Universal Scaling and Dynamics at Quantum Phase Transitions in the Kitaev Chain

Emma Catherine King

Thesis presented in partial fulfillment of the requirements for the degree of Master of Science in the Faculty of Science at Stellenbosch University.

The financial assistance of the National Research Foundation (NRF) towards this research is hereby acknowledged. Opinions expressed, and conclusions arrived at, are those of the author and are not necessarily to be attributed to the NRF.

Supervised by Dr. JN Kriel and Prof. M Kastner

Departement Fisika · Department of Physics
Universiteit · Stellenbosch · University
December 2021

Declaration

By submitting this thesis electronically, I declare that the entirety of the work contained therein is my own, original work, that I am the sole author thereof (save to the extent explicitly otherwise stated), that reproduction and publication thereof by Stellenbosch University will not infringe any third party rights and that I have not previously in its entirety or in part submitted it for obtaining any qualification.

Date: December 2021

Abstract

Universal Scaling and Dynamics at Quantum Phase Transitions in the Kitaev Chain

E.C. King

Department of Physics
Stellenbosch University

Thesis: MSc (Theoretical Physics)

December 2021

Experimental advances in ultracold gases present physicists with the opportunity to explore a diverse range of new phenomena in a controllable manner. In turn, this has fuelled significant interest in the field of non-equilibrium quantum many-body dynamics. A common theme in several theoretical studies has been the dynamics that emerge when a quantum system is driven out of equilibrium through a continuous ramp, or sudden quench, of a control parameter in the system's Hamiltonian. Of particular interest is the case where the ramp results in the system approaching, or crossing, a quantum phase transition, and where properties of the associated critical point are then imprinted on the system's dynamics. A classical version of this notion was already proposed by Kibble and Zurek in the 1980s in the context of thermal phase transitions. There it was shown that the equilibrium critical exponents of the phase transition govern certain scaling laws which emerge following a parameter ramp across a phase transition. This mechanism subsequently also received considerable attention in the context of zero-temperature quantum phase transitions. Fundamental to this framework is the breakdown in adiabatic evolution at the critical point, leading to the production of excitations. The scaling of the resulting excitation density with the ramp rate, and how the equilibrium critical exponents are encoded in this scaling law, are some of the central predictions of the Kibble-Zurek framework.

We study extensions of this framework and investigate parameter ramps at finite temperatures, as well as ramps of the temperature itself, in the vicinity of a quantum phase transition. The overarching goal is to formulate scaling laws and identify universal features resulting from such ramps. We single out the one-dimensional, long-range fermionic Kitaev chain as a setting for this investigation. The quadratic nature of this model makes it amenable to both analytic and numeric treatments, even after introducing a coupling to a thermal bath within the Lindblad formalism. We derive analytic scaling laws for the excitation density resulting from ramps to the critical point, both for an isolated chain and for one in contact with a thermal environment. In the former case, our results are found to agree with the predictions of the Kibble-Zurek framework, except for the case of long-range hopping along the chain. Despite this, we find excellent agreement between our analytic scaling predictions and exact numeric results obtained from solving the relevant equations of motion. For the open Kitaev chain the scaling of, and competition between, the contributions of the coherent and incoherent excitation mechanisms is analysed in detail. To support our analytic predictions, we exploit the superoperator formalism of Prosen to solve the Lindblad master equation numerically for chains with several thousand sites. We also consider the cooling of the system towards the quantum critical point, and investigate how the final residual excitation density scales with the cooling rate and the initial temperature. This work presents new results for these temperature ramps towards critical points, and extends several other results appearing in the literature.

Uittreksel

Universele Skalering en Dinamika by Kwantum Faseoorgange in die Kitaev Ketting

E.C. King

Departement Fisika
Universiteit Stellenbosch

Tesis: MSc (Teoretiese Fisika)

Desember 2021

Eksperimentele vooruitgang in ultrakoue kwantumgasse bied fisici die geleentheid om ’n uiteenlopende reeks nuwe verskynsels op ’n beheerbare wyse te ondersoek. Hierdie vooruitsig het ook aansienlike belangstelling in nie-ewewig veeldeeltjie kwantumdinamika aangewakker. ’n Sentrale tema in verskeie teoretiese studies is die dinamika van ’n kwantumsisteem wat uit ewewig gedryf word deur ’n kontinue of skielike variasie van ’n kontroleparameter in die sisteem se Hamiltoniaan. Van besondere belang is die geval waar die parameter variasie daartoe lei dat die sisteem ’n kwantum-faseoorgang nader of oorsteek, en waar eienskappe van die gepaardgaande kritiese punt dan in die dinamika vervat word. ’n Klassieke weergawe van hierdie idee is reeds in die negentien-tagtigs in die konteks van termiese faseoorgange deur Kibble en Zurek voorgestel. Daar is gevind dat die ewewig kritiese eksponente van die faseoorgang ’n rol speel in sekere skaleringswette wat na vore kom na ’n parameter variasie wat die faseoorgang oorsteek. Hierdie meganisme het sedertdien ook aansienlike aandag in die konteks van nul-temperatuur kwantum-faseoorgange geniet. ’n Fundamentele aspek van hierdie raamwerk is hoe adiabatiese evolusie by die kritiese punt afbreek wat dan lei tot die skep van opwekkings. Die skalering van die resulterende opwekkingsdigtheid met die tempo waarteen die parameter gevarieer word, asook hoe die ewewig kritiese eksponente in hierdie skaleringswet verskyn, is van die sentrale voorspellings van die Kibble-Zurek raamwerk.

Ons bestudeer veralgemenings van hierdie raamwerk en ondersoek kontroleparameter variasies by eindige temperature, asook temperatuur variasies na aan ’n kwantum-faseoorgang. Die oorhoofse doelwit is om skaleringswette te formuleer en universele kenmerke te identifiseer. Ons fokus op die een-dimensionele, langreikwydte fermioniese Kitaev ketting as ’n konteks vir hierdie studie. Die kwadratiese aard van hierdie model maak beide analitiese en numeriese ondersoeke moontlik, selfs wanneer dit aan ’n termiese bad gekoppel word binne die Lindblad-formalisme. Ons lei analitiese skaleringswette af vir die opwekkingsdigtheid wat volg uit parameter variasies wat eindig by die kritiese punt, beide vir ’n geïsoleerde sisteem asook vir een wat in kontak met ’n termiese omgewing is. Vir die geïsoleerde sisteem stem ons resultate ooreen met die voorspellings van die standaard Kibble-Zurek raamwerk, behalwe in die geval van langreikwydte hopprosesse in die ketting. Ten spyte hiervan vind ons steeds uitstekende ooreenstemming tussen ons analitiese voorspellings en eksakte numeriese resultate wat verkry word deur die relevante bewegingsvergelykings op te los. Vir die sisteem wat in kontak met ’n termiese bad is ontleed ons beide die skalering van die koherente en nie-koherente bydraes tot die opwekkingsdigtheid, asook die kompetisie tussen hierdie bydraes. Om ons analitiese resultate te ondersteun gebruik ons die superoperator formalisme van Prosen om die Lindblad-meestervergelyking numeries op te los vir kettings met ’n paar duisend eenhede. Ons beskou ook die afkoel van die sisteem na die kwantum kritiese punt, en ontleed hoe die finale oorblywende opwekkingsdigtheid met die afkoeltempo asook die aanvanklike temperatuur skaleer. Hierdie werk bevat nuwe resultate vir hierdie temperatuur variasies by kritiese punte, en brei ook verskeie ander resultate uit wat in die literatuur verskyn.

Contents

List of Figures

Chapter 1

Introduction

This thesis investigates the non-equilibrium dynamics of quantum many-body systems in the vicinity of quantum critical points, with a strong focus on Kibble-Zurek (KZ) physics and realisations thereof in the Kitaev chain. The overarching goal is to formulate scaling laws and identify universal features that arise either when ramping a coupling constant, or control parameter, across a critical point at finite temperature, or when cooling a quantum system towards criticality. Drawing inspiration from the dynamic KZ scaling results for the closed fermionic Kitaev chain, the non-equilibrium dynamics of the chain in the presence of weak dissipation is studied. This provides an interesting setting for exploring the interplay between quantum and thermal fluctuations, and the connection between the dynamical and equilibrium properties of quantum critical systems. Section 1.1 will introduce important theoretical concepts that are used extensively throughout this thesis. This is followed by a brief literature review on the adiabatic dynamics of isolated and dissipative open quantum systems in Section 1.2. In Section 1.3 we summarise the aims and applications of this research. The chapter ends with Section 1.4 in which an outline of the thesis is provided.

1.1 Theoretical background

This section provides some essential theoretical background on quantum phase transitions, the Landau-Zener problem, the Kibble-Zurek Mechanism (KZM) and open quantum systems.

1.1.1 Quantum phase transitions

Phase transitions are of paramount importance in many fields within the physical sciences and play an essential role in nature [1, 2]. A phase transition marks an abrupt and fundamental change in the state of a system [1], which is often characterised by non-analytic behaviour in the system's free energy [3]. Fundamental changes from one phase of matter to another can be seen everywhere [1]. Everyday examples include the freezing of rivers, the boiling of water or the melting of ice. This macroscopic change that occurs when a physical system crosses the boundary between distinct phases of matter is driven by microscopic fluctuations [2, 4]. Traditionally, phase transitions are classified as either first-order or continuous. This work concentrates on continuous (second-order) phase transitions, where the two phases do not co-exist at the transition point [2].

The notion of a continuous phase transition was first introduced by Andrews in 1869 [5, 6]. Andrews' discovery of critical opalescence in carbon dioxide [5] led to the first observation of a diverging correlation length at a continuous phase transition [5, 6]. Over the past century, scientists have delved deeply into this topic, leading to an expansive understanding of critical phenomena. Presently, many systems that display second-order phase transitions are known to exhibit universal features close to critical points. These universal features are independent of the particular microscopic details of the system. Amongst these universal features are the critical exponents that characterise divergences in time and length scales at the critical point [7].

More recently, considerable progress has also been made in the field of quantum phase transitions (QPTs) [2, 7, 8]. While classical (thermal) phase transitions[1] and QPTs share some similarities, QPTs are fundamentally different to their classical counterparts [2, 8]. QPTs are driven by microscopic quantum fluctuations (as opposed to thermal fluctuations) [4, 6, 8], typically at very low temperatures where thermal

[1]The terms *classical phase transition* and *thermal phase transition* will be used interchangeably. It can be justified that all thermal phase transitions are indeed classical. Refer to the work published in Ref. [6] for a discussion on this.

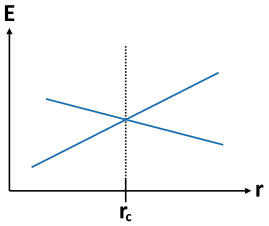

(a) True level-crossing

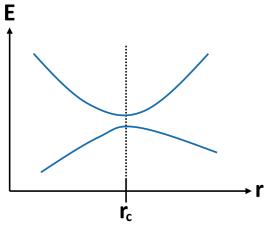

(b) Avoided level-crossing

Figure 1.1: (Reproduced from [7]) (a) A true level-crossing, which is often characteristic of a first-order quantum phase transition. (b) An avoided level-crossing, signifying a second-order quantum phase transition.

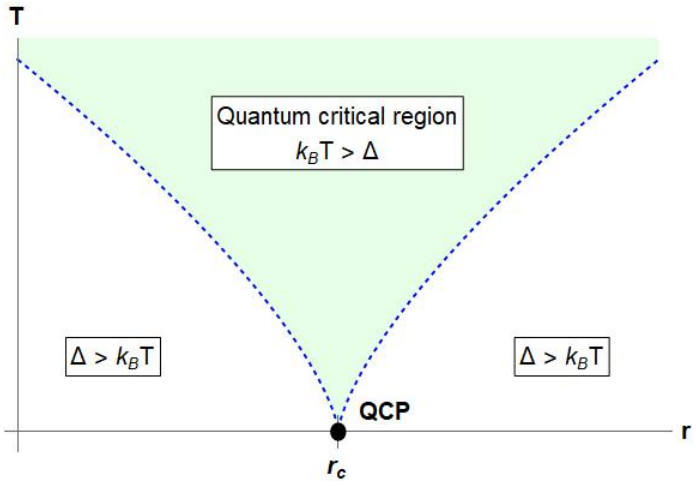

Figure 1.2: (Reproduced from [7]) The r-axis corresponds to the system's zero-temperature phase diagram, with the critical value of r marking the quantum phase transition. The dashed lines are not phase transitions, but crossovers at $T \sim |r - r_c|^{\nu z}$ with critical exponent νz. These crossovers between the semi-classical ($\Delta > k_B T$) and quantum critical ($\Delta < k_B T$) regions are based on a comparison of the temperature T with the system's excitation gap Δ.

fluctuations are largely absent [4, 7]. As a result, QPTs are accessed at zero absolute temperature by varying a non-thermal control parameter, for example pressure, an external magnetic field or the chemical potential [2, 6]. When the control parameter is varied across a critical value, the properties of the ground state change in a non-analytic way.

When the existence of QPTs was first predicted by the physicist John Hertz in 1976 [9], the study of critical phenomena in quantum mechanical systems at zero temperature was believed to be of purely academic interest [6]. This belief was reasonable since (i) QPTs are accessed strictly at zero temperature, which is inaccessible in an experiment, and (ii) QPTs occur at a precise, critical control parameter value [2, 6]. However, in recent years, QPTs have attracted attention in both theoretical and experimental settings. After the experimental realization of a quantum phase transition from a superfluid to a Mott insulator in a gas of ultracold atoms [4, 10], condensed matter physicists have become intrigued by the important — and experimentally relevant — consequences of QPTs [6]. Despite being a very active field of modern physics research over the past decade, quantum phase transitions and critical phenomena continue to challenge physicists' understanding of condensed matter systems.

In this thesis a quantum phase transition will be formally defined as any point of non-analyticity in the ground state energy or ground state properties of a quantum system [2, 7]. Points of non-analyticity could arise from either an actual level-crossing or an avoided level-crossing (see Fig. 1.1), where the latter is more commonly observed [7]. To describe these level-crossings, consider a many-body system with Hamiltonian $H(r)$, where $H(r)$ varies as a function of a control parameter (coupling constant) r [2, 7]. For a finite system, the ground state energy of $H(r)$ as a function of r will typically be a smooth, analytic function [7]. However, for the case where r couples solely to a conserved quantity, it is possible that a previously excited level becomes the ground state at some point $r = r_c$. This is known as a true level-crossing, and at the transition point the level-crossing produces a non-analyticity in the ground state energy as a function of r [2, 7]. If the excited level cannot become equal in energy to the ground state, i.e. they cannot *cross*, then it is known as an avoided level-crossing. The point at which an avoided level-crossing occurs is commonly referred to as a quantum critical point (QCP)[2]. This avoided level-crossing becomes sharper with an increase in system size [3, 7], resulting in a point of non-analyticity in the thermodynamic limit, i.e. an infinitely sharp transition is obtained in the limit of an infinite system size [2].

[2]Formally, a QCP is a point at which the correlation length diverges upon variation of the control parameter r at exactly zero temperature [3]. In some cases a QCP is at a physically inaccessible parameter value [7].

It is requisite to point out that according to the definition above QPTs occur strictly at zero temperature. Focusing on second-order phase transitions, these transitions can be loosely characterised by an energy gap between the ground state manifold and the rest of the spectrum [7, 11] which vanishes as the critical point is approached. More specifically, second-order QPTs involve a characteristic energy scale, say Δ, where $\Delta \to 0$ as $r \to r_c$ [11]. However, the inaccessibility of zero temperature in experimental settings motivates the expansion of this theory to also include transitions and crossovers at $T > 0$. At finite temperatures a second important energy scale enters, namely $k_B T$ [7]. It is the comparison of the competing energy scales Δ and $k_B T$ that leads to the diagram in Fig. 1.2. This figure combines the system's zero-temperature phase diagram and the the crossovers resulting from the comparison of the competing energy scales. The smooth crossover lines at $T \sim |r - r_c|^{\nu z}$, with critical exponent νz, separate the semi-classical regions from the quantum critical region. The so-called *quantum critical region*, where $\Delta < k_B T$, will play an important role in this thesis. Within this region both quantum and thermal fluctuations impact on the system dynamics [7]. This fascinating interplay between quantum and thermal fluctuations will be further explored, with a focus on the universal features which may arise in the vicinity of QCPs. An important tool for understanding how the universal properties of QPTs imprint on the system's dynamics, and the extension of this idea into the finite-temperature domain, is the so-called Kibble-Zurek mechanism. Fundamental to the KZ mechanism is the breakdown of adiabaticity at the critical point. A simple, paradigmatic example of this breakdown of adiabaticity is the Landau-Zener model [12], which we consider next.

1.1.2 The Landau-Zener problem

During the late 1920s there was considerable interest in the crossing of energy levels. According to the adiabatic theorem [13], a system governed by a time-dependent Hamiltonian $H(t)$, with the initial state being a stationary state, will pass through all the corresponding stationary states of $H(t)$ for all t, provided that the Hamiltonian varies infinitely slowly. However, when the spectrum is no longer gapped, as is the case when crossing a second-order phase transition [7], there will be a deviation from the adiabatic dynamics no matter how slowly the Hamiltonian changes. These ideas can be straightforwardly demonstrated using the Landau-Zener (LZ) problem[3], a well-known and extensively studied paradigm in quantum physics [18, 19].

The LZ model is a two-state (two-level) quantum mechanical system described by the time-dependent Hamiltonian

$$H(t) = \begin{bmatrix} \varepsilon(t) & \bar{\Delta} \\ \bar{\Delta} & -\varepsilon(t) \end{bmatrix} \tag{1.1}$$

in the diabatic basis $\{|1\rangle, |2\rangle\}$. Here $\bar{\Delta} \geq 0$ is a constant coupling and $\varepsilon(t)$ is the energy level spacing (or detuning). The solution $|\psi(t)\rangle$ of the Schrödinger equation

$$i\frac{\mathrm{d}}{\mathrm{d}t}|\psi(t)\rangle = H(t)|\psi(t)\rangle \tag{1.2}$$

can be written in the form

$$|\psi(t)\rangle = C_1(t)|1\rangle + C_2(t)|2\rangle . \tag{1.3}$$

Here the probability amplitudes $C_1(t)$ and $C_2(t)$ of the diabatic states $|1\rangle$ and $|2\rangle$ satisfy [11, 19, 20]

$$i\frac{\mathrm{d}}{\mathrm{d}t}C_1(t) = \varepsilon(t)C_1(t) + \bar{\Delta}C_2(t) \qquad \text{and} \qquad i\frac{\mathrm{d}}{\mathrm{d}t}C_2(t) = \bar{\Delta}C_1(t) - \varepsilon(t)C_2(t). \tag{1.4}$$

Since only the characteristics in the vicinity of the crossing are of interest to us, the detuning is chosen to have a linear time-dependence, $\varepsilon(t) = \vartheta t$ [15, 18], which is a realistic approximation for many physical problems [18]. Here ϑ can be regarded as the ramp rate for the variation of $\varepsilon(t)$ with time. At $t = 0$ the detuning vanishes and produces for $\bar{\Delta} = 0$ a true crossing of the energy levels, while for $\bar{\Delta} > 0$ the coupling between diabatic states results in level repulsion and an avoided level-crossing.

At any given time, the Hamiltonian has two instantaneous eigenstates (adiabatic states): the ground state $|g(t)\rangle$ and the excited state $|e(t)\rangle$ [11]. The adiabatic states written in the diabatic basis $\{|1\rangle, |2\rangle\}$ of the Hamiltonian are [11, 18]

$$|g(t)\rangle = \cos(\theta/2)|1\rangle - \sin(\theta/2)|2\rangle \qquad \text{and} \qquad |e(t)\rangle = \sin(\theta/2)|1\rangle + \cos(\theta/2)|2\rangle , \tag{1.5}$$

[3] As early as 1932, Landau [14] and Zener [15] (see also work published in Refs. [16, 17]) rigorously derived an analytical description of the excitation probability for this model when it is driven through an avoided level-crossing by adiabatic variation of a control parameter. This excitation probability later became known as the LZ transition probability.

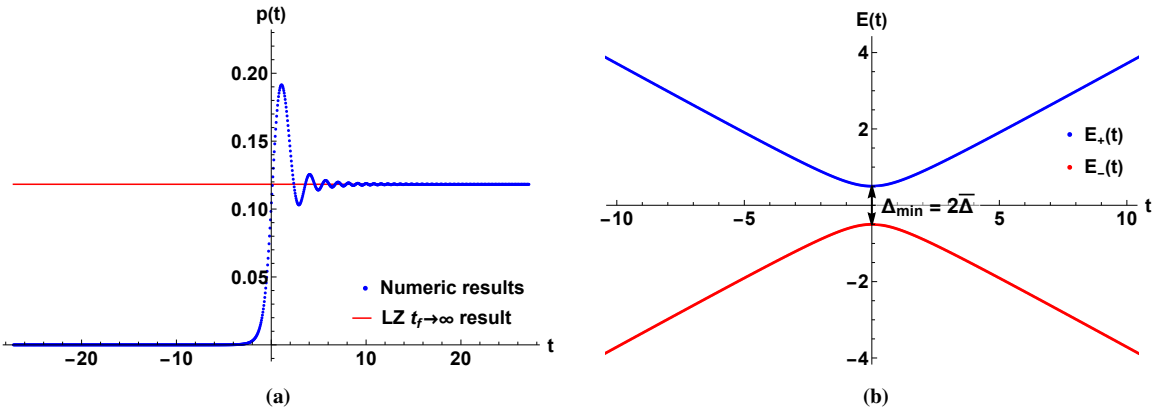

Figure 1.3: **(a)** The excitation probability as a function of time. At late times there is good agreement with the LZ result. Parameters are chosen as follows: $\bar{\Delta} = 0.5$ and $\vartheta = e^{-1}$. **(b)** The eigenenergies as a function of time, showing the instantaneous excitation gap $\Delta(t)$ which is minimal at $t = 0$.

where $\tan(\theta) = -\bar{\Delta}/\varepsilon(t)$, $0 \leq \theta \leq \pi$. The corresponding eigenenergies are

$$E_{\pm}(t) = \pm\sqrt{\varepsilon^2(t) + \bar{\Delta}^2}, \tag{1.6}$$

hence the instantaneous energy gap $\Delta(t) = E_+ - E_-$ is minimal at the avoided level-crossing, where $\varepsilon(t) = 0$, with a value of $\Delta_{\text{min}} = 2\bar{\Delta}$ [18]. The LZ model is exactly solvable, making it useful to understand the breakdown of adiabaticity due to the vanishing energy gap.

In the LZ problem the system is typically prepared in the instantaneous ground state $|g(t_i)\rangle$ at some initial time t_i. The solution to the differential equations (1.4) can be used to determine the probability $p(t_f)$ that the system is excited at some final time t_f [11]. Using the state of the system introduced in Eq. (1.3), the probability to undergo a transition is

$$p(t_f) = |\langle e(t_f)|\psi(t_f)\rangle|^2 = 1 - |\langle g(t_f)|\psi(t_f)\rangle|^2 . \tag{1.7}$$

In the limit $t_f \to \infty$ this non-adiabatic transition probability $p(t_f)$ is given by the well-known exponential Landau-Zener formula [21]

$$p_{\text{LZ}} = e^{-\pi\bar{\Delta}^2/\vartheta}, \tag{1.8}$$

assuming the system was initially prepared in its ground state at time $t_i \to -\infty$. Figure 1.3a shows the numeric results obtained from solving Eq. (1.4), together with the LZ result in Eq. (1.8). At late times the LZ formula accurately approximates the exact excitation probability. The minimum in the system's excitation gap at $t = 0$ (see Fig. 1.3b) results in a breakdown of adiabaticity if the adiabatic-following condition[4]

$$\sqrt{\vartheta} \ll \Delta(t)/2 \tag{1.9}$$

is violated in the neighbourhood of $t = 0$. This leads to the excitation probability increasing rapidly close to $t = 0$ before stabilising to its long-time value given by the LZ formula. For a true closing of the excitation gap, i.e. when $\Delta_{\text{min}} = 2\bar{\Delta} = 0$, we have $p_{\text{LZ}} = 1$ regardless of how slowly the Hamiltonian is varied. In other words, the violation of the adiabatic-following condition is unavoidable if the excitation gap truly vanishes.

Generalisation of this two-state case can be achieved for several integrable spin models by using a Jordan–Wigner transformation to perform a mapping to non-interacting fermions [11]. In a translationally invariant system of non-interacting fermions, a phase transition can be viewed as a set of independent LZ avoided crossings [11]. The details of this general LZ argument are summarised in work by Dziarmaga [11], with useful technicalities addressed in Refs. [19, 20]. Of particular interest is the expression for the probability p_k that an excitation mode with momentum k of the final Hamiltonian at $t \to \infty$ is excited after the system has passed through a phase transition as a result of ramping some control parameter. In general, this probability is given by [11]

$$p_k = e^{-\pi\tau_Q\Delta^2(k)/a(k)}, \tag{1.10}$$

[4] Refer to Appendix A for details on the derivation of this condition.

where $\Delta(k)$ is the minimal gap function and $a(k)$ is a model-dependent parameter. The ramp rate τ_Q^{-1} plays the role of ϑ above, and characterises the rate at which the control parameter in the Hamiltonian is varied. Averaging the excitation probability in Eq. (1.10) over the first Brillouin zone gives the density of quasiparticle excitations in the final state at the end of the parameter ramp as[5]

$$n_{\text{ex}} = \frac{1}{L}\sum_k p_k \approx \int \frac{d^d k}{(2\pi)^d}\, p_k, \tag{1.11}$$

where L is the system size (number of lattice sites) and d is the system's dimensionality [11, 22, 23].

In the past two decades, the LZ formalism has been applied extensively in quantum optics [24–27], atomic and molecular physics [28] and condensed matter physics (see for example work published in Refs. [29–36]). Remarkably, physicists continue discovering more systems that are governed by (or well approximated by) the LZ problem. In the context of quantum non-equilibrium dynamics, the two-level Landau-Zener model is also a powerful tool for exploring Kibble-Zurek physics.

1.1.3 The Kibble-Zurek mechanism

The Kibble-Zurek mechanism (KZM), a powerful theory describing the universality of dynamical behaviour near a phase transition, has brought about substantial development in the study of slow passages through critical points. This theory was originally introduced by Kibble [37] in the context of the formation of domain walls, strings and monopoles in the early universe due to the occurrence of symmetry breaking phase transitions [37, 38]. Zurek identified that similar behaviour is observed in phase transitions taking place in the laboratory [39]. Subsequently, Zurek recast the theory for application in the study of critical phenomena in statistical mechanics and condensed matter physics. In the years that followed, experiments in superfluid helium and liquid crystals shed light on the dynamics of the defect formation process [38]. A plethora of experiments in condensed matter systems have since rigorously tested the dynamical KZM for classical phase transitions [11], and shown results to be consistent with the theory. Today, the KZM is a well-established theory for the prediction of how the number of defects generated in a system being driven through a continuous finite-temperature phase transition scales with the driving rate [40].

Although the KZM was first proposed for classical phase transitions, the concepts have since been extended to include quantum phase transitions. Generalization to the quantum setting was achieved by the work of Zurek [41], Polkovnikov [42] and Dziarmaga [43]. The quantum version of the KZM is similar to its classical (finite-temperature) counterpart in that the excitations scale with a power of the driving rate [11]. The fundamental differences reside in the underlying physics. To thoroughly understand the mechanism at zero temperature, consider a quantum condensed matter system that is driven (or ramped) slowly across a critical point $r = r_c$ at $T = 0$ by varying the coupling constant r.[6] Near the isolated critical point there is a divergence in the system's reaction time τ and correlation length ξ [7, 11]. More specifically, τ and ξ diverge as [11]

$$\tau \sim |\varepsilon|^{-\nu z} \qquad \text{and} \qquad \xi \sim |\varepsilon|^{-\nu}, \tag{1.12}$$

where

$$\varepsilon = \frac{r - r_c}{r_c} \tag{1.13}$$

is a dimensionless distance parameter describing the proximity of r to its critical value [21], ν is the correlation length critical exponent, and z is the dynamical critical exponent. Both ν and z are determined by the universality class of the underlying phase transition. Note that the reaction time, which governs how quickly the system can respond to external perturbations, is set by the inverse energy gap, $\tau \simeq \Delta^{-1}$ [11]. It then follows from Eq. (1.12) that

$$\Delta \sim |\varepsilon|^{\nu z}. \tag{1.14}$$

The vanishing of the gap results in non-adiabatic system evolution near the critical point, no matter how slow the driving speed (ramp rate) [11].

[5] Note that (i) the integral approximation in Eq. (1.11) only becomes accurate in the thermodynamic limit $L \to \infty$, and (ii) the dominant contributions to n_{ex} come from the long-wavelength modes [11, 22].

[6] In the context of our work, the *slowness* of the driving or ramping is understood by comparing the relevant timescales in the problem when we are far from the QPT. Therefore, 'ramping slowly' should be interpreted as follows: away from the QCP, the control parameter or coupling constant is varied on a timescale that is much longer than the typical timescales of the system, i.e. it is possible for the adiabatic-following condition to be satisfied.

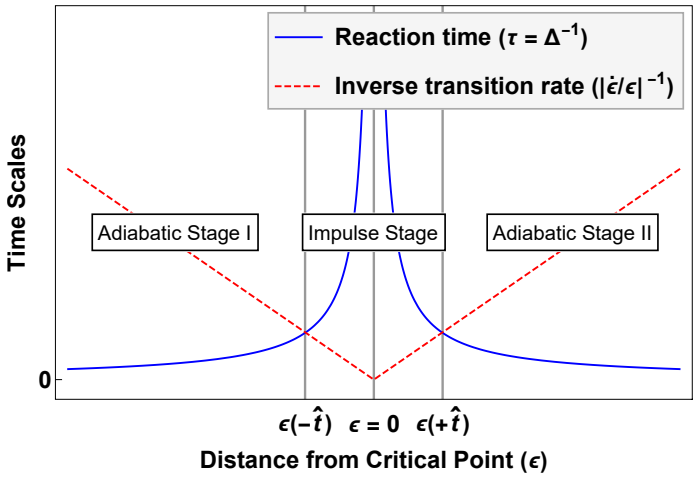

Figure 1.4: (Reproduced from [11, 21]) The reaction time $\tau(\simeq \Delta^{-1})$ and the inverse transition rate $|t|$ as a function of the dimensionless parameter ε which indicates the distance from the critical point. The energy gap Δ equals the transition rate at the crossover points $\varepsilon(-\hat{t})$ and $\varepsilon(\hat{t})$. These boundaries differentiate between the impulse and adiabatic stages of evolution. Starting in adiabatic stage I, the system evolves adiabatically until $\varepsilon(-\hat{t})$ is reached, where the impulse stage is entered. This impulse stage lasts until the reactions of the system again become faster than the transition rate.

The study of linear ramping protocols constitute a great proportion of the literature, and will also be the focus of this thesis. However, it is possible to implement a slow nonlinear ramp across a quantum critical point. The first theoretical investigation of the production of defects as a consequence of a nonlinear ramp was conducted by Sen et al. [44]. In what follows, the parameter ε will be varied linearly at a finite ramp rate set by the ramp timescale $\tau_Q = \left| \frac{\mathrm{d}\varepsilon}{\mathrm{d}t}\big|_{t\to 0} \right|^{-1}$ [11, 21]. We write this as

$$\varepsilon(t) = -\frac{t}{\tau_Q}. \tag{1.15}$$

The system is prepared in the ground state at $t \to -\infty$, and evolves with varying ε. There are three distinct stages for the system's evolution: adiabatic stage I, impulse, and adiabatic stage II [21], as shown in Figure 1.4. Initially, the system's state will follow the instantaneous adiabatic ground state since the reaction time is fast enough or, equivalently, the gap Δ is large enough. The relative rate of change of the energy gap, $|\dot{\Delta}/\Delta|$, is introduced as a qualitative measure of the rate at which the Hamiltonian is changing. This measure is referred to as the *transition rate*, and from Eqs. (1.14) and (1.15) it is postulated that [45]

$$|\dot{\Delta}/\Delta| \simeq |\dot{\varepsilon}/\varepsilon| = |t|^{-1}. \tag{1.16}$$

Therefore, the first adiabatic stage lasts until the inverse reaction time Δ (1.14) equals the transition rate (1.16) at an instant $t = -\hat{t}$. This leads to the freeze-out time [21]

$$\hat{t} \sim \tau_Q^{\frac{\nu z}{1+\nu z}}. \tag{1.17}$$

After $t = -\hat{t}$, the impulse stage is entered (see Figure 1.4). Adiabaticity breaks down since the system's reaction time is too slow. In the adiabatic–impulse approximation, the evolution becomes *impulse*, i.e. the state becomes 'frozen' and does not change until adiabatic evolution resumes at time $\hat{t}$ [11]. Close to the freeze-out time, $-\hat{t}$, the system is in its instantaneous ground state with correlation length $\hat{\xi}$ [11]. According to the definition in Eq. (1.12), this correlation length is given by $\hat{\xi} \sim |\varepsilon(-\hat{t})|^{-\nu}$. It follows from the definition of the parameter ε (1.15) and the freeze-out time (1.17) that

$$\hat{\xi} \sim |\varepsilon(-\hat{t})|^{-\nu} \sim \tau_Q^{\frac{\nu}{1+\nu z}}. \tag{1.18}$$

This ground state, which gets 'frozen' exactly at $-\hat{t}$, becomes an excited initial state for the system's evolution after the transition into the final adiabatic stage at $\hat{t}$ [11]. While the simplification made by the adiabatic–impulse approximation captures the important details of the non-equilibrium dynamics, strictly speaking, the evolution in the system does not stop [21]. During the impulse stage the system's state will still evolve as dictated by its Hamiltonian, but ceases to be adiabatic. Sufficiently long after passing the critical point, the

system can 'catch up' locally.

The characteristic timescale $\hat{t}$ (1.17) and correlation length $\hat{\xi}$ (1.18) predicted by the KZ mechanism can be used to estimate other physical observables [11, 21]. In this work, the focus is on the scaling of the density of quasiparticle excitations generated during the slow passage through a quantum phase transition. In the limit of long ramp timescales, i.e. slow ramp rates, the density of excitations n_{ex} is expected to scale as [11]

$$n_{\text{ex}} \simeq \hat{\xi}^{-d} \sim \tau_Q^{-\frac{d\nu}{1+\nu z}} = v^{\frac{d\nu}{1+\nu z}}, \tag{1.19}$$

where d is the (spatial) dimensionality of the system, $v = \tau_Q^{-1}$ is the ramp rate and $\frac{d\nu}{1+\nu z}$ is the KZ scaling exponent. While the KZM does not provide an exact prediction for the excitation density, it does predict that n_{ex} obeys a power law in the ramp rate, where the power exponent is given in terms of the critical exponents associated with the phase transition. This prediction reflects an element of universality in the non-equilibrium dynamics of systems in the vicinity of QCPs.

At the end of Section 1.1.2 it was claimed that the Landau-Zener model is a powerful tool to explore Kibble-Zurek physics. Recently, work by Damski [12] showed that the Kibble-Zurek theory of the production of defects, which was introduced above, gives an accurate account of the quantum non-equilibrium dynamics across a LZ transition. This intriguing connection between the KZM and LZ crossing has subsequently been verified experimentally, with results published in Refs. [46–48]. As a result, the two-level LZ model is useful to gain new insight into the non-equilibrium dynamics of quantum phase transitions. Undoubtedly, most important many-body quantum systems, such as spin systems and cold atoms in optical lattices, are substantially more complex than the LZ model [12]. However, the generic nature of avoided level-crossings at a second-order QPT suggests that changes to the system's properties incurred during a phase transition can be qualitatively described by the Landau-Zener problem [11, 12].

1.1.4 Open quantum systems

Over the past decade, open many-body quantum systems have received considerable attention. Despite the formidable challenges, the theoretical study of open quantum systems is warranted by the major role these systems play in numerous applications of quantum physics [49]. This wide-spread applicability can be attributed to the fact that the perfect isolation of quantum systems in experimental settings is not viable [49, 50]. Any realistic system will be in contact with some uncontrollable environment which may significantly alter it, as well as its dynamics. Consequently, it is necessary to understand the highly non-trivial interplay between unitary quantum dynamics and dissipation [51] in order to address pertinent questions about quantum phenomena and the dynamics of open systems. To this end, many noteworthy experiments have been conducted in atomic and molecular optical systems and superconducting circuits [52, 53]. The ability to experimentally control both coherent and dissipative dynamics will allow for exciting future developments in the field of general open-system quantum simulation. However, modeling open quantum system dynamics from a theoretical standpoint presents several difficulties. Two notable issues are (i) the numeric description of many-body quantum systems requires significant computational power, with the computational complexity increasing exponentially with the number of particles, and (ii) the tools used to describe isolated quantum systems cannot trivially be extended to deal with open systems.

1.1.4.1 Quantum master equations

One of the most well-known approaches for treating open quantum systems is through a quantum master equation [49], which is an equation of motion for the system's density matrix, $\varrho(t)$ [49]. Such an equation of motion is useful for (approximately) describing the time evolution of an open system, as well as understanding its dynamics. Under the assumption that the total quantum system (the system plus the environment) is closed and the environmental correlation times are short (the Markovian assumption), the Markovian quantum master equation is [49, 54, 55]

$$\frac{\mathrm{d}\varrho(t)}{\mathrm{d}t} = \hat{\mathcal{L}}\varrho(t), \tag{1.20}$$

where $\hat{\mathcal{L}}$—the *Liouvillean* or the *Liouville (super-) operator*—is the generator of the quantum dynamical semigroup [54]. A general expression for the generator $\hat{\mathcal{L}}$ can be derived from first-principles under the Born–Markov and rotating wave approximations (refer to Refs. [49, 54, 55] for detailed discussions). Omitting the

specific details of the derivation, the widely used Markovian Lindblad master equation is [49, 54, 55]

$$\frac{\mathrm{d}\varrho(t)}{\mathrm{d}t} = \hat{\mathcal{L}}\varrho(t) = -i[H_{\mathrm{S}} + H_{\mathrm{LS}}, \varrho(t)] + \sum_{\alpha} \gamma_{\alpha} \left(L_{\alpha}\varrho(t)L_{\alpha}^{\dagger} - \frac{1}{2}\{L_{\alpha}^{\dagger}L_{\alpha}, \varrho(t)\} \right) \tag{1.21}$$

where the operators L_{α}—commonly referred to as Lindblad bath operators—encode information about the system's couplings to the bath(s). The system–bath couplings describe how the system interacts with the bath(s), as well as the strength of the interaction. Note that the first term of the generator in Eq. (1.21) accounts for the unitary part of the dynamics generated by the effective Hamiltonian, $H_{\mathrm{S}} + H_{\mathrm{LS}}$ [55], which is a combination of the system Hamiltonian H_{S} and the Lamb-Shift Hamiltonian H_{LS}. The remaining terms are responsible for the non-unitary (dissipative) evolution [55]. Finally, it is important to note that Lindblad master equations can be restrictive due to the various assumptions and approximations introduced in the description of both the system and the environment [49, 54, 56].

In this thesis a simple model of a quadratic quantum many-body system in the presence of a thermal bath will be treated within the Lindblad formalism using a quantum master equation of the form given in Eq. (1.21). D'Abbruzzo and Rossini's recent paper [51] provides a self-consistent microscopic derivation of this Markovian master equation for open quadratic quantum systems. Following this approach, the Lindblad bath operators for quadratic fermionic or bosonic models can be found. In some cases, local master equations may violate the second law of thermodynamics, fail to accurately describe the dissipative dynamics, or result in unphysical behaviour (refer to work by Konopik and Lutz [57] for an in-depth discussion). Importantly, the derivation in the work published in Ref. [51] leads to a non-local form of the master equation. Solving this master equation is computationally infeasible for very large systems since the dimensionality of the problem increases exponentially with the system size. In Refs. [58, 59] a general method to solve master equations for quadratic open Fermi systems is presented, where computational complexity increases only linearly with system size. Using this approach of "third quantisation", numeric calculations for larger systems can be performed. We will present this approach in Section 3.1.

1.2 The adiabatic dynamics of isolated and open dissipative quantum systems

With the advancement of experimental platforms in the past two decades came a succession of noteworthy experiments on the non-equilibrium dynamics of many-body systems [60–67], and in particular highly controllable ultracold atomic gases [4, 68–73] (refer to [74] for an extensive review). These experiments probed various many-body critical phenomena and shed light on out-of-equilibrium quantum dynamics of various different systems. Inevitably, this swiftly stirred up fresh interest in the theoretical study of the dynamics of isolated (closed) quantum many-body systems. Most of the theoretical studies have been devoted to one simple approach: the controlled variation (hereafter referred to as 'ramping') of a parameter or coupling constant in a Hamiltonian. These ramping protocols can be split into two broad categories: sudden ramps (quenches) and slow (adiabatic) ramps. Over the years many studies on sudden quenches have been conducted, for example: the study of universality in the quench dynamics [75, 76], the evolution of entanglement entropy [77, 78] and the use of work statistics to formulate descriptions of generic sudden quenches [79, 80]. In this thesis the focus will be on parameter ramps in which the ramp rate is slow compared to the other relevant timescales of the system.

The adiabatic dynamics of a system become particularly fascinating when a critical point is traversed. The breakdown of adiabaticity in the vicinity of a critical point results in interesting out-of-equilibrium dynamics and the formation of (topological) defects. Many tools have been developed for the theoretical study of the non-equilibrium physics of interacting systems, including, but not limited to, the density matrix renormalization group, the Keldysh technique, quantum kinetic equations and functional integral methods [45]. This work focuses on another one of these tools, the so-called Kibble-Zurek mechanism (KZM) which was introduced in Section 1.1.3.

When the KZM was first generalised to the quantum setting, explicit calculations were only performed for the Quantum Ising model [41, 43] and Boson Hubbard model [42]. For these models it was successfully shown that the excitation density scaling is compatible with the general KZM theory [41–43]. Subsequently, KZ scaling laws have been observed for various other models. More recently, this has been extended to also include long-range systems. Work by Puebla et al. [81] explored the Kibble-Zurek physics in a

one-dimensional transverse-field Ising model with algebraically decaying long-range interactions. The non-equilibrium behaviour was found to obey the predicted scaling laws. In work by Dutta and Dutta [22] the effect of long-range interactions on the non-equilibrium dynamics of a p-wave superconducting chain was studied. The scaling of the defects generated was found to be universal and the KZ scaling exponents dictating the power-law decay of the defect density were extracted. For the short-range model the scaling exponent turns out to be $1/2$, a well-known result for the nearest-neighbour Kitaev chain [22]. For long-range interactions the scaling exponent depends non-trivially on the long-range parameter [22]. Recent work published in Ref. [82] focused on signatures of universality that are beyond the KZM. Experimental verification that the distribution of topological defects can be determined by the universality class of the underlying phase transition is a powerful extension of the KZ theory, with potential applications in adiabatic quantum computation error analysis [82].

The discussions above focused on unitary, non-dissipative dynamics of quantum systems at zero temperature, under the implicit assumption that the system is initially prepared in the ground state. Strictly speaking, QPTs occur only at zero temperature, as discussed in Section 1.1.1. However, it is well-known that in equilibrium the universality of the scaling governed by QCPs extends into the finite-temperature domain within the bounds of the quantum critical region (refer to Fig. 1.2) [7, 8]. It is anticipated that this is also the case for non-equilibrium systems. Therefore a natural question that arises is how the investigations discussed above can be extended to the finite-temperature domain. On this point, two interesting questions are (i) how would finite-temperature effects in isolated systems modify the response of the system, and (ii) how would dissipation, or the coupling to some thermal bath, affect these non-equilibrium processes. These remain very much open questions.

The work published in Refs. [83, 84] provides some insight into the first question, and gives finite-temperature generalisations of sudden quench dynamics, with a focus on the sine-Gordon model. Finite-temperature generalisations to slow adiabatic dynamics are somewhat less explored, with recent investigations published in Refs. [23, 50, 85, 86]. In the work published in Refs. [23, 50, 85], the critical point is approached by ramping a control parameter $r \to r_c$ at $T > 0$. The finite temperature introduces thermal fluctuations, which impact on the system's dynamics. Despite the sensitivity of the dynamics to these fluctuations for generic open quantum systems, the defect formation resulting from the parameter ramp obeys a general scaling law characterised by the equilibrium critical exponents. A QCP can also be approached by cooling a system towards criticality, i.e. $T \to 0$ at $r = r_c$ [2]. By lowering the temperature at $r = r_c$, the QPT is approached and both $1/k_B T$ and τ will diverge. It is expected that both quantum and thermal fluctuations will impact on the dynamics. To the best of our knowledge, results for such a protocol in which systems are cooled towards the critical point are reported for the first time in the present thesis.

1.3 Aims and applications

With the experimental advances in ultracold gases comes a need for a better theoretical understanding of the non-equilibrium dynamics of quantum systems. One promising avenue of investigation is the identification of universal features in systems which are driven through, or towards, a quantum phase transition. It has already been established that close to critical points systems exhibit a breakdown in adiabaticity, resulting in the production of excitations when control parameters are varied [42]. The overarching goal of this thesis is to formulate scaling laws for the excitations generated when slowly ramping coupling constants in the Hamiltonian at finite temperatures, and ramps of the temperature itself, in the vicinity of QCPs. Accordingly, we study three ramping protocols in detail: the standard zero-temperature quantum KZ protocol, parameter ramps at finite temperatures and the cooling of systems at the critical point.

In line with our main aim, we will first study the standard quantum KZ ramping protocol to establish a framework for the study of parameter ramps at finite temperatures. This KZ protocol is performed at zero temperature, and the density of excitations is expected to show signatures of the quantum phase transition and exhibit universal features. After establishing this foundation, we aim to understand the impact of the presence of dissipation on the universal scaling that emerges in closed systems. To achieve this, we couple systems to thermal baths, which are effectively described in the Lindblad formalism, and develop scaling theories for certain aspects of the non-equilibrium physics.

The final part of this research will involve a detailed investigation into the analytic scaling arguments, using as a model system the one-dimensional, long-range Kitaev chain. This model is amenable to (partially)

analytic calculations—even in the presence of a bosonic bath. As such, it is an ideal choice to make further quantitative statements on the scaling laws and their regimes of validity, as well as numerically support the analytic results by using an exact numeric treatment of an appropriate Lindblad master equation. Hereby we aim to verify the scaling behaviour in both weakly long-range and short-range regimes.

In addition to the fundamental theoretical interest of this research, the study of the dynamics associated with QPTs and universal features in quantum systems may have an impact on future technologies [45]. Systematically understanding the breakdown of the adiabatic dynamics across quantum critical points will provide useful insights into adiabatic quantum state preparation for quantum simulation [11]. This work could also contribute towards developing techniques for engineering interesting many-body quantum states in experimental settings, studying ultracold quantum gases and better understanding the cooling of systems to lower temperatures.

Another potential application is adiabatic quantum computation [11]. Two of the main driving forces behind the successful realisation of quantum computing are (i) the fast speed at which certain problems can be solved when compared to using known classical methods [87], and (ii) problems believed to be intractable on classical computers may be solvable with a quantum computer [88]. Advances in *conventional* quantum computing have been hindered by the decoherence caused by unavoidable interactions with the environment [87–89]. Scientists have looked to adiabatic quantum computation as a means to overcome the challenges associated with noise and flaws in quantum computers. By encoding the solution to a problem in the ground state of some suitably engineered Hamiltonian, the adiabatic theorem can be exploited to extract the solution [87]. This is possible since the quantum state remains close to the instantaneous ground state of the Hamiltonian governing the evolution, provided the evolution is sufficiently slow [88]. Our work, which focuses on traversing or approaching quantum phase transitions by adiabatically ramping parameters in the system Hamiltonian, is qualitatively very similar to adiabatic quantum algorithms. Consequently, the work may facilitate a better understanding of these algorithms. Gardas et al. [89] have also shown that adiabatic quenches of exactly solvable many-body systems may be used to study defects in quantum computers by quantifying the extent to which the quantum computer is imperfect [89].

1.4 Thesis outline

We conclude this chapter by summarising the content of the remaining chapters. In Chapter 2 the Kitaev chain model is introduced, as well as a description of its coupling to a thermal bath. We exploit the quadratic nature of the model Hamiltonian and map it to a free-quasiparticle system by performing a Fourier transform followed by a Bogoliubov transformation. Since our focus is to study the non-equilibrium dynamics of systems in the vicinity of QCPs, we also provide brief discussions on the zero-temperature phase structure of the Kitaev chain and how the phases are distinguished, as well as the properties of the model's low-energy spectrum. The open system dynamics is then formulated in terms of an appropriate Markovian Lindblad master equation, with the environment consisting of identical, independent bosonic baths and a linear coupling between these baths and the sites of the fermionic chain. A careful analysis of the environment correlation functions and eigenoperators of the system Hamiltonian leads to a dissipator in Lindblad form.

Chapter 3 focuses on an approach to solve the Lindblad dynamics of the Kitaev chain. We start by summarising the general method of "third quantisation", which was introduced by Prosen [58] to solve master equations for quadratic fermionic problems. Within this formalism, we derive a matrix differential equation that governs the time evolution of particular correlation functions. This is useful for studying the dynamic response of systems. We proceed by focusing specifically on the Kitaev chain model. It is shown that this model reaches the expected thermal steady state in the long-time limit, with the expectation values of the steady state (of which only the occupation numbers are non-zero) tending to the Fermi-Dirac distribution associated with the thermal baths. The excitation density dynamics for the Kitaev chain is described using the matrix differential equation for the correlation functions. To reduce computational complexity, these correlation functions are reformulated in terms of Fourier Majorana fermions, resulting in a convenient block-diagonal structure for the relevant matrices.

In Chapter 4 we study the dynamic KZ scaling for the isolated Kitaev chain using the tools introduced in previous chapters. We start with a general description of the standard quantum KZ ramping protocol, followed by a detailed derivation of the scaling laws. These scaling laws are derived directly from the Landau-Zener theory and later compared to the Kibble-Zurek scaling predictions. A numeric treatment of

the Kitaev chain is used to verify the analytic scaling results, with good agreement observed for both weakly long-range and short-range systems. The concepts and results of this chapter are used as building blocks to later study the universal features of the dissipative open Kitaev chain.

Chapter 5 further develops the work on dynamic scaling laws to include the scaling behaviour of the open Kitaev chain. There are two time dependencies of interest to us: $\mu(t)$ and $T(t)$, where μ is the chemical potential in the system Hamiltonian and T is the temperature of the thermal bath to which the system is coupled. First we consider the finite-temperature ramping protocol, whereby the chemical potential μ is ramped towards the quantum critical point at $T > 0$. Provided the temperature is sufficiently low, the system will still "feel" the presence of the quantum critical point and universal scaling is expected. Thereafter we investigate the cooling of the Kitaev chain towards quantum criticality, where critical slowing down is expected once the temperature is sufficiently low. For both ramping protocols we derive a set of analytic scaling laws, which are supported by numeric results.

Finally, in Chapter 6 we provide a summary of the work in this thesis, together with possible future avenues of investigation. A natural extension of the work in Chapter 4 and Chapter 5 could be research focused on the strongly long-range Kitaev chain, which is intriguing since we expect it to exhibit a topological quantum phase transition at finite temperatures. The use of novel non-local observables, which are sensitive to the proximity of the topological critical point, should allow us to identify signatures of the transition and investigate potential universal behaviour. The solvability of the Kitaev chain can also be exploited to study non-equilibrium stationary states within the framework we developed in Chapter 2 and Chapter 3. Although unrelated to the Kitaev chain, we also mention the possibility of exploring systems that exhibit true finite-temperature phase transitions, with a focus on identifying how the scaling behaviour differs in weakly long-range versus strongly long-range regimes.

Chapter 2

The Kitaev chain and its coupling to a thermal bath

In this chapter we introduce the long-range Kitaev chain. This is a simple model of spinless fermions undergoing hopping and pairing processes on a one-dimensional lattice. The strength of the hopping and pairing terms decay in a power-law fashion with distance. In later chapters the Kitaev chain will be used to investigate the validity of scaling relations and for benchmarking analytic results against numeric data. After introducing the model in Section 2.1, we will consider the coupling of the chain to a thermal bath. This will enable us to address whether universal scaling relations, similar to those emerging in closed systems at zero temperature, exist in the context of such an open quantum system. The open system dynamics can be described by an appropriate Markovian Lindblad master equation, with important details summarised in Section 2.2.

2.1 The Model

In this section we start by providing a definition of the Kitaev chain. This model is exactly solvable. We first outline a general procedure to obtain the spectral decomposition of generic fermionic quadratic Hamiltonians and then apply this to the Kitaev chain. This is followed by discussions on the zero-temperature phase structure of the model, how the various phases can be distinguished, and the properties of the low-energy spectrum.

2.1.1 Definition of the Kitaev chain Hamiltonian

The Hamiltonian for the Kitaev chain of spinless fermionic particles on a closed one-dimensional lattice of length L, with long-range hopping and pairing, is [22, 90]

$$H_{\text{LRK}} = \underbrace{J\sum_{j=1}^{L}\sum_{l=1}^{\lfloor L/2\rfloor} d_l^{-\phi}\left(c_j^\dagger c_{j+l} + c_{j+l}^\dagger c_j\right)}_{H_{\text{hop}}} + \underbrace{\frac{\Delta}{2}\sum_{j=1}^{L}\sum_{l=1}^{\lfloor L/2\rfloor} d_l^{-\alpha}\left(c_j c_{j+l} + c_{j+l}^\dagger c_j^\dagger\right)}_{H_{\text{pair}}} + \underbrace{2\mu\sum_{j=1}^{L} c_j^\dagger c_j}_{N}, \tag{2.1}$$

where $c_j^\dagger$ (c_j) creates (annihilates) a fermionic particle at lattice site j [91] and satisfies the standard anticommutation relations [58]

$$\{c_i, c_j\} = 0, \qquad \{c_i^\dagger, c_j^\dagger\} = 0, \qquad \{c_i, c_j^\dagger\} = \delta_{i,j}, \qquad i,j = 1,\ldots,L. \tag{2.2}$$

We have implemented periodic boundary conditions, that is

$$c_{j+L} = c_j, \qquad j = 1,\ldots,L, \tag{2.3}$$

which give rise to translational invariance. In Eq. (2.1) J is the hopping parameter, Δ is the pairing parameter, μ is the on-site (local) chemical potential, and ϕ and α are the distance decay (or long-range) parameters [22,

92]. The hopping and pairing terms, H_{hop} and H_{pair} respectively, decay with distance

$$d_l = \begin{cases} l & \text{if } l < L/2 \\ 2^{1/\zeta} l & \text{if } l = L/2 \end{cases} \tag{2.4}$$

in a power-law fashion characterised by the long-range parameter $\zeta = \phi, \alpha$ [22, 90]. In the limit $\phi, \alpha \to \infty$ only nearest-neighbour terms are present.

2.1.2 Diagonalisation

The Kitaev chain constitutes a paradigmatic example of an exactly solvable quantum many-body system, which can be described in terms of free quasiparticles. While this implies that such models are not truly interacting, a wealth of insight can still be acquired from the study of such systems. In Section 2.1.2.1 the procedure for diagonalising a generic quadratic fermionic Hamiltonian is summarised. We then take advantage of the quadratic nature of the Kitaev chain Hamiltonian H_{LRK} to explicitly diagonalise it in Section 2.1.2.2.

2.1.2.1 A generic fermionic quadratic Hamiltonian

The spectral decomposition of a generic fermionic quadratic Hamiltonian [90, 93]

$$H_{\text{S}} = \sum_{i,j=1}^{L} \left[c_i^\dagger Q_{ij} c_j + \frac{1}{2}\left(c_i^\dagger P_{ij} c_j^\dagger + \text{h.c.}\right) \right] \tag{2.5}$$

is obtained through a Bogoliubov transformation. Note that the anticommutation relations in Eq. (2.2) and the Hermiticity of H_{S} impose the following conditions on the coefficient matrices [51, 93]:

$$P = -P^{\text{T}} \text{ (antisymmetric matrix)} \qquad \text{and} \qquad Q = Q^\dagger \text{ (Hermitian matrix).} \tag{2.6}$$

We define the $2L$-dimensional Nambu field vectors as [51]

$$\underline{\mathbf{c}} = \begin{bmatrix} \vec{c} \\ \vec{c}^\dagger \end{bmatrix} \qquad \text{and} \qquad \underline{\mathbf{c}}^\ddagger = \begin{bmatrix} \vec{c}^\dagger \\ \vec{c} \end{bmatrix}^{\text{T}}, \tag{2.7}$$

where the column vector $\vec{c}\,(\vec{c}^\dagger)$ of fermionic operators c_i $(c_i^\dagger)$ is defined as

$$\vec{c} = [c_1, c_2, \ldots, c_L]^{\text{T}} \qquad \left(\vec{c}^\dagger = \left[c_1^\dagger, c_2^\dagger, \ldots, c_L^\dagger\right]^{\text{T}}\right). \tag{2.8}$$

In this notation, the anticommutation relations read [51]

$$\{\underline{\mathbf{c}}_\mu, \underline{\mathbf{c}}_\nu^\ddagger\} = \mathbb{J}_{\mu\nu}, \qquad \text{where} \qquad \mathbb{J} \equiv \begin{bmatrix} \mathbb{I}_L & 0 \\ 0 & -\mathbb{I}_L \end{bmatrix}, \tag{2.9}$$

with $\mathbb{I}_L$ the $L \times L$ identity matrix. Now the quadratic Hamiltonian can be written in the compact form

$$H_{\text{S}} = \frac{1}{2}\left(\underline{\mathbf{c}}^\ddagger \mathbb{H} \underline{\mathbf{c}} + \text{Tr}[Q]\right), \qquad \text{where} \qquad \mathbb{H} = H_{\text{BdG}} = \begin{bmatrix} Q & P \\ -P^* & -Q^* \end{bmatrix} \tag{2.10}$$

is the Bogoliubov–de Gennes (BdG) Hamiltonian.

We can introduce a new set of fermionic operators, $\{\eta_k^\dagger, \eta_k\}$, through the linear canonical transformation

$$c_j = \sum_k \left(V_{jk}\eta_k + S_{jk}\eta_k^\dagger\right), \tag{2.11}$$

or, equivalently,

$$\underline{\mathbf{c}} = \begin{bmatrix} \vec{c} \\ \vec{c}^\dagger \end{bmatrix} = \mathbb{T} \begin{bmatrix} \vec{\eta} \\ \vec{\eta}^\dagger \end{bmatrix} \qquad \text{where} \qquad \mathbb{T} = \begin{bmatrix} V & S \\ S^* & V^* \end{bmatrix}. \tag{2.12}$$

The anticommutation relations impose the conditions

$$VV^\dagger + SS^\dagger = \mathbb{I}, \quad VS^{\text{T}} + SV^{\text{T}} = 0, \quad V^\dagger V + S^{\text{T}} S^* = \mathbb{I}, \quad \text{and} \quad S^{\text{T}} V^* + V^\dagger S = 0 \tag{2.13}$$

on the V and S matrices. It is possible to choose V and S such that $\mathbb{T}^\dagger \mathbb{H} \mathbb{T}$ is diagonal. This can be achieved through an appropriate singular value decomposition (SVD) of the matrix $Q+P$ [93]. After performing the SVD, we obtain the diagonalised form of the Hamiltonian as

$$H_{\text{S}} = \sum_k \lambda_k \eta_k^\dagger \eta_k + \frac{1}{2}\left(\text{Tr}[Q] - \sum_k \lambda_k\right), \tag{2.14}$$

where $\{\lambda_k \geq 0\}$ is the spectrum of excitations and $\eta_k^\dagger$ (η_k) is the creation (annihilation) operator of a quasiparticle excitation with energy λ_k.

2.1.2.2 The Kitaev chain Hamiltonian

Following the general procedure in the previous section, we show how the Hamiltonian in Eq. (2.1) can be solved exactly. First we introduce the Fourier transforms of the fermionic site operators through

$$a_k = \frac{1}{\sqrt{L}} \sum_j e^{ijk} c_j \qquad \text{such that} \qquad c_j = \frac{1}{\sqrt{L}} \sum_k e^{-ijk} a_k. \tag{2.15}$$

Here the lattice momenta $k \in \{2\pi n/L : n \in \mathbb{Z}_L\}$ run over the first Brillouin zone. Based on Eq. (2.15), the matrix $A_{c\to a}$ which transforms between the site and Fourier fermions is

$$\begin{bmatrix} \vec{a} \\ \vec{a}^\dagger \end{bmatrix} = \underbrace{\begin{bmatrix} A_1 & 0 \\ 0 & A_1^* \end{bmatrix}}_{A_{c\to a}} \begin{bmatrix} \vec{c} \\ \vec{c}^\dagger \end{bmatrix} \tag{2.16}$$

with entries $A_{1(k,j)} = \frac{1}{\sqrt{L}} e^{ijk}$, $j = 0, 1, \ldots, L-1$. In terms of the Fourier fermion operators, the hopping, pairing and chemical potential terms in the Kitaev chain Hamiltonian (2.1) are

$$H_{\text{hop}} = J \sum_k g_\phi(k)(a_k^\dagger a_k - a_{-k} a_{-k}^\dagger + 1), \tag{2.17}$$

$$H_{\text{pair}} = i\frac{\Delta}{2} \sum_k f_\alpha(k)(a_k^\dagger a_{-k}^\dagger - a_{-k} a_k), \tag{2.18}$$

$$N = \mu \sum_k (a_k^\dagger a_k - a_{-k} a_{-k}^\dagger + 1), \tag{2.19}$$

where

$$g_\phi(k) = \sum_{l=1}^{\lfloor L/2 \rfloor} d_l^{-\phi} \cos(kl) \qquad \text{and} \qquad f_\alpha(k) = \sum_{l=1}^{\lfloor L/2 \rfloor} d_l^{-\alpha} \sin(kl). \tag{2.20}$$

Neglecting the constant terms in H_{hop} and N, the Hamiltonian in terms of the Fourier fermions has a convenient block-diagonal form

$$H_{\text{LRK}} = \sum_k \begin{bmatrix} a_k^\dagger & a_{-k} \end{bmatrix} \begin{bmatrix} Jg_\phi(k) + \mu & i\Delta/2 f_\alpha(k) \\ -i\Delta/2 f_\alpha(k) & -(Jg_\phi(k) + \mu) \end{bmatrix} \begin{bmatrix} a_k \\ a_{-k}^\dagger \end{bmatrix}. \tag{2.21}$$

The final diagonalisation step uses the Bogoliubov transformation

$$\begin{bmatrix} \eta_k^\dagger \\ \eta_{-k} \end{bmatrix} = \begin{bmatrix} \cos\beta_k & i\sin\beta_k \\ i\sin\beta_k & \cos\beta_k \end{bmatrix} \begin{bmatrix} a_k^\dagger \\ a_{-k} \end{bmatrix} \tag{2.22}$$

with the Bogoliubov angle β_k defined by $\tan(2\beta_k) = \frac{-\Delta f_\alpha(k)}{2Jg_\phi(k)+2\mu}$. This transformation relates the Fourier fermions to those of the free quasiparticle η_k modes of the diagonalised Hamiltonian. Considering all the modes, the transformation is given by

$$\begin{bmatrix} \vec{\eta} \\ \vec{\eta}^\dagger \end{bmatrix} = \underbrace{\begin{bmatrix} B_1 & B_2 \\ B_2^* & B_1^* \end{bmatrix}}_{B_{a\to\eta}} \begin{bmatrix} \vec{a} \\ \vec{a}^\dagger \end{bmatrix} \tag{2.23}$$

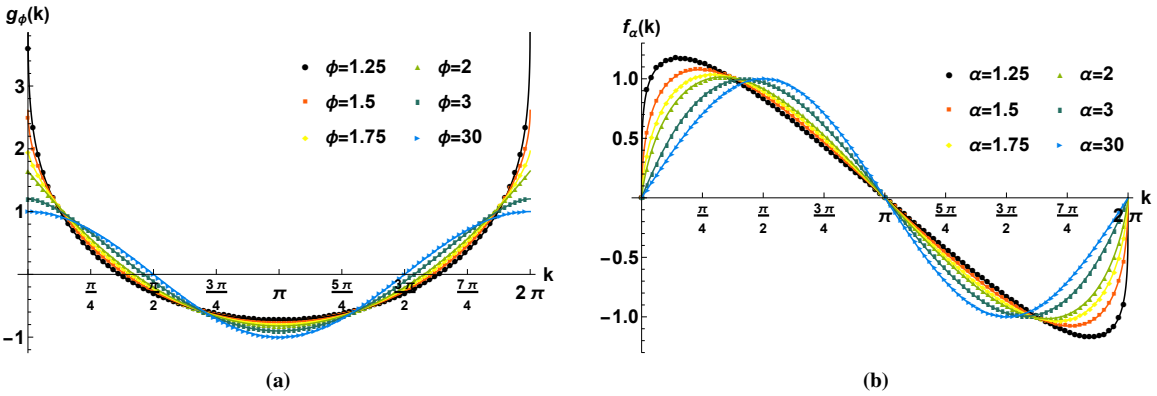

(a) (b)

Figure 2.1: **(a)** The functions $g_\phi(k)$ (2.20) and $g_\phi^\infty(k)$ (2.28) as functions of the lattice momentum k for nearest-neighbour pairing and various values of ϕ. Data points correspond to $g_\phi(k)$ with a system size of $L = 250$, while the $L \to \infty$ results are given by the solid lines. The locations of the roots of the function are dependent on the long-range parameter ϕ. **(b)** $f_\alpha(k)$ (2.20) and $f_\alpha^\infty(k)$ (2.29) for nearest-neighbour hopping and various values of $\alpha > 1$. The data points correspond to $f_\alpha(k)$ with a system size of $L = 250$, and the solid lines represent the $L \to \infty$ results. There are two roots: one at $k = 0$ and the other at $k = \pi$.

where $B_{1(k,k')} = \delta_{k,k'} \cos\beta_k$ and $B_{2(k,k')} = -i\delta_{k,-k'} \sin\beta_k$. It can be shown that $B_1 B_1^\dagger + B_2 B_2^\dagger = \mathbb{I}_L$ and $B_1 B_2^{\mathrm{T}} + B_2 B_1^{\mathrm{T}} = 0$, which ensures that the η fermions satisfy the canonical anticommutation relations. Combining the Fourier and Bogoliubov transformations in Eqs. (2.16) and (2.23) yields

$$\begin{bmatrix} \vec{c} \\ \vec{c}^\dagger \end{bmatrix} = A^*_{c\to a} B^\dagger_{a\to\eta} \begin{bmatrix} \vec{\eta} \\ \vec{\eta}^\dagger \end{bmatrix} = \underbrace{\begin{bmatrix} A_1^* B_1^\dagger & A_1^* B_2^{\mathrm{T}} \\ A_1 B_2^\dagger & A_1 B_1^{\mathrm{T}} \end{bmatrix}}_{\mathbb{T}} \begin{bmatrix} \vec{\eta} \\ \vec{\eta}^\dagger \end{bmatrix}, \tag{2.24}$$

from which we identify $V = A_1^* B_1^\dagger$ and $S = A_1^* B_2^T$ from Eq. (2.12). This transformation then brings H_{LRK} (2.1) into a diagonal form as [22, 90]

$$H_{\mathrm{LRK}} = \sum_k \lambda_{\phi,\alpha}(k) \left(\eta_k^\dagger \eta_k - \frac{1}{2} \right). \tag{2.25}$$

The dispersion relation for the η_k fermions is [90]

$$\lambda_{\phi,\alpha}(k) = \sqrt{(2Jg_\phi(k) + 2\mu)^2 + (\Delta f_\alpha(k))^2}. \tag{2.26}$$

In the thermodynamic limit $L \to \infty$ the lattice momentum k assumes continuous values, and the dispersion relation becomes [22]

$$\lambda^\infty_{\phi,\alpha}(k) = \sqrt{(2Jg^\infty_\phi(k) + 2\mu)^2 + (\Delta f^\infty_\alpha(k))^2}, \tag{2.27}$$

where [22, 90, 94]

$$g^\infty_\phi(k) = \lim_{L\to\infty} g_\phi(k) = \frac{1}{2} \sum_{l=1}^{\infty} \frac{e^{ilk} + e^{-ilk}}{l^\phi} = \frac{1}{2} \left(\mathbf{Li}_\phi(e^{ik}) + \mathbf{Li}_\phi(e^{-ik}) \right) \tag{2.28}$$

and

$$f^\infty_\alpha(k) = \lim_{L\to\infty} f_\alpha(k) = \frac{1}{2i} \sum_{l=1}^{\infty} \frac{e^{ilk} - e^{-ilk}}{l^\alpha} = -\frac{i}{2} \left(\mathbf{Li}_\alpha(e^{ik}) - \mathbf{Li}_\alpha(e^{-ik}) \right). \tag{2.29}$$

The function $\mathbf{Li}_\zeta(z) = \sum_{l=1}^\infty l^{-\zeta} z^l$ above is the polylogarithmic function of order ζ [22, 94]. Figure 2.1 shows the g_ϕ and f_α functions for various long-range parameter values.

2.1.3 Zero-temperature phase structure

Studying the phase structure of the Kitaev chain will provide insight into the location and nature of the quantum phase transitions in this model. The Kitaev chain exhibits second-order phase transitions at zero

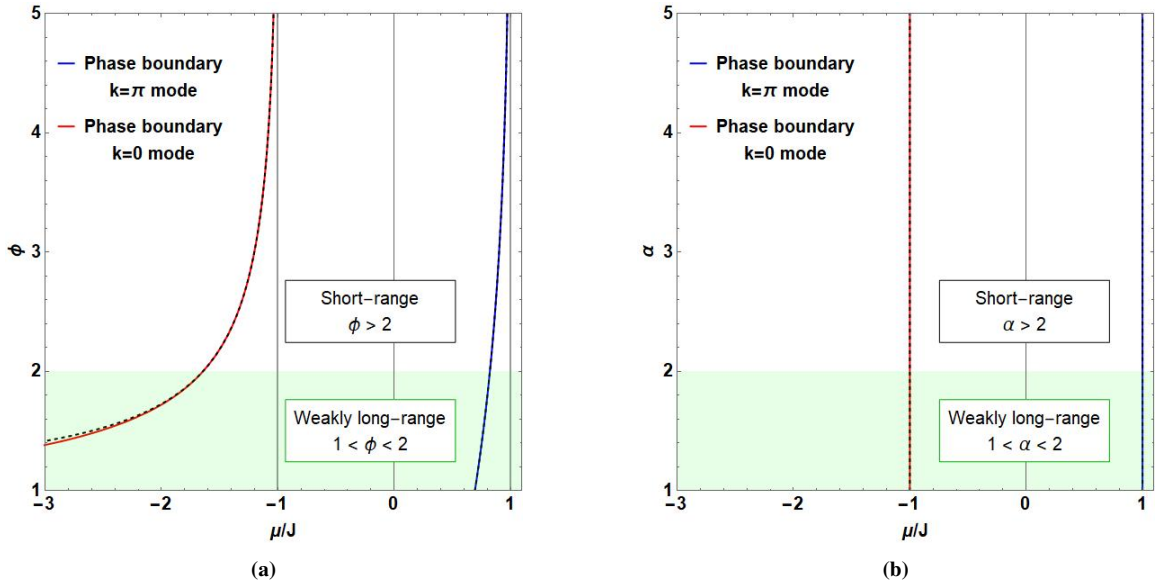

Figure 2.2: **(a)** The phase boundaries for the Kitaev chain with short-range pairing and a range of long-range hopping parameter values. For $\phi \gg 1$ the locations of the critical lines tend towards $\mu/J = \mp 1$ for the 0 and π modes, respectively. When there is long-range hopping, the phase boundaries deviate from the $\mu/J = \mp 1$ lines. **(b)** The phase boundaries for the Kitaev chain with short-range hopping and a range of long-range pairing parameter values. The phase boundaries occur at $\mu/J = \mp 1$ for the 0 and π modes, respectively. In both (a) and (b) the solid lines correspond to a system size of $L = 1500$, while the dashed lines give the results in the thermodynamic limit.

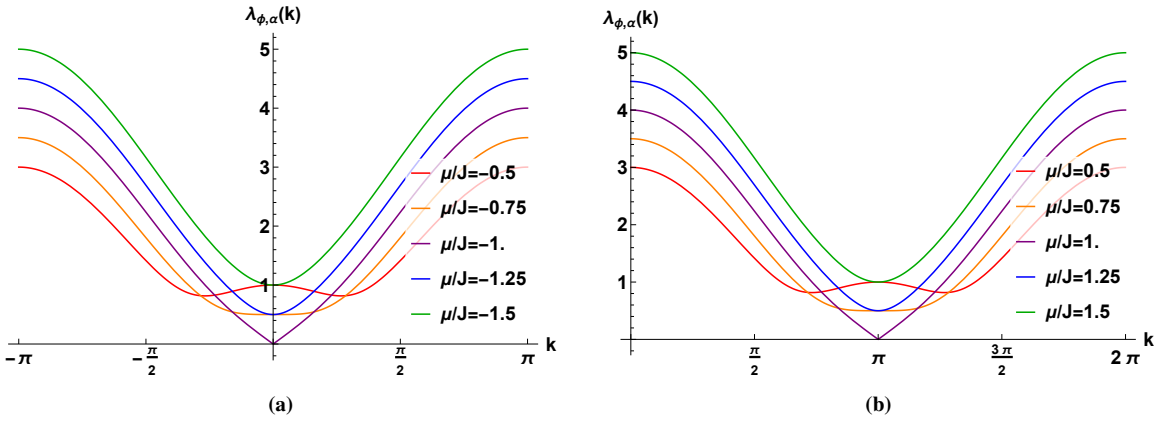

Figure 2.3: **(a)** The dispersion relation of the nearest-neighbour Kitaev chain as a function of k, centered around the critical mode $k_c = 0$. The gap in the spectrum closes for the $k = 0$ mode when $\mu/J = -1$. The pairing parameter is set to $\Delta = 1$. **(b)** The dispersion relation as a function of k, centered around the critical mode $k_c = \pi$. The gap in the spectrum closes for the $k = \pi$ mode when $\mu/J = 1$. Parameters are set as in (a).

absolute temperature.[1] A second-order quantum phase transition is commonly signaled by the *closure of the excitation gap* in the system's spectrum. If we denote the minimum excitation gap of the Kitaev chain quasiparticle spectrum by $\breve{\Delta} = \min_k \lambda_{\phi,\alpha}(k)$, then the spectrum is gapless when $\breve{\Delta} = 0$. Therefore, from Eq. (2.26), we require $f_\alpha(k) = 0$ and $-g_\phi(k) = \mu/J$ for $\breve{\Delta} = 0$.[2] The lines along which these conditions are simultaneously satisfied correspond to the phase boundaries.

To determine the location of the phase boundaries, note that $f_\alpha(k)$ vanishes for all $\alpha > 1$ at $k = 0$ and $k = \pi$ (see Fig. 2.1b). This signals the existence of two critical lines in the $\phi - \mu/J$ and $\alpha - \mu/J$ planes: one corresponding to $-g_\phi(0) = \mu/J$ and the other to $-g_\phi(\pi) = \mu/J$. The phase diagrams are provided in Fig. 2.2. We split these phase diagrams into two regions, short-range and weakly long-range, based on the values of the distance decay parameters. If $\phi > 2$ ($\alpha > 2$) we consider the hopping (pairing)

[1] The identification of topological phase transitions at finite temperatures requires tools which are beyond the scope of this thesis. See the work published in Ref. [95] for further details.

[2] We will disregard the null-pairing case here.

to be short-range. Setting $\mu = \mp J$ in the Kitaev chain with nearest-neighbour hopping and arbitrary range pairing results in a gapless spectrum for the $k = 0$ and π modes, respectively (see Fig. 2.3). Consequently, the critical lines in the short-range regimes are either located at, or tend towards, $\mu/J = \mp 1$ for the critical modes $k_c = 0, \pi$. However, in the $\phi - \mu/J$ plane the critical lines deviate from $\mu/J = \mp 1$ when the hopping starts becoming longer ranged. More precisely, for weakly long-range hopping, i.e. when $\phi \in (1, 2)$, $g_\phi(0)$ diverges as $\phi \to 1$, which results in $\mu_c = -Jg_\phi(0) \to -\infty$. Subsequent discussions will focus only on the QCP associated with the $k = 0$ mode, which is at $\mu = -Jg_\phi(0)$.

2.1.4 Distinguishing the phases

The Kitaev chain with nearest-neighbour hopping and pairing is equivalent to the transverse field Ising model through a Jordan–Wigner transformation [96]. Applying the Jordan–Wigner transformation [96]

$$\sigma_j^+ = c_j^\dagger \exp\left(i\pi \sum_{l<j} c_l^\dagger c_l\right), \qquad \sigma_j^z = 2c_j^\dagger c_j - 1, \tag{2.30}$$

where $\sigma_j^+ = (\sigma_j^x + i\sigma_j^y)/2$, allows us to map the fermionic operators onto the spin operators. Taking as an example the case where $\Delta = -2J$, this produces[3]

$$H_{\text{TFIM}} = \sum_i \left[-\mu\sigma_i^x + J\sigma_i^z\sigma_{i+1}^z\right]. \tag{2.31}$$

The first term describes the interaction of the spins with an external field pointing along the x-direction, and the second to a ferromagnetic ($J < 0$) or anti-ferromagnetic ($J > 0$) interaction between neighbouring spins. When $|\mu| < |J|$ this model's ground state exhibits (anti-)ferromagnetic ordering of the spins along the z-directions. This suggests the introduction of a local order parameter which is sensitive to this ordering, and which will be non-zero in this phase. When $|\mu| > |J|$ the spins instead align along the field direction, leading to the order parameter vanishing.

Using the Jordan–Wigner transformation (2.30), such an order parameter can be translated into the fermionic language, and used to distinguish the phases of the Kitaev chain. However, the non-local nature of the transformation in Eq. (2.30) means that this order parameter will necessarily be non-local in the fermionic site operators. Furthermore, the equivalence between the Ising model and the Kitaev chain breaks down when the latter contains hopping or pairing terms with finite values for ϕ or α. The use of an order parameter derived from the magnetic model therefore might not be appropriate in this case. In fact, it does not seem possible to identify a local fermionic order parameter for distinguishing the two phases of the chain. For this reason the Kitaev chain's phase transition is often described as being topological in nature, and it is from this perspective that the model has received considerable attention. See the work published in Ref. [98] and references therein.

Topological quantities have been proposed with which to characterise the two phases. These include a winding number derived from the Bogoliubov–de Gennes matrix in Eq. (2.21), as well as the fermionic parity of the ground state [99]. Both these quantities only assume discrete values, and vary discontinuously at the phase boundaries. We will be focussing on the dynamics of the excitation density, and so will not investigate the topological classification of the phases further. An interesting extension of this work would be to investigate how the topological phase transition imprints itself on the dynamics of suitable non-local topological quantities due to a finite-temperature ramp. Questions surrounding the finite-temperature signatures of this topological phase transition have already been considered in the literature [95].

2.1.5 Properties of the low-energy spectrum

The properties of the low-energy spectrum of the Kitaev chain will be central to our derivation of various scaling relations in later chapters. We focus on the critical line associated with the $k = 0$ mode. Close to this line, the small-k modes that are in the neighbourhood of the zero mode are also the modes with the lowest energies. We will therefore use the terms *small-k* and *low-energy* synonymously in this section.

[3] There are some technicalities related to the boundary conditions on the chain which we will ignore here. See Appendix A of the work by Calabrese et al. [97] for details.

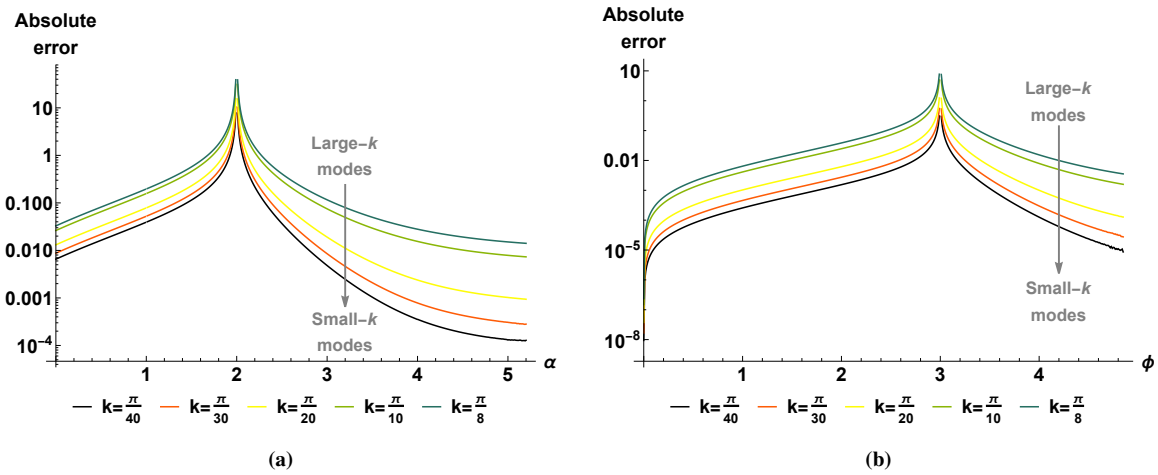

Figure 2.4: **(a)** The absolute value of the errors introduced when approximating the function $f_\alpha^\infty(k)$ by its leading-order expansion in Eq. (2.34) for $\alpha \in (0, 5.2)$. The errors are noticeably larger around $\alpha = 2$ where the powers of the dominant terms are competing, and large-k modes (high-energy modes) consistently have larger errors. **(b)** The absolute value of the errors introduced when approximating the function $g_\phi^\infty(k)$ by its leading-order expansion in Eq. (2.38) for $\phi \in (0, 4.8)$. When the powers of the dominant terms are competing, i.e. around $\phi = 3$, the errors are noticeably larger. As expected, the larger-k modes (higher-energy modes) are not well approximated by the small-k expansion.

First it will be useful to study the small-k behaviour of the $f_\alpha^\infty(k)$ and $g_\phi^\infty(k)$ functions in Eqs. (2.29) and (2.28) which appear in the dispersion relation (2.27). The main results are summarised in Section 2.1.5.1 and Section 2.1.5.2. This provides us with the necessary tools to approximate the Kitaev chain's dispersion relation at low energies for different distance decay parameters. The expressions in Section 2.1.5.3 will be used in Chapter 4 and Chapter 5 to derive scaling relations for the excitation density.

2.1.5.1 Small-k behaviour of $f_\alpha^\infty(k)$

For $\alpha \notin \mathbb{Z}$, we expand the function $f_\alpha^\infty(k)$ in Eq. (2.29) around the critical mode $k = 0$ as

$$f_\alpha^\infty(k) = a_1(\alpha)k^{\alpha-1} + a_2(\alpha)k + a_3(\alpha)k^3 + \mathcal{O}(k^5), \tag{2.32}$$

where the coefficients $a_i(\alpha)$ are given by

$$a_1(\alpha) = \cos\left(\frac{\pi\alpha}{2}\right)\Gamma(1-\alpha), \qquad a_2(\alpha) = \zeta(\alpha-1) \qquad \text{and} \qquad a_3(\alpha) = -\frac{\zeta(\alpha-3)}{6}. \tag{2.33}$$

Here Γ and ζ are the standard Gamma and Riemann-Zeta functions. When considering small-k modes, the first and second terms in Eq. (2.32) will be dominant for $\alpha \in (0, 2)$ and $\alpha > 2$, respectively. This suggests that, to leading order in k, we can approximate $f_\alpha^\infty(k)$ by

$$f_\alpha^\infty(k) \approx \begin{cases} a_1(\alpha)k^{\alpha-1}, & 0 < \alpha < 2 \\ a_2(\alpha)k, & \alpha > 2 \\ k, & \alpha = \infty \end{cases}. \tag{2.34}$$

The leading-order approximation for nearest-neighbour pairing in Eq. (2.34) is obtained from the small-k expansion of $\sin(k)$. In Fig. 2.4a we show the absolute errors introduced by the small-k approximations (2.34) of $f_\alpha^\infty(k)$. These approximations work well, provided the parameter α is not within the regime where the powers of the dominant terms are competing, i.e. around $\alpha = 2$. To accurately describe the function in this regime, a linear combination of the terms is required:

$$f_\alpha^\infty(k) \approx a_1(\alpha)k^{\alpha-1} + a_2(\alpha)k. \tag{2.35}$$

2.1.5.2 Small-k behaviour of $g_\phi^\infty(k)$

A similar small-k expansion can be performed for the function $g_\phi^\infty(k)$ in Eq. (2.28). For $\phi \notin \mathbb{Z}$, we have

$$g_\phi^\infty(k) = b_1(\phi) + b_2(\phi)k^{\phi-1} + b_3(\phi)k^2 + b_4(\phi)k^4 + \mathcal{O}(k^5) \tag{2.36}$$

with the coefficients

$$b_1(\phi) = \zeta(\phi), \qquad b_2(\phi) = \sin\left(\frac{\pi\phi}{2}\right)\Gamma(1-\phi), \qquad b_3(\phi) = -\frac{\zeta(\phi-2)}{2} \qquad \text{and} \qquad b_4(\phi) = \frac{\zeta(\phi-4)}{24}. \tag{2.37}$$

The powers of k in the expansion (2.36) suggest that when $\phi \in (0,3)$ the first and second terms in the expansion of g_ϕ^∞ will be dominant, while for $\phi > 3$ the first and third terms will make the most significant contribution. As a result, to leading-order in k, $g_\phi^\infty(k)$ can be approximated by

$$g_\phi^\infty(k) \approx \begin{cases} b_1(\phi) + b_2(\phi)k^{\phi-1}, & 0 < \phi < 3 \\ b_1(\phi) + b_3(\phi)k^2, & \phi > 3 \\ 1 - \frac{1}{2}k^2, & \phi = \infty \end{cases}. \tag{2.38}$$

The leading-order approximation for nearest-neighbour hopping in Eq. (2.38) is obtained from the small-k expansion of $\cos(k)$. Figure 2.4b shows the errors introduced by the leading-order approximation (2.38). We observe that the approximation in Eq. (2.38) well approximates $g_\phi^\infty(k)$ for small-k modes, provided that ϕ is not within the vicinity of $\phi = 3$ where the powers of the dominant terms are competing.

In Chapter 4 and Chapter 5 we will use the properties of the low-energy spectrum at the critical point $\mu = \mu_c$ to extract scaling laws, and to determine the dynamical critical exponent z for the long-range Kitaev chain. From Eq. (2.27) we write the Kitaev chain dispersion relation at the critical point as

$$\lambda_{\phi,\alpha}^\infty(k) = \sqrt{(2Jg_\phi^\infty(k) + 2\mu_c)^2 + (\Delta f_\alpha^\infty(k))^2}. \tag{2.39}$$

The small-k behaviour of the term containing $f_\alpha^\infty(k)$ has already been addressed in Section 2.1.5.1, with the remaining term being $(2Jg_\phi^\infty(k) + 2\mu_c)$. Based on the discussion in Section 2.1.3, the QCP associated with the $k = 0$ mode is at $\mu = \mu_c = -Jg_\phi^\infty(0)$. In the nearest-neighbour case, where $\phi = \infty$, this simplifies to $\mu_c = -J$. Therefore, using the small-k approximation (2.38), we write $(2Jg_\phi^\infty(k) + 2\mu_c)$ to leading order in k as

$$(2Jg_\phi^\infty(k) + 2\mu_c) \approx \begin{cases} 2Jb_2(\phi)k^{\phi-1}, & 0 < \phi < 3 \\ 2Jb_3(\phi)k^2, & \phi > 3 \\ -Jk^2, & \phi = \infty \end{cases}. \tag{2.40}$$

2.1.5.3 Low-energy approximation of the dispersion relation

We combine Eqs. (2.34) and (2.40) to acquire the low-energy spectrum of the Kitaev chain on the $k = 0$ critical line shown in Fig. 2.2:

$$\lambda_{\phi,\alpha}^\infty(k) \approx \begin{cases} |\Delta||k| & \text{for nearest-neighbour hopping and pairing } (\phi, \alpha = \infty) \\ |\Delta a_2(\alpha)||k| & \text{for short-range hopping and pairing } (\phi, \alpha > 2) \\ |\Delta a_1(\alpha)||k|^{\alpha-1} & \text{for nearest-neighbour hopping and long-range pairing } (\phi = \infty,\ \alpha < 2) \\ |2Jb_2(\phi)||k|^{\phi-1} & \text{for long-range hopping and nearest-neighbour pairing } (\phi < 2,\ \alpha = \infty) \end{cases}. \tag{2.41}$$

Figure 2.5 provides comparisons between the approximations above and the exact dispersion relation for small-k modes, with the approximations for long-range hopping and pairing rapidly deteriorating outside the immediate vicinity of $k = 0$. We emphasise that this low-energy approximation is derived in the large-L limit, and to leading order in k. Scaling relations for the excitation density derived using these expressions will eventually be benchmarked against exact, finite-L numeric calculations. The agreement we will observe there will be determined, in part, by how well the low-energy spectrum of the finite chain is described by these expressions. Two factors are expected to play a role here. The first is how well f_α and g_ϕ are approximated

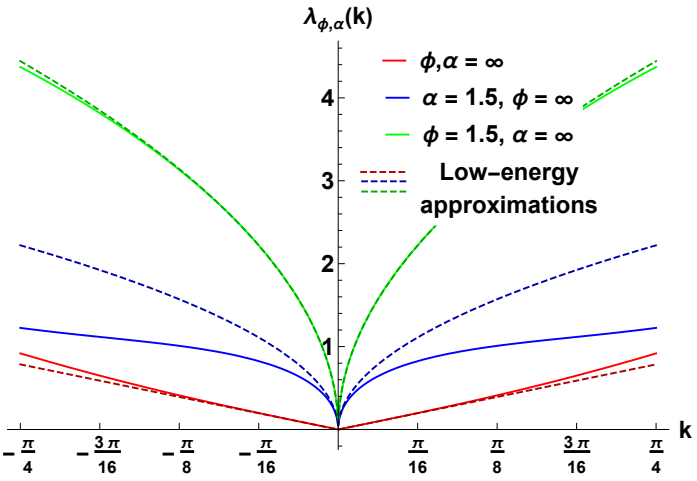

Figure 2.5: The dispersion relation $\lambda_{\phi,\alpha}(k)$ as a function of the lattice momentum k for small-k modes. We show three choices for the distance decay parameters: (i) $\phi, \alpha = \infty$ which corresponds to nearest-neighbour hopping and pairing, (ii) $\alpha = 1.5$ with $\phi = \infty$ which corresponds to a Kitaev chain with long-range pairing and nearest-neighbour hopping, and (iii) $\phi = 1.5$ with $\alpha = \infty$ which corresponds to long-range hopping and nearest-neighbour pairing. For each case the solid line is the exact dispersion relation (2.27) in the thermodynamic limit, and the dashed line is the corresponding low-energy approximation from Eq. (2.41).

by their $L \to \infty$ versions f_α^∞ and g_ϕ^∞. Figure 2.1 suggests that already at $L = 250$ this agreement will be quite good. A more subtle issue is that these leading-order expansions might only be accurate for very small values of k, especially if the leading-order and next-to-leading order terms are of roughly the same power in k. Since the k discretisation is set by $2\pi/L$, it could require an extremely large value of L and a very slow ramp rate to ensure that the modes which make the dominant contribution to the excitation density have energies which follow the behaviour in Eq. (2.41). Indeed, this turns out to be one of the major challenges in the benchmarking of the analytic scaling results for long-range hopping and pairing parameters within the range $\phi, \alpha \in (0, 3)$.

2.2 Coupling to a bath

We will now focus on deriving a Markovian Lindblad master equation to study the open system dynamics of the Kitaev chain when it is coupled to a thermal bath. In Section 2.2.1 we briefly discuss the general form of the master equation and the system–environment interaction. Thereafter, the remainder of this chapter is dedicated to the derivation of the dissipator and Lindblad operators specifically for our model.

2.2.1 The Lindblad master equation

The open system dynamics is formulated in terms of an appropriate Markovian Lindblad master equation. Our system and thermal environment together form an isolated (closed) quantum system which evolves unitarily according to the Hamiltonian

$$H = H_{\mathrm{S}} \otimes \mathbb{I}_{\mathrm{E}} + \mathbb{I}_{\mathrm{S}} \otimes H_{\mathrm{E}} + H_{\mathrm{int}} \tag{2.42}$$

with the system Hamiltonian $H_{\mathrm{S}} = H_{\mathrm{LRK}}$ from Eq. (2.1), the environment Hamiltonian H_{E} and the system–environment interaction H_{int} [49, 51]. The identity operators $\mathbb{I}_{\mathrm{S}}$ and $\mathbb{I}_{\mathrm{E}}$ act on the system and the environment, respectively. In this case, the environment consists of a set of N_{B} independent thermal baths, indexed by n. Each thermal bath is modeled as a large collection of uncoupled harmonic oscillators with mode frequencies $\omega_{n,q}$. We also associate with each bath the temperature T_n and chemical potential μ_n. The Hamiltonian of the n'th thermal bath is

$$H_{\mathrm{B},n} = \int dq\, \omega_{n,q} b_{n,q}^\dagger b_{n,q}, \tag{2.43}$$

where $b_{n,q}$ and $b_{n,q}^\dagger$, which satisfy the standard bosonic commutation relations [51, 100]

$$[b_{n,k}, b_{m,q}] = 0, \qquad [b_{n,k}^\dagger, b_{m,q}^\dagger] = 0 \qquad \text{and} \qquad [b_{n,k}, b_{m,q}^\dagger] = \delta_{nm}\delta(k-q), \tag{2.44}$$

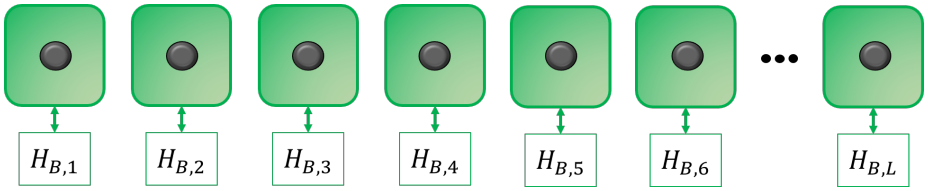

Figure 2.6: Schematic image of the system–environment interactions. The gray dots represent the Kitaev chain lattice sites, while the coloured squares are the independent external baths. Each lattice site is coupled to its own bath, and all the baths together compose the environment.

are the bosonic operators associated with the n'th bath. The resulting environment Hamiltonian is [51]

$$H_{\mathrm{E}} = \sum_{n=1}^{N_{\mathrm{B}}} H_{\mathrm{B},n}. \tag{2.45}$$

For the system–environment interaction we consider a linear coupling between the bosonic baths of the environment and the sites of the fermionic chain. When each site of the system (site fermion) is coupled to its own independent bosonic bath (see Fig. 2.6), the general interaction Hamiltonian is[4] [51]

$$\begin{aligned} H_{\mathrm{int}} = \sum_{n=1}^{L} O_n \otimes R_n &= \sum_{n=1}^{L} \Bigg[\underbrace{\left(c_n + c_n^\dagger\right)}_{O_n} \otimes \underbrace{\int dq\, g_{n,q} \left(b_{n,q} + b_{n,q}^\dagger\right)}_{R_n} \Bigg] \\ &= \sum_{n=1}^{L} \int dq\, g_{n,q} \left(c_n + c_n^\dagger\right) \otimes \left(b_{n,q} + b_{n,q}^\dagger\right), \end{aligned} \tag{2.46}$$

where O_n acts on the system and R_n acts on the environment. Here $g_{n,q}$ determines the system–bath coupling strength (interaction strength) between the q'th mode of the n'th bath and site fermion n [51].

The density matrix $\varrho_{\mathrm{SE}}(t)$ of the combined system and thermal environment evolves unitarily according to the von Neumann equation [49]

$$i\frac{\mathrm{d}\varrho_{\mathrm{SE}}(t)}{\mathrm{d}t} = [H, \varrho_{\mathrm{SE}}(t)], \tag{2.47}$$

with H the Hamiltonian in Eq. (2.42). We assume that the baths are prepared in thermal equilibrium states at a temperature T_n, and that their coupling to the system has a negligible effect on their dynamics. Based on this we write

$$\varrho_{\mathrm{SE}}(t) \approx \varrho(t) \otimes \varrho_{\mathrm{E}}, \tag{2.48}$$

with $\varrho(t)$ the system's density matrix and ϱ_{E} being the stationary thermal state of the environment. We insert this form of $\varrho_{\mathrm{SE}}(t)$ into the von Neumann equation (2.47), and then trace out the environment degrees of freedom. After a standard series of approximations [49, 54], this leads to a description of the system's dynamics in terms of the master equation

$$\frac{\mathrm{d}\varrho(t)}{\mathrm{d}t} = \hat{\mathcal{L}}\varrho(t) = -i[H_{\mathrm{S}} + H_{\mathrm{LS}}, \varrho(t)] + \mathcal{D}[\varrho]. \tag{2.49}$$

We write the dissipator $\mathcal{D}[\varrho]$ as [49, 51, 54]

$$\mathcal{D}[\varrho] = \sum_{\alpha,\beta,\lambda} \bar{\Gamma}_{\alpha\beta}(\lambda) \left[2O_\beta(\lambda)\varrho O_\alpha^\dagger(\lambda) - \{O_\alpha^\dagger(\lambda)O_\beta(\lambda), \varrho\}\right], \tag{2.50}$$

where

$$\bar{\Gamma}_{\alpha\beta}(\lambda) = \frac{1}{2}\int_{-\infty}^{\infty} d\tau\, e^{i\lambda\tau}\langle \tilde{R}_\alpha^\dagger(\tau) R_\beta\rangle \qquad \text{with} \qquad \tilde{R}_\alpha(\tau) = e^{iH_{\mathrm{E}}\tau} R_\alpha e^{-iH_{\mathrm{E}}\tau} \tag{2.51}$$

are the Fourier transforms of the environment correlation functions, and $O_\beta(\lambda)$ are the eigenoperators of

[4] Note that a consequence of choosing each site fermion to be coupled to its own independent bath is that the number of thermal baths N_{B} is equivalent to the number of lattice sites L in the system. Hence, taking the upper limit of the summation to be L is no different from using N_{B}.

H_S [49, 51]. The dissipator (2.50) accounts for the non-unitary (dissipative) evolution of the system [55]. In comparison, the first term of the generator (2.49) accounts for the unitary part of the dynamics generated by the effective Hamiltonian, $H_S + H_{LS}$ [55], which is a combination of the system Hamiltonian $H_S = H_{LRK}$ (2.1) and the Lamb-shift Hamiltonian H_{LS}. We write the Lamb-shift Hamiltonian in terms of the eigenoperators $O_\beta(\lambda)$ as

$$H_{LS} = \sum_\lambda \sum_{\alpha,\beta} S_{\alpha\beta}(\lambda) O_\alpha^\dagger(\lambda) O_\beta(\lambda), \tag{2.52}$$

where $S_{\alpha\beta}(\lambda) = \frac{1}{2i}\left(\bar{\Gamma}_{\alpha\beta} - \bar{\Gamma}^*_{\beta\alpha}\right)$ is the imaginary part of $\bar{\Gamma}_{\alpha\beta}$ (2.51).

In Section 2.2.2 and Section 2.2.3 the environment correlation functions and eigenoperators of H_S are calculated explicitly. These results are used in Section 2.2.4 to bring the dissipator (2.50) into Lindblad form, and extract the Lindblad bath operators. We end the chapter with a brief discussion in Section 2.2.5 on the Lamb-shift Hamiltonian (2.52). The work in these sections closely follows work by D'Abbruzzo and Rossini [51]. Before proceeding, we specialise our general description of the thermal environment and the system–environment interaction (2.46). In particular, we will consider *identical* thermal baths fixed at a temperature of T and with zero chemical potential. The mode frequencies of each thermal bath are therefore also identical, and will be denoted by ω_q. Finally, we choose the system–bath coupling strength $g_{n,q}$ to be equivalent for each interaction, such that $g_{n,q} = g_q$.

2.2.2 Environment correlation functions

The one-sided Fourier transforms (2.51) of the environment correlation functions are [49, 51]

$$\bar{\Gamma}_{nm}(\lambda) = \frac{1}{2}\int_{-\infty}^{\infty} d\tau\, e^{i\lambda\tau} \langle \tilde{R}_n^\dagger(\tau) R_m \rangle, \tag{2.53}$$

where, from Eq. (2.46),

$$\langle \tilde{R}_n^\dagger(\tau) R_m \rangle = \int dk \int dq\ g_k^* g_q \left\langle e^{iH_E\tau}(b_{n,k} + b_{n,k}^\dagger) e^{-iH_E\tau}(b_{m,q} + b_{m,q}^\dagger) \right\rangle. \tag{2.54}$$

In Eqs. (2.53) and (2.54), $\langle \bullet \rangle = \mathrm{Tr}_B[\bullet \varrho_E]$ is the expectation value calculated by tracing over the bath degrees of freedom, ϱ_E is the thermal equilibrium state for the environment and $\tilde{R}_n(\tau) = e^{iH_E\tau} R_n e^{-iH_E\tau}$ [49, 51]. Now Eq. (2.54) is simplified using the Baker-Campbell-Hausdorff (BCH) formula [101]. For two generic operators X and Y, the BCH formula states that [101]

$$e^X Y e^{-X} = e^v Y \qquad \text{if} \qquad [X, Y] = vY,\ v \in \mathbb{C}. \tag{2.55}$$

Noting that the bath operators satisfy

$$[H_E, b_{n,k}] = -\omega_k b_{n,k} \qquad \text{and} \qquad [H_E, b_{n,k}^\dagger] = \omega_k b_{n,k}^\dagger, \tag{2.56}$$

it follows that

$$e^{iH_E\tau}(b_{n,k} + b_{n,k}^\dagger) e^{-iH_E\tau} = e^{-i\omega_k\tau} b_{n,k} + e^{i\omega_k\tau} b_{n,k}^\dagger, \tag{2.57}$$

resulting in

$$\langle \tilde{R}_n^\dagger(\tau) R_m \rangle = \int dk \int dq\, g_k^* g_q \left(e^{-i\omega_k\tau} \left\langle b_{n,k}(b_{m,q} + b_{m,q}^\dagger) \right\rangle + e^{i\omega_k\tau} \left\langle b_{n,k}^\dagger (b_{m,q} + b_{m,q}^\dagger) \right\rangle \right). \tag{2.58}$$

Under the condition that baths are strictly independent and identical, the two-point expectation values for the bath operators are [51]

$$\langle b_{n,k} b_{m,q} \rangle = \langle b_{n,k}^\dagger b_{m,q}^\dagger \rangle = 0 \qquad \text{and} \qquad \langle b_{n,k}^\dagger b_{m,q} \rangle = \delta_{nm}\delta(k-q) n_{BE}(\omega_k), \tag{2.59}$$

where $n_{BE}(\omega_k) = \left(1 - e^{\omega_k/T}\right)^{-1}$ is the Bose-Einstein distribution. The environment correlation functions can be simplified using these two-point expectation values, giving

$$\langle \tilde{R}_n^\dagger(\tau) R_m \rangle = \delta_{nm} \int dk\, |g_k|^2 \left(e^{-i\omega_k\tau} \left(n_{BE}(\omega_k) + 1 \right) + e^{i\omega_k\tau} n_{BE}(\omega_k) \right). \tag{2.60}$$

Performing a one-sided Fourier transform of $\langle \tilde{R}_n^\dagger(\tau) R_m \rangle$ results in a diagonal matrix with entries $\bar{\Gamma}_{nm}(\lambda) = \delta_{nm}\bar{\Gamma}(\lambda)$. The diagonal entries $\bar{\Gamma}(\lambda)$ are

$$\begin{aligned}\bar{\Gamma}(\lambda) &= \pi \int dk\, |g_k|^2 \big(\delta(\lambda-\omega_k)(n_{\text{BE}}(\omega_k)+1) + \delta(\lambda+\omega_k) n_{\text{BE}}(\omega_k)\big) \\ &= \mathcal{J}(\lambda)(n_{\text{BE}}(\lambda)+1) + \mathcal{J}(-\lambda) n_{\text{BE}}(-\lambda),\end{aligned} \tag{2.61}$$

where

$$\mathcal{J}(\lambda) = \pi \int dk\, |g_k|^2 \delta(\lambda - \omega_k) \tag{2.62}$$

is the density of states associated with each identical bath. Assuming the mode frequencies are non-negative, $\bar{\Gamma}(\lambda)$ (2.61) can be expressed as

$$\bar{\Gamma}(\lambda) = \begin{cases} \mathcal{J}(\lambda)(n_{\text{BE}}(\lambda)+1) & \text{if} \quad \lambda > 0 \\ \mathcal{J}(-\lambda) n_{\text{BE}}(-\lambda) & \text{if} \quad \lambda < 0 \\ \mathcal{J}(0)(2n_{\text{BE}}(0)+1) & \text{if} \quad \lambda = 0. \end{cases} \tag{2.63}$$

2.2.3 Eigenoperators of the system Hamiltonian

The eigenoperators $O_n(\lambda)$ associated with the operator O_n are found by decomposing the interaction Hamiltonian (2.46) into eigenoperators of the system Hamiltonian H_{S}. Suppose the spectrum of H_{S} is discrete and that $\{|\mathbf{x}\rangle = |x_{k_1}, \ldots, x_{k_L}\rangle\}$ is the orthonormal basis of the diagonalised quadratic Hamiltonian in Eq. (2.14), with $x_{k_n} = \{0, 1\}$, where $k_n = 2\pi n/L$, being the occupation number associated with the η_k mode which has an excitation energy of λ_k. We denote the eigenvalue of $|\mathbf{x}\rangle$ with respect to H_{S} by $E(\mathbf{x}) = \sum_k x_k \lambda_k$. Now the eigenoperators $O_n(\lambda)$ of the system associated with $O_n = (c_n + c_n^\dagger)$ are

$$O_n(\lambda) = \sum_{\mathbf{x},\mathbf{y}} \delta_{E(\mathbf{y})-E(\mathbf{x}),\lambda} \, |\mathbf{x}\rangle \langle \mathbf{x}| \left(c_n + c_n^\dagger\right) |\mathbf{y}\rangle \langle \mathbf{y}| \,, \tag{2.64}$$

where the delta function restricts the sum to pairs of H_{S} eigenstates with a fixed energy difference of λ. Making use of the connection between the c_n and η_k fermions in Eq. (2.11), we find that

$$\langle \mathbf{x}| \, c_n \, |\mathbf{y}\rangle = \sum_k (V_{nk} \langle \mathbf{x}| \, \eta_k \, |\mathbf{y}\rangle + S_{nk} \langle \mathbf{x}| \, \eta_k^\dagger \, |\mathbf{y}\rangle). \tag{2.65}$$

The expression for $\langle \mathbf{x}| \, c_n \, |\mathbf{y}\rangle$ can therefore only be non-zero if the states $|\mathbf{x}\rangle$ and $|\mathbf{y}\rangle$ differ in the occupation of a single η_k mode. Consequently, when we have non-zero values for the matrix elements $\langle \mathbf{x}| \, c_n \, |\mathbf{y}\rangle$ and $\langle \mathbf{x}| \, c_n^\dagger \, |\mathbf{y}\rangle$, the energy difference $E(\mathbf{y}) - E(\mathbf{x})$ in Eq. (2.64) will be either λ_k or $-\lambda_k$. Now we can substitute Eq. (2.65) into the expression for $O_n(\lambda)$. The result is simplified using the resolution of the identity, $\sum_{\mathbf{x}} |\mathbf{x}\rangle \langle \mathbf{x}| = \mathbb{I}$ and $\sum_{\mathbf{y}} |\mathbf{y}\rangle \langle \mathbf{y}| = \mathbb{I}$, yielding

$$\begin{aligned} O_n(\lambda) &= \sum_k \left(V_{nk}\delta_{\lambda,\lambda_k}\eta_k + S_{nk}\delta_{\lambda,-\lambda_k}\eta_k^\dagger\right) + \sum_k \left(S_{nk}^*\delta_{\lambda,\lambda_k}\eta_k + V_{nk}^*\delta_{\lambda,-\lambda_k}\eta_k^\dagger\right) \\ &= \sum_k \left(\phi_{nk}\delta_{\lambda,\lambda_k}\eta_k + \phi_{nk}^*\delta_{\lambda,-\lambda_k}\eta_k^\dagger\right), \end{aligned} \tag{2.66}$$

where

$$\phi = V + S^*. \tag{2.67}$$

2.2.4 Calculation of the dissipator and Lindblad bath operators

In Section 2.2.2 we found that the matrix comprising of the environment correlation functions is diagonal, with the entries $\delta_{nm}\bar{\Gamma}(\lambda)$ given by Eq. (2.61). The dissipator in Eq. (2.50) therefore acquires the form

$$\mathcal{D}[\varrho] = \sum_{n,\lambda} \bar{\Gamma}(\lambda) \Big[2 \underbrace{O_n(\lambda)\varrho O_n^\dagger(\lambda)}_{(a)} - \underbrace{\{O_n^\dagger(\lambda)O_n(\lambda), \varrho\}}_{(b)} \Big]. \tag{2.68}$$

In the calculations that follow it will be important to account for the presence of degenerate single quasiparticle eigenenergies. For the Kitaev chain the degeneracies come in pairs, where the energy associated with

the k and $-k$ modes are the same. We will group the η_k modes according to their energies λ_k, and let $\mathcal{A}_m$ denote the set of modes with energy λ_m. Here the index $m = 1, \ldots, M$ keeps track of the sets of modes with the same energy, and M is the number of unique eigenenergies in the energy spectrum. Assuming for the moment that there are no zero-energy modes, the first term in the square brackets of Eq. (2.68), which is denoted by (a), is

$$O_n(\lambda)\varrho O_n^\dagger(\lambda) = \sum_{m=1}^{M} \sum_{k,q\in\mathcal{A}_m} \left(\phi_{nk}\phi_{nq}^* \delta_{\lambda,\lambda_m} \eta_k \varrho \eta_q^\dagger + \phi_{nk}^* \phi_{nq} \delta_{\lambda,-\lambda_m} \eta_k^\dagger \varrho \eta_q\right), \tag{2.69}$$

where the result for the system eigenoperators $O_n(\lambda)$ in Eq. (2.66) has been used. Following a similar approach, the second term in the square brackets, denoted by (b), is given by

$$\{O_n^\dagger(\lambda)O_n(\lambda), \varrho\} = \sum_{m=1}^{M} \sum_{k,q\in\mathcal{A}_m} \left(\phi_{nk}^* \phi_{nq} \delta_{\lambda,\lambda_m} \{\eta_k^\dagger \eta_q, \varrho\} + \phi_{nk}\phi_{nq}^* \delta_{\lambda,-\lambda_m} \{\eta_k \eta_q^\dagger, \varrho\}\right). \tag{2.70}$$

Combining Eqs. (2.69) and (2.70), the dissipator now reads

$$\mathcal{D}[\varrho] = \sum_{n;m} \sum_{k,q\in\mathcal{A}_m} \left[\Phi_{kq}^n \bar{\Gamma}(\lambda_m)(2\eta_k \varrho \eta_q^\dagger - \{\eta_q^\dagger \eta_k, \varrho\}) + \Phi_{qk}^n \bar{\Gamma}(-\lambda_m)(2\eta_k^\dagger \varrho \eta_q - \{\eta_q \eta_k^\dagger, \varrho\})\right] \tag{2.71}$$

with

$$\Phi_{kq}^n = \phi_{nk}\phi_{nq}^* \qquad \text{and} \qquad \Phi_{qk}^n = \Phi_{kq}^{n*} = \phi_{nq}\phi_{nk}^*. \tag{2.72}$$

The dissipator $\mathcal{D}[\varrho]$ in Eq. (2.71) can be brought into Lindblad form by enforcing a set of constraints on the V and S matrices. In Eq. (2.13) we provided the conditions imposed on V and S by the canonical anticommutation relations. Additional constraints are placed on the V and S matrices by the symmetries of the Kitaev chain Hamiltonian. The relevant symmetries here are particle-hole (PH) symmetry and time-reversal (TR) symmetry. It is shown in Appendix B that these symmetries impose the condition

$$V^\dagger S^* + S^{\mathrm{T}} V = 0. \tag{2.73}$$

Using these constraints on V and S, we show that ϕ is unitary:

$$\phi^\dagger \phi = (V^\dagger + S^{\mathrm{T}})(V + S^*) = (V^\dagger V + S^{\mathrm{T}} S^*) + (V^\dagger S^* + S^{\mathrm{T}} V) = \mathbb{I}. \tag{2.74}$$

Noting that the n summation index only enters in the $\Phi_{kq}^n = \phi_{nk}\phi_{nq}^*$ factors in Eq. (2.71) allows us to use Eq. (2.74) to simplify the dissipator $\mathcal{D}[\varrho]$. Let us first write the dissipator as

$$\mathcal{D}[\varrho] = \sum_{m} \sum_{k,q\in\mathcal{A}_m} \left[\left(\sum_n \Phi_{kq}^n\right)\bar{\Gamma}(\lambda_m)(2\eta_k \varrho \eta_q^\dagger - \{\eta_q^\dagger \eta_k, \varrho\}) + \left(\sum_n \Phi_{qk}^n\right)\bar{\Gamma}(-\lambda_m)(2\eta_k^\dagger \varrho \eta_q - \{\eta_q \eta_k^\dagger, \varrho\})\right]. \tag{2.75}$$

Now we use Eq. (2.74) to show that

$$\sum_n \Phi_{kq}^n = \sum_n \phi_{nk}\phi_{nq}^* = \sum_n \phi_{kn}^{\mathrm{T}} \phi_{nq}^* = (\phi^\dagger \phi)_{kq}^* = \delta_{kq}, \tag{2.76}$$

which leads to the simplified form of the dissipator

$$\mathcal{D}[\varrho] = \sum_k \left[\bar{\Gamma}(\lambda_k)(2\eta_k \varrho \eta_k^\dagger - \{\eta_k^\dagger \eta_k, \varrho\}) + \bar{\Gamma}(-\lambda_k)(2\eta_k^\dagger \varrho \eta_k - \{\eta_k \eta_k^\dagger, \varrho\})\right]. \tag{2.77}$$

Here the k summation index runs over the first Brillouin zone.

The final task of this chapter is to extract the Lindblad operators. Using the general form of the master equation (2.49) and the dissipator (2.77), the full master equation for the Kitaev chain in Lindblad form is

$$\frac{\mathrm{d}\varrho(t)}{\mathrm{d}t} = -i[H_{\mathrm{LRK}} + H_{\mathrm{LS}}, \varrho(t)] + \gamma \sum_k \sum_{\sigma=\pm} \left[L_{k,\sigma} \varrho(t) L_{k,\sigma}^\dagger - \frac{1}{2}\left\{L_{k,\sigma}^\dagger L_{k,\sigma}, \varrho(t)\right\}\right], \tag{2.78}$$

where the Lindblad bath operators are

$$L_{k,+} = \sqrt{\Gamma_{k,+}}\eta_k^\dagger \qquad \text{and} \qquad L_{k,-} = \sqrt{\Gamma_{k,-}}\eta_k, \tag{2.79}$$

with bath coupling constants

$$\Gamma_{k,+} = 2\bar{\Gamma}(-\lambda_k) = 2\mathcal{J}(\lambda_k)n_{\text{BE}}(\lambda_k) \qquad \text{and} \qquad \Gamma_{k,-} = 2\bar{\Gamma}(\lambda_k) = 2\mathcal{J}(\lambda_k)(n_{\text{BE}}(\lambda_k)+1). \tag{2.80}$$

In Eq. (2.78) we have made the system–bath coupling γ explicit by factoring it out of the spectral density function. In the majority of our work, and in particular the numeric calculations, we choose the spectral density function to be ohmic. This leads to

$$\mathcal{J}(\lambda_k) = \pi\delta\lambda_k e^{-\lambda_k/\lambda_c}, \tag{2.81}$$

with dimensionless parameter δ and cutoff frequency λ_c.

The results in Eqs. (2.78)–(2.80) are valid provided that the energies of the η_k-modes are strictly positive. For the Kitaev chain the closure of the excitation gap at one of the critical points results from the energy of either the $k = 0$ or $k = \pi$ mode vanishing. If we suppose that $\lambda_0 = 0$ then, by following the same series of steps as before, we would obtain a modified $k = 0$ contribution to the sum which defines the dissipator in Eq. (2.77). This takes the form

$$\mathcal{D}_0[\varrho] = \bar{\Gamma}(0)\left[2(\eta_0+\eta_0^\dagger)\varrho(\eta_0+\eta_0^\dagger) - \{(\eta_0+\eta_0^\dagger)^2, \varrho\}\right], \tag{2.82}$$

which suggests that there is now a single Lindblad operator $L_0 = \sqrt{2\bar{\Gamma}(0)}(\eta_0+\eta_0^\dagger)$ associated with this mode. While the difference in the $k = 0$ terms in Eqs. (2.77) and (2.82) would affect some aspects of this mode's dynamics, it can be shown that these two dissipators generate exactly the same evolution of the mode occupation $\langle\eta_0^\dagger\eta_0\rangle$. Since the latter is our primary quantity of interest, the Lindblad master equation in Eq. (2.78) will suffice to treat all modes, including the zero-energy mode at the critical point.

2.2.5 The Lamb-shift Hamiltonian

While the dissipation is of primary interest to us, it is worth mentioning some details about the unitary dynamics of the system, which is described by the first term in the Lindblad master equation (2.78). The Hamiltonian governing the unitary dynamics is the free system Hamiltonian H_{LRK} with a Lamb-shift correction H_{LS}. The Lamb-shift Hamiltonian (2.52) amounts to a bath-induced modification of the system's unitary dynamics. The form of H_{LS} can be simplified through an identical series of steps as was used for the dissipator in the previous section. This produces

$$H_{\text{LS}} = \sum_k \left[S(\lambda_k) - S(-\lambda_k)\right]\eta_k^\dagger\eta_k, \tag{2.83}$$

where $S(\lambda) = \text{Im}[\bar{\Gamma}(\lambda)]$, with $\bar{\Gamma}(\lambda)$ given in Eq. (2.63). We first note that H_{LS} is diagonal in the η_k fermions, and therefore commutes with the system Hamiltonian. This ensures that H_{LS} will not introduce any non-trivial "mixing" of the system's elementary excitation modes. Instead, it introduces a shift of order γ, the system–bath coupling strength, into the mode energies appearing in the unitary part of the master equation (2.78). The potential impact of this shift on the quantities we consider later is as follows. In Chapter 4 we focus on the dynamics of the closed Kitaev chain, in which the Lamb-shift Hamiltonian is completely absent. Bath-induced excitations are considered in detail in Chapter 5, but for the class of observables we study the Lamb-shift also plays no role. It is only in the coherently generated excitations at finite temperature, which result from a breakdown of adiabaticity, that the Lamb-shift could have an impact. However, we consider a weak system–bath coupling throughout, which is also consistent with the assumptions under which the master equation is derived. This suggests that the coherent excitation density will be dominated by the dynamics resulting from the system Hamiltonian. In the chapters that follow we will therefore neglect the contribution of the Lamb-shift Hamiltonian (2.83) to the master equation (2.78).

Chapter 3

Solving the Lindblad dynamics of the Kitaev chain

This chapter commences with a summary of Prosen's method of "third quantisation" [58], a general technique of canonical quantisation in Liouville space [102]. This approach allows one to solve master equations for quadratic fermionic problems, making it applicable to the study of the Lindblad dynamics of the Kitaev chain. After establishing some important preliminaries in Section 3.1, we use the third quantisation formalism to study the dynamics of two-point correlation functions in Section 3.2. Section 3.3 and Section 3.4 apply the general methods of the preceding sections to the Kitaev chain, which provides insight into the model's equilibration and excitation density dynamics.

3.1 The method of third quantisation

Consider a general quadratic system of L interacting fermionic modes. These modes are coupled to a general set of Markovian baths, written in terms of Lindblad operators that are linear in fermionic variables. Under these conditions, work published in Ref. [58] shows that the Liouvillean $\hat{\mathcal{L}}$ can be diagonalised. In this section a summarised version of this method of "third quantisation" will be presented, which closely follows work by Prosen [58].[1] To be consistent with Ref. [58], we work with a master equation of the form

$$\frac{\mathrm{d}\varrho(t)}{\mathrm{d}t} = \hat{\mathcal{L}}\varrho(t) = -i[H, \varrho(t)] + \sum_{\mu} \left[2L_\mu \varrho(t) L_\mu^\dagger - \left\{L_\mu^\dagger L_\mu, \varrho(t)\right\}\right], \tag{3.1}$$

where $\hbar = 1$ and H is the Hamiltonian. In Section 3.3 we will tailor this method to treat the Kitaev chain master equation (2.78).

The Hamiltonian H and Lindblad operators L_μ in the master equation (3.1) can be expressed in quadratic and linear forms, respectively, in terms of $2L$ anti-commuting Hermitian Majorana operators w_j, satisfying

$$\{w_j, w_k\} = 2\delta_{jk} \qquad \text{with} \qquad j, k = 1, 2, \ldots, 2L. \tag{3.2}$$

We write the Hamiltonian and Lindblad operators in terms of these Majorana operators as

$$H = \sum_{j,k=1}^{2L} w_j H_{jk} w_k = \underline{w} \cdot \mathbf{H}\underline{w} \qquad \text{and} \qquad L_\mu = \sum_{j=1}^{2L} l_{\mu,j} w_j = \underline{l}_\mu \cdot \underline{w}, \tag{3.3}$$

where $l_{\mu,j}$ are the bath coupling constants. Here $\underline{x} = (x_1, x_2, \ldots)^{\mathrm{T}}$ denotes a column vector of either scalars or operators. The $2L \times 2L$ matrix $\mathbf{H}$ is chosen to be antisymmetric, such that $\mathbf{H}^{\mathrm{T}} = -\mathbf{H}$. The Majorana fermions w_j introduced in Eq. (3.2) can be expressed in terms of canonical (Dirac) fermions d_m as

$$w_{2m-1} = d_m + d_m^\dagger \qquad \text{and} \qquad w_{2m} = i(d_m - d_m^\dagger), \qquad m = 1, 2, \ldots, L, \tag{3.4}$$

[1] The formalism considers time-independent Hamiltonians and Lindblad operators, but can be generalised for the treatment of Hamiltonians and Lindblad operators depending explicitly on time [58, 102]. In work by Prosen and Žunkovič [102] the treatment of time-dependent master equations written in third-quantised form is briefly discussed.

where the Dirac fermions satisfy the standard anticommutation relations. While Majorana fermions can be expressed in terms of the Dirac fermions, the two are fundamentally different. In the case of a Dirac fermion, the creation and annihilation operators, $d_m^\dagger$ and d_m, are distinct. In comparison, a Majorana fermion is mathematically equivalent to its antiparticle. This is consistent with Eq. (3.4) where $w_{2m-1} = w_{2m-1}^\dagger$ and $w_{2m} = w_{2m}^\dagger$.

Now define a 4^L dimensional vector space $\mathcal{K}$ of operators, spanned by a canonical basis $\left|P_{\underline{\alpha}}\right\rangle$, with

$$P_{\alpha_1,\alpha_2,\ldots,\alpha_{2L}} := 2^{-L/2} w_1^{\alpha_1} w_2^{\alpha_2} \cdots w_{2L}^{\alpha_{2L}}, \qquad \alpha_j \in \{0,1\} \tag{3.5}$$

forming a complete orthonormal basis with respect to the Hilbert-Schmidt inner product $\langle x|y\rangle = \mathrm{tr}[x^\dagger y]$. Elements of this vector space $\mathcal{K}$ of operators acts on the system's fermionic Fock space $\mathcal{F}$, and the system's density matrix $\varrho = |\varrho\rangle$ is an element of $\mathcal{K}$. We now define on $\mathcal{K}$ a set of adjoint creation and annihilation superoperators as

$$\hat{c}_j^\dagger \left|P_{\underline{\alpha}}\right\rangle = \delta_{\alpha_j,0} \left|w_j P_{\underline{\alpha}}\right\rangle \qquad \text{and} \qquad \hat{c}_j \left|P_{\underline{\alpha}}\right\rangle = \delta_{\alpha_j,1} \left|w_j P_{\underline{\alpha}}\right\rangle, \tag{3.6}$$

which satisfies the canonical anticommutation relations

$$\{\hat{c}_j, \hat{c}_k\} = 0, \qquad \{\hat{c}_j^\dagger, \hat{c}_k^\dagger\} = 0, \qquad \{\hat{c}_j, \hat{c}_k^\dagger\} = \delta_{jk}, \qquad j,k = 1,\ldots,2L. \tag{3.7}$$

In turn, we can now introduce $4L$ Majorana (superoperator) maps

$$\hat{a}_{2j-1} := \frac{1}{\sqrt{2}}(\hat{c}_j + \hat{c}_j^\dagger) \qquad \text{and} \qquad \hat{a}_{2j} := \frac{i}{\sqrt{2}}(\hat{c}_j - \hat{c}_j^\dagger), \tag{3.8}$$

which satisfy $\hat{a}_r = \hat{a}_r^\dagger$ and the anticommutation relation $\{\hat{a}_r, \hat{a}_s\} = \delta_{rs}$. Using these Majorana maps, the master equation (3.1), which governs the time evolution of $\varrho = |\varrho\rangle$, can be expressed in the Liouville-Fock picture as

$$\frac{\mathrm{d}\,|\varrho\rangle}{\mathrm{d}t} = \hat{\mathcal{L}}\,|\varrho\rangle = (\underline{\hat{a}} \cdot \acute{\mathbf{A}} \underline{\hat{a}} - A_0 \mathbb{I})\,|\varrho\rangle\,. \tag{3.9}$$

If we restrict ourselves to study only observables which are products of an even number of Majorana operators, then the $4L \times 4L$ antisymmetric complex *structure matrix* $\acute{\mathbf{A}}$ of the Liouvillean has entries

$$\begin{aligned}
\acute{\mathbf{A}}_{2j-1,2k-1} &= -2i\mathbf{H}_{jk} - \mathbf{M}_{kj} + \mathbf{M}_{jk}, \\
\acute{\mathbf{A}}_{2j-1,2k} &= 2i\mathbf{M}_{kj}, \\
\acute{\mathbf{A}}_{2j,2k-1} &= -2i\mathbf{M}_{jk}, \\
\acute{\mathbf{A}}_{2j,2k} &= -2i\mathbf{H}_{jk} + \mathbf{M}_{kj} - \mathbf{M}_{jk},
\end{aligned} \tag{3.10}$$

where

$$\mathbf{M} := \sum_\mu \underline{l}_\mu \otimes \underline{l}_\mu^* \tag{3.11}$$

is the $2L \times 2L$ Hermitian Lindblad bath matrix encoding the Lindblad operators, and $A_0 = 2\mathrm{tr}[\mathbf{M}]$.

Under the assumption that the structure matrix $\acute{\mathbf{A}}$ in Eq. (3.9) can be diagonalised, there exists $4L$ linearly independent vectors $\underline{v}_q$, $q = 1,\ldots,4L$, with corresponding eigenvalues $r_1, -r_1, r_2, -r_2, \ldots, r_{2L}, -r_{2L}$. Hereafter the eigenvalues r_j will be referred to as rapidities. It can be shown that these rapidities coincide with the eigenvalues of the $2L \times 2L$ non-Hermitian matrix [59, 103]

$$\mathbf{X} = -2i\mathbf{H} + 2\mathbf{M}_r, \tag{3.12}$$

where $\mathbf{H}$ is defined in Eq. (3.3) and $\mathbf{M}_r = \mathrm{Re}[\mathbf{M}]$ is the real part of $\mathbf{M}$ in Eq. (3.11). The vectors $\underline{v}_q$ are ordered according to the real parts of the rapidities, such that $\mathrm{Re}[r_1] \geq \mathrm{Re}[r_2] \cdots \geq \mathrm{Re}[r_{2L}] \geq 0$. The normalisation condition imposed on $\underline{v}_q$ is

$$\underline{v}_q \cdot \underline{v}_s = \mathbf{J}_{qs}, \qquad \text{where} \qquad \mathbf{J} = \mathbb{I}_{2L} \otimes \sigma^x = \mathbb{I}_{2L} \otimes \begin{bmatrix} 0 & 1 \\ 1 & 0 \end{bmatrix}. \tag{3.13}$$

Now using the $4L$ linearly independent vectors, the $4L \times 4L$ matrix $\acute{\mathbf{V}}$ can be constructed, where its q'th

row is given by $\underline{v}_q$. The normalisation condition in Eq. (3.13) reduces to $\acute{\mathbf{V}}\acute{\mathbf{V}}^{\mathrm{T}} = \mathbf{J}$, and the matrix $\acute{\mathbf{V}}$ diagonalises $\acute{\mathbf{A}}$ such that

$$\acute{\mathbf{V}}^{-\mathrm{T}}\acute{\mathbf{A}}\acute{\mathbf{V}}^{\mathrm{T}} = \mathbf{D}, \tag{3.14}$$

where $\mathbf{D} = \mathrm{diag}\{r_1, -r_1, r_2, -r_2, \ldots, r_{2L}, -r_{2L}\}$.

The construction of the $\acute{\mathbf{V}}$ matrix is such that it diagonalises the structure matrix $\acute{\mathbf{A}}$, as demonstrated in Eq. (3.14). We can therefore introduce a new set of superoperators in terms of which the Liouvillean $\hat{\mathcal{L}}$ is diagonal. This allows us to explicitly calculate the complete spectrum of the Liouvillean, as well as the equilibrium expectation value of any quadratic observable $w_j w_k$, using the rapidities and matrices defined previously. Given a sequence of occupation numbers $\underline{\nu} = (\nu_1, \nu_2, \ldots, \nu_{2L})$ with $\nu_j \in \{0, 1\}$, the complete spectrum of the Liouvillean is [104]

$$\lambda_{\underline{\nu}} = -2\sum_{j=1}^{2L} r_j \nu_j. \tag{3.15}$$

The non-equilibrium steady states $|\mathrm{NESS}\rangle$ represent the stationary solutions of the Liouville-Fock Lindblad equation (3.9), and satisfy

$$\hat{\mathcal{L}}\,|\mathrm{NESS}\rangle = 0. \tag{3.16}$$

If, and only if, the rapidity spectrum $\{r_j\}$ does not contain zero, i.e. $r_{2L} \neq 0$, the non-equilibrium steady state is unique. Under this assumption, the expectation value of any quadratic observable $w_j w_k$ in the unique NESS is

$$\begin{aligned}\langle w_j w_k\rangle_{\mathrm{NESS}} &= \delta_{jk} + \langle \mathbb{I}|\, \hat{c}_j \hat{c}_k\, |\mathrm{NESS}\rangle \\ &= \delta_{jk} + \frac{1}{2}\sum_{m=1}^{2L} (v_{2m,2j-1} - i v_{2m,2j})(v_{2m-1,2k-1} - i v_{2m-1,2k}),\end{aligned} \tag{3.17}$$

where $|\mathbb{I}\rangle$ represents the identity operator acting on the fermionic Fock space $\mathcal{F}$ and $v_{x,y}$ denotes the entry of the matrix $\acute{\mathbf{V}}$ in row x and column y. Expectation values of more general observables which are even in the fermionic operators can be determined using Wick contractions. Refer to the work published in Refs. [105, 106] for more detail.

Up to now, the ordering of the Majorana superoperators, $\hat{a}_{2j-1}$ and $\hat{a}_{2j}$, has been $\underline{\hat{a}} = (\hat{a}_1, \hat{a}_2, \cdots, \hat{a}_{2L})^{\mathrm{T}}$. By introducing a second convenient ordering, we can bring the $\acute{\mathbf{A}}$ and $\acute{\mathbf{V}}$ matrices into a useful block-structured form. If we define the mappings $(2j-1) \to (1, j)$ and $(2j) \to (2, j)$, the Majorana superoperators (3.8) can be relabeled as [59, 103]

$$\hat{a}_{1,j} = \hat{a}_{2j-1} \qquad \text{and} \qquad \hat{a}_{2,j} = \hat{a}_{2j}, \tag{3.18}$$

which obey the anticommutation relation $\{\hat{a}_{\nu,j}, \hat{a}_{\nu',j'}\} = \delta_{\nu\nu'}\delta_{jj'}$. This relabeling of the Majorana superoperators in Eq. (3.18) leads to the ordering $\underline{\hat{a}} = (\hat{a}_{1,1}, \hat{a}_{1,2}, \cdots, \hat{a}_{1,2L}, \hat{a}_{2,1}, \cdots, \hat{a}_{2,2L})^{\mathrm{T}}$. Implementing this ordering convention in Eq. (3.9) results in a structure matrix of the form [59]

$$\mathbf{A} = \mathcal{P}\acute{\mathbf{A}}\mathcal{P}^{\mathrm{T}} = \begin{bmatrix} -2i\mathbf{H} + 2i\mathbf{M}_i & 2i\mathbf{M} \\ -2i\mathbf{M}^{\mathrm{T}} & -2i\mathbf{H} - 2i\mathbf{M}_i \end{bmatrix}, \tag{3.19}$$

where $\mathcal{P}$ is the $4L \times 4L$ permutation matrix encoding the mappings $(2j-1) \to (1, j)$ and $(2j) \to (2, j)$ and $\mathbf{M}_i = \mathrm{Im}[\mathbf{M}]$ refers to the imaginary part of the matrix $\mathbf{M}$. Similarly, transforming $\acute{\mathbf{V}}$ with the permutation matrix $\mathcal{P}$ yields

$$\mathbf{V} = \mathcal{P}\acute{\mathbf{V}}\mathcal{P}^{\mathrm{T}} = \begin{bmatrix} \mathbf{V_a} & \mathbf{V_b} \\ \mathbf{V_c} & \mathbf{V_d} \end{bmatrix}. \tag{3.20}$$

Using the submatrices of $\mathbf{V}$, the expectation values $\langle w_j w_k\rangle_{\mathrm{NESS}}$ in the unique NESS can be calculated as

$$\langle w_j w_k\rangle_{\mathrm{NESS}} = \left[\mathbb{I}_{2L} + \frac{1}{2}(\mathbf{V_a} - i\mathbf{V_b})(\mathbf{V_c}^{\mathrm{T}} - i\mathbf{V_d}^{\mathrm{T}})\right]_{jk}. \tag{3.21}$$

This second ordering convention for the Majorana maps, as well as the $\mathbf{A}$ and $\mathbf{V}$ matrices in Eqs. (3.19) and (3.20), will be used extensively in our application of this general method to the Kitaev chain.

3.2 Correlation function dynamics

Within the third quantisation formalism, we can study the dynamics of two-point correlation functions in quadratic open quantum systems [103]. In this section we summarise the approach of Kos and Prosen [103]. This approach will be used in Section 3.4 to study the time dependence of the correlation functions for the Kitaev chain, which will provide insight into the dynamic response of the system to various ramping protocols. In the summary of the work published in Ref. [103] below we will consider only two-point correlation functions, since higher-order correlations can be determined directly from the former using Wick contractions.

The two-point correlation functions can be combined into a correlation matrix $\mathbf{C}(t)$ with entries

$$\mathbf{C}_{jk}(t) = \mathrm{Tr}(w_j w_k \varrho(t)) - \delta_{jk} = 2\,\langle \mathbb{I}|\, \hat{a}_{1,j}\hat{a}_{1,k}\,|\varrho(t)\rangle - \delta_{jk}. \tag{3.22}$$

To describe the dynamics of $\mathbf{C}(t)$, which follows from the Liouville-Fock master equation (3.9), the time derivative of Eq. (3.22) is computed. After some manipulation, the matrix differential equation governing the time evolution of the two-point correlation functions is [103]

$$-\frac{1}{2}\frac{\mathrm{d}\mathbf{C}(t)}{\mathrm{d}t} = \mathbf{X}^{\mathrm{T}}\mathbf{C}(t) + \mathbf{C}(t)\mathbf{X} + 4i\mathbf{M}_i, \tag{3.23}$$

where $\mathbf{X} = -2i\mathbf{H} + 2\mathbf{M}_r$ is the matrix that was introduced in Eq. (3.12), and $\mathbf{M}_i$ is the imaginary part of $\mathbf{M}$ in Eq. (3.11). The time evolution of the correlation functions is considered to be closed and Markovian, since the evolution only depends on the instantaneous correlation matrix $\mathbf{C}(t)$ and not the entire history of the density matrix. We now express the correlation matrix as

$$\mathbf{C}(t) = \mathbf{C}^{\infty} + (\mathbf{C}(t) - \mathbf{C}^{\infty}), \tag{3.24}$$

where $\mathbf{C}^{\infty}$ is the stationary solution of the matrix differential equation (3.23). This stationary solution, which is associated with the NESS, is defined by $\frac{\mathrm{d}\mathbf{C}^{\infty}}{\mathrm{d}t} = 0$, which results in

$$\mathbf{X}^{\mathrm{T}}\mathbf{C}^{\infty} + \mathbf{C}^{\infty}\mathbf{X} + 4i\mathbf{M}_i = 0. \tag{3.25}$$

Inserting Eq. (3.24) into the matrix differental equation (3.23) yields the general solution for $\mathbf{C}(t)$, which is given by

$$\mathbf{C}(t) = e^{-2t\mathbf{X}^{\mathrm{T}}}(\mathbf{C}(0) - \mathbf{C}^{\infty})e^{-2t\mathbf{X}} + \mathbf{C}^{\infty} \qquad \text{with} \qquad \mathbf{C}_{jm}(0) = \mathrm{tr}[w_j w_m \varrho(0)] - \delta_{jm}. \tag{3.26}$$

It is possible to solve for $\mathbf{C}^{\infty}$ from Eq. (3.25) by diagonalising $\mathbf{X}$. This leads to a convenient expression for the two-point equilibrium correlations in the NESS. We therefore express $\mathbf{C}^{\infty}$ as

$$\mathbf{C}^{\infty} = \mathbf{P}^{-\mathrm{T}}(\mathbf{P}^{\mathrm{T}}\mathbf{C}^{\infty}\mathbf{P})\mathbf{P}^{-1} \qquad \text{with} \qquad (\mathbf{P}^{\mathrm{T}}\mathbf{C}^{\infty}\mathbf{P})_{kl} = -4i\frac{(\mathbf{P}^{\mathrm{T}}\mathbf{M}_i\mathbf{P})_{kl}}{\Lambda_k + \Lambda_l}, \tag{3.27}$$

where the spectral decomposition of the matrix $\mathbf{X}$ (3.12) is used to define $\mathbf{P}$ and $\mathbf{\Lambda}$ as

$$\mathbf{X}\mathbf{P} = \mathbf{P}\mathbf{\Lambda} \qquad \text{with} \qquad \mathbf{\Lambda} = \mathrm{diag}(\ldots, r_j, \ldots). \tag{3.28}$$

The entries of the diagonal matrix $\mathbf{\Lambda}$ are the rapidities r_j.

The result in Eq. (3.26) provides important information about the dynamics in quadratic open quantum systems. From this result we can also extract the relaxation times of the correlation functions. Performing a basis transformation

$$\mathbf{G}(t) = \mathbf{P}^{\mathrm{T}}(\mathbf{C}(t) - \mathbf{C}^{\infty})\mathbf{P}, \tag{3.29}$$

the time evolution of the correlations is described by a simple propagation of the initial condition in the new basis as

$$\mathbf{G}_{jm}(t) = e^{-2(r_j + r_m)t}\mathbf{G}_{jm}(0). \tag{3.30}$$

This shows that the correlation functions will relax on timescales set by the real parts of the rapidities. The overall relaxation time can be bounded by calculating $\min_{j,m}(r_j + r_m)$.

3.3 The Kitaev chain: Equilibration

The Lindblad master equation governing the time evolution of the density matrix $\varrho(t)$ of the Kitaev chain, of which the final form appears in Eq. (2.78), can be treated using the method of third quantisation outlined in Section 3.1. Here we will apply this method to determine the steady state solution of the Kitaev chain master equation, and subsequently verify that the steady state corresponds to a thermal equilibrium state. From this we can confirm that at late times the system produces the equilibration we would expect.

We start with the diagonalised Kitaev chain Hamiltonian in terms of the Dirac fermions from Eq. (2.25), which is given by

$$H_{\text{LRK}} = \sum_k \lambda_{\phi,\alpha}(k) \left(\eta_k^\dagger \eta_k - \frac{1}{2} \right). \tag{3.31}$$

Using Eq. (3.4), the Dirac fermions in the expression for H_{LRK} above can be expressed in terms of the Majorana fermions as

$$w_{2n-1} = \eta_{k_n} + \eta_{k_n}^\dagger \qquad \text{and} \qquad w_{2n} = i(\eta_{k_n} - \eta_{k_n}^\dagger), \tag{3.32}$$

which satisfy the anti-commutation relation $\{w_i, w_j\} = 2\delta_{ij}$ with $i, j = 1, 2, \ldots, 2L$. In Eq. (3.32) we introduced the notation k_n to be consistent with the labeling of the Majorana fermions. These k_n subscripts of the Dirac fermions are directly related to the n labels through $k_n = 2\pi n/L$. In this notation, the Hamiltonian (3.31) is written in terms of the Majorana operators (3.32) as

$$H_{\text{LRK}} = \frac{i}{2} \sum_{n=0}^{L-1} \lambda_{\phi,\alpha}(k_n) w_{2n} w_{2n-1}. \tag{3.33}$$

The specific form of the master equation in Eq. (2.78) suggests that the various η_k modes equilibrate independently, and the system therefore factorises into L copies of a single fermion in a bath. To this end, studying the trivial single-fermion example first will be useful.

3.3.1 Trivial example: A single fermion in a bath

In Ref. [58] the method of third quantisation is demonstrated using a single fermion in a thermal bath. We will outline the results given in Ref. [58] for this simple example, but in a notation that will allow for these results to be extended to the Kitaev chain. In addition, we supplement the results with a brief discussion on the relaxation of the single-fermion system, which will be useful when looking at the per-mode equilibration of the Kitaev chain.

The most general single-fermion Hamiltonian is

$$H_{\text{SF}} = -ihw_1 w_2 + c_1 = 2hc^\dagger c + c_2, \tag{3.34}$$

where c_1, c_2 and $h > 0$ are constants. For this trivial case the Lindblad operators are

$$L_1 = \sqrt{\Gamma_-}c = \frac{1}{2}\sqrt{\Gamma_-}(w_1 - iw_2) \qquad \text{and} \qquad L_2 = \sqrt{\Gamma_+}c^\dagger = \frac{1}{2}\sqrt{\Gamma_+}(w_1 + iw_2). \tag{3.35}$$

As in the full Lindblad master equation (2.78), the bath coupling constants $\Gamma_\pm$ encode information on the system–bath coupling and the properties of the bath. In particular, the bath temperature T is set by the ratio of these coupling constants as $\Gamma_-/\Gamma_+ = e^{2h/T}$. Following the method outlined in Section 3.1, the structure matrix of the Liouvillean $\hat{\mathcal{L}}$ in Eq. (3.9) is found to be

$$\mathbf{A} = -h\mathbf{R} + \mathbf{B}_{\Gamma_1,\Gamma_2}, \tag{3.36}$$

where

$$\mathbf{R} := \begin{bmatrix} 0 & 0 & 1 & 0 \\ 0 & 0 & 0 & 1 \\ -1 & 0 & 0 & 0 \\ 0 & -1 & 0 & 0 \end{bmatrix}, \qquad \mathbf{B}_{\Gamma_1,\Gamma_2} := \begin{bmatrix} 0 & \frac{i}{2}\Gamma_1 & -\frac{i}{2}\Gamma_2 & \frac{1}{2}\Gamma_2 \\ -\frac{i}{2}\Gamma_1 & 0 & \frac{1}{2}\Gamma_2 & \frac{i}{2}\Gamma_2 \\ \frac{i}{2}\Gamma_2 & -\frac{1}{2}\Gamma_2 & 0 & \frac{i}{2}\Gamma_1 \\ -\frac{1}{2}\Gamma_2 & -\frac{i}{2}\Gamma_2 & -\frac{i}{2}\Gamma_1 & 0 \end{bmatrix}, \tag{3.37}$$

and $\Gamma_{1,2} = \Gamma_+ \pm \Gamma_-$. It is also found that $A_0 = \Gamma_1$, while the rapidities are given by $r_{1,2} = \frac{1}{2}\Gamma_1 \pm ih$.

Applying Eq. (3.17) we find that in the steady state

$$\langle c^\dagger c\rangle = \frac{1}{2} - \frac{i}{2}\langle w_1 w_2\rangle = \frac{1}{2}\left(\frac{\Gamma_1+\Gamma_2}{\Gamma_1}\right) = \left(\frac{\Gamma_-}{\Gamma_+}+1\right)^{-1}, \tag{3.38}$$

which reduces to the expected Fermi-Dirac distribution $n_{\text{FD}} = (e^{2h/T}+1)^{-1}$. The single-fermion system will therefore relax to a thermal equilibrium state at a rate set by the real part of the rapidities.

3.3.2 Per-mode equilibration of the Kitaev chain

The diagonalised Kitaev chain Hamiltonian (3.33) can be viewed as a sum of L independent single-fermion Hamiltonians of the form in Eq. (3.34). The bath operators (2.79) are given in terms of the η Majorana fermions as

$$L_{k_n,-} = \sqrt{\Gamma_{k_n,-}}\eta_{k_n} = \frac{1}{2}\sqrt{\Gamma_{k_n,-}}(w_{2n-1} - iw_{2n}) \tag{3.39}$$

and

$$L_{k_n,+} = \sqrt{\Gamma_{k_n,+}}\eta^\dagger_{k_n} = \frac{1}{2}\sqrt{\Gamma_{k_n,+}}(w_{2n-1} + iw_{2n}). \tag{3.40}$$

Following the steps in Section 3.1, with the notation $\underline{\hat{a}} = (\hat{a}_{1,1}, \hat{a}_{2,1}, \cdots, \hat{a}_{1,2L}, \hat{a}_{2,2L})$ for the vector of superoperators (3.18), and drawing inspiration from the single-fermion example, the structure matrix is found to have a simple block-diagonal form:

$$\mathbf{A} = \begin{bmatrix} \mathbf{A}_0 & \mathbf{0} & \mathbf{0} & \cdots & \mathbf{0} \\ \mathbf{0} & \mathbf{A}_1 & \mathbf{0} & \cdots & \mathbf{0} \\ \mathbf{0} & \mathbf{0} & \mathbf{A}_2 & \cdots & \mathbf{0} \\ \vdots & \vdots & \vdots & \ddots & \vdots \\ \mathbf{0} & \mathbf{0} & \mathbf{0} & \cdots & \mathbf{A}_{L-1} \end{bmatrix}, \tag{3.41}$$

where

$$\mathbf{A}_n = -\frac{\lambda_{\phi,\alpha}(k_n)}{2}\mathbf{R} + \gamma\mathbf{B}_{\Gamma_{k_n,1},\Gamma_{k_n,2}}, \qquad n = 0,\ldots,L-1. \tag{3.42}$$

The matrices $\mathbf{R}$ and $\mathbf{B}_{\Gamma_{k_n,1},\Gamma_{k_n,2}}$ are defined as in Eq. (3.37), with $\Gamma_{k_n,1} = \Gamma_{k_n,+} + \Gamma_{k_n,-}$ and $\Gamma_{k_n,2} = \Gamma_{k_n,+} - \Gamma_{k_n,-}$. The $2L$ rapidities are found to be

$$r_{\pm,n} = \frac{1}{2}\Big(\gamma(\Gamma_{k_n,+}+\Gamma_{k_n,-}) \pm i\lambda_{\phi,\alpha}(k_n)\Big) = \frac{1}{2}\Big(\gamma\Gamma_{k_n,1} \pm i\lambda_{\phi,\alpha}(k_n)\Big). \tag{3.43}$$

The $\mathbf{V}$ matrix is constructed from the eigenvectors of $\mathbf{A}$ (3.41), ordered by the real parts of the rapidities (3.43). To obtain the correct ordering of rows in $\mathbf{V}$, we calculate the *overlap* between all eigenvectors of $\mathbf{A}$ and pair those which have the largest *overlap*. This is consistent with pairing the eigenvectors corresponding to the rapidity pairs $r_j, -r_j$, as discussed in the work published in Ref. [58]. Using the block-diagonal form of $\mathbf{A}$ in Eq. (3.41), $\mathbf{V}$ is constructed as

$$\mathbf{V} = \begin{bmatrix} \mathbf{V}_0 & \mathbf{0} & \mathbf{0} & \cdots & \mathbf{0} \\ \mathbf{0} & \mathbf{V}_1 & \mathbf{0} & \cdots & \mathbf{0} \\ \mathbf{0} & \mathbf{0} & \mathbf{V}_2 & \cdots & \mathbf{0} \\ \vdots & \vdots & \vdots & \ddots & \vdots \\ \mathbf{0} & \mathbf{0} & \mathbf{0} & \cdots & \mathbf{V}_{L-1} \end{bmatrix}, \tag{3.44}$$

where

$$\mathbf{V}_n = \begin{bmatrix} \frac{1}{2}\zeta_{n,-}(1+\frac{\Gamma_{k_n,2}}{\Gamma_{k_n,1}}) & -\frac{i}{2\zeta_{n,-}} & \frac{i}{2}\zeta_{n,-}(1+\frac{\Gamma_{k_n,2}}{\Gamma_{k_n,1}}) & \frac{1}{2\zeta_{n,-}} \\ \frac{1}{2\zeta_{n,-}} & \frac{i}{2\zeta_{n,-}} & -\frac{i}{2\zeta_{n,-}} & \frac{1}{2\zeta_{n,-}} \\ -\frac{1}{2}\zeta_{n,+}(1-\frac{\Gamma_{k_n,2}}{\Gamma_{k_n,1}}) & \frac{i}{2\zeta_{n,+}} & \frac{i}{2}\zeta_{n,+}(1-\frac{\Gamma_{k_n,2}}{\Gamma_{k_n,1}}) & \frac{1}{2\zeta_{n,+}} \\ -\frac{1}{2\zeta_{n,+}} & -\frac{i}{2\zeta_{n,+}} & -\frac{i}{2\zeta_{n,+}} & \frac{1}{2\zeta_{n,+}} \end{bmatrix} \tag{3.45}$$

with

$$\zeta_{n,-} = \sqrt{\frac{\Gamma_{k_n,1}}{\Gamma_{k_n,1}-\Gamma_{k_n,2}}} \qquad \text{and} \qquad \zeta_{n,+} = \sqrt{\frac{\Gamma_{k_n,1}}{\Gamma_{k_n,1}+\Gamma_{k_n,2}}}. \tag{3.46}$$

It can be shown that the matrix $\mathbf{V}$ in Eq. (3.44) satisfies the normalisation condition $\mathbf{V}\mathbf{V}^{\mathrm{T}} = \mathbf{J} = \mathbb{I}_{2L} \otimes \sigma^x$ from Eq. (3.13). The condition introduced in Eq. (3.14) is also satisfied, such that the matrix $\mathbf{V}$ (3.44) diagonalises $\mathbf{A}$ (3.41) as $\mathbf{V}^{-\mathrm{T}}\mathbf{A}\mathbf{V}^{\mathrm{T}} = \mathbf{D}$, where $\mathbf{D}$ is a diagonal matrix with the rapidities (3.43) on the diagonal.

Recalling from Eq. (3.17) that the expectation values $\langle w_j w_k \rangle$ are given by

$$\langle w_j w_k \rangle_{\mathrm{NESS}} = \delta_{jk} + \frac{1}{2} \sum_{m=1}^{2L} (v_{2m,2j-1} - i v_{2m,2j})(v_{2m-1,2k-1} - i v_{2m-1,2k}), \tag{3.47}$$

a matrix $\mathbf{W}$ with entries $\mathbf{W}_{ij} = \langle w_i w_j \rangle$, $i, j = 1, \ldots, 2L$, can be constructed. This matrix has a simple structure, and only depends on the ratios of the bath coupling constants, $\Gamma_{k_n,1}$ and $\Gamma_{k_n,2}$. Compactly, we write

$$\mathbf{W} = \begin{bmatrix} \mathbf{W}_0 & \mathbf{0} & \mathbf{0} & \cdots & \mathbf{0} \\ \mathbf{0} & \mathbf{W}_1 & \mathbf{0} & \cdots & \mathbf{0} \\ \mathbf{0} & \mathbf{0} & \mathbf{W}_2 & \cdots & \mathbf{0} \\ \vdots & \vdots & \vdots & \ddots & \vdots \\ \mathbf{0} & \mathbf{0} & \mathbf{0} & \cdots & \mathbf{W}_{L-1} \end{bmatrix}, \tag{3.48}$$

where

$$\mathbf{W}_n = \begin{bmatrix} 1 & i\frac{\Gamma_{k_n,2}}{\Gamma_{k_n,1}} \\ -i\frac{\Gamma_{k_n,2}}{\Gamma_{k_n,1}} & 1 \end{bmatrix}. \tag{3.49}$$

The entries of $\mathbf{W}$ reduce to hyperbolic tangent functions with arguments depending only on the bath temperature $T = \beta^{-1}$ and the dispersion relation (2.26). More precisely, we have

$$\frac{\Gamma_{k_n,2}}{\Gamma_{k_n,1}} = \frac{\Gamma_{k_n,+} - \Gamma_{k_n,-}}{\Gamma_{k_n,+} + \Gamma_{k_n,-}} = -\tanh\left(\frac{\lambda_{\phi,\alpha}(k_n)\beta}{2}\right). \tag{3.50}$$

Using the entries of $\mathbf{W}$, the equilibrium (steady state) expectation values of the fermionic number operators $\langle \eta_{k_n}^\dagger \eta_{k_n} \rangle$ can be calculated as

$$\langle \eta_{k_n}^\dagger \eta_{k_n} \rangle = \frac{1}{2}\big(1 + i\langle w_{2n} w_{2n-1} \rangle\big) = \left(e^{\lambda_{\phi,\alpha}(k_n)\beta} + 1\right)^{-1}. \tag{3.51}$$

In equilibrium the expectation values of the number operators therefore reduce to the Fermi-Dirac distribution, $n_{\mathrm{FD}}(\lambda\beta)$.

3.4 The Kitaev chain: Excitation density dynamics

In Section 3.2 we introduced a matrix differential equation (3.23) that describes the dynamics of the two-point correlation functions $\langle w_j w_k \rangle$. One challenge is that the dimension of the correlation matrix $\mathbf{C}(t)$ increases linearly with the system size. For the Kitaev chain we can overcome this challenge by exploiting the properties of momentum conservation. Due to momentum conservation in our model, the same factorisation as observed in Section 3.3 will enter in the matrix differential equation (3.23). We therefore reduce the full matrix differential equation into a set of 4×4 matrix differential equations, which are easier to treat numerically. From the solutions of these 4×4 matrix differential equations, the excitation density of the system will be extracted.

We will first reformulate the correlation functions (3.22) in terms of the Fourier Majorana fermions, and then derive the set of 4×4 matrix differential equations. Switching to the Fourier Majorana fermions will be convenient in the subsequent chapters, where we implement ramping protocols to study the non-equilibrium dynamics of the Kitaev chain. This is due to the Fourier operators a_k and $a_k^\dagger$ remaining unaffected by any change in the ramping parameter. Now define the Fourier Majorana operators for the k and $-k$ modes as

$$\begin{aligned} w_1 &= a_k + a_k^\dagger, & w_2 &= i(a_k - a_k^\dagger), \\ w_3 &= a_{-k} + a_{-k}^\dagger, & w_4 &= i(a_{-k} - a_{-k}^\dagger). \end{aligned} \tag{3.52}$$

We will use the definitions above, together with momentum conservation, to write the $\mathbf{H}$, $\mathbf{M}$ and $\mathbf{X}$ matrices in block-diagonal form, where each submatrix on the diagonal corresponds to a particular $\{k, -k\}$ mode

pair. To determine the general 4×4 submatrices on the diagonal of $\mathbf{H}$, which are denoted by $\mathbf{H}_{\{k,-k\}}$, we write the diagonalised Hamiltonian (2.25) in terms of the Majorana fermions (3.52) by using the Bogoliubov transformation (2.22). Now based on the definition in Eq. (3.3), the general 4×4 submatrices $\mathbf{H}_{\{k,-k\}}$ for the $\{k,-k\}$ mode pairs on the diagonal of $\mathbf{H}$ are found to be

$$\mathbf{H}_{\{k,-k\}} = \frac{i}{4}\lambda_{\phi,\alpha}(k)\begin{bmatrix} 0 & -\cos(2\beta_k) & -\sin(2\beta_k) & 0 \\ \cos(2\beta_k) & 0 & 0 & \sin(2\beta_k) \\ \sin(2\beta_k) & 0 & 0 & -\cos(2\beta_k) \\ 0 & -\sin(2\beta_k) & \cos(2\beta_k) & 0 \end{bmatrix}. \tag{3.53}$$

Here β_k is the Bogoliubov angle, which is defined below Eq. (2.22). The 0 and π modes[2] are special cases for which the following 2×2 submatrices are computed:

$$\mathbf{H}_{k=0} = \frac{i}{4}\lambda_{\phi,\alpha}(0)\cos(2\beta_k)\begin{bmatrix} 0 & -1 \\ 1 & 0 \end{bmatrix} \quad \text{and} \quad \mathbf{H}_{k=\pi} = \frac{i}{4}\lambda_{\phi,\alpha}(\pi)\begin{bmatrix} 0 & 1 \\ -1 & 0 \end{bmatrix}. \tag{3.54}$$

The general 4×4 submatrix $\mathbf{M}_{\{k,-k\}}$ on the diagonal of $\mathbf{M}$ can be constructed directly from the Lindblad bath operators $L_{k,\pm}$ (2.79). After rewriting the η_k fermion operators in terms of the Fourier fermion operators as

$$\eta_k^\dagger = \cos(\beta_k)a_k^\dagger + i\sin(\beta_k)a_{-k} \quad \text{and} \quad \eta_k = \cos(\beta_k)a_k - i\sin(\beta_k)a_{-k}^\dagger, \tag{3.55}$$

Eq. (3.52) can be used to obtain the Lindblad operators in terms of the Fourier Majorana fermions. We find that

$$L_{k,\pm} = \frac{1}{2}\sqrt{\Gamma_{k,\pm}}\Big(\cos(\beta_k)(w_1 \pm iw_2) \pm i\sin(\beta_k)(w_3 \mp iw_4)\Big). \tag{3.56}$$

Making use of Eq. (3.56) above and the definition in Eq. (3.3), we find the submatrix

$$\mathbf{M}_{\{k,-k\}} = \frac{\gamma}{4}\begin{bmatrix} \Gamma_{k,1} & -i\Gamma_{k,2}\cos(2\beta_k) & -i\Gamma_{k,2}\sin(2\beta_k) & 0 \\ i\Gamma_{k,2}\cos(2\beta_k) & \Gamma_{k,1} & 0 & i\Gamma_{k,2}\sin(2\beta_k) \\ i\Gamma_{k,2}\sin(2\beta_k) & 0 & \Gamma_{k,1} & -i\Gamma_{k,2}\cos(2\beta_k) \\ 0 & -i\Gamma_{k,2}\sin(2\beta_k) & i\Gamma_{k,2}\cos(2\beta_k) & \Gamma_{k,1} \end{bmatrix}. \tag{3.57}$$

Again the 0 and π modes will be treated separately. For these we find

$$\mathbf{M}_{k=0} = \frac{\gamma}{4}\begin{bmatrix} \Gamma_{0,1} & i\Gamma_{0,2} \\ -i\Gamma_{0,2} & \Gamma_{0,1} \end{bmatrix} \quad \text{and} \quad \mathbf{M}_{k=\pi} = \frac{\gamma}{4}\begin{bmatrix} \Gamma_{\pi,1} & i\Gamma_{\pi,2} \\ -i\Gamma_{\pi,2} & \Gamma_{\pi,1} \end{bmatrix}. \tag{3.58}$$

Based on Eq. (3.12), a submatrix of $\mathbf{X}$ now follows directly from $\mathbf{H}_{\{k,-k\}}$ (3.53) and $\mathbf{M}_{\{k,-k\}}$ (3.57), giving

$$\mathbf{X}_{\{k,-k\}} = -2i\mathbf{H}_{\{k,-k\}} + 2\mathrm{Re}[\mathbf{M}_{\{k,-k\}}]. \tag{3.59}$$

In this formulation the correlation matrix entries are

$$[\mathbf{C}_{\{k,-k\}}(t)]_{ij} = \mathrm{tr}(w_i w_j \varrho) - \delta_{ij}, \tag{3.60}$$

where w_i, w_j, with $i,j = 1,\ldots,4$, are the Fourier Majorana fermions introduced in Eq. (3.52). We can therefore write the set of 4×4 matrix differential equations as

$$-\frac{1}{2}\frac{\mathrm{d}\mathbf{C}_{\{k,-k\}}(t)}{\mathrm{d}t} = \mathbf{X}_{\{k,-k\}}^{\mathrm{T}}\mathbf{C}_{\{k,-k\}}(t) + \mathbf{C}_{\{k,-k\}}(t)\mathbf{X}_{\{k,-k\}} + 4i\mathrm{Im}[\mathbf{M}_{\{k,-k\}}], \tag{3.61}$$

which can be solved numerically. An analogous expression holds for the $k = 0, \pi$ cases.

The solution to Eq. (3.61) provides two-point correlation functions for the Fourier Majorana fermions. However, in the study of the excitation density dynamics it is the occupations of the η_k modes, which correspond to the elementary excitations of the system, that are of interest. We can use a series of linear transformations to relate the occupations $\langle\eta_k^\dagger\eta_k\rangle$ to the correlation functions of the Fourier Majorana fermions in

[2] The π mode is present only when the number of lattice sites L is even.

$\mathbf{C}_{\{k,-k\}}(t)$. Combining the transformations

$$\begin{bmatrix} w_1 \\ w_2 \\ w_3 \\ w_4 \end{bmatrix} = \underbrace{\begin{bmatrix} 1 & 1 & 0 & 0 \\ i & -i & 0 & 0 \\ 0 & 0 & 1 & 1 \\ 0 & 0 & i & -i \end{bmatrix}}_{Q^{-1}} \begin{bmatrix} a_k \\ a_k^\dagger \\ a_{-k} \\ a_{-k}^\dagger \end{bmatrix} \quad \text{and} \quad \begin{bmatrix} \eta_k \\ \eta_{-k} \end{bmatrix} = \underbrace{\begin{bmatrix} \cos(\beta_k) & 0 \\ 0 & i\sin(\beta_k) \\ 0 & \cos(\beta_k) \\ -i\sin(\beta_k) & 0 \end{bmatrix}^{\mathrm{T}}}_{R^{\mathrm{T}}} \begin{bmatrix} a_k \\ a_k^\dagger \\ a_{-k} \\ a_{-k}^\dagger \end{bmatrix} \tag{3.62}$$

allows us to write

$$\begin{bmatrix} \eta_k \\ \eta_{-k} \end{bmatrix} = S \begin{bmatrix} w_1 & w_2 & w_3 & w_4 \end{bmatrix}^{\mathrm{T}} \qquad \text{with} \qquad S = RQ. \tag{3.63}$$

From this we can express the correlations of the η_k fermions in terms of the Fourier Majorana correlations as

$$\langle \eta_q^\dagger \eta_{q'} \rangle = S_{qi}^* \langle w_i w_j \rangle S_{q'j}. \tag{3.64}$$

Hence, the excitation probability for a $\{k, -k\}$ mode pair is

$$\langle \eta_k^\dagger \eta_k \rangle + \langle \eta_{-k}^\dagger \eta_{-k} \rangle = \sum_{q=\{k,-k\}} S_{qi}^* S_{qj} \langle w_i w_j \rangle = \mathrm{Tr}\left[S^{\mathrm{T}} S^* \mathbf{C}_{\{k,-k\}}(t) \right] + 1. \tag{3.65}$$

The tools developed in this section will be used in the subsequent chapters to study the dynamics of the Kitaev chain and the Kibble-Zurek physics associated with various ramping protocols. It is important to mention that when we numerically solve the matrix differential equations (3.61) to study the dynamics of the Kitaev chain, we require the initial condition $\mathbf{C}(0)$. In our work we will initialise the system in a thermal state, and therefore the initial condition $\mathbf{C}(0)$ in terms of the Fourier Majorana fermion correlations can be found from the transformation in Eq. (3.64).

Chapter 4

Dynamic Kibble-Zurek scaling for the isolated Kitaev chain

In this chapter we study the non-equilibrium dynamics of the isolated long-range Kitaev chain. In particular, we implement what we call the standard quantum Kibble-Zurek (KZ) protocol. This ramping protocol describes a procedure in which a control parameter or coupling constant in the isolated system's Hamiltonian is varied, or ramped, continuously. The dynamics becomes particularly fascinating when the control parameter or coupling constant approaches a critical value associated with a QPT. For the Kitaev chain we focus on ramping the chemical potential μ, which enters through the dispersion relation $\lambda_{\phi,\alpha}$ of the system Hamiltonian (2.25). During the ramp we will monitor the density of excitations $\mathcal{E}$, which is expected to display universal scaling behaviour following a sufficiently slow ramp of μ through, or towards, the QCP. A ramp is regarded as *sufficiently slow* when only the low-energy modes—for which the energies $\lambda_{\phi,\alpha}(k)$ are accurately described by a power law in terms of the critical exponents—make a significant contribution to the excitation density.

The universal behaviour emerging in quantities such as the excitation density has already been studied for various models, including the short- and long-range Kitaev chain. In work by Dutta et al. [22] the role of long-range pairing on the non-equilibrium dynamics of the Kitaev chain is studied, with a focus on deriving the KZ scaling exponent that dictates the power-law behaviour of the excitation density. This scaling exponent is found to depend non-trivially on the distance decay parameter α of the pairing term. In this chapter we extend the results published in Ref. [22] to also include the case of long-range hopping, and provide a more general derivation of the scaling relations which does not depend on the asymptotic Landau-Zener transition probability (1.10).

In Section 4.1 we start with an introduction to the standard KZ protocol, and then illustrate the breakdown of adiabaticity in the vicinity of the QCP using numeric results for the Kitaev chain. Section 4.2 makes use of the Landau-Zener model introduced in Section 1.1.2 to derive a set of scaling relations for the isolated Kitaev chain. These analytic scaling predictions are subsequently supported by numeric results. We conclude with Section 4.3 in which we provide a brief summary of this chapter.

4.1 Standard quantum Kibble-Zurek protocol

In the context of the Kitaev chain Hamiltonian (2.25), the quantum Kibble-Zurek protocol describes the ramping of the chemical potential μ towards its critical value μ_c. We ramp the chemical potential linearly at a constant rate v, such that

$$\mu(t) = vt + \mu_i, \tag{4.1}$$

where the ramp starts at some large negative initial value μ_i and ends at μ_f. At μ_i the system is prepared in the many-particle ground state, which, for the diagonalised Kitaev chain Hamiltonian (2.25), is the vacuum state of the η-quasiparticles. At early times, the system will remain in its instantaneous ground state, and no η-quasiparticle modes are excited. Hence, the quasiparticle occupations $\langle \eta_k^\dagger \eta_k \rangle$ remain zero. However, if we ramp in the vicinity of the QCP, the inherent timescale of the system's dynamics becomes very long, referred to as *critical slowing down*. As explained in Section 1.1.2 and Section 1.1.3, this results in a breakdown of adiabaticity whereby the system is unable to transition through a sequence of instantaneous ground states and, as a result, will start populating exciting states.

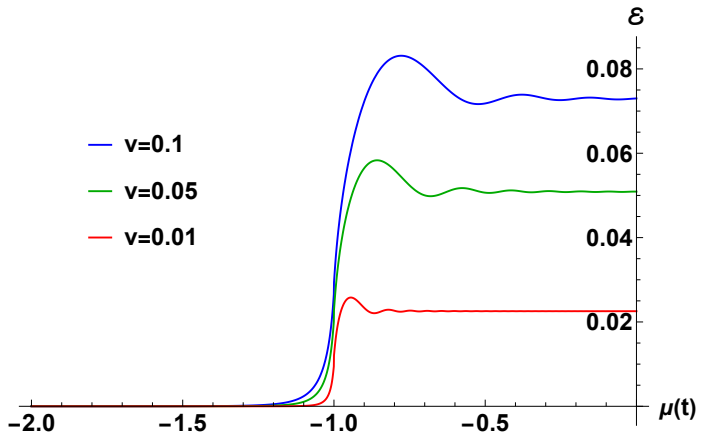

Figure 4.1: The excitation density $\mathcal{E}$ of the nearest-neighbour Kitaev chain during a ramp as a function of the chemical potential $\mu(t)$. Results are shown for three different ramp rates, $v = 0.1, 0.05$ and 0.01, with faster ramps resulting in the system being pushed further out of equilibrium. Parameter values are set to $L = 450$, $J = 1$, $\Delta = 1$, $\mu_i = -5$ and $\mu_f = 0$.

The loss of adiabaticity associated with this critical slowing down can be observed by monitoring the excitation density during the ramp. We will define the excitation density as the sum of the occupation numbers (excitation probabilities) $\mathcal{P}_k(t) = \langle \eta_k^\dagger \eta_k \rangle(t)$ over all the instantaneous quasiparticle modes at time t, divided by the system size L. We write this compactly as

$$\mathcal{E}(t) = \frac{1}{L}\sum_k \mathcal{P}_k(t) = \frac{1}{L}\sum_k \langle \eta_k^\dagger \eta_k \rangle(t). \tag{4.2}$$

In the thermodynamic limit $L \to \infty$ the lattice momentum k assumes continuous values and Eq. (4.2) becomes

$$\mathcal{E}(t) = \frac{1}{2\pi}\int_{-\pi}^{\pi} dk\, \mathcal{P}_k(t) = \frac{1}{2\pi}\int_{-\pi}^{\pi} dk\, \langle \eta_k^\dagger \eta_k \rangle(t) \tag{4.3}$$

for the one-dimensional chain. The excitation probability $\mathcal{P}_k$ for each k-mode can be computed directly from the time-dependent correlation functions $\mathbf{C}_{\{k,-k\}}(t)$ using Eq. (3.65) in Chapter 3. Upon application of Eq. (4.2), we can then determine the excitation density. Numeric results for $\mathcal{E}$ are presented in Fig. 4.1 for the nearest-neighbour Kitaev chain. The figure illustrates the generation of excitations—and subsequent breakdown of adiabaticity—when the critical point at $\mu_c = -1$ is traversed during the ramp. For faster ramp rates the loss of adiabaticity sets in earlier, i.e. at smaller values of μ, and the system is driven further out of equilibrium. This can be understood through the condition for adiabatic evolution, which for a particular k-mode is[1]

$$\sqrt{v} \ll \lambda_{\phi,\alpha}(k). \tag{4.4}$$

For lower-energy modes this condition is violated more readily, leading to the generation of excitations. Furthermore, the unavoidable closure of the energy gap for the $k = 0$ mode in the Kitaev chain spectrum means that condition (4.4) cannot be satisfied at the QCP, no matter how slow the ramp. The density of excitations that emerge as a result of the breakdown of adiabaticity at the phase transition is expected to scale universally with the ramp rate v. We regard the scaling as universal, since the scaling laws describing the functional relationship between the excitation density and ramp rate depend only on the equilibrium critical exponents. These critical exponents, which describe the behaviour of physical quantities near a QPT, are independent of the model's specific details [107, 108]. This allows us to group a collection of models with similar behaviour and general features into a single universality class, where all the models within this prescribed class share the same critical exponents [107, 108]. As such, the behaviour of systems in the vicinity of QPTs can be deduced without any comprehensive knowledge of the details of the system itself. In the next section we derive scaling relations that describe the universal behaviour of the density of excitations.

[1] In Appendix A we provide details on the derivation of the adiabatic-following condition for the Landau-Zener problem, which was introduced in Section 1.1.2. Within the context of the Landau-Zener model and Section 4.2.1, the results in the appendix can be generalised to the isolated Kitaev chain to obtain the condition in Eq. (4.4).

4.2 Scaling relations for the coherent excitation density

The excitations that are generated during the KZ ramping protocol are expected to scale with the ramp rate in a power-law fashion. In Section 4.2.1 we study the single-mode excitation probability for the Kitaev chain within the Landau-Zener picture. This will provide us with several important tools for deriving scaling relations for the density of quasiparticle excitations in Section 4.2.2. In preparation for the work that follows in Chapter 5, we consider ramps ending at the critical point. The scaling exponents are found to exhibit a non-trivial dependence on the long-range parameters ϕ and α, where $\phi, \alpha = 2$ pinpoints the boundary between the short- and long-range scaling behaviours. In Section 4.2.3 the Kibble-Zurek scaling predictions are derived and compared to our analytic results. We observe agreement with these predictions, except for the case of long-range hopping. Finally, Section 4.2.4 presents numeric results to verify the analytically derived scaling relations.

4.2.1 Single-mode excitation probability within the Landau-Zener picture

The evolution of the excitation probability $\langle \eta_k^\dagger \eta_k \rangle(t)$ for a single η_k-mode in the Kitaev chain can be described by mapping this problem onto the Landau-Zener model introduced in Section 1.1.2. This important link between the fermionic and Landau-Zener pictures is discussed further in Appendix C. The two-level description of the excitation probability dynamics in the LZ language forms the basis from which we will derive scaling relations for the density of quasiparticle excitations in Section 4.2.2.

The 2×2 matrices defining the system Hamiltonian H_{LRK} in Eq. (2.21) are used to map the single η_k-mode excitation probabilities of the Kitaev chain onto the two-level LZ model. In the diabatic basis $\{|1\rangle, |2\rangle\}$, this two-level representation for a single η_k-mode is described by the time-dependent Hamiltonian

$$H_k(t) = \begin{bmatrix} A_k(t) & iB_k \\ -iB_k & -A_k(t) \end{bmatrix}, \tag{4.5}$$

with eigenenergies

$$\pm \lambda_k(t) = \pm \sqrt{A_k^2(t) + B_k^2}, \tag{4.6}$$

where $A_k(t) = A_{-k}(t) = 2Jg_\phi(k) + 2\mu(t)$ and $B_k = -B_{-k} = \Delta f_\alpha(k)$. The coupling B_k is time-independent, while the energy-level spacing has a linear time dependence given by $\mu(t)$ in Eq. (4.1). The two-level Hamiltonian (4.5) governs the evolution of the time-dependent state $|\psi_k(t)\rangle$ of the system. This state is given by

$$|\psi_k(t)\rangle = u_k(t)\,|1\rangle + v_k(t)\,|2\rangle\,, \tag{4.7}$$

where $|1\rangle = \begin{bmatrix} 1 & 0 \end{bmatrix}^{\text{T}}$ and $|2\rangle = \begin{bmatrix} 0 & 1 \end{bmatrix}^{\text{T}}$. From the Schrödinger equation (1.2), together with Eqs. (4.5) and (4.7), we find the equations of motion governing the dynamics of the state $|\psi_k(t)\rangle$ to be

$$i\frac{d}{dt}u_k(t) = A_k(t)u_k(t) + iB_k v_k(t) \qquad \text{and} \qquad i\frac{d}{dt}v_k(t) = -iB_k u_k(t) - A_k(t)v_k(t). \tag{4.8}$$

At any given time, the Hamiltonian $H_k(t)$ in Eq. (4.5) has two instantaneous eigenstates. The $-\lambda_k$ and $+\lambda_k$ eigenstates of $H_k(t)$ will be denoted by $|g(t)\rangle$ and $|e(t)\rangle$, respectively. We can therefore write the transition amplitude at time t in terms of the system's state $|\psi_k(t)\rangle$ and the instantaneous eigenstate $|e(t)\rangle$ as $\langle \psi_k(t)|e(t)\rangle$. This transition amplitude will depend on the various parameters entering through the A_k and B_k functions. In the work that follows, it will be convenient to formulate this amplitude in terms of dimensionless parameters. To this end, we introduce

$$\chi(k,t) = \frac{A_k(t)}{\sqrt{2v}} = \frac{2Jg_\phi(k) + 2\mu(t)}{\sqrt{2v}} \qquad \text{and} \qquad \omega(k) = \frac{B_k}{\sqrt{2v}} = \frac{\Delta f_\alpha(k)}{\sqrt{2v}}, \tag{4.9}$$

where v is the ramp rate. In terms of the dimensionless parameters $\chi(k,t)$ and $\omega(k)$, we write the probability amplitude as

$$A[\chi(k,t), \omega(k)] = \langle \psi_k(t)|e(t)\rangle\,. \tag{4.10}$$

An exact expression for $A[\chi(k,t), \omega(k)]$ can be derived, provided we have the initial conditions at the initial time t_i. In our analytic work we start in the ground state $|g(t_i)\rangle = |1\rangle$ at $\mu(t_i) = \mu_i = -\infty$. To obtain the probability amplitude $A[\chi(k,t), \omega(k)]$ (4.10), we first solve for u_k and v_k in Eq. (4.8) in terms of parabolic

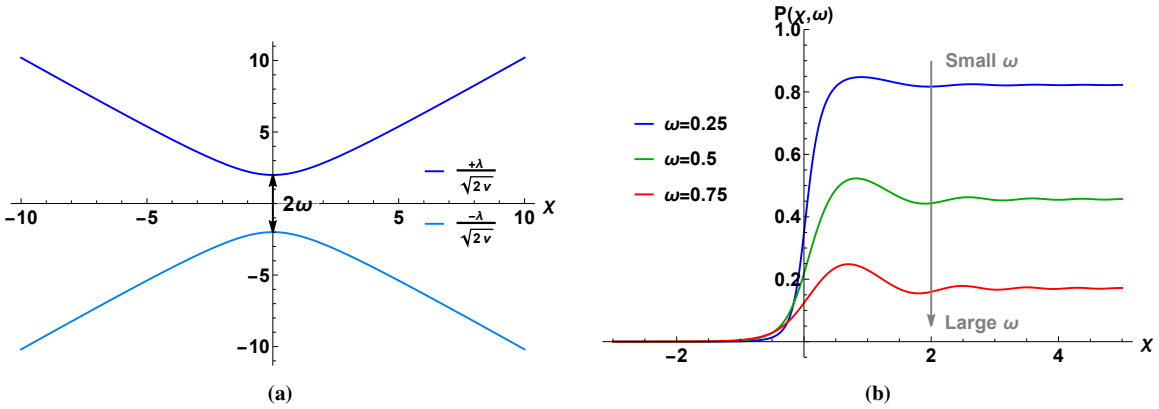

Figure 4.2: **(a)** The dimensionless eigenenergies $\pm\lambda_k(t)/\sqrt{2v}$ as functions of χ, showing the instantaneous excitation gap which is minimal at $\chi = 0$ with a value of 2ω. **(b)** The excitation probability $P(\chi,\omega)$ as a function of χ for $\omega = 0.25, 0.5$ and 0.75. $P(\chi,\omega)$ increases rapidly close to the avoided level-crossing at $\chi = 0$ before stabilising to its long-time value.

cylinder functions $D_n(z)$, which are solutions to the Weber equation [15, 20, 109]. It is then possible to calculate the inner product in Eq. (4.10). Details on the solution to the differential equations (4.8), as well as the derivation of the probability amplitude, are provided in Appendix C. This leads to

$$\begin{aligned} A(\chi,\omega) = {} & \frac{1}{\sqrt{\pi}}(1+i)2^{-2+\frac{i\omega^2}{4}} e^{-\frac{3\pi\omega^2}{8}+\frac{i}{2}} \\ & \times \left[(1-i)\sqrt{1+\frac{\chi}{\sqrt{\chi^2+\omega^2}}}\,\Gamma\left(1-\frac{i\omega^2}{2}\right)\left(e^{\frac{\pi\omega^2}{2}} D_{\frac{i\omega^2}{2}-1}((1-i)\chi) + D_{\frac{i\omega^2}{2}-1}((-1+i)\chi)\right)\right. \\ & \left. - i\omega\sqrt{1-\frac{\chi}{\sqrt{\chi^2+\omega^2}}}\,\Gamma\left(-\frac{i\omega^2}{2}\right)\left(D_{\frac{i\omega^2}{2}}((-1+i)\chi) - e^{\frac{\pi\omega^2}{2}} D_{\frac{i\omega^2}{2}}((1-i)\chi)\right)\right]. \end{aligned} \tag{4.11}$$

Using the result above, we now write the occupation $\langle\eta_k^\dagger\eta_k\rangle(t_f)$ of the η_k-mode at a final time $t = t_f$ as

$$p_k = \langle\eta_k^\dagger\eta_k\rangle(t_f) = |A[\chi(k,t_f),\omega(k)]|^2 =: P[\chi(k,t_f),\omega(k)]. \tag{4.12}$$

The behaviour of the excitation probability $P(\chi,\omega)$ will be essential for making a series of sensible approximations in Section 4.2.2 to extract the scaling of the excitation density with v.

Our understanding of the behaviour of $P(\chi,\omega)$ will rely heavily on the physical interpretation of the dimensionless parameters χ and ω. The parameter χ is an effective measure of the closeness to the avoided level-crossing at $\chi = 0$, and ω is an effective measure of the minimum value of the excitation gap. Using Eqs. (4.6) and (4.9), we express the excitation gap of H_k in terms of χ and ω as

$$\lambda_k(t) = \sqrt{2v}\sqrt{\chi^2(k,t)+\omega^2(k)}. \tag{4.13}$$

This excitation gap is illustrated in Fig. 4.2a, with the minimum gap occurring at the avoided level-crossing. This minimum in the system's excitation gap at $\chi = 0$ corresponds to a slowing down of the system's dynamics. Subsequently, there is potentially a breakdown in the adiabatic evolution, as discussed in Section 1.1.2 for the LZ model. This leads to the excitation probability increasing rapidly close to $\chi = 0$ before stabilising to its long-time value, as observed in Fig. 4.2b where we used the exact analytic expressions (4.11) and (4.12) with various choices for ω. As discussed earlier, the value of ω impacts on the size of the gap in the excitation spectrum at the avoided level-crossing. Since the gap closes with decreasing ω, a smaller ω value results in a noticeably larger excitation probability, as observed in Fig. 4.2b.

We now discuss some qualitative trends of the function $P(\chi,\omega)$, which will be important for deriving scaling relations in subsequent sections. These discussions will closely reference Fig. 4.2, and rely on the physical interpretation of χ and ω in the previous paragraph. First note that the ramps are terminated at the critical point μ_c at a final time t_f, where $\mu_f = \mu_c = -Jg_\phi(0)$. As a result, $\chi(k,t_f) < 0$ for all $k \neq 0$ modes. The zero mode is a special case for which $\chi(0,t_f) = 0$. When χ is identically zero we are

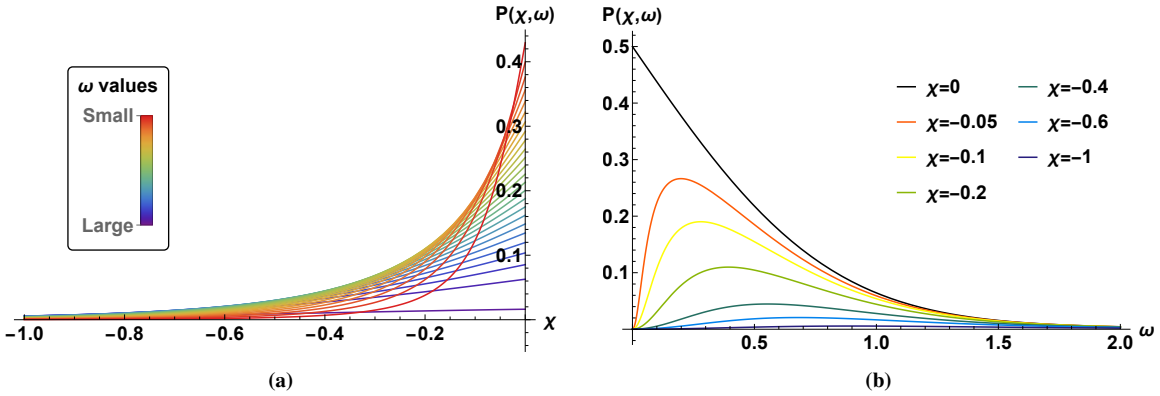

Figure 4.3: (a) $P(\chi,\omega)$ is a strictly decreasing function of χ for $\chi \leq 0$. **(b)** $P(\chi,\omega)$ is an increasing function of ω for $\chi \leq 0$ and small ω, and a decreasing function of ω when ω is large.

stopping the ramp at the avoided level-crossing, as illustrated in Fig. 4.2a. In all other cases χ is strictly negative, implying that the ramp is terminated before the level-crossing for the mode in question is reached. The further χ is from the level-crossing, the easier it becomes to satisfy the adiabatic-following condition in Eq. (4.4). We therefore expect the excitation probability $P(\chi,\omega)$ to be small for sufficiently large negative χ. This is equivalent to stating that $P(\chi,\omega)$ is small for the high momentum modes. In fact, the excitation probability for increasingly high momenta quickly becomes negligible, allowing it to be safely neglected in later calculations. However, when χ is in the neighbourhood of $\chi = 0$, the condition in Eq. (4.4) is potentially violated, resulting in a breakdown of adiabaticity and subsequently non-negligible excitation probabilities. It is therefore the low momentum modes which will contribute significantly to the excitation density. This is supported by Fig. 4.3a, where $P(\chi,\omega)$ is shown to be a decreasing function of χ when $\chi \leq 0$.

The behaviour of the excitation probability $P(\chi,\omega)$ with ω is more subtle. Recall that ω is an effective measure of the closure of the excitation gap. Based on this interpretation and Fig. 4.2a, it is unsurprising that $P(\chi,\omega)$ is a decreasing function of ω at $\chi = 0$. Both the figures in 4.3 show this trend. For $\chi < 0$, $P(\chi,\omega)$ is an increasing function of ω when ω is small, and a decreasing function when ω is large. This is supported by Fig. 4.3b, confirming that the low momentum modes will correspond to the largest excitation probabilities. In the next section we will use these qualitative trends of the excitation probability $P(\chi,\omega)$ to derive asymptotic scaling relations for the coherent excitation density.

4.2.2 Derivation of asymptotic scaling relations for the coherent excitation density

In the previous section we focused on the single-mode excitation probability within the Landau-Zener picture. The exact analytic expression for the excitation probability in the two-level representation will now be used to study the coherent excitation density $\mathcal{E}_{\text{coh}}$. Using the notation introduced above and the definition in Eq. (4.3), the density of excitations is

$$\mathcal{E}_{\text{coh}} = \frac{1}{2\pi}\int_{-\pi}^{\pi} dk\, P(\chi(k,t_f),\omega(k)) = \frac{1}{\pi}\int_{0}^{\pi} dk\, P(\chi(k,t_f),\omega(k)), \tag{4.14}$$

where we exploited the $k \leftrightarrow -k$ symmetry of the modes. According to the integral expression above, the excitation density $\mathcal{E}_{\text{coh}}$ is determined by the values of the excitation probability $P(\chi,\omega)$ along the curve $\{(\chi(k,t_f),\omega(k)) : k \in [0,\pi]\}$ in the $\chi-\omega$ plane. Figure 4.4a shows three such curves for different distance decay parameters. To eliminate the simple, but ultimately very important dependence of χ and ω on the ramp rate v we have chosen to scale the two axes by factors of $\sqrt{v}$. This emphasises that curves for different ramp rates just differ by a simple rescaling. In all cases the curves start at the point $(\chi(0,t_f),\omega(0)) = (0,0)$, and terminate at a point $(\chi(\pi,t_f) < 0, 0)$. As was argued in the previous section, we expect the low momentum modes to make the dominant contribution to $\mathcal{E}_{\text{coh}}$. Figure 4.4b reiterates this by illustrating that $P(\chi,\omega)$ will be negligible for the high momentum modes. In the context of Fig. 4.4a, it is the modes for which $(\chi(k,t_f),\omega(k))$ lies close to the origin for which the excitation probability $P(\chi,\omega)$ will be non-negligible. Since both $\chi(k,t_f)$ and $\omega(k)$ are proportional to $v^{-1/2}$, the range of contributing modes is expected to shrink with decreasing v, as illustrated in Fig. 4.4b. More precisely, only the modes in a small neighbourhood of $k = 0$ contribute to $\mathcal{E}_{\text{coh}}$ when the ramp rate is very slow. This motivates the introduction of the lowest order in k approximations of χ and ω.

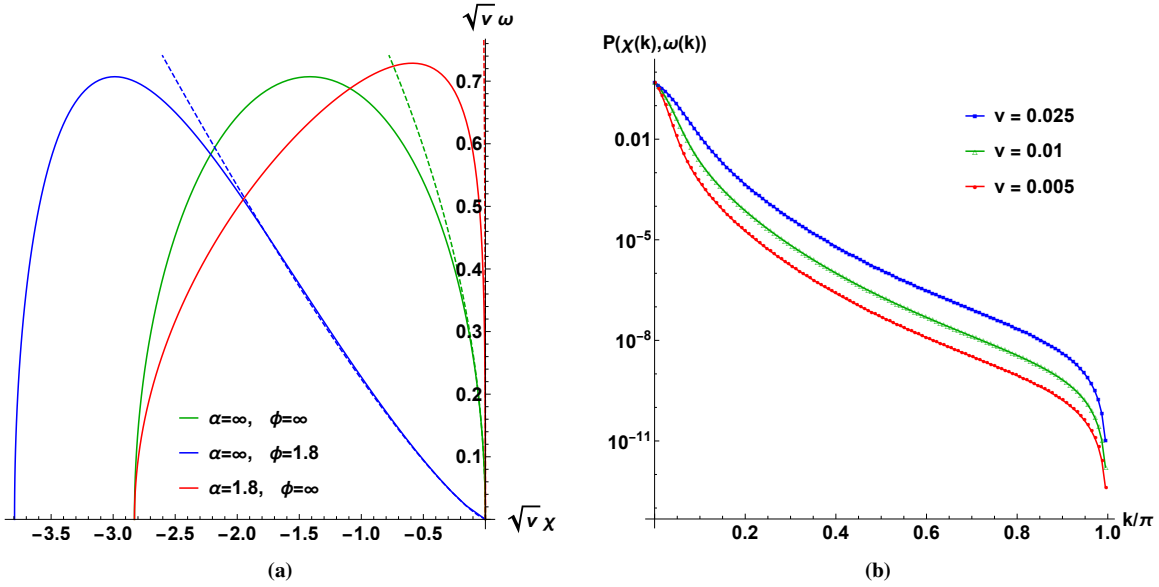

Figure 4.4: **(a)** Three curves $\{(\chi(k,t_f),\omega(k)) \,:\, k\in[0,\pi]\}$ in the $\chi-\omega$ plane, parametrised by k, for different distance decay parameters. The two axes are scaled by factors of $\sqrt{v}$ to eliminate the dependence of χ and ω on the ramp rate v. For the low momentum modes, for which $(\chi(k,t_f),\omega(k))$ lies close to the origin, the curves are well approximated by the lowest order in k approximations in Eq. (4.15), which are indicated by the dashed curves. **(b)** An indication of the range of contributing modes to $P(\chi,\omega)$ for three ramp rates, $v=0.005$, 0.01 and 0.025. The range of modes which contribute significantly shrinks with decreasing v, and the dominant contribution to the excitation density $\mathcal{E}_{\text{coh}}$ will come from modes around $k=0$, where $P(\chi,\omega)$ is noticeably larger.

For sufficiently slow ramp rates, χ and ω in Eq. (4.9) can be replaced by their lowest order in k approximations

$$\chi(k,t_f)\approx\chi_0(k)=-\frac{\mathcal{G}(\phi)}{\sqrt{v}}k^a \qquad \text{and} \qquad \omega(k)\approx\omega_0(k)=\frac{\mathcal{F}(\alpha)}{\sqrt{v}}k^b, \qquad k\geq 0, \tag{4.15}$$

as motivated above. Here the a and b exponents are the powers of the leading-order terms in the small-k expansions of $g_\phi^\infty(k)$ and $f_\alpha^\infty(k)$ in Eqs. (2.40) and (2.34), while $\mathcal{G}(\phi)$ and $\mathcal{F}(\alpha)$ are ϕ- and α-dependent coefficients. Replacing $\chi(k,t_f)$ and $\omega(k)$ in $P(\chi,\omega)$ by their approximations in Eq. (4.15) results in the approximate excitation probability $P(\chi_0(k),\omega_0(k))$. We expect $P(\chi_0(k),\omega_0(k))$ to agree with the exact excitation probability for low momentum modes, where the contribution to $\mathcal{E}_{\text{coh}}$ is largest. This is validated by Fig. 4.4a where $\chi(k,t_f)$ and $\omega(k)$ are shown to be well approximated by $\chi_0(k)$ and $\omega_0(k)$ for the low momentum modes. In addition, we note that the magnitudes of $\chi_0(k)$ and $\omega_0(k)$ grow with increasing k. Hence, in the regions where $\chi(k,t_f)$ and $\omega(k)$ are not well approximated by their lowest-order approximations, i.e. for large-k modes, the contribution of $P(\chi_0(k),\omega_0(k))$ to the excitation density will be negligible. Based on these observations, we extend the upper bound of the integral in Eq. (4.14) to ∞, and replace $\chi(k,t_f)$ and $\omega(k)$ in the integrand by their lowest order in k approximations, $\chi_0(k)$ and $\omega_0(k)$, from Eq. (4.15). This leads to

$$\mathcal{E}_{\text{coh}}=\frac{1}{\pi}\int_0^\infty dk\, P[\chi_0(k),\omega_0(k)]=\frac{1}{\pi}\int_0^\infty dk\, P\left[-\frac{\mathcal{G}(\phi)}{\sqrt{v}}k^a,\frac{\mathcal{F}(\alpha)}{\sqrt{v}}k^b\right]. \tag{4.16}$$

For the sake of clarity, we write the a and b exponents in the leading-order approximations (4.15) in terms of the distance decay parameters from Eqs. (2.40) and (2.34) as

$$a=\begin{cases}\phi-1, & 1<\phi<3\\ 2, & \phi>3\end{cases} \qquad \text{and} \qquad b=\begin{cases}\alpha-1, & 1<\alpha<2\\ 1, & \alpha>2\end{cases}. \tag{4.17}$$

The small-v asymptotic behaviour of $\mathcal{E}_{\text{coh}}$ in Eq. (4.16) varies depending on the values of the hopping and pairing parameters, ϕ and α. In Section 4.2.2.1 we will study the small-v asymptotic behaviour of $\mathcal{E}_{\text{coh}}$ for short-range hopping $(\phi>2)$ and arbitrary-range pairing $(\alpha>1)$. Following the same procedure in Section 4.2.2.2, we derive exact asymptotic results for the scaling of $\mathcal{E}_{\text{coh}}$ when the Kitaev chain hopping term is long-range $(1<\phi<2)$ and the pairing term is short-range $(\alpha>2)$.

4.2.2.1 Asymptotic scaling relation for short-range hopping and arbitrary pairing

For short-range hopping ($\phi > 2$) and arbitrary pairing ($\alpha > 1$) we have that $b \leq a$ from Eq. (4.17). The change of variable $k \to [\sqrt{v}/\mathcal{F}]^{1/b} k$ in Eq. (4.16) then leads to

$$\mathcal{E}_{\text{coh}} = \frac{1}{\pi}\left[\frac{\sqrt{v}}{\mathcal{F}}\right]^{1/b} \int_0^\infty dk\, P\left(\frac{-\mathcal{G}}{\mathcal{F}^{a/b}}\sqrt{v}^{(a/b-1)}k^a, k^b\right). \tag{4.18}$$

To extract the small-v asymptotic behaviour of $\mathcal{E}_{\text{coh}}$ from the expression above we require that the $v \to 0$ limit of the integral exists and is finite. Provided these requirements are met, the dominant scaling behaviour will come from the prefactor in Eq. (4.18). We will motivate that the integral has a well defined $v \to 0$ limit by first considering the small-v behaviour of the integrand in Eq. (4.18). Based on earlier discussions on the excitation probability, the integrand $P\left(\frac{-\mathcal{G}}{\mathcal{F}^{a/b}}\sqrt{v}^{(a/b-1)}k^a, k^b\right)$ will be a decreasing function of $\frac{\mathcal{G}}{\mathcal{F}^{a/b}}\sqrt{v}^{(a/b-1)}k^a$. More precisely, the integrand increases as the ramp rate v slows down. However, it is important to mention that the integrand does not increase indefinitely, since it is bounded from above by its $v \to 0$ value of $P\left(0, k^b\right)$. The integral therefore exists, and the leading-order result for the excitation density is written as

$$\mathcal{E}_{\text{coh}} = v^{1/(2b)}\left[\frac{\mathcal{F}^{-1/b}}{\pi}\int_0^\infty dk\, P\left(0, k^b\right)\right], \tag{4.19}$$

which scales with the ramp rate v as $\mathcal{E}_{\text{coh}} \propto v^{1/(2b)}$. A necessary condition for the integral in Eq. (4.19) to converge is $4b > 1$, since it can be shown that $P(0,\omega) \sim 1/\omega^4$.

4.2.2.2 Asymptotic scaling relation for long-range hopping and short-range pairing

In this section we will consider the small-v asymptotic behaviour of $\mathcal{E}_{\text{coh}}$ for long-range hopping ($1 < \phi < 2$) and short-range pairing ($\alpha > 2$). According to Eq. (4.17), long-range hopping and short-range pairing translates into the condition that $b > a$. We now perform the change of variable $k \to [\sqrt{v}/\mathcal{G}]^{1/a} k$ in Eq. (4.16) which gives

$$\mathcal{E}_{\text{coh}} = \frac{1}{\pi}\left[\frac{\sqrt{v}}{\mathcal{G}}\right]^{1/a} \int_0^\infty dk\, P\left(-k^a, \frac{\mathcal{F}}{\mathcal{G}^{b/a}}\sqrt{v}^{(b/a-1)}k^b\right). \tag{4.20}$$

Extracting the small-v asymptotic behaviour of $\mathcal{E}_{\text{coh}}$ from the expression above is slightly more difficult than in the previous case.

In order to follow the same procedure as in Section 4.2.2.1, we reformulate Eq. (4.20) as

$$\mathcal{E}_{\text{coh}} = \frac{1}{\pi}\left[\frac{\sqrt{v}}{\mathcal{G}}\right]^{1/a} v^{b/a-1} \int_0^\infty dk\, v^{1-b/a} P\left(-k^a, \frac{\mathcal{F}}{\mathcal{G}^{b/a}}\sqrt{v}^{(b/a-1)}k^b\right). \tag{4.21}$$

Unlike in Section 4.2.2.1, the function $P\left(-k^a, \frac{\mathcal{F}}{\mathcal{G}^{b/a}}\sqrt{v}^{(b/a-1)}k^b\right)$ does not behave in a simple, monotonic way as $v \to 0$ or, equivalently, as $\omega \to 0$. See for example Fig. 4.3b. If we identify $\omega = \frac{\mathcal{F}}{\mathcal{G}^{b/a}}\sqrt{v}^{(b/a-1)}k^b$ in the excitation probability function P in Eq. (4.21), then it follows that $v^{1-b/a} \sim 1/\omega^2$. From Fig. 4.5 we observe that the integrand $\sim P(\chi,\omega)/\omega^2$ in Eq. (4.21) is a monotonically decreasing function of ω. As discussed previously, the integrand therefore increases with decreasing v, but is bounded from above by its $v \to 0$ value of

$$\lim_{\omega\to 0}\frac{P(\chi,\omega)}{\omega^2} = \frac{1}{8\pi\chi^2}h(\chi), \tag{4.22}$$

where $h(\chi)$ is a function of χ containing parabolic cylinder functions and their derivatives. The exact expression for $h(\chi)$ is provided in Appendix G. Based on the arguments made above, the dominant scaling behaviour will reside in the prefactor of Eq. (4.21), and the exact small-v asymptotic result for the excitation density when $b > a$ is

$$\mathcal{E}_{\text{coh}} = v^{(1+2b)/(2a)-1}\left[\frac{\mathcal{F}^2}{8\pi^2}\mathcal{G}^{-1/a-2b/a}\int_0^\infty dk\, k^{2(b-a)}h\left(-k^a\right)\right]. \tag{4.23}$$

As expected, $\mathcal{E}_{\text{coh}}$ scales with v as $\mathcal{E}_{\text{coh}} \propto v^{(1+2b)/(2a)-1}$. The scaling prediction (4.23) is only valid when the condition for integral convergence, $6a - 2b > 1$, is met.

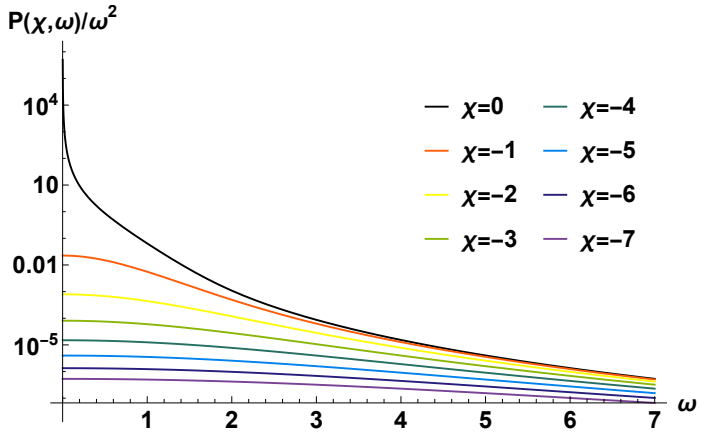

Figure 4.5: $P(\chi,\omega)/\omega^2$ as a function of ω for a series of $\chi \leq 0$ values. The function $P(\chi,\omega)/\omega^2$ is monotonically decreasing with ω for all $\chi \leq 0$.

4.2.2.3 Summary of scaling relations

In the preceding sections we derived asymptotic scaling relations for the coherent excitation density for various distance decay parameter values. These results, as given in Eqs. (4.19) and (4.23), can be reformulated in terms of the Kitaev chain distance decay parameters ϕ and α using Eq. (4.17). In summary, the exact $v \to 0$ asymptotic results are

$$\mathcal{E}_{\text{coh}} \propto \begin{cases} v^{1/2} & \text{if} \quad \phi, \alpha > 2 \\ v^{1/[2(\alpha-1)]} & \text{if} \quad \phi > 2, \quad 0 < \alpha < 2 \\ v^{3/[2(\phi-1)]-1} & \text{if} \quad \alpha > 2, \quad 3/2 < \phi < 2 \end{cases} . \tag{4.24}$$

Based on the theoretical scaling predictions (4.24), we expect the scaling exponent to saturate to the short-range value of $1/2$ for $\phi, \alpha > 2$. In contrast, the scaling exponent for the long-range hopping and pairing cases will depend non-trivially on the distance decay parameters. For long-range pairing the predicted scaling exponent of $1/[2(\alpha-1)]$ is in agreement with the results published in Ref. [22]. We extended the results in Ref. [22] to also consider long-range hopping, for which the scaling exponent is $3/[2(\phi-1)]-1$. Both of the long-range scaling exponents reduce to the short-range value of $1/2$ when $\phi, \alpha \to 2$, marking the boundary between the short- and long-range scaling behaviours.

The asymptotic results in Eq. (4.24) are only applicable in the limit of very slow ramp rates. It is therefore important to question the extent to which this scaling behaviour will emerge if the ramp rate v is finite. This will depend on the magnitudes of the sub-leading terms that were neglected in multiple steps of our derivation. A more detailed analysis on the expected range of validity for the scaling in the nearest-neighbour Kitaev chain for finite v appears in Appendix D. We find that, in the majority of cases, a necessary condition for the predicted scaling in v to materialise in $\mathcal{E}_{\text{coh}}$ is

$$v \ll \frac{2\pi^2 \Delta^4}{J^2}. \tag{4.25}$$

As expected, the scaling emerges when the ramp rate v is sufficiently slow.

4.2.3 Kibble-Zurek scaling prediction

In Section 1.1.3 we showed that the general Kibble-Zurek scaling result predicts that the density of excitations scales in a power-law fashion with the ramp rate v. More precisely, according to Eq. (1.19) we have

$$\mathcal{E}_{\text{coh}} \propto v^{\frac{d\nu}{1+\nu z}}. \tag{4.26}$$

For the Kitaev chain $d = 1$ is the number of space dimensions, and the critical exponents ν and z need to be determined. It is possible to obtain these critical exponents by determining the universality class of our model. Here we will use a different approach, whereby the exponents are extracted via the asymptotics of the dispersion relation (2.26). The relevant energy scale, which is given by $\lambda_{\phi,\alpha}(k)$ in Eq. (2.26), vanishes

for the $k = 0$ mode as the critical value μ_c is approached. This energy gap that vanishes can be related to the reaction time τ (1.12), which governs how quickly the system can respond to external perturbations, as $\tau^{-1} \simeq \lambda_{\phi,\alpha}(0)$. Using Eq. (1.14), the critical exponent νz is therefore determined directly from the dispersion relation at $k = 0$ as

$$\lambda_{\phi,\alpha}(0) \sim |\mu - \mu_c|^{z\nu} = |\mu - \mu_c|, \tag{4.27}$$

which leads to $z\nu = 1$. Work published in Ref. [110] notes that at a quantum critical point the dynamical critical exponent z is a property of the gapless dispersion relation. To this end, we extract the exponent z from the dispersion relation (2.26) by considering the leading-order behaviour in k at the critical point where $\mu = \mu_c$. In general we have

$$\lambda_{\phi,\alpha}(k) \sim k^z \tag{4.28}$$

at the quantum critical point [50, 110]. With reference to the low-energy approximations (2.41) of the dispersion relation, a combination of Eqs. (4.27) and (4.28) leads to

$$z = \nu^{-1} = \begin{cases} 1 & \text{(SR pairing and hopping)} \\ \alpha - 1 & \text{(LR pairing and SR hopping)} \\ \phi - 1 & \text{(LR hopping and SR pairing)} \end{cases}, \tag{4.29}$$

where SR and LR denote short-range and long-range, respectively. It follows from Eqs. (4.26) and (4.29) that the predicted Kibble-Zurek scaling is

$$\mathcal{E}_{\text{coh}} \propto \begin{cases} v^{1/2} & \text{if} \quad \alpha > 2 \text{ and } \phi > 2 & \text{(SR pairing and hopping)} \\ v^{1/[2(\alpha-1)]} & \text{if} \quad 1 < \alpha < 2 \text{ and } \phi > 2 & \text{(LR pairing)} \\ v^{1/[2(\phi-1)]} & \text{if} \quad \alpha > 2 \text{ and } 1 < \phi < 2 & \text{(LR hopping)} \end{cases}. \tag{4.30}$$

The scaling laws derived using the LZ model in Section 4.2.2 are in agreement with the Kibble-Zurek scaling predictions for the Kitaev chain with short-range hopping ($\phi > 2$) and arbitrary-range pairing ($\alpha > 1$). When considering the Kitaev chain with long-range hopping, i.e. $\phi \in (1, 2)$, the scaling exponent $(3/[2(\phi - 1)] - 1)$ in Eq. (4.24), which was derived from the exact expression for the excitation probability, differs from the KZ prediction of $1/[2(\phi - 1)]$ in Eq. (4.30). This discrepancy may be a consequence of the point at which the ramp is terminated. For short-range systems it is known that the end point of the ramp—whether that be at the critical point or after leaving the quantum critical region—does not alter the scaling laws [111]. For sufficiently long-range systems, however, it has been shown in work by Defenu et al. [111] that ending the ramp at different points can lead to the emergence of different scaling laws. In our work we terminate the ramp exactly at the critical point, where the correlation length diverges. This is different from the KZ argument, where the ramp is terminated after passing through the QCP in a region where the correlation length is finite. It is therefore not surprising that the results differ. Further investigation into the Kitaev chain's spatial correlations and correlation lengths is required to provide further insight on this matter. Despite the discrepancy, $\mathcal{E}_{\text{coh}}$ is still expected to scale universally with the ramp rate. In the next section we show that the numeric results for the Kitaev chain support the analytic scaling laws (4.24), including the case of long-range hopping.

4.2.4 Numeric results

In this section we will benchmark our analytic predictions for the scaling behaviour of the excitation density against results obtained by evaluating the integral expression in Eq. (4.16) numerically. The latter represents the excitation density in the $L \to \infty$ limit. This calculation requires an efficient means of evaluating the excitation probability $P(\chi, \omega)$, for which different techniques were used depending on the regime of $\chi - \omega$ parameter space we were considering. It was found that using the analytic expression in Eq. (4.11) was not always tractable, due to the parabolic cylinder functions being slow to evaluate. In the region $\chi < -5$ or $\omega > 5$ the excitation probability is small and varies slowly, which allows it to be calculated using interpolation on a set of data points obtained from solving the differential equations (4.8) numerically. When $-5 < \chi < 0$ and $0 < \omega < 5$ the excitation probability is large and varies rapidly, and so in this regime we use the analytic result for the probability amplitude in Eq. (4.11). Combining these two approaches enables us to efficiently compute the integral for the excitation density in Eq. (4.16).

In Fig. 4.6 the excitation density $\mathcal{E}_{\text{coh}}$ is shown as a function of the ramp rate v for a series of long-range pairing and hopping parameters, all greater than the boundary value of 2. The a- and b-dependencies, or

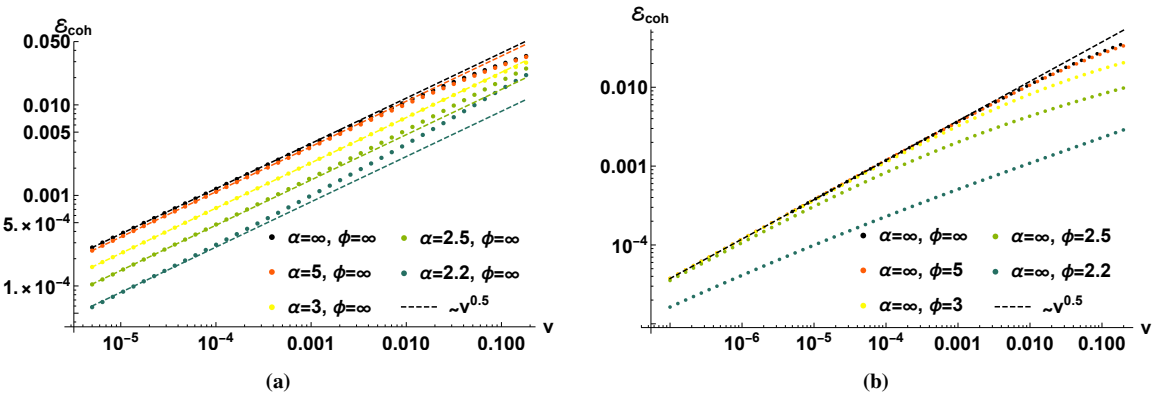

Figure 4.6: **(a)** The excitation density $\mathcal{E}_{\text{coh}}$ as a function of the ramp rate v for a series of pairing parameter values, $\alpha > 2$, with the hopping parameter fixed at $\phi \to \infty$ (nearest-neighbour hopping). The dashed lines correspond to the analytic scaling result in Eq. (4.24). **(b)** The same as (a), but for a series of hopping parameter values, $\phi > 2$, with the pairing parameter fixed at $\alpha \to \infty$ (nearest-neighbour pairing). The remaining parameters in both (a) and (b) are set to $L = \infty$, $J = 1$, $\Delta = 1$, $\mu_i = -\infty$ and $\mu_f = \mu_c = -1$.

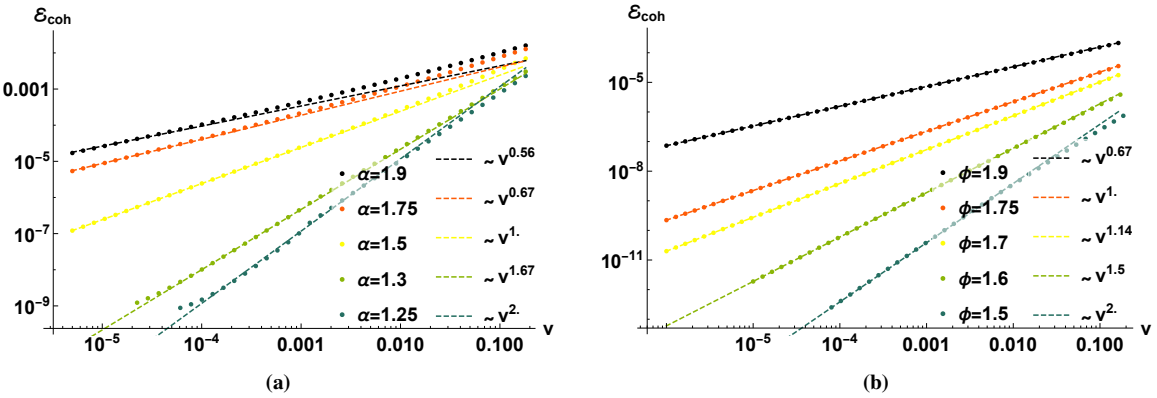

Figure 4.7: **(a)** The excitation density $\mathcal{E}_{\text{coh}}$ as a function of the ramp rate v for a series of long-range pairing parameter values, $1 < \alpha < 2$, with the hopping parameter fixed at $\phi \to \infty$ (nearest-neighbour hopping). We terminate the ramp at the critical point, corresponding to $\mu_f = \mu_c = -1$. The dashed lines are the analytic scaling prediction in Eq. (4.24), which depends non-trivially on the pairing parameter α. **(b)** The same as (a), but for a series of long-range hopping parameter values, $1 < \phi < 2$, with the pairing parameter fixed at $\alpha \to \infty$ (nearest-neighbour pairing). Here the ramp is also terminated at the critical point where $\mu_f = \mu_c = -g_\phi^\infty(0)$. The remaining parameters in both (a) and (b) are set to $L = \infty$, $J = 1$, $\Delta = 1$ and $\mu_i = -\infty$.

equivalently the ϕ- and α-dependencies, of the predicted scaling in Eq. (4.19) suggest that for $\phi, \alpha > 2$ the scaling exponent saturates to $1/2$ in the limit of slow ramp rates and that the intercept of the scaling function changes with α only. This is evident in the numeric results, where Fig. 4.6a illustrates that changing α produces a shift in the excitation density data, and the intercepts of the analytic scaling predictions differ for the various α values. In contrast, Fig. 4.6b demonstrates a certain ϕ-independence where the excitation density data collapses onto the same curve at slow ramp rates, and the intercepts of the analytic scaling predictions remain unchanged. The deviations from the predicted scaling at fast ramp rates are expected, since the scaling predictions only hold for sufficiently slow ramp rates. Additionally, as ϕ, α approach the boundary separating short- and long-range scaling behaviours, the expected scaling will only emerge for very slow ramp rates.

The numeric results exhibiting long-range scaling behaviour are shown in Fig. 4.7. For both long-range pairing and hopping the numeric data shows a clear dependence on the distance decay parameters. The data is also in good agreement with the analytic results (4.24), indicated by the dashed lines in Fig. 4.7.

4.3 Conclusion

The aim of this chapter was to study the non-equilibrium dynamics of the isolated long-range Kitaev chain. We started with a general description of the quantum KZ ramping protocol, which describes a procedure in which a control parameter or coupling constant in the system's Hamiltonian is varied continuously. For the Kitaev chain we focused on ramping the chemical potential μ linearly from an initial value μ_i to its critical value μ_c, according to Eq. (4.1). Of primary interest was the dynamics of the chain, and the universal behaviour thereof, in the vicinity of the QCP associated with the QPT for the $k = 0$ mode. To study the universal behaviour, we looked at the density of excitations $\mathcal{E}_{\text{coh}}$, as defined in Eq. (4.3).

The universal scaling behaviour emerging in the coherent excitation density $\mathcal{E}_{\text{coh}}$ following a sufficiently slow ramp of μ towards the QCP was studied both analytically and numerically. Our analytic results were derived in Section 4.2.2 within the Landau-Zener picture. The scaling laws, which are summarised in Eq. (4.24), agree with the results in the publication by Dutta et al. [22], where a more restrictive approach was followed. In comparison, our more general derivation in Section 4.2 does not depend on the asymptotic Landau-Zener transition probability (1.10), and is based on weaker hypotheses.[2] For both long-range hopping and pairing we found that the scaling exponents depend non-trivially on the distance decay parameters ϕ and α. Comparisons between the asymptotic scaling relations (4.24) we derived and the Kibble-Zurek predictions (4.30) are consistent in the majority of cases. The discrepancy arising between the long-range hopping scaling exponents is expected to be a consequence of the point at which the ramp is terminated, but requires further investigation. Finally, in Section 4.2.4 a numeric treatment of the Kitaev chain was used to verify the analytic scaling results (4.24), with good agreement observed for both weakly long-range and short-range systems. We will use the concepts and results of this chapter as building blocks to study the universal features of the open Kitaev chain with dissipation in Chapter 5.

[2] Details on the asymptotic Landau-Zener transition probability for the Kitaev chain are included in Appendix C.

Chapter 5

Dynamic scaling relations for the dissipative open Kitaev chain

In this chapter we study the dynamic scaling of the dissipative open Kitaev chain. In the past, most studies assumed unitary Hamiltonian dynamics, and little was known about the adiabatic dynamics of open systems close to criticality. More recently, there has been renewed interest in open system dynamics, since it is crucial to understanding the effect of an external environment on the dynamics of a system. This is important in a variety of contexts, including adiabatic quantum computation, state preparation and for overcoming the challenges associated with decoherence, which is present due to the unavoidable system–environment coupling. Pioneering work in Refs. [23, 50, 85] has led to general scaling laws for the density of excitations generated when a system is driven across a QCP by slowly ramping a parameter of the Hamiltonian at finite temperature. It was found that the excitation density scales universally as a function of the ramp rate and the bath temperature—even in the presence of dissipation [50]. The scaling laws have been verified for the XY spin chain locally coupled to bosonic baths by numerically solving a set of kinetic equations [23, 50], and for a one-dimensional fermionic wire in the presence of dissipative mechanisms, including local pumping, decay and dephasing [85]. In our work, we extend the existing results to also include scaling laws for the cooling of systems in the vicinity of the QCP.

The primary focus of this chapter will be studying a class of scaling relations in the open Kitaev chain using the "third quantisation" framework introduced in Chapter 3. There are two time dependencies of interest to us: $\mu(t)$ and $T(t)$, where μ is the chemical potential in the system Hamiltonian (2.1) and T is the temperature of the thermal bath to which the system is coupled. In the third quantisation formalism the bath temperature enters through the Lindblad bath coupling constants in Eq. (2.80). Section 5.1 focuses

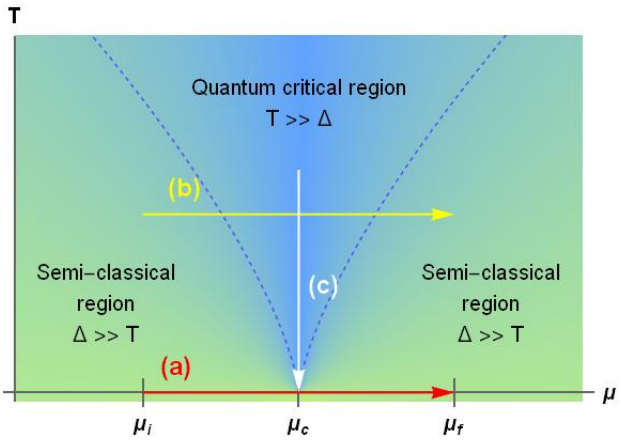

Figure 5.1: An illustration of the three ramping protocols studied in this thesis on the finite-temperature crossover phase diagram in the vicinity of the quantum critical point. Arrow (a) corresponds to the standard quantum Kibble-Zurek protocol, which was addressed in Chapter 4, (b) is the finite-temperature ramping protocol which involves the ramping of the parameter μ across its critical value at some non-zero temperature, and (c) represents a ramp of the temperature from $T > 0$ towards $T = 0$ at the critical value μ_c. The values μ_i and μ_f correspond to the start and end points of the ramp, respectively, for protocols (a) and (b).

on a finite-temperature ramping protocol, whereby the chemical potential μ is ramped towards the quantum critical point $\mu = \mu_c$ at $T > 0$. Provided the temperature is sufficiently low, the system will still be sensitive to the presence of the quantum critical point, and universal scaling of the excitation density is expected. In Section 5.2 the cooling of the long-range Kitaev chain towards quantum criticality is studied. In this protocol the temperature is ramped from some finite value $T > 0$ towards zero absolute temperature at the critical point. Critical slowing down is expected once the temperature is sufficiently low. These ramping protocols are summarised in Fig. 5.1 on the finite-temperature crossover phase diagram which appeared in Fig. 1.2.

In Section 5.1 and Section 5.2 the above-mentioned protocols are applied to the one-dimensional, long-range Kitaev chain in the presence of a bosonic bath. Although we restrict the majority of our discussions to this one model, it should be possible to extend our results to be applicable to other models with similar system–bath couplings. For each ramping protocol, we will derive a set of analytic scaling relations using the definitions and methods introduced in Chapter 2 and Chapter 3. To support the scaling arguments, we treat the Lindblad master equation (2.78) numerically to study the excitation density dynamics, where our approach follows the methods outlined in Section 3.4.

5.1 Parameter ramps at finite temperatures

Parameter ramps at finite temperatures involve a slow variation of a parameter or coupling constant in the Hamiltonian across its critical value while keeping the temperature fixed at some low, finite value. In this work, the chemical potential $\mu(t)$ is ramped linearly from μ_i to μ_f at a constant rate v as

$$\mu(t) = vt + \mu_i. \tag{5.1}$$

The system is initialised at μ_i in equilibrium with the bath at temperature T. As the chemical potential approaches its critical value μ_c, the system will be sensitive to the presence of the quantum critical point, and excitations will be generated.

In this ramping protocol there are two mechanisms contributing to the total excitation density: the coherent contribution and the incoherent contribution. The coherent contribution $\mathcal{E}_{\text{coh}}$ results from the unitary dynamics generated by the system Hamiltonian and the breakdown of adiabaticity, while the incoherent contribution $\mathcal{E}_{\text{inc}}$ refers to the thermal excitations that are introduced through the coupling to the bath. We will derive scaling laws for $\mathcal{E}_{\text{coh}}$ and $\mathcal{E}_{\text{inc}}$ by considering the two contributions separately. While these contributions are studied in isolation for the analytical scaling analysis, they cannot in general be disentangled to write the total excitation density $\mathcal{E}_{\text{tot}}$ as the sum

$$\mathcal{E}_{\text{tot}} = \mathcal{E}_{\text{coh}} + \mathcal{E}_{\text{inc}}. \tag{5.2}$$

Although Eq. (5.2) is expected to hold approximately for sufficiently weak system–bath coupling ($\gamma \ll 1$), a numeric treatment of the full Lindblad master equation (2.78) is required to get a complete and accurate understanding of the total excitation density $\mathcal{E}_{\text{tot}}$.

In Chapter 4 the coherently generated excitations for the long-range Kitaev chain were studied in detail, hence the remainder of this section will focus primarily on the incoherent contribution. For our model and choice of system–bath coupling, which are discussed in Section 2.1 and Section 2.2, the thermal excitations contributing to $\mathcal{E}_{\text{inc}}$ can be described by a set of rate equations, one for each η_k mode. This rate equation is derived in Section 5.1.1 by explicitly "turning off" the unitary dynamics in the master equation (2.78). Equipped with the rate equation description of the incoherent excitation density, we show that $\mathcal{E}_{\text{inc}}$ scales with the ramp rate and the bath temperature in a power-law fashion, characterised by the equilibrium critical exponents. To arrive at these analytic scaling laws, several approximations are made. Based on these approximations, the validity of the open Kitaev chain scaling laws is found to be restricted to certain regimes of parameter space. In Section 5.1.3 the regimes in which scaling is expected, and where it breaks down, are discussed. We also define a quantitative *crossover rate* that distinguishes between the regions in which the two mechanisms of excitation dominate. Section 5.1.4 focuses on verifying the analytic scaling results for the short- and long-range Kitaev chain using the set of 4×4 correlation matrix differential equations (3.61) in Section 3.4.

5.1.1 Incoherent contribution to the excitation density

The thermal excitations generated by the bath can be studied in isolation by *turning off* the unitary dynamics. In practice, this is achieved by adding a "correction term" to the correlation function matrix differential equation (3.61) and setting all the entries of the $\mathbf{H}$ matrix, as defined in Eq. (3.3), to zero. We show that this leads to a rate equation, providing a convenient, numerically efficient description of the incoherent excitations.

First recall from Section 3.4 that the matrix differential equation (3.61) for a $\{k,-k\}$ mode pair is formulated in terms of the two-point correlation matrix $\mathbf{C}_{\{k,-k\}}(t)$ for the Fourier Majorana fermions. Here we are interested in the correlation functions of the η_k fermions. It will therefore be convenient to perform a series of transformations to recast the matrix differential equation (3.61) as one which describes the dynamics of the correlation matrix

$$\boldsymbol{\mathcal{N}}(t) = \frac{1}{4}\mathbf{Z}(\mathbf{C}_{\{k,-k\}}(t)+\mathbb{I})\mathbf{Z}^\dagger = \begin{bmatrix} \langle \eta_k^\dagger \eta_k\rangle & \langle \eta_k^\dagger \eta_{-k}\rangle & \langle \eta_k^\dagger \eta_k^\dagger\rangle & \langle \eta_k^\dagger \eta_{-k}^\dagger\rangle \\ \langle \eta_{-k}^\dagger \eta_k\rangle & \langle \eta_{-k}^\dagger \eta_{-k}\rangle & \langle \eta_{-k}^\dagger \eta_k^\dagger\rangle & \langle \eta_{-k}^\dagger \eta_{-k}^\dagger\rangle \\ \langle \eta_k \eta_k\rangle & \langle \eta_k \eta_{-k}\rangle & \langle \eta_k \eta_k^\dagger\rangle & \langle \eta_k \eta_{-k}^\dagger\rangle \\ \langle \eta_{-k} \eta_k\rangle & \langle \eta_{-k} \eta_{-k}\rangle & \langle \eta_{-k} \eta_k^\dagger\rangle & \langle \eta_{-k} \eta_{-k}^\dagger\rangle \end{bmatrix}, \tag{5.3}$$

where $\mathbf{C}_{\{k,-k\}}(t)$ is defined in Eq. (3.60), $\mathbb{I}$ is the 4×4 identity matrix and the entries of $\boldsymbol{\mathcal{N}}(t)$ are time-dependent correlation functions of the η_k fermions for a particular $\{k,-k\}$ mode pair. The matrix

$$\mathbf{Z} = \begin{bmatrix} \cos\beta_k & i\cos\beta_k & i\sin\beta_k & \sin\beta_k \\ -i\sin\beta_k & -\sin\beta_k & \cos\beta_k & i\cos\beta_k \\ \cos\beta_k & -i\cos\beta_k & -i\sin\beta_k & \sin\beta_k \\ i\sin\beta_k & -\sin\beta_k & \cos\beta_k & -i\cos\beta_k \end{bmatrix} \tag{5.4}$$

performs a linear transformation between the Fourier Majorana fermions and the η_k fermions, with the time-dependence entering through the Bogoliubov angle $\beta_k(t)=\beta_k$ defined by

$$\tan(2\beta_k(t)) = \frac{-\Delta f_\alpha(k)}{2Jg_\phi(k)+2\mu(t)}. \tag{5.5}$$

With the definitions in Eqs. (5.3) and (5.4) we write the 4×4 matrix differential equation for the correlation matrix $\boldsymbol{\mathcal{N}}(t)$ for a $\{k,-k\}$ mode pair as

$$\frac{\mathrm{d}\boldsymbol{\mathcal{N}}(t)}{\mathrm{d}t} = -\Bigg[\Bigg(\underbrace{\mathbf{Z}\mathbf{X}^{\mathrm{T}}\mathbf{Z}^\dagger}_{①} - \frac{1}{2}\underbrace{\dot{\mathbf{Z}}\mathbf{Z}^\dagger}_{②}\Bigg)\boldsymbol{\mathcal{N}}(t) + \boldsymbol{\mathcal{N}}(t)\Bigg(\underbrace{\mathbf{Z}\mathbf{X}\mathbf{Z}^\dagger}_{①} - \frac{1}{2}\underbrace{\mathbf{Z}\dot{\mathbf{Z}}^\dagger}_{②}\Bigg) \underbrace{-\frac{1}{2}\mathbf{Z}(\mathbf{X}+\mathbf{X}^{\mathrm{T}}-4i\mathbf{M}_i)\mathbf{Z}^\dagger}_{③}\Bigg], \tag{5.6}$$

where $\mathbf{X}\equiv\mathbf{X}_{\{k,-k\}}$ from Eq. (3.59) and $\mathbf{M}\equiv\mathbf{M}_{\{k,-k\}}$ from Eq. (3.57), with the subscript i referring to the imaginary part of the matrix $\mathbf{M}$. The subscripts $\{k,-k\}$ have been suppressed in Eq. (5.6) for notational simplicity. The additional terms in the matrix differential equation (5.6) emerge due to the time-dependent transformation $\mathbf{Z}$ applied to the correlation matrices $\mathbf{C}_{\{k,-k\}}(t)$.

Systematically studying the terms appearing in the matrix differential equation (5.6) will allow us to identify which parts contribute to the unitary dynamics. This identification will provide a means of *turning off* the unitary dynamics, resulting in a matrix differential equation that governs the evolution of only the thermal excitations generated by the bath. We will discuss each of the unique terms in Eq. (5.6), denoted by ①, ② and ③, to understand which matrices, or parts thereof, contribute to the unitary dynamics of the Kitaev chain:

1. The diagonal matrices denoted by ① in Eq. (5.6) are defined as

$$\mathbf{Z}\mathbf{X}^{\mathrm{T}}\mathbf{Z}^\dagger = (\mathbf{Z}\mathbf{X}\mathbf{Z}^\dagger)^* = \mathrm{diag}\left[\gamma\Gamma_{k,1}-i\lambda, \gamma\Gamma_{k,1}-i\lambda, \gamma\Gamma_{k,1}+i\lambda, \gamma\Gamma_{k,1}+i\lambda\right], \tag{5.7}$$

   where $\Gamma_{k,1}=\Gamma_{k,+}+\Gamma_{k,-}$ is a combination of the Lindblad bath coupling constants $\Gamma_{k,\pm}$ (2.80), γ is the system–bath coupling and $\lambda_k=\lambda$ is the mode energy (4.6). We can distinguish between the unitary and dissipative dynamics through the γ-dependence that enters in the matrix. More precisely, the "turning off" of the unitary dynamics in the $\mathbf{Z}\mathbf{X}^{\mathrm{T}}\mathbf{Z}^\dagger$ and $\mathbf{Z}\mathbf{X}\mathbf{Z}^\dagger$ matrices involves dropping the terms with no γ-dependence. This amounts to setting $\mathbf{H}=0$, which eliminates the complex $i\lambda$s in Eq. (5.7).

2. The matrices denoted by ② in the matrix differential equation (5.6) appear as a result of the time-dependence of the transformation matrix $\mathbf{Z}$ (5.4). The time derivative of $\mathbf{Z}$ will introduce derivatives of the Bogoliubov angle β_k, leading to

$$\dot{\mathbf{Z}}\mathbf{Z}^\dagger = -\mathbf{Z}\dot{\mathbf{Z}}^\dagger = 2\frac{\mathrm{d}\beta_k}{\mathrm{d}t}\begin{bmatrix} 0 & 0 & 0 & i \\ 0 & 0 & -i & 0 \\ 0 & -i & 0 & 0 \\ i & 0 & 0 & 0 \end{bmatrix}. \tag{5.8}$$

The $\dot{\mathbf{Z}}\mathbf{Z}^\dagger$ and $\mathbf{Z}\dot{\mathbf{Z}}^\dagger$ matrices can be viewed as Bogoliubov coupling terms in the matrix differential equation (5.6). Since there is no γ-dependence, these terms will not impact on the dissipative dynamics of the system.

3. Term ③ in Eq. (5.6) can be written in terms of the system–bath coupling γ and combinations of the Lindblad bath coupling constants as

$$\begin{aligned} ③ &= -\frac{1}{2}\mathbf{Z}(\mathbf{X} + \mathbf{X}^{\mathrm{T}} - 4i\mathbf{M}_i)\mathbf{Z}^\dagger \\ &= -\gamma\ \mathrm{diag}\left[(\Gamma_{k,1} + \Gamma_{k,2}),\ (\Gamma_{k,1} + \Gamma_{k,2}),\ (\Gamma_{k,1} - \Gamma_{k,2}),\ (\Gamma_{k,1} - \Gamma_{k,2})\right] \qquad (5.9) \\ &= -2\gamma\Gamma_{k,1}\ \mathrm{diag}\left[\frac{1}{2}\left(1 + \frac{\Gamma_{k,2}}{\Gamma_{k,1}}\right),\ \frac{1}{2}\left(1 + \frac{\Gamma_{k,2}}{\Gamma_{k,1}}\right),\ \frac{1}{2}\left(1 - \frac{\Gamma_{k,2}}{\Gamma_{k,1}}\right),\ \frac{1}{2}\left(1 - \frac{\Gamma_{k,2}}{\Gamma_{k,1}}\right)\right], \qquad (5.10) \end{aligned}$$

where $\Gamma_{k,1}$ and $\Gamma_{k,2}$ are defined in terms of the bath coupling constants (2.80) as

$$\Gamma_{k,1} = \Gamma_{k,+} + \Gamma_{k,-} \qquad \text{and} \qquad \Gamma_{k,2} = \Gamma_{k,+} - \Gamma_{k,-}. \tag{5.11}$$

This matrix contributes purely to the description of the dissipative dynamics, since turning off the bath, which amounts to setting $\gamma = 0$, will set this matrix to zero.

In the three points above we established that the unitary dynamics introduce the complex $i\lambda$s in the matrices $\mathbf{Z}\mathbf{X}^{\mathrm{T}}\mathbf{Z}^\dagger$ and $\mathbf{Z}\mathbf{X}\mathbf{Z}^\dagger$ in Eq. (5.7), and the Bogoliubov coupling terms in Eq. (5.8). We therefore *turn off* the unitary dynamics by setting $\mathbf{H} = 0$, which eliminates the contribution to the unitary dynamics in the terms denoted by ① in the matrix differential equation, and secondly by dropping the Bogoliubov coupling terms denoted by ②. After doing so, Eq. (5.6) reduces to

$$\frac{\mathrm{d}\boldsymbol{\mathcal{N}}(t)}{\mathrm{d}t} = -\left[\mathrm{Re}[\mathbf{Z}\mathbf{X}^{\mathrm{T}}\mathbf{Z}^\dagger]\,\boldsymbol{\mathcal{N}}(t) + \boldsymbol{\mathcal{N}}(t)\,\mathrm{Re}[\mathbf{Z}\mathbf{X}\mathbf{Z}^\dagger] - \frac{1}{2}\mathbf{Z}(\mathbf{X} + \mathbf{X}^{\mathrm{T}} - 4i\mathbf{M}_i)\mathbf{Z}^\dagger\right], \tag{5.12}$$

which describes only the dissipative dynamics.

The set of 4×4 matrix differential equations (5.12) describe the dissipative dynamics for all the η_k correlation functions. For our purposes, we are interested only in the occupations $\langle \eta_k^\dagger \eta_k \rangle$, which correspond to the diagonal entries of the $\boldsymbol{\mathcal{N}}$ matrix in Eq. (5.3). According to Eq. (5.12), the diagonal entries of $\boldsymbol{\mathcal{N}}$ evolve according to the rate equation

$$\frac{\mathrm{d}}{\mathrm{d}t}\mathcal{P}_k(t) = -\frac{1}{\tau_k}\left[\mathcal{P}_k(t) - \mathcal{P}_k^{\mathrm{th}}\left(\frac{\lambda_k}{T}\right)\right], \tag{5.13}$$

where $\mathcal{P}_k(t) = \langle \eta_k^\dagger \eta_k \rangle(t)$ is the excitation probability of the k'th mode, $\lambda_k(t) = \lambda_k$ is the mode energy (2.26), $\tau_k^{-1} = 2\gamma\Gamma_{k,1}$ is the relaxation rate and $\mathcal{P}_k^{\mathrm{th}}(\lambda_k/T) = n_{\mathrm{FD}}(\lambda_k/T)$ is the thermal equilibrium distribution at time t. The Fermi-Dirac distribution n_{FD} emerges from the ratios $\Gamma_{k,2}/\Gamma_{k,1}$ in Eq. (5.10), which can be calculated using Eq. (5.11) and the bath coupling constants (2.80) as

$$\frac{\Gamma_{k,2}}{\Gamma_{k,1}} = \frac{\Gamma_{k,+} - \Gamma_{k,-}}{\Gamma_{k,+} + \Gamma_{k,-}} = \frac{2\mathcal{J}(\lambda_k)}{2\mathcal{J}(\lambda_k)(2n_{\mathrm{BE}}(\lambda_k) + 1)} = \frac{1}{(2n_{\mathrm{BE}}(\lambda_k) + 1)}. \tag{5.14}$$

If we identify the prefactor in Eq. (5.10) as $\tau_k^{-1} = 2\gamma\Gamma_{k,1}$, and apply the result in Eq. (5.14), we find that the diagonal entries of Eq. (5.10) are $-\tau_k^{-1} n_{\mathrm{FD}}(\lambda_k/T)$. This is consistent with the rate equation (5.13). The rate equation, which describes the dynamics of the incoherent excitation probability $\mathcal{P}_k$, will be central to our work on deriving analytic scaling relations for the incoherent contribution $\mathcal{E}_{\mathrm{inc}}$.

In the rate equation above we introduced the so-called relaxation rate τ_k^{-1}, which is defined in terms of

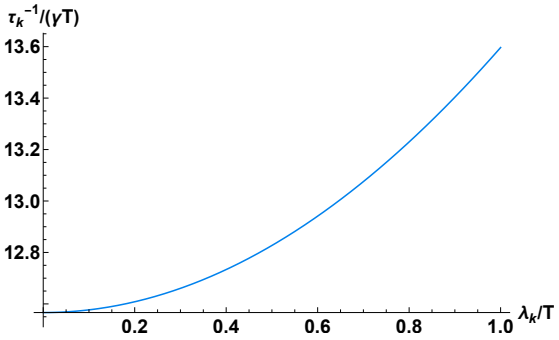

Figure 5.2: The Kitaev chain relaxation rate τ_k^{-1} for a single η_k-mode of the form in Eq. (5.18), scaled by $1/(\gamma T)$, as a function of λ_k/T. This illustrates that τ_k^{-1} is an increasing function of the mode energy λ_k. Here we set $s = 1$.

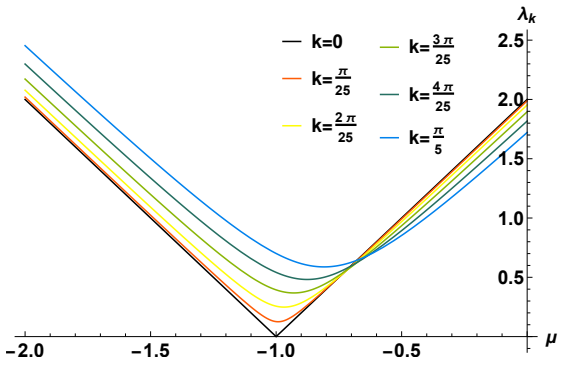

Figure 5.3: The mode energy λ_k for the short-range Kitaev chain as a function of the chemical potential μ for various k values. The $k = 0$ mode energy λ_0 reaches a minimum of zero at the critical value $\mu = \mu_c = -1$. For $k > 0$ the minima of the mode energies λ_k are located to the right of the critical point $\mu_c = -1$. As a result, the mode energy λ_k is a monotonic function of μ for all k values when $\mu \leq \mu_c$.

the system–bath coupling and bath coupling constants as

$$\tau_k^{-1} = 2\gamma\Gamma_{k,1}, \tag{5.15}$$

where $\Gamma_{k,1}$ is defined in Eq. (5.11). To establish whether the identification of $2\gamma\Gamma_{k,1}$ as a relaxation rate is sensible and consistent, we look at the evolution of the correlations for the time-independent case which was discussed in Section 3.2. Recall that after performing a basis transformation, the time evolution of the correlations is described by a simple propagation of the initial condition $\mathbf{G}(0)$ [103]. According to Eq. (3.30) we have [103]

$$\mathbf{G}_{jm}(t) = e^{-2(r_j+r_m)t}\mathbf{G}_{jm}(0), \tag{5.16}$$

where r_j and r_m are the rapidities (3.43). We therefore expect that the correlation functions will relax on timescales set by the real parts of the rapidities. For the Kitaev chain the real parts of the rapidities can be extracted from Eq. (3.43), leading to the identification of τ_k^{-1} as

$$\tau_k^{-1} = 4\mathrm{Re}[r_{+,k}] = 2\gamma\Gamma_{k,1} = 2\gamma\mathcal{J}(\lambda_k)(2n_{\mathrm{BE}}(\lambda_k) + 1), \tag{5.17}$$

which is consistent with Eq. (5.15).

If we now consider a bosonic bath with a spectral function $\mathcal{J}(\lambda_k)$ of the form $\mathcal{J}(\lambda_k) \propto \lambda_k^s$, the relaxation rate can be written as

$$\tau_k^{-1} = \gamma T^s m(\lambda_k/T) \qquad \text{with} \qquad m(\lambda_k/T) = 2\pi \left(\frac{\lambda_k}{T}\right)^s \left(\frac{2}{e^{\lambda_k/T} - 1} + 1\right). \tag{5.18}$$

It follows from the expression above that τ_k^{-1} is an increasing function of T. From a physical perspective, this suggests that modes will relax more rapidly at higher temperatures. Figure 5.2 illustrates another important feature of the relaxation rate, namely that τ_k^{-1} is an increasing function of the mode energy λ_k. Consequently, the high-energy modes in the Kitaev chain, which in our case are synonymous with the large-k modes, will relax faster than the low-energy modes. The form of the relaxation rate in Eq. (5.18) will be used in the next section.

5.1.2 Scaling laws for the incoherent contribution to the excitation density

In the absence of an environment, the excitation density will exhibit the scaling laws derived in Chapter 4. These scaling laws for the isolated Kitaev chain are summarised in Eq. (4.24). In this section we use the results in Section 5.1.1 to demonstrate how a set of scaling laws for the incoherent contribution $\mathcal{E}_{\mathrm{inc}}$ can be derived directly from the rate equation (5.13). As a matter of convenience, we will ramp the chemical potential μ according to $\mu(t) = vt$ in the analytic work that follows. If we define t appropriately, this is equivalent to Eq. (5.1) which will be used in the numerics in Section 5.1.4.

In the derivation of the set of scaling laws for the incoherent contribution we terminate the parameter ramp at a final time t_f. At this final time we define $\mathcal{E}_{\text{inc}}$ in terms of the incoherent excitation probability $\mathcal{P}_k$ as

$$\mathcal{E}_{\text{inc}}(t_f) = \frac{1}{\pi}\int_0^\infty dk\, \mathcal{P}_k(t_f). \tag{5.19}$$

Under the assumption that the spectral function takes the form $\mathcal{J}(\lambda_k) \propto \lambda_k^s$, a direct integration of the rate equation (5.13) yields an implicit integral equation for the excitation probability

$$\mathcal{P}_k(t_f) = -\gamma \int_{t_i}^{t_f} dt\, T^s m\left(\frac{\lambda_k(t)}{T}\right)\left[\mathcal{P}_k(t) - \mathcal{P}_k^{\text{th}}\left(\frac{\lambda_k(t)}{T}\right)\right]. \tag{5.20}$$

Here the relaxation rate τ_k^{-1} from the rate equation has been replaced by the form in Eq. (5.18), $\lambda_k(t)$ is the mode energy (2.26) with the t-dependence entering via the chemical potential (5.1), and t_f is the time at which the ramp is terminated. The lower bound t_i of the integral in Eq. (5.20) is chosen such that $\lambda_k(t_i)/T \gg 1$. An initial time t_i for which $\lambda_k(t_i)/T \gg 1$ will coincide with a ramp start point $\mu(t_i) = \mu_i$ at which $\mathcal{P}_k(t_i)$ is essentially zero. Since the mode energy λ_k is a monotonic function of μ for all k values when $\mu \leq \mu_c$, as shown in Fig. 5.3, we extend the lower bound to $-\infty$. This will not impact on the nature of the ramp in any way. The form of Eq. (5.20) with $t_i \to -\infty$ now allows for an iterative expansion of $\mathcal{P}_k$ in orders of the system–bath coupling γ. Inserting the zeroth-order solution $\mathcal{P}_k(t_i = -\infty) = 0$ for $\mathcal{P}_k(t)$ on the right-hand side of the implicit integral equation (5.20) leads to

$$\mathcal{P}_k(t_f) = \gamma \int_{-\infty}^{t_f} dt\, T^s m\left(\frac{\lambda_k(t)}{T}\right)\mathcal{P}_k^{\text{th}}\left(\frac{\lambda_k(t)}{T}\right) + \mathcal{O}(\gamma^2). \tag{5.21}$$

The expression above gives the excitation probability $\mathcal{P}_k(t_f)$ to linear order in the system–bath coupling, which we expect to be valid for sufficiently weak couplings. Equation (5.21) forms the basis for the remainder of the derivation of the scaling relations.

To sensibly study the universal behaviour of the dissipative dynamics, it is important to terminate parameter ramps exactly at the critical point where $\mu(t_f) = \mu_c$. Ramping beyond the critical point results in significant bath-induced relaxation which is not expected to be universal [50]. Hereafter, the ramp is assumed to always end at the critical point μ_c, corresponding to the time $t_f = \mu_c/v$. This specific choice for the ramp end point results in the function $t \to \lambda_k(t)/T$ being invertible, since the mode energy $\lambda_k(t)$ for $\mu \leq \mu_c$ is a monotonic function of μ. To illustrate this, we include Fig. 5.3. The function $t \to \lambda_k(t)/T$ being invertible allows for the change of variable

$$x = \frac{\lambda_k(t)}{T}, \qquad \text{with} \qquad dx = \frac{\lambda_k'(t)}{T}\, dt. \tag{5.22}$$

Implementing the change of variables above, Eq. (5.21) can be reformulated as

$$\mathcal{P}_k(t_f) = \gamma \int_{\infty}^{\lambda_k(t_f)/T} dx\, T^s m(x)\mathcal{P}_k^{\text{th}}(x)\frac{T}{\lambda_k'(t)} + \mathcal{O}(\gamma^2), \tag{5.23}$$

where the thermal equilibrium distribution $\mathcal{P}_k^{\text{th}}$ is given by the Fermi-Dirac distribution $\mathcal{P}_k^{\text{th}}(x) = (e^x + 1)^{-1}$. When the excitation energy λ_k is large compared to the temperature T, i.e. when $x \gg 1$, we have that $\mathcal{P}_k^{\text{th}}(x) \ll 1$. As a result, the modes for which $x \gg 1$ will make a negligible contribution to the excitation probability. It is therefore only necessary to consider those modes for which $\lambda_k(t_f) \lesssim T$. At low temperatures this will correspond to the low-energy modes around $k = 0$. Further simplification of the excitation probability (5.23) requires the short- and long-range cases to be considered separately.

We will simplify the excitation probability (5.23) for the nearest-neighbour case where $\alpha, \phi = \infty$. It is possible to extend the methods and reasoning we apply here to the long-range case. As argued at the end of the previous paragraph, only the low-energy modes will contribute significantly to the excitation probability $\mathcal{P}_k(t_f)$ if the temperature is low. This motivates the introduction of the approximation of the mode energy λ_k to lowest order in k. From the expansions in Eqs. (2.34) and (2.38) λ_k is written to lowest order in k as

$$\lambda_k^2(t) = 4[J + \mu(t)]^2 + [\Delta^2 - 4J(J + \mu(t))]k^2. \tag{5.24}$$

The above expression for the mode energy performs well, provided the temperature is low. The time deriva-

tive of $\lambda_k(t)$ in Eq. (5.24) is calculated as

$$\lambda_k'(t) = -\frac{2v}{\lambda_k(t)}(\lambda_k^2(t) - \Delta^2 k^2)^{1/2} = -2v\frac{T}{\lambda_k(t)}\left(\frac{\lambda_k^2(t)}{T^2} - \frac{\Delta^2 k^2}{T^2}\right)^{1/2}. \tag{5.25}$$

Recalling that $x = \lambda_k(t)/T$ from Eq. (5.22), we insert the result for $\lambda_k'(t)$ into Eq. (5.23). This leads to

$$\mathcal{P}_k(t_f) = -\frac{1}{2}\gamma v^{-1}T^{s+1}\int_{\infty}^{\lambda_k(t_f)/T} dx\, m(x)\mathcal{P}_k^{\text{th}}(x)x\left(x^2 - \frac{\lambda_k^2(t_f)}{T^2}\right)^{-1/2} + \mathcal{O}(\gamma^2), \tag{5.26}$$

where we have used the low-energy approximation $\lambda_k(t_f) = |\Delta||k|$ from Eq. (2.41). Now we write $\mathcal{E}_{\text{inc}}$ (5.19) in terms of the incoherent excitation probability $\mathcal{P}_k(t_f)$ (5.26) as

$$\mathcal{E}_{\text{inc}}(t_f) = -\frac{1}{2\pi|\Delta|}\gamma v^{-1}T^{s+1}\int_0^{\infty} dE \underbrace{\int_{\infty}^{E/T} dx\, m(x)\mathcal{P}_k^{\text{th}}(x)x\left(x^2 - \frac{E^2}{T^2}\right)^{-1/2}}_{\psi(E/T)} + \mathcal{O}(\gamma^2), \tag{5.27}$$

where we have introduced the function $\psi(E/T)$ and $E = \lambda_k(t_f) = |\Delta||k|$ from Eq. (2.41) is the mode energy at the critical point $\mu(t_f) = \mu_c$ to lowest order in k. After performing the change of variable

$$y = E/T \qquad \text{with} \qquad dE = T\,dy, \tag{5.28}$$

we have to leading order in γ for the nearest-neighbour case that

$$\mathcal{E}_{\text{inc}} = -\frac{1}{2\pi|\Delta|}\gamma v^{-1}T^{s+2}\int_0^{\infty} dy\,\psi(y) \propto \gamma v^{-1}T^{s+2}. \tag{5.29}$$

From this result we extract the scaling law for the nearest-neighbour Kitaev chain as

$$\mathcal{E}_{\text{inc}} \propto \gamma v^{-1}T^{s+2}. \tag{5.30}$$

We expect the above scaling relation to also be applicable to fermionic chains with short-range pairing and hopping, provided $\alpha, \phi > 2$.

Following a similar approach, the scaling behaviour of the incoherent contribution to the density of excitations for long-range pairing with $\alpha \in (1,2)$ and long-range hopping with $\phi \in (1,2)$ can be determined. Using the expansions of $f_\alpha^\infty(k)$ and $g_\phi^\infty(k)$ in Eqs. (2.34) and (2.38), as well as the low-energy approximation (2.41) of the dispersion relation, the scaling laws for long-range pairing and long-range hopping are found to be

$$\mathcal{E}_{\text{inc}} \propto \gamma v^{-1}T^{s+1+\frac{1}{\alpha-1}} \qquad \text{and} \qquad \mathcal{E}_{\text{inc}} \propto \gamma v^{-1}T^{s+1+\frac{1}{\phi-1}}, \tag{5.31}$$

respectively. Consequently, for all distance decay parameters we expect $\mathcal{E}_{\text{inc}}$ to exhibit power-law scaling in v, with exponent -1, and power-law scaling in the temperature T. We summarise the scaling laws (5.30) and (5.31) in terms of the dynamical and correlation length critical exponents, z and ν, as

$$\mathcal{E}_{\text{inc}} \propto \gamma v^{-1}T^{s+\nu+\frac{1}{\nu z}}, \tag{5.32}$$

with z and ν given in Eq. (4.29). This suggests a dependence on the equilibrium critical exponents, and is supported by the results published in Refs. [23, 50].

5.1.3 Scaling laws: regimes of validity

The scaling results obtained in Section 4.2.2 and Section 5.1.2 correspond to leading-order expansions in the ramp rate v and system–bath coupling γ. In this section we report results for explicit bounds on v and γ, which should ensure that the predicted scaling behaviour is observed. We first discuss the scaling law regimes of validity for the two contributions independently, starting with the coherent contribution $\mathcal{E}_{\text{coh}}$, followed by the incoherent contribution $\mathcal{E}_{\text{inc}}$. Although the study of the two contributions in isolation provides valuable insights into the universal behaviour exhibited close to the phase transition, it is restrictive since the total excitation density cannot in general be written as a combination of the two contributions, as in Eq. (5.2). Therefore, we conclude this section by determining a *crossover rate* which distinguishes between the regions in which the two mechanisms of excitation dominate. This should indicate whether the scaling with the ramp

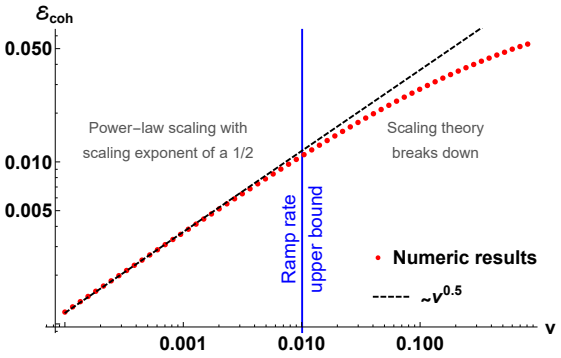

Figure 5.4: Numeric results for $\mathcal{E}_{\text{coh}}$ as a function of v for the nearest-neighbour Kitaev chain with parameters set to $L = 2^{12}$ and $J, \Delta = 1$. The condition in Eq. (5.33), indicated by the solid line, distinguishes between regimes in which power-law scaling is expected and where the scaling breaks down.

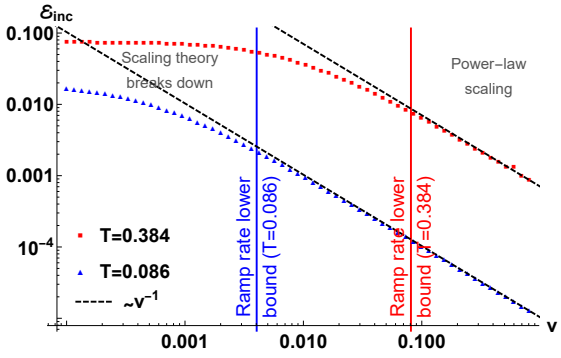

Figure 5.5: Numeric results for $\mathcal{E}_{\text{inc}}$ as a function of v for the nearest-neighbour Kitaev chain with parameters set to $L = 2^{12}$, $J, \Delta = 1$ and $\gamma = 0.005$. The condition in Eq. (5.34), indicated by the solid lines, distinguishes between regimes in which power-law scaling is expected and where the scaling breaks down for two temperatures, $T = 0.086$ and $T = 0.384$.

rate will also be observed in the total excitation density, and not only when the contributions are considered in isolation.

For $\mathcal{E}_{\text{coh}}$ a necessary condition for the predicted scaling in Eq. (4.24) to emerge for the nearest-neighbour Kitaev chain is

$$\frac{J\sqrt{v}}{\sqrt{2}\Delta^2\pi} \ll 1. \tag{5.33}$$

Details on the derivation of this condition are included in Appendix D.[1] Therefore we do not expect perfect scaling to be exhibited for fast ramps, since, for a fixed J and Δ, condition (5.33) places an upper bound on the ramp rate. Figure 5.4 shows the numeric results for $\mathcal{E}_{\text{coh}}$, together with this condition on the ramp rate. We observe that the scaling becomes more accurate for slower ramp rates. However, it should be noted that the numeric data may also deviate from the predicted scaling at very slow ramp rates. This is due to finite-size effects. At slow ramp rates it is only the modes in an increasingly narrow interval around $k = 0$ which will contribute significantly to the excitation density. In the numerics we approximate the integral $\int dk$ in Eq. (4.3) by a discrete sum $\sum_k$ over modes, as in Eq. (4.2). If only a narrow interval of modes make a contribution to $\mathcal{E}_{\text{coh}}$, this translates to us requiring a larger system size to observe the predicted power-law scaling.

A necessary condition for the predicted scaling in Eqs. (5.30) and (5.31) to emerge in $\mathcal{E}_{\text{inc}}$ can be derived by analysing the $k = 0$ mode contribution to $\mathcal{E}_{\text{inc}}$ within the linear-order approximation (5.21). Details are provided in Appendix E, where the condition for the power-law scaling to emerge is found to be[2]

$$\frac{\pi T^2 \gamma \delta}{v} < \frac{1}{35} \approx 0.02857. \tag{5.34}$$

The dimensionless parameter δ enters via the relaxation rate as a part of the spectral function $\mathcal{J}$ in Eq. (2.81). Condition (5.34) suggests that the predicted power-law scaling will emerge provided that the ramp rate v is sufficiently fast, the bath temperature T is sufficiently low or the system–bath coupling γ is sufficiently weak. All three of these conditions would suppress the generation of the incoherent excitations, and thereby ensure that $\mathcal{P}_k$ remains sufficiently small for the linear-order approximation in Eq. (5.21) to hold. This is supported by Fig. 5.5, where the incoherent contribution $\mathcal{E}_{\text{inc}}$ only exhibits power-law scaling at sufficiently fast ramp rates and sufficiently low temperatures.

Studying the two mechanisms of excitation independently is valuable, but does not provide the full picture. To determine whether the scaling of the two contributions makes an appearance in the total excitation density, we define a quantitative *crossover rate*, v_{cross}. This crossover rate will distinguish between the regions

[1] We only include details on the nearest-neighbour case, but these results can be generalised to long-range pairing and hopping with some additional work.

[2] This result is specifically for the nearest-neighbour Kitaev chain, but can be generalised to also include long-range systems.

in which one of the two mechanisms of excitation dominate. The different scaling of the two contributions implies that for slow ramp rates, where $v < v_{\text{cross}}$, the incoherent mechanism of excitation will be dominant, while for fast ramp rates, where $v > v_{\text{cross}}$, the coherent mechanism dominates over the incoherent one. If the conditions (5.33) and (5.34) are met in regions where the appropriate contribution is dominant, then the scaling should materialise in $\mathcal{E}_{\text{tot}}$.

We restrict our discussion here to the case of nearest-neighbour hopping and pairing, with a pairing parameter $\Delta > 0$. The crossover rate can be determined by equating $\mathcal{E}_{\text{coh}} = \mathcal{E}_{\text{inc}}$. To obtain a quantitative description of this rate, it is important to also consider the prefactors and not only the quantities with which the excitation density scales. To this end, we make use of the result in Appendix D to write

$$\mathcal{E}_{\text{coh}} \approx \frac{1}{\pi}\frac{\sqrt{2v}}{\Delta}\int_0^\infty d\omega_0\, P_0(\omega_0) \approx \frac{0.119}{\Delta}v^{1/2}, \tag{5.35}$$

which provides a quantitative analytic description of $\mathcal{E}_{\text{coh}}$. For the incoherent excitations the result in Eq. (5.29) gives

$$\mathcal{E}_{\text{inc}} \approx -\frac{\gamma}{2\pi\Delta}v^{-1}T^{s+2}\int_0^\infty dy\, \psi(y) \approx \frac{3.776\gamma}{\Delta}v^{-1}T^{s+2}. \tag{5.36}$$

Now equating (5.35) and (5.36) yields

$$v_{\text{cross}} = 10.023\gamma^{2/3}T^{2(s+2)/3}. \tag{5.37}$$

Note that the temperature T and system–bath coupling γ shift the crossover point. For low temperatures, or weak system–bath couplings, the excitations generated by the incoherent mechanism will only be visible at very slow ramp rates, with the coherent mechanism dominating at faster ramp rates. In contrast, a high temperature, or strong system–bath coupling, increases v_{cross}, implying that the incoherent contribution will be visible at faster ramp rates.

The result in Eq. (5.37) provides us with a quantitative description of the crossover point between the regions in which the incoherent and coherent mechanisms of excitation dominate. This is useful for deriving conditions on the ramp rate v for which the scaling will emerge in $\mathcal{E}_{\text{tot}}$. First note that the emergence of scaling in the total excitation density requires that conditions (5.33) and (5.34) are satisfied in the region where the appropriate contribution is dominant. We handle the two scaling cases separately in the list below. Point one provides a condition on the ramp rate v for the coherent scaling (4.24) to emerge in $\mathcal{E}_{\text{tot}}$, while point two gives a condition on v for which the incoherent scaling (5.30) should be visible in $\mathcal{E}_{\text{tot}}$.

1. The coherent mechanism of excitation is dominant when $v > v_{\text{cross}}$. Based on condition (5.33), the ramp rate must be bounded from above to observe scaling behaviour. Therefore combining (5.33) and (5.37), we find the condition on v to be

$$10.023\gamma^{2/3}T^{2(s+2)/3} < v \ll \frac{2\pi^2\Delta^4}{J^2}. \tag{5.38}$$

   If the ramp rate v satisfies the condition above, the scaling $\mathcal{E}_{\text{coh}} \propto v^{1/2}$ is expected to emerge in $\mathcal{E}_{\text{tot}}$. Consequently, scaling will be observed only in a very specific regime of ramp rates, with very slow ramp rates resulting in the coherent contribution not being dominant and fast ramp rates leading to condition (5.33) being violated.

2. The incoherent mechanism of excitation is dominant when $v < v_{\text{cross}}$. The scaling $\mathcal{E}_{\text{inc}} \propto v^{-1}$ will therefore emerge in $\mathcal{E}_{\text{tot}}$ only if condition (5.34) and $v < v_{\text{cross}}$ are satisfied simultaneously. We write this condition for observing scaling compactly by combining Eqs. (5.34) and (5.37) as[3]

$$35\pi T^2\gamma < v < 10.023\gamma^{2/3}T^{2(s+2)/3}. \tag{5.39}$$

   Obtaining an interval of ramp rates that satisfies (5.39) is challenging, since the temperature and system–bath coupling enter in both the upper and lower bound on v. If $s > 1$ we expect high temperatures to broaden the interval over which the incoherent scaling will emerge. The system–bath coupling γ enters in condition (5.39) in such a way that stronger couplings lead to a narrower range of ramp rates for which the scaling in Eq. (5.30) will emerge. It is possible that sufficiently strong

[3]Note that we have absorbed the dimensionless parameter δ, which enters in condition (5.34), into the system–bath coupling γ to be consistent with the expression in Eq. (5.37), which makes use of the relaxation rate (5.18).

system-bath couplings suppress the scaling behaviour entirely due to it being impossible to satisfy condition (5.39). As a result, we anticipate that the incoherent scaling (5.30) will not materialise in $\mathcal{E}_{\text{tot}}$, unless γ is very weak.

With reference to points one and two above, we conclude that the coherent and incoherent scaling behaviours will only materialise in $\mathcal{E}_{\text{tot}}$ if we consider a range of ramp rates for which the conditions (5.38) and (5.39) are satisfied. For low temperatures, condition (5.38) on the ramp rate should be easy to satisfy. The second condition on v suggests that there will be a suppression of the scaling behaviour for the incoherent contribution in $\mathcal{E}_{\text{tot}}$, unless the system–bath coupling is sufficiently weak.

5.1.4 Numeric results for the Kitaev chain

In Section 5.1.4.1 we report some numeric results for the scaling of the incoherent contribution to the excitation density for the Kitaev chain coupled to a bosonic bath, which is maintained at a temperature T. When considering the incoherent contribution in isolation, a numeric treatment of the rate equation (5.13) suffices. Obtaining the total excitation density is a more challenging task, requiring an exact numeric treatment of the Lindblad master equation (2.78). To this end, we first reduce the matrix differential equation (3.61), which governs the open system dynamics of the Kitaev chain, to a set of three ordinary coupled differential equations. This permits a computationally feasible numeric evaluation of $\mathcal{E}_{\text{tot}}$, even for system sizes in the order of thousands of fermions. In Section 5.1.4.2 we summarise this approach for computing $\mathcal{E}_{\text{tot}}$ and discuss the results that follow from it.

5.1.4.1 Incoherent contribution

In our numeric analysis we consider a bosonic bath with an ohmic spectral function $\mathcal{J}(\lambda_k) = \pi\delta\lambda_k e^{-\lambda_k/\lambda_c}$, as defined in Eq. (2.81). If the cutoff frequency λ_c is sufficiently large compared to the mode energy, the spectral function can be approximated by $\mathcal{J}(\lambda_k) \approx \pi\delta\lambda_k$. Consequently, $s = 1$ and the analytic scaling laws (5.30) and (5.31) are written as

$$\mathcal{E}_{\text{inc}} \propto \begin{cases} \gamma v^{-1} T^{3} & \text{(SR pairing and hopping)} \\ \gamma v^{-1} T^{2+1/(\alpha-1)} & \text{(LR pairing)} \\ \gamma v^{-1} T^{2+1/(\phi-1)} & \text{(LR hopping)} \end{cases} . \tag{5.40}$$

To verify these scaling laws, we solve the rate equation numerically for each η_k mode. With the excitation probabilities at our disposal, it is possible to calculate $\mathcal{E}_{\text{inc}}$ and corroborate our scaling predictions.

Results for the nearest-neighbour Kitaev chain are shown in Fig. 5.6. The power-law scaling emerging in the numeric results for both $\mathcal{E}_{\text{inc}}$ versus v (Fig. 5.6a) and $\mathcal{E}_{\text{inc}}$ versus T (Fig. 5.6b) is consistent with the analytic scaling prediction in Eq. (5.40). As expected, the universal scaling behaviour vanishes when condition (5.34) is not met. In the case of long-range pairing or hopping, the scaling of $\mathcal{E}_{\text{inc}}$ with T will depend non-trivially on either α or ϕ. Figure 5.7 shows the numeric results for long-range pairing and long-range hopping, together with the analytic scaling predictions from Eq. (5.40). Deviations from the expected scaling at low temperatures is a consequence of using a finite system size.

5.1.4.2 Total excitation density

It is important to note that hitherto the two contributions to $\mathcal{E}_{\text{tot}}$ were considered independently. In this section we study the *exact* total excitation density through a numeric treatment of the Kitaev chain master equation (2.78).[4] We also address the extent to which the total excitation density can be approximated by the sum of the two contributions, $\mathcal{E}_{\text{coh}}$ and $\mathcal{E}_{\text{inc}}$.

The computational expense associated with numerically solving the matrix differential equation (3.61) for the Fourier Majorana fermion correlation functions, in particular for large system sizes and slow ramp rates, motivates first simplifying these equations analytically as far as possible. After some manipulation, the

[4] Refer to Chapter 3 for a detailed discussion on solving the Lindblad dynamics of the Kitaev chain. This section provides a simplification of the methodology and tools already established in Chapter 3 in order to make the calculation of the total excitation density computationally feasible.

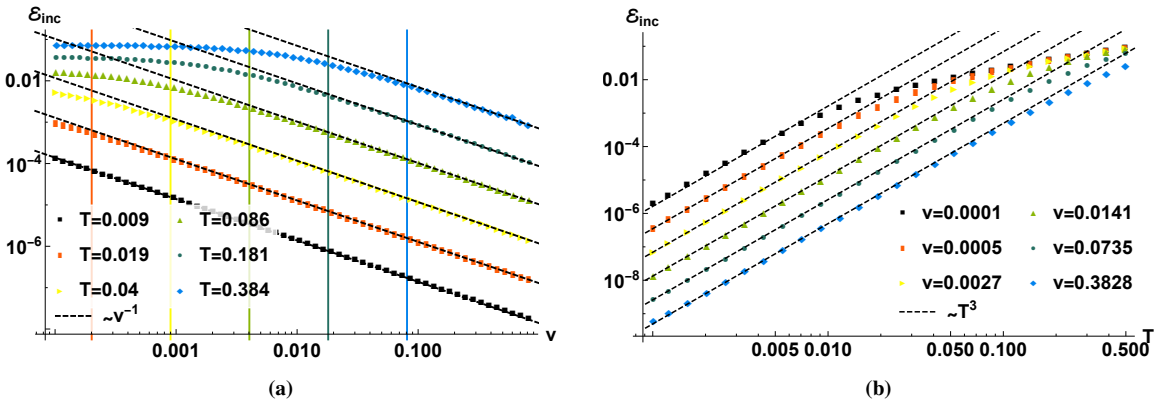

Figure 5.6: **(a)** The incoherent contribution $\mathcal{E}_{\text{inc}}$ to the excitation density as a function of v for a range of temperatures and $\gamma = 0.005$, together with the analytic scaling result (5.30) (dashed black lines) to which the exact numeric results converge when $v > 35\pi T^2\gamma\delta$. Solid vertical lines, corresponding to $v = 35\pi T^2\gamma\delta$ from (5.34), distinguish between regimes in which power-law scaling is expected and where the scaling breaks down. **(b)** The incoherent contribution to the excitation density $\mathcal{E}_{\text{inc}}$ as a function of T for several ramp rates and $\gamma = 0.05$, together with the analytic scaling result (5.30) (dashed black lines) to which the exact numeric results converge as the temperature tends to zero. The parameters in both (a) and (b) are set as follows: $L = 2^{12}$, $J = \Delta = \delta = 1$, $\phi = \alpha = \infty$, $\lambda_c = 4000$, $\mu_i = -3$ and $\mu_f = -1$.

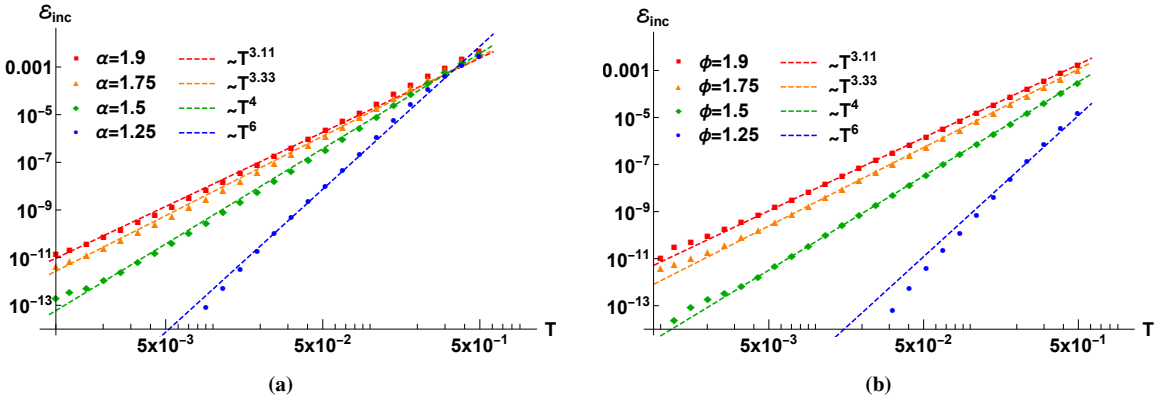

Figure 5.7: The incoherent contribution $\mathcal{E}_{\text{inc}}$ to the excitation density as a function of T for the long-range Kitaev chain, together with the analytic scaling predictions (5.31) (dashed lines). **(a)** Data for weakly long-range pairing ($1 < \alpha < 2$) and nearest-neighbour hopping ($\phi = \infty$). **(b)** Data for weakly long-range hopping ($1 < \phi < 2$) and nearest-neighbour pairing ($\alpha = \infty$). The remaining parameters in both (a) and (b) are set to $L = 10^6$, $J = \Delta = \delta = 1$, $v = 0.5$, $\gamma = 0.01$, $\lambda_c = 4000$, $\mu_i = -5$ and $\mu_f = -1$.

set of 16 equations per mode can be reduced exactly to three ordinary coupled differential equations of the form

$$\begin{aligned}
\frac{\mathrm{d}f_{k,1}}{\mathrm{d}t} &= \gamma(\Gamma_{k,1} + \cos(2\beta_k)\Gamma_{k,2} - 2\Gamma_{k,1}f_{k,1}) - 2\sin(2\beta_k)\lambda_k f_{k,2},\\
\frac{\mathrm{d}f_{k,2}}{\mathrm{d}t} &= -\sin(2\beta_k)\lambda_k + 2\sin(2\beta_k)\lambda_k f_{k,1} - 2\gamma\Gamma_{k,1}f_{k,2} - 2\cos(2\beta_k)\lambda_k f_{k,3},\\
\frac{\mathrm{d}f_{k,3}}{\mathrm{d}t} &= \gamma\sin(2\beta_k)\Gamma_{k,2} + 2\cos(2\beta_k)\lambda_k f_{k,2} - 2\gamma\Gamma_{k,1}f_{k,3},
\end{aligned} \tag{5.41}$$

where $f_{k,1} = \langle a_k^\dagger a_k\rangle$, $f_{k,2} = \mathrm{Re}[\langle a_k^\dagger a_{-k}^\dagger\rangle]$ and $f_{k,3} = \mathrm{Im}[\langle a_k^\dagger a_{-k}^\dagger\rangle]$. The initial conditions are given by

$$\begin{aligned}
f_{k,1}(0) &= \cos(2\beta_k[t=0])\,\langle\eta_k^\dagger\eta_k\rangle_{t=0} + \frac{1}{2}\Big(1 - \cos(2\beta_k[t=0])\Big),\\
f_{k,2}(0) &= 0,\\
f_{k,3}(0) &= \sin(2\beta_k[t=0])\left(\langle\eta_k^\dagger\eta_k\rangle_{t=0} - \frac{1}{2}\right).
\end{aligned} \tag{5.42}$$

Note that there is an implicit time-dependence sitting in all the coefficients in the differential equations (5.41).

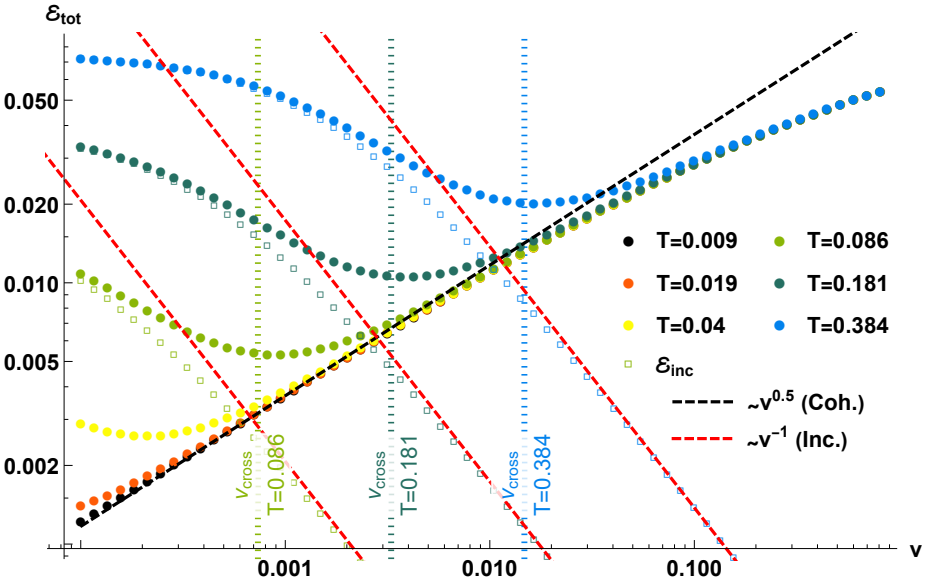

Figure 5.8: The total excitation density $\mathcal{E}_{\text{tot}}$ versus the ramp rate v for a range of temperatures. We terminate the ramp at the QCP, with $\mu_f = \mu_c = -1$. Empty data points correspond to the incoherent contribution of $\mathcal{E}_{\text{tot}}$, which is calculated directly from a numeric treatment of the rate equation (5.13). The vertical dotted lines correspond to v_{cross} in Eq. (5.37). Dashed lines are the analytic scaling predictions, $\mathcal{E}_{\text{coh}} \propto v^{1/2}$ and $\mathcal{E}_{\text{inc}} \propto v^{-1}$, with only the coherent scaling emerging in $\mathcal{E}_{\text{tot}}$. The remaining parameters are set to $L = 2^{12}$, $J = \Delta = \delta = 1$, $\alpha = \phi = \infty$, $\gamma = 0.001$, $\lambda_c = 4000$ and $\mu_i = -3$.

For the $k = 0, \pi$ modes, only a single differential equation needs to be solved:

$$\frac{\mathrm{d}f_{k,1}}{\mathrm{d}t} = \gamma(\Gamma_{k,1} - \Gamma_{k,2} - 2\Gamma_{k,1} f_{k,1}) \qquad \text{with} \qquad f_{k,1}(0) = 1 - \langle \eta_k^\dagger \eta_k \rangle. \tag{5.43}$$

Once the differential equations have been solved, the excitation density for $k \neq 0, \pi$ can be extracted using

$$\langle \eta_k^\dagger \eta_k \rangle = \cos(2\beta_k) f_{k,1}(t_f) + \sin(2\beta_k) f_{k,3}(t_f) + (1 - \cos(2\beta_k))/2, \tag{5.44}$$

whilst the zero and π mode excitations are

$$\langle \eta_0^\dagger \eta_0 \rangle = \begin{cases} 0.5 & \text{if} \quad \mu_f = -J, \\ 1 - f_{0,1}(t_f) & \text{if} \quad \mu_f < -J, \\ f_{0,1}(t_f) & \text{if} \quad \mu_f > -J, \end{cases} \qquad \text{and} \qquad \langle \eta_\pi^\dagger \eta_\pi \rangle = \begin{cases} 0.5 & \text{if} \quad \mu_f = J, \\ 1 - f_{\pi,1}(t_f) & \text{if} \quad \mu_f < J, \\ f_{\pi,1}(t_f) & \text{if} \quad \mu_f > J. \end{cases} \tag{5.45}$$

While the set of differential equations (5.41) has a simple form, it is found to be very *stiff*. This *stiffness* is due to the very different scales of the independent variable on which the dependent variables are changing [112]. The issue with stiff differential equations is that they are numerically unstable unless the step size in t is extremely small. Consequently, any of the conventional explicit methods for solving the differential equations quickly become very computationally expensive. To solve stiff systems it is best to use higher-order implicit methods. The results in Figs. 5.8 and 5.9 are obtained using the Bulirsch-Stoer method with a few generalisations, in particular a semi-implicit extrapolation method due to Bader and Deuflhard [112].

The results for the total excitation density as a function of the ramp rate are shown in Fig. 5.8. To be consistent with our analytic work, the ramping protocol is always halted at the critical point. The six data sets visible in the figure correspond to different bath temperatures. For the data sets with higher temperatures we explicitly show the crossover rates, as well as the incoherent contribution. We observe that the coherent mechanism of excitation dominates when $v > v_{\text{cross}}$. Increasing the ramp rate beyond v_{cross} results in the incoherent contribution very quickly becoming small. At slow ramp rates, where the condition $v < v_{\text{cross}}$ is satisfied, the incoherent mechanism of excitation is the dominant one. In this region the coherent mechanism becomes inconsequential and $\mathcal{E}_{\text{tot}} \approx \mathcal{E}_{\text{inc}}$. The range of ramp rates for which each mechanism of excitation is dominant is crucial for understanding why the scaling laws for the two contributions are suppressed in the total excitation density. With reference to the theoretical arguments in Section 5.1.3, the regime in which the scaling is expected to emerge does not fall in the region where the appropriate contribution is dominant. One

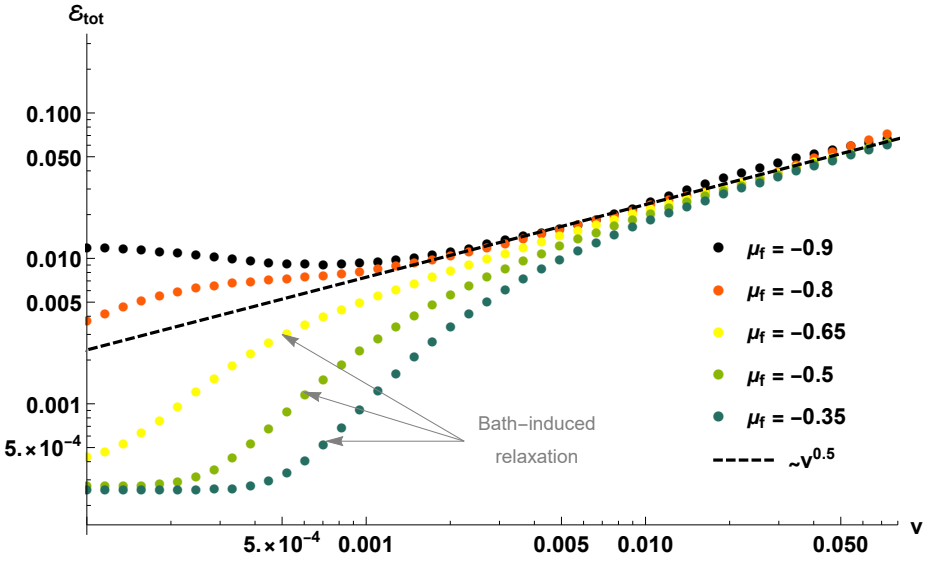

Figure 5.9: $\mathcal{E}_{\text{tot}}$ versus the ramp rate v for $T = 0.086$ and $\mu_f = -0.9, -0.8, -0.65, -0.5$ and -0.35. Bath-induced relaxation is prominent for slow ramp rates. The remaining parameters are set to $L = 2^{12}$, $J = \Delta = \delta = 1$, $\alpha = \phi = \infty$, $\gamma = 0.001$, $\lambda_c = 4000$ and $\mu_i = -3$.

exception is when the temperature of the thermal bath is sufficiently low. In this case, the coherent scaling behaviour does materialise, as observed in Fig. 5.8.

Earlier we claimed that ramping past the critical point results in significant bath-induced relaxation, which is not expected to be universal. Numeric results can be used to support this claim. In particular, Fig. 5.9 shows $\mathcal{E}_{\text{tot}}$ versus v for a range of μ_f values past the critical value $\mu_c = -1$. The relaxation induced by the bath, as seen in Fig. 5.9, is a consequence of the system leaving the quantum critical region and crossing the semi-classical region [50]. Naturally, the further one ramps past the critical point, the more prominent the effect of the bath-induced relaxation. Also note that the relaxation occurs predominantly at small v, since the time spent in the semi-classical region is prolonged [50]. The plateauing observed at slow ramp rates for $\mu_f = -0.35$ and $\mu_f = -0.5$ in Fig. 5.9 indicates that the system has relaxed to a point where it is approaching thermal equilibrium at the end of the ramp. From this discussion we conclude that ramping beyond the critical point leads to an unavoidable relaxation of the excitations generated in the vicinity of the critical point due to the coupling with the bath.

In Section 5.1.3, as well as in our discussion of Fig. 5.8, we focused on regimes where one of the two excitation mechanisms dominate, and formulated conditions under which the associated scaling behaviour will be observed in the total excitation density. A natural question is the extent to which the total excitation density can generally be regarded as a sum of independent coherent and incoherent contributions, as in Eq. (5.2). The structure of the coupled differential equations (5.41) suggests that disentangling the contributions from these two mechanisms will not be a simple task, or even possible at all in general. There are certainly parameter regimes where a complicated interplay between the generation of coherent excitations and the bath-induced dissipation will result in the total excitation density deviating significantly from being a sum of the two independent contributions. For example, a fast ramp rate could generate coherent excitations which push the system far out of equilibrium with the bath. This will result in the system losing some of this excess energy through dissipation, rather than absorbing energy from the bath as it would in the absence of the coherent excitations. A more detailed analysis of the full set of coupled differential equations would be necessary to determine whether scaling behaviour in the excitation density could emerge in regimes where it is necessary to account for both the coherent excitations and the system–bath coupling simultaneously.

5.2 Cooling quantum critical systems to zero temperature

In Section 5.1 we used the "third quantisation" framework introduced in Chapter 3 to study the universal behaviour of the long-range Kitaev chain when ramping the chemical potential $\mu(t)$ towards the critical value $\mu = \mu_c$ at a finite temperature. Here we focus on the second time dependency of interest to us, $T(t)$, which involves the cooling of the Kitaev chain (2.1) towards quantum criticality. In this temperature

ramping protocol the chain is initialised at the critical value $\mu = \mu_c$ in equilibrium with the thermal bath at temperature T_i. We then cool the system by ramping the temperature linearly from the initial temperature $T_i > 0$ towards $T = 0$ at a rate v according to

$$T(t) = T_i - vt. \tag{5.46}$$

During the ramp, the system is held at the critical value μ_c, and we expect a critical slowing down of the dynamics as the quantum critical point is approached. As with the previous ramping protocols, the excitation density $\mathcal{E}$ is monitored during the temperature ramp. We define this excitation density as

$$\mathcal{E} = \frac{1}{2\pi}\int_{-\pi}^{\pi} dk\, \mathcal{P}_k, \tag{5.47}$$

where $\mathcal{P}_k$ is the excitation probability for the k'th mode. The sections that follow focus on investigating the loss of adiabaticity and universal features that emerge in the density of excitations (5.47) when cooling the Kitaev chain according to the above-mentioned temperature ramping protocol.

We will start with a discussion of the adiabatic and non-adiabatic cooling regimes in Section 5.2.1, which are fundamental to the accurate interpretation of the results for the temperature ramping protocol. In Section 5.2.2 we show that, under certain conditions, the excitation density $\mathcal{E}$ exhibits scaling behaviour characterised by power laws involving v and T_i. These analytic scaling predictions for the long-range Kitaev chain are subsequently verified by numeric results. The numeric results presented in Section 5.2.3 suggest that an appropriate rescaling of the data can collapse the various data sets onto a universal scaling function. This idea is explored further in the final section of this chapter, Section 5.2.4.

5.2.1 Adiabatic and non-adiabatic cooling regimes

When cooling the Kitaev chain at the critical value $\mu = \mu_c$ there are two important regimes: the initially adiabatic (early time) regime and the non-adiabatic (late time) regime. In the context of Chapter 4, *adiabatic evolution* referred to an isolated system's ability to follow its instantaneous ground state. Here the notion of adiabaticity is conceptually similar. We use the terms *adiabatic* and *non-adiabatic* to describe the extent to which the system instantaneously remains in thermal equilibrium with the bath. If the system has the ability to cool down through a sequence of thermal states corresponding to the instantaneous bath temperature, then the evolution is adiabatic. As soon as the system evolves out of equilibrium with the bath, the evolution is deemed to be non-adiabatic. The temperature at which the system dynamics switches from the adiabatic to the non-adiabatic regime will be called the *crossover temperature*, T_{cr}.

Before quantitatively characterising the crossover temperature, we provide a more detailed discussion on the adiabatic and non-adiabatic evolution in the context of the temperature ramping protocol. Suppose we start the temperature ramp at a sufficiently high initial temperature T_i. Here we expect the system to start in the adiabatic regime, since the relaxation rate (5.18) is an increasing function of the temperature T. Over time, the system is cooled according to (5.46). Provided $T > T_{\text{cr}}$, the evolution is adiabatic, since the relaxation rate is sufficiently fast for the system to cool down in unison with the bath. At some point we expect the temperature to have decreased sufficiently such that $T = T_{\text{cr}}$. After this point there is a breakdown in adiabaticity, and the slow relaxation rate results in the system evolving out of thermal equilibrium. These concepts are well illustrated in Fig. 5.10. Figure 5.10a demonstrates adiabatic cooling at early times and high temperatures, followed by a region in which the instantaneous excitation density can no longer track the excitation density $\mathcal{E}^{\text{th}}$ of the thermal equilibrium distribution. In Fig. 5.10b we show the excess excitations that are generated over time after starting from a thermal initial state at $T_i = 15$. As the temperature is lowered, the system's evolution transitions from being adiabatic to non-adiabatic, resulting in an increase of excess excitations.

A sensible comparison of the relaxation rate and the relative rate of change of the thermal equilibrium occupation can be used to quantitatively characterise the crossover temperature. To consider the relaxation rate $\tau_k^{-1}(\lambda_k)$ of all η_k modes simultaneously, we introduce the average relaxation rate

$$\left\langle \tau^{-1} \right\rangle = \frac{1}{\pi}\int_{0}^{\pi} dk\, \rho_{\text{th}}(\lambda_k/T)\tau_k^{-1}(\lambda_k), \tag{5.48}$$

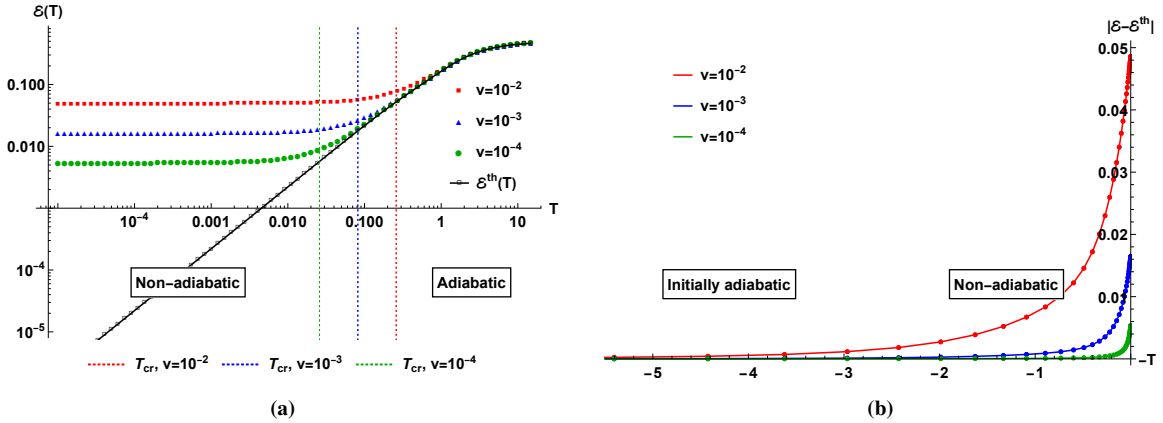

Figure 5.10: **(a)** The excitation density $\mathcal{E}$ as a function of $T(t)$ for temperature ramps with ramp rates $v = 10^{-2}, 10^{-3}, 10^{-4}$. For comparison, the excitation density $\mathcal{E}^{\text{th}}$ of the thermal equilibrium distribution with temperature $T(t)$ is shown in black. In all cases the dynamics starts from a thermal initial state at $T_i = 15$. The dotted lines in the corresponding colours mark the crossover temperatures T_{cr} at which the dynamics switches from the adiabatic to the non-adiabatic regime. **(b)** The excess excitations $|\mathcal{E}(T) - \mathcal{E}^{\text{th}}(T)|$ as a function of $-T = vt - T_i$ for temperature ramps with ramp rates $v = 10^{-2}, 10^{-3}, 10^{-4}$. The parameters in both (a) and (b) are set to $L = 10^6$, $J = \Delta = \delta = 1$, $\alpha = \phi = \infty$, $\gamma = 0.01$, $\lambda_c = 4000$ and $\mu = \mu_c = -1$.

weighted by the normalised thermal equilibrium distribution

$$\rho_{\text{th}}(\lambda_k/T) = N^{-1} n_{\text{FD}}(\lambda_k/T) \qquad \text{with} \qquad N = \frac{1}{\pi}\int_0^\pi dk\, n_{\text{FD}}(\lambda_k/T). \tag{5.49}$$

In the expressions above we have exploited the $k \leftrightarrow -k$ mode symmetry to produce integrals which run over only half of the domain $k \in [-\pi, \pi]$. The average relaxation rate (5.48) is compared to the average value of the relative rate of change of the equilibrium occupation

$$\left\langle \left| \frac{\dot{n}_{\text{FD}}}{n_{\text{FD}}} \right| \right\rangle = \frac{1}{\pi}\int_0^\pi dk\, \rho_{\text{th}}(\lambda_k/T) \left| \frac{\dot{n}_{\text{FD}}(\lambda_k/T)}{n_{\text{FD}}(\lambda_k/T)} \right|. \tag{5.50}$$

The time dependence in the expression above enters through the temperature $T = T(t)$ according to (5.46), and we define $\dot{n}_{\text{FD}}(\lambda_k/T) \equiv \frac{\mathrm{d}}{\mathrm{d}t}[n_{\text{FD}}(\lambda_k/T)]$. We now interpret the crossover temperature T_{cr} as the temperature at which the average rates (5.48) and (5.50) are equal, i.e. $\langle \tau^{-1} \rangle = \langle |\dot{n}_{\text{FD}}/n_{\text{FD}}| \rangle$. This provides a quantitative indication of the point where, on average, the system's relaxation rate matches the rate at which the thermal equilibrium distribution changes. We proceed by calculating T_{cr} explicitly for the nearest-neighbour and long-range Kitaev chains.

In general, the derivation of T_{cr} requires several approximations to be made. In both the nearest-neighbour and long-range cases we assume the temperature T is sufficiently low, such that only the low-energy modes around $k = 0$ will contribute significantly to the average rates in Eqs. (5.48) and (5.50). This allows us to replace the mode energies by their low-energy approximations (2.41). Within the low-energy approximation, we can also extend the upper bounds of the integrals in Eqs. (5.48) and (5.50) to infinity. Under these assumptions, it is now possible to calculate the integrals. In the nearest-neighbour case we use the low-energy approximation (2.41) for λ_k to perform the change of variable $k \to \lambda/|\Delta|$ in both the average relaxation rate and the average value of the relative rate of change of the equilibrium occupation. This leads to

$$\langle \tau^{-1} \rangle_{\text{NN}} = \frac{1}{\pi|\Delta|}\int_0^\infty d\lambda\, \rho_{\text{th}}(\lambda/T)\tau^{-1}(\lambda) \quad \text{and} \quad \left\langle \left| \frac{\dot{n}_{\text{FD}}}{n_{\text{FD}}} \right| \right\rangle_{\text{NN}} = \frac{1}{\pi|\Delta|}\int_0^\infty d\lambda\, \rho_{\text{th}}(\lambda/T) \left| \frac{\dot{n}_{\text{FD}}(\lambda/T)}{n_{\text{FD}}(\lambda/T)} \right|. \tag{5.51}$$

Following the same set of steps, we find the normalisation factor of $\rho_{\text{th}}(\lambda/T)$ (5.49) to be

$$N = \frac{1}{\pi|\Delta|}\int_0^\infty d\lambda\, n_{\text{FD}}(\lambda/T) = \frac{T\ln(2)}{\pi|\Delta|}. \tag{5.52}$$

To simplify the average rates $\langle \tau^{-1} \rangle_{\text{NN}}$ and $\langle |\dot{n}_{\text{FD}}/n_{\text{FD}}| \rangle_{\text{NN}}$ further, we approximate the relaxation rate $\tau^{-1}(\lambda)$ in Eq. (5.17) by taking the cutoff frequency λ_c in the spectral function (2.81) to be sufficiently large. For

large λ_c we find that[5]

$$\tau^{-1}(\lambda) \approx 2\pi\gamma\lambda\,(2n_{\text{BE}}(\lambda/T)+1)\,. \tag{5.53}$$

We now insert expression (5.49) for ρ_{th}, with the normalisation factor (5.52) and relaxation rate (5.53), into the average rates in Eq. (5.51). After some manipulation, the average rates are found to be

$$\langle\tau^{-1}\rangle_{\text{NN}} = \frac{1}{\pi|\Delta|N}\frac{\pi^3}{3}(\gamma T^2) \qquad \text{and} \qquad \left\langle\left|\frac{\dot{n}_{\text{FD}}}{n_{\text{FD}}}\right|\right\rangle_{\text{NN}} = \frac{1}{\pi|\Delta|N}v\ln(2). \tag{5.54}$$

The crossover temperature for the cooling of the Kitaev chain with nearest-neighbour hopping and pairing is the temperature at which the average rates in Eq. (5.54) match. Accordingly, we have

$$\langle\tau^{-1}\rangle_{\text{NN}} = \left\langle\left|\frac{\dot{n}_{\text{FD}}}{n_{\text{FD}}}\right|\right\rangle_{\text{NN}} \quad\Rightarrow\quad \frac{\pi^3}{3}(\gamma T_{\text{cr}}^2) = v\ln(2) \quad\Rightarrow\quad T_{\text{cr}}\left(\frac{v}{\gamma}\right) = \sqrt{\frac{3v\ln(2)}{\gamma\pi^3}}, \tag{5.55}$$

where the crossover temperature depends only on the ratio of the ramp rate v and system–bath coupling γ. In Fig. 5.10a we find that the analytic expression (5.55) accurately marks the temperature at which the dynamics switches from the adiabatic to the non-adiabatic regime.

The crossover temperature for the cooling of a long-range Kitaev chain can be found in a similar way. We start by implementing the same set of approximations we made for the nearest-neighbour case. More precisely, we assume that the temperature is sufficiently low, allowing us to approximate the mode energy by its low-energy approximations (2.41), and that the integral upper bounds in Eqs. (5.48) and (5.50) can be extended to infinity. Before we proceed, we note that the crossover temperature for the long-range case will exhibit a non-trivial dependence on the distance decay parameters α and ϕ. In order to treat the long-range hopping and pairing cases simultaneously, we introduce the parameter ζ, and define the α- and ϕ-dependent coefficients in the mode energy λ_k as C_ζ. Here either $\zeta = \alpha$ or $\zeta = \phi$, depending on whether long-range pairing or hopping is being considered. For the weakly long-range distance decay parameters we are considering, we have the condition $1 < \zeta < 2$. Within the low-energy approximation, we use Eq. (2.41) to perform the change of variables $k \to (\lambda/C_\zeta)^{1/(\zeta-1)}$ in the integrals appearing the the average rates in Eqs. (5.48) and (5.50). This leads to

$$\langle\tau^{-1}\rangle_{\text{LR}} = \frac{1}{\pi C_\zeta(\zeta-1)}C_\zeta^{\frac{\zeta-2}{\zeta-1}}\int_0^\infty d\lambda\,\lambda^{\frac{2-\zeta}{\zeta-1}}\rho_{\text{th}}(\lambda/T)\tau^{-1}(\lambda) \tag{5.56}$$

and

$$\left\langle\left|\frac{\dot{n}_{\text{FD}}}{n_{\text{FD}}}\right|\right\rangle_{\text{LR}} = \frac{1}{\pi C_\zeta(\zeta-1)}C_\zeta^{\frac{\zeta-2}{\zeta-1}}\int_0^\infty d\lambda\,\lambda^{\frac{2-\zeta}{\zeta-1}}\rho_{\text{th}}(\lambda/T)\left|\frac{\dot{n}_{\text{FD}}(\lambda/T)}{n_{\text{FD}}(\lambda/T)}\right|. \tag{5.57}$$

Under an identical set of approximations and change of variables, the normalisation factor of the thermal equilibrium distribution in Eq. (5.49) for the long-range case is

$$\begin{aligned} N &= \frac{1}{\pi C_\zeta(\zeta-1)}C_\zeta^{\frac{\zeta-2}{\zeta-1}}\int_0^\infty d\lambda\,\lambda^{\frac{2-\zeta}{\zeta-1}}n_{\text{FD}}(\lambda/T) \\ &= \frac{1}{\pi C_\zeta(\zeta-1)}C_\zeta^{\frac{\zeta-2}{\zeta-1}}\left(1-2^{\frac{\zeta-2}{\zeta-1}}\right)T^{\frac{1}{\zeta-1}}\Gamma\left[\frac{1}{\zeta-1}\right]\zeta_{\text{R}}\left[\frac{1}{\zeta-1}\right], \end{aligned} \tag{5.58}$$

where Γ and ζ_{R} are the standard Gamma and Riemann Zeta functions. For the values of ζ we are considering, the integral in Eq. (5.58) converges. If we again consider the cutoff frequency λ_c to be large, the relaxation rate τ^{-1} is given by Eq. (5.53). Inserting the expression for ρ_{th} and τ^{-1} into the average relaxation rate (5.56) leads to

$$\langle\tau^{-1}\rangle_{\text{LR}} = \left[\frac{1}{\pi C_\zeta(\zeta-1)N}C_\zeta^{\frac{\zeta-2}{\zeta-1}}\right]2\pi\gamma T^{\frac{\zeta}{\zeta-1}}\Gamma\left[\frac{\zeta}{\zeta-1}\right]\mathbf{Li}_{\frac{\zeta}{\zeta-1}}(1) \tag{5.59}$$

The function $\mathbf{Li}_{\frac{\zeta}{\zeta-1}}(1)$ is the polylogarithmic function of order $\frac{\zeta}{\zeta-1}$. After some manipulation, we find the

[5] For simplicity, we have absorbed the dimensionless parameter δ in the spectral density function into the system–bath coupling γ.

average rate $\langle|\dot{n}_{\text{FD}}/n_{\text{FD}}|\rangle_{\text{LR}}$ in Eq. (5.57) to be

$$\begin{aligned}\left\langle\left|\frac{\dot{n}_{\text{FD}}}{n_{\text{FD}}}\right|\right\rangle_{\text{LR}} &= -\frac{1}{\pi C_\zeta(\zeta-1)N} C_\zeta^{\frac{\zeta-2}{\zeta-1}} v T^{\frac{2-\zeta}{\zeta-1}} \underbrace{\int_0^\infty d\lambda' \, (\lambda')^{\frac{2-\zeta}{\zeta-1}+1} n'_{\text{FD}}(\lambda')}_{\mathcal{I}_\zeta} \\ &= \left[\frac{1}{\pi C_\zeta(\zeta-1)N} C_\zeta^{\frac{\zeta-2}{\zeta-1}}\right] v T^{\frac{2-\zeta}{\zeta-1}} |\mathcal{I}_\zeta|, \end{aligned} \tag{5.60}$$

where we have labeled the ζ-dependent integral by $\mathcal{I}_\zeta$ and n'_{FD} is the derivative of the Fermi-Dirac distribution with respect to the integration variable λ'. In the final line of (5.60) we made use of the fact that $\mathcal{I}_\zeta < 0$ for $1 < \zeta < 2$. Equating the two rates (5.59) and (5.60) yields the crossover temperature in terms of the long-range parameter $\zeta = \phi, \alpha$:

$$\begin{aligned}\langle \tau^{-1} \rangle_{\text{LR}} = \left\langle\left|\frac{\dot{n}_{\text{FD}}}{n_{\text{FD}}}\right|\right\rangle_{\text{LR}} \quad &\Rightarrow \quad 2\pi\gamma T^{\frac{\zeta}{\zeta-1}} \Gamma\left[\frac{\zeta}{\zeta-1}\right] \mathbf{Li}_{\frac{\zeta}{\zeta-1}}(1) = v T^{\frac{2-\zeta}{\zeta-1}} |\mathcal{I}_\zeta| \\ &\Rightarrow \quad T_{\text{cr}}\left(\frac{v}{\gamma}\right) = \sqrt{\frac{v|\mathcal{I}_\zeta|}{2\pi\gamma}} \left(\Gamma\left[\frac{\zeta}{\zeta-1}\right] \mathbf{Li}_{\frac{\zeta}{\zeta-1}}(1)\right)^{-1/2}. \end{aligned} \tag{5.61}$$

The integral $\mathcal{I}_\zeta$ must be computed numerically.

As will be clear from later numeric results in Section 5.2.3, these quantitative values for the crossover temperature will separate the two cooling regimes. In summary, when $T > T_{\text{cr}}$ the evolution is adiabatic and we expect the excitation density to track its changing thermal equilibrium value. However, when $T < T_{\text{cr}}$, the system relaxes too slowly and therefore cannot remain in thermal equilibrium with the bath.

5.2.2 Asymptotic scaling laws for temperature ramps

In the temperature ramping protocol we are restricted to the quantum critical region (see Fig. 5.1) in which thermal excitations are generated due to the temperature exceeding the excitation gap. These thermal excitations are expected to display universal features at the end of the temperature ramp. In this section we will study some of the universal features by examining the scaling behaviour of the excitation density (5.47). More precisely, we will show that, under certain conditions, the excitation density $\mathcal{E}$ exhibits scaling behaviour characterised by power laws involving either the ratio v/γ of the ramp rate and system–bath coupling or the initial temperature T_i. Here we specialise our discussions and derivation of the scaling laws to the one-dimensional Kitaev chain. At the end of the section, the applicability of this work to other models is briefly reviewed.

Unlike for the parameter ramps at finite temperatures in Section 5.1, there is no coherent contribution to the excitation density for the temperature ramping protocol. Hence, the rate equation (5.13) describes the full (incoherent) contribution to the excitation density $\mathcal{E}$. Since the rate equation has an analytic solution, scaling laws for the temperature ramping protocol can be derived directly from the exact analytic solution for the excitation density. From Section 5.1.1 we know that inside the quantum critical region the dynamics of the incoherent excitation probability $\mathcal{P}_k$ is described by the rate equation

$$\frac{\mathrm{d}}{\mathrm{d}t}\mathcal{P}_k = -\tau_k^{-1}(\lambda_k, T)\left(\mathcal{P}_k - \mathcal{P}_k^{\text{th}}(\lambda_k/T)\right), \tag{5.62}$$

where $\mathcal{P}_k^{\text{th}}$ is the thermal equilibrium distribution. We will consider a relaxation rate τ_k^{-1} of the form in Eq. (5.18). As a matter of convenience, we express τ_k^{-1} with important functional dependencies as

$$\tau_k^{-1}(\lambda_k, T) = \gamma T^s m(\lambda_k/T) \qquad \text{with} \qquad m(\lambda_k/T) = 2\pi\left(\frac{\lambda_k}{T}\right)^s \left(\frac{2}{e^{\lambda_k/T}-1}+1\right). \tag{5.63}$$

To obtain the expression for the relaxation rate above, we have assumed that the spectral function $\mathcal{J}$ has the form $\mathcal{J}(\lambda_k) \propto \lambda_k^s$. On the surface, the differential equation (5.62) appears to be simple. However, recall that a non-trivial time dependence enters via the temperature according to Eq. (5.46) in both the relaxation rate and thermal equilibrium distribution. This leads to a complicated analytic solution for the excitation probability $\mathcal{P}_k$. To write down this analytic solution, it will be useful to first recast the rate equation into a different form. We will do this in two steps. First we perform the change of variables $t \to (T_i - T)/v$ in the

rate equation (5.62) with the relaxation rate given by (5.63). This leads to

$$\frac{\mathrm{d}}{\mathrm{d}T}\mathcal{P}_k = \frac{\gamma T^s m(\lambda_k/T)}{v}\left(\mathcal{P}_k - \mathcal{P}_k^{\mathrm{th}}\left(\frac{\lambda_k}{T}\right)\right). \tag{5.64}$$

Now introducing a new variable $y = -T/\lambda_k$, we write Eq. (5.64) as

$$\frac{\mathrm{d}}{\mathrm{d}y}\mathcal{P}_k = -\frac{\gamma\lambda_k^{s+1}m(-1/y)}{v}(-y)^s\mathcal{P}_k + \frac{\gamma\lambda_k^{s+1}m(-1/y)}{v}(-y)^s\mathcal{P}_k^{\mathrm{th}}\left(\frac{-1}{y}\right). \tag{5.65}$$

According to Ref. [113], the solution to a first-order linear differential equation of the form

$$g(x)\frac{\mathrm{d}y(x)}{\mathrm{d}x} = f_1(x)y(x) + f_0(x) \tag{5.66}$$

is

$$y(x) = Ce^F + e^F\int dx\, e^{-F}\frac{f_0(x)}{g(x)}, \qquad \text{with} \qquad F(x) = \int dx\,\frac{f_1(x)}{g(x)}. \tag{5.67}$$

Here C is an arbitrary constant, which is determined by the initial conditions of the problem. It follows from (5.66) and (5.67) that the excitation probability $\mathcal{P}_k$ for a single η_k mode is

$$\mathcal{P}_k = \mathcal{P}\left(y, \frac{T_i}{\lambda_k}, \frac{\gamma\lambda_k^{s+1}}{v}\right) = Ce^{F(y)} + \frac{\gamma\lambda_k^{s+1}}{v}e^{F(y)}\int_{-\frac{T_i}{\lambda_k}}^{y} dy'\, e^{-F(y')}(-y')^s m(-1/y')\mathcal{P}_k^{\mathrm{th}}\left(\frac{-1}{y'}\right), \tag{5.68}$$

where

$$C = \mathcal{P}_k^{\mathrm{th}}(\lambda_k/T_i) \qquad \text{and} \qquad F(y) = -\frac{\gamma\lambda_k^{s+1}}{v}\int_{-\frac{T_i}{\lambda_k}}^{y} dy'\,(-y')^s m(-1/y'). \tag{5.69}$$

The analytic expression (5.68) for the thermal excitations can be integrated over all η_k modes according to Eq. (5.47) to get the total excitation density $\mathcal{E}$. First we reduce the domain $k \in [-\pi, \pi]$ over which the integral (5.47) runs to $k \in [0, \pi]$ by exploiting the $k \leftrightarrow -k$ mode symmetry. This leads to

$$\mathcal{E} = \frac{1}{\pi}\int_0^\pi dk\,\mathcal{P}_k = \frac{1}{\pi}\int_0^\pi dk\,\mathcal{P}\left(y, \frac{T_i}{\lambda_k}, \frac{\gamma\lambda_k^{s+1}}{v}\right). \tag{5.70}$$

We rely on several approximations to simplify the excitation density in the expression above. As mentioned earlier, the system is held at the critical value μ_c during the temperature ramp. Consequently, for the low-energy modes, we have [50, 110]

$$\lambda_k \propto k^z, \tag{5.71}$$

where z is the dynamical equilibrium critical exponent. Within this low-energy approximation, we extend the upper bound of the integral in Eq. (5.70) to infinity and perform the change of variables $k \to \lambda^{1/z}$. Up to a proportionality constant, the excitation density is now given by

$$\mathcal{E} \propto \int_0^\infty d\lambda\,(\lambda)^{\frac{1}{z}-1}\mathcal{P}\left(y, \frac{T_i}{\lambda}, \frac{\gamma\lambda^{s+1}}{v}\right). \tag{5.72}$$

We are interested in the scaling behaviour of $\mathcal{E}$ when the temperature ramp is terminated at the quantum critical point at $T = 0$. Provided that only the low-energy modes of the system's spectrum contribute significantly to the excitation density $\mathcal{E}$ (5.72) at $T = 0$, i.e. $y = 0$, we expect $\mathcal{E}$ to display universal behaviour with both v/γ and T_i. For the sake of clarity, these two cases are treated separately below.

5.2.2.1 Asymptotic scaling relation for small v/γ

We start by performing the change of variables $\lambda \to (v/\gamma)^{1/(s+1)}\lambda$ in Eq. (5.72). After performing the change of variables, the excitation density at the end of the ramp, i.e. at $y = 0$, is found to be

$$\mathcal{E} \propto \left(v\gamma^{-1}\right)^{1/[z(s+1)]}\int_0^\infty d\lambda\,(\lambda)^{\frac{1}{z}-1}\mathcal{P}\left(0, \frac{T_i}{\lambda(v/\gamma)^{1/(s+1)}}, \lambda^{s+1}\right). \tag{5.73}$$

To extract the small-v/γ asymptotic behaviour of $\mathcal{E}$ from the expression above we require that the $v/\gamma \to 0$ limit of the integral exists and is finite. Provided these requirements are met, the dominant scaling behaviour will come from the prefactor in Eq. (5.73). The approach here is identical to that of Section 4.2.2.1 and Section 4.2.2.2. We therefore reserve a detailed analysis of the existence and convergence of the $v/\gamma \to 0$ limit of the integral in Eq. (5.73) for Appendix F. Based on the small-v/γ asymptotics of the excitation probability $\mathcal{P}\left(0, \frac{T_i}{\lambda(v/\gamma)^{1/(s+1)}}, \lambda^{s+1}\right)$ in Appendix F, we conclude that the integral has a well defined $v/\gamma \to 0$ limit and is finite. Therefore, in the limit of slow ramp rates, the leading-order behaviour of $\mathcal{E}$ results in

$$\mathcal{E} \propto (v/\gamma)^{1/[z(s+1)]}. \tag{5.74}$$

The result above suggests that for sufficiently slow ramp rates the excitation density $\mathcal{E}$ obeys a power law in the ramp rate v.

5.2.2.2 Asymptotic scaling relation for small T_i

The scaling behaviour with the initial temperature can be found in a similar way. First we perform the change of variables $\lambda \to \lambda T_i$ in Eq. (5.72). This leads to

$$\mathcal{E} \propto (T_i)^{1/z} \int_0^\infty d\lambda\, (\lambda)^{\frac{1}{z}-1} \mathcal{P}\left(0, \frac{1}{\lambda}, \frac{\gamma(\lambda T_i)^{s+1}}{v}\right), \tag{5.75}$$

where the ramp is terminated at $T = 0$. We can extract the small-T_i asymptotic behaviour of $\mathcal{E}$ from the expression above by considering the leading-order scaling behaviour of the integral at small T_i. In Appendix F we motivate that the $T_i \to 0$ limit of the integral in Eq. (5.75) exists and is finite. Therefore, under the assumption that the initial temperature is sufficiently low, the excitation density scales universally with T_i as

$$\mathcal{E} \propto (T_i)^{1/z}. \tag{5.76}$$

5.2.2.3 Discussion on the asymptotic scaling results

The scaling relations (5.74) and (5.76) were derived specifically with the Kitaev chain in mind. Despite the derivation being focused on a single model, we expect these results to be applicable to other models with similar system–bath couplings. We anticipate that changing the model or the description of the bath will impact on the exponent s, which is determined by the properties of the bath and, in some cases, potentially the equilibrium critical exponents. In addition to this, we point out that the derivation is consistent for different forms of the function $m(\lambda_k/T)$ (5.63).[6] This allows for the treatment of models that have a different functional form for the relaxation rate. Our results can also be extended to d-dimensional systems, since the dimensionality in the scaling exponent always enters in a ratio with the dynamical critical exponent as d/z. In the next section we test our analytic predictions against numeric results for the Kitaev chain. This is followed by Section 5.2.4 where we analyse the work of this section again, but using a different approach in which the proportionality constants are included.

5.2.3 Temperature ramp numeric results for the Kitaev chain

In this section we will test the scaling predictions (5.74) and (5.76) derived in Section 5.2.2 against numeric results for the long-range Kitaev chain. Quantitative comparisons between the analytic and numeric results require that we first calculate the exponent s, which is determined by the properties of the bath. Here we work with the description of the Kitaev chain and bosonic bath from Section 2.2, where the bath has an ohmic spectral density function $\mathcal{J}(\lambda_k) = \pi\delta\lambda e^{-\lambda_k/\lambda_c}$ (2.81). If we assume the cutoff frequency λ_c is high, the relaxation rate (5.15) is approximated as

$$\tau_k^{-1}(\lambda_k, T) \approx 2\pi\gamma\lambda_k \left(\frac{2}{e^{\lambda_k/T} - 1} + 1\right), \tag{5.77}$$

[6] Although the derivation is consistent for different forms of the function $m(\lambda_k/T)$ (5.63), there are certain conditions that must be satisfied by the function to ensure that the integrals in Eqs. (5.73) and (5.75) have well-defined $v/\gamma \to 0$ and $T_i \to 0$ limits and are finite. Refer to Appendix F for further details.

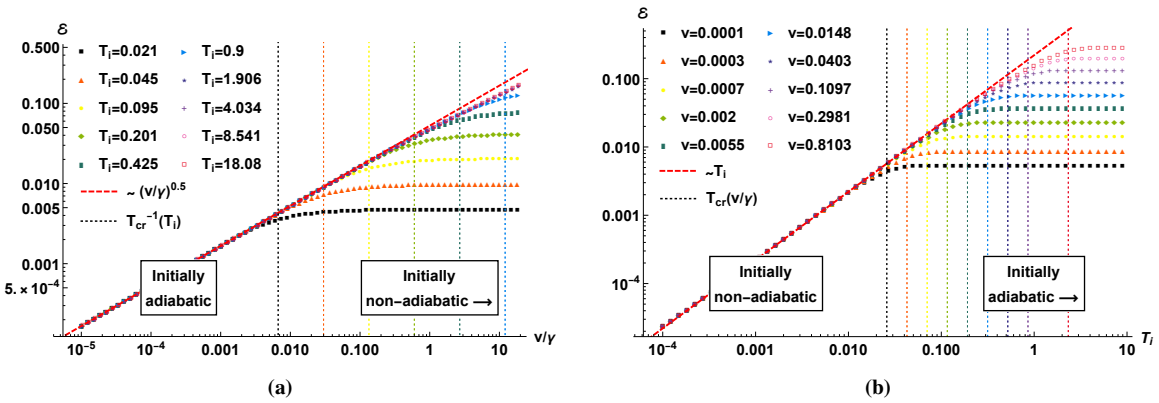

Figure 5.11: (a) The excitation density $\mathcal{E}$ for the nearest-neighbour Kitaev chain as a function of v/γ for a range of initial temperatures and $\gamma = 0.1$. This is shown together with the asymptotic result (5.79) (dashed red line) to which the exact numeric results converge as v/γ tends to zero. The dotted vertical lines in the corresponding colours are the crossover points $T_{\text{cr}}^{-1}(T_i)$ (5.55) between the initially adiabatic and initially non-adiabatic regimes. **(b)** The excitation density as a function of T_i for a series of ramp rates and $\gamma = 0.01$, together with the asymptotic result (5.79) (dashed red line) to which the exact numeric results converge as T_i tends to zero. The dotted vertical lines in the corresponding colours are the crossover points $T_{\text{cr}}(v/\gamma)$ (5.55) between the initially adiabatic and initially non-adiabatic regimes. The parameters in both (a) and (b) are set as follows: $L = 4 \times 10^4$, $J = \Delta = \delta = 1$, $\phi = \alpha = \infty$, $\lambda_c = 4000$, $\mu = \mu_c = -1$ and $T_f \simeq 0$. In

where we have absorbed the dimensionless parameter δ into the system–bath coupling γ for convenience. The approximate relaxation rate above is recast into the form of Eq. (5.63) to give

$$\tau_k^{-1}(\lambda_k, T) \approx (\gamma T)\left[2\pi\frac{\lambda_k}{T}\left(\frac{2}{e^{\lambda_k/T}-1}+1\right)\right] = \gamma T m(\lambda_k/T). \tag{5.78}$$

A comparison of (5.63) and (5.78) indicates that $s = 1$. For the short-range Kitaev chain the dynamical equilibrium critical exponent is found to be $z = 1$, as illustrated in Section 4.2.3. Substituting the appropriate values of s and z into the scaling relations (5.74) and (5.76) yields

$$\mathcal{E} \propto (v/\gamma)^{1/2} \qquad \text{and} \qquad \mathcal{E} \propto T_i. \tag{5.79}$$

These analytic scaling predictions (5.79) are compared with the numeric results in Fig. 5.11.

Figure 5.11 shows the exact numeric results for the density of excitations $\mathcal{E}$ at the end of the temperature ramp for the nearest-neighbour Kitaev chain. In Fig. 5.11a the excitation density is plotted as a function of v/γ for a range of initial temperatures, together with the asymptotic scaling law (5.79). For each initial temperature two cooling regimes are visible: the initially adiabatic regime and the initially non-adiabatic regime. The former refers to a regime in which the system dynamics starts out adiabatically, but at some point during the temperature ramp adiabaticity is lost. The latter corresponds to completely non-adiabatic ramps, in the sense that the dynamics is non-adiabatic from the instance the ramp is started. In Fig. 5.11a these initially adiabatic and non-adiabatic regimes are distinguished for each data set by a dotted line corresponding to the point $(v/\gamma) = T_{\text{cr}}^{-1}(T_i)$, which is the inverse of the crossover temperature $T_{\text{cr}}(v/\gamma)$ in Eq. (5.55). In the initially adiabatic regime, i.e. in the region to the left of the crossover lines, we are ramping more slowly or coupling more strongly to the thermal baths. As a result, the system cools down more effectively with the bath, and the exact numeric results converge to the predicted scaling function (5.79) with a scaling exponent of $1/2$. To the right of the crossover lines, a *plateauing* in the excitation density is observed, where the final value of $\mathcal{E}$ is essentially identical to its initial thermal value at T_i. This is a consequence of the ramp rate being so fast, or the system–bath coupling being so weak, that the comparatively slow relaxation time of the system does not allow the chain to cool down with the bath.

Numeric results for the excitation density $\mathcal{E}$ as a function of the initial temperature T_i for a range of ramp rates are summarised in Fig. 5.11b. We observe qualitatively similar behaviour to Fig. 5.11a, with distinct power-law scaling in one cooling regime and a plateauing of the excitation density in the other. The two regimes, initially adiabatic and initially non-adiabatic, are separated by dotted lines for each data set. These crossover points $T_{\text{cr}}(v/\gamma)$ are given by Eq. (5.55). At high initial temperatures, i.e. when $T_i > T_{\text{cr}}(v/\gamma)$, the initial relaxation rate is fast enough for the system to cool effectively with the bath—at least until the

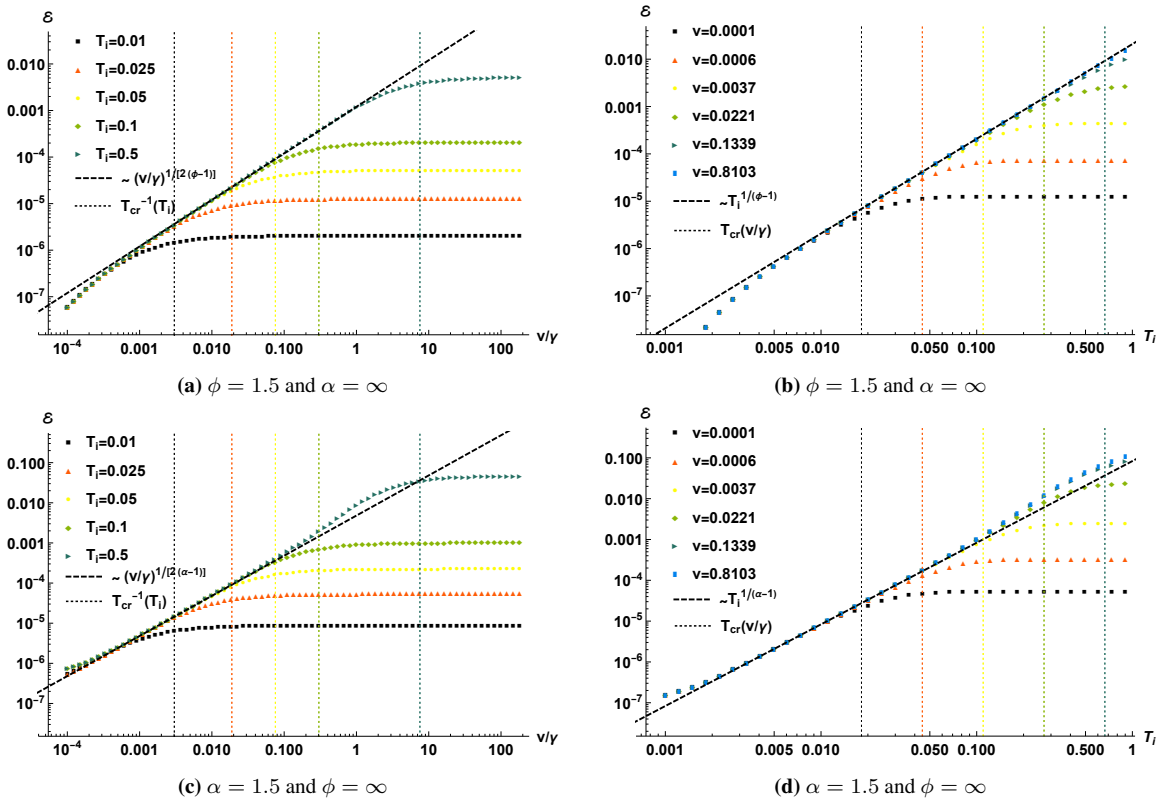

(a) $\phi = 1.5$ and $\alpha = \infty$ **(b)** $\phi = 1.5$ and $\alpha = \infty$

(c) $\alpha = 1.5$ and $\phi = \infty$ **(d)** $\alpha = 1.5$ and $\phi = \infty$

Figure 5.12: (a) and (c): The excitation density $\mathcal{E}$ for the long-range Kitaev chain as a function of v/γ for a range of initial temperatures, together with the asymptotic result (dashed black line) to which the exact numeric results converge as v/γ tends to zero. The dotted vertical lines in the corresponding colours are the crossover points $T_{\text{cr}}^{-1}(T_i)$ (5.61) between the initially adiabatic and initially non-adiabatic regimes. **(b) and (d):** The excitation density for the long-range Kitaev chain as a function of T_i for a series of ramp rates. This is shown together with the asymptotic result (dashed black line) to which the exact numeric results converge as T_i tends to zero. The crossover points $T_{\text{cr}}(v/\gamma)$ (5.61) between the initially adiabatic and initially non-adiabatic regimes are marked by the vertical dotted lines. The parameters in (a)-(d) are set as follows: $L = 4 \times 10^6$, $J = \Delta = \delta = 1$, $\lambda_c = 4000$, $\mu = \mu_c = -g_\phi(0)$ (long-range hopping), $\mu = \mu_c = -1$ (long-range pairing) and $T_f \simeq 0$.

temperature T drops below $T_{\text{cr}}(v/\gamma)$. As a result, we observe a plateauing behaviour in $\mathcal{E}$, since the initial temperature does not impact on the final excitation density at the end of the ramp. In the initially non-adiabatic regime the ramps are by definition non-adiabatic from the start. The system therefore cannot follow the cooling of the bath, so it remains in its initial thermal state. Hence we find that when $T_i < T_{\text{cr}}(v/\gamma)$ the excitation density converges to the predicted power-law scaling function.

If we now consider the Kitaev chain with long-range hopping and pairing, the scaling relations will depend non-trivially on the distance decay parameters ϕ and α. These long-range parameters are introduced through the dynamical critical exponent z. The result in Eq. (4.29) gives $z = \phi - 1$ for long-range hopping. It follows from the asymptotic scaling relations (5.74) and (5.76) that

$$\mathcal{E} \propto (v/\gamma)^{1/[2(\phi-1)]} \qquad \text{and} \qquad \mathcal{E} \propto T_i^{1/(\phi-1)}. \tag{5.80}$$

Similarly, for long-range pairing we have $z = \alpha - 1$, which leads to the two asymptotic scaling relations

$$\mathcal{E} \propto (v/\gamma)^{1/[2(\alpha-1)]} \qquad \text{and} \qquad \mathcal{E} \propto T_i^{1/(\alpha-1)}. \tag{5.81}$$

These analytic scaling predictions are supported by the numeric results in Fig. 5.12 for $\phi = 1.5$ with nearest-neighbour pairing ($\alpha = \infty$), as well as for $\alpha = 1.5$ with nearest-neighbour hopping ($\phi = \infty$). The results are qualitatively similar to those for the nearest-neighbour case, with the only noteworthy difference being the power-law scaling exponent which now depends on ϕ or α. Finite-size effects cause deviations from the predicted scaling for small v/γ and T_i, however, there is still good agreement between the predicted scaling laws (5.80) and (5.81) and the numeric results. It is possible to verify the scaling laws numerically for other choices of $\phi \in (1, 2)$ and $\alpha \in (1, 2)$.

5.2.4 A universal scaling function for temperature ramps

In the context of non-equilibrium physics, in particular the study of the dynamics of continuous phase transitions, we often find that in the vicinity of the critical point(s) different systems in various parameter regimes show qualitatively similar features, but on differing scales. The numeric results for the Kitaev chain in Section 5.2.3 suggest that an appropriate rescaling can collapse the various data sets onto a single curve, corresponding to a universal scaling function. The key to producing such a *data collapse* is to exploit the similarity of the data sets and, through an appropriate rescaling, bring the data sets to lie on a single curve [114]. A neat collapse of the data indicates that the various data sets are related by power laws in the parameters that were used for the rescaling. This is of interest to us since temperature ramps with different parameters can be unified through a single scaling function. We proceed by deriving a set of scaling functions onto which all the data sets from Section 5.2.3 collapse asymptotically.

Our derivation of a universal scaling function for the cooling of the Kitaev chain to criticality starts with the description of the total excitation density $\mathcal{E}$ within the low-energy approximation. If the temperature ramp is terminated at $T = 0$, recall from Eq. (5.72) that the total excitation density at the end of the ramp is approximated by

$$\mathcal{E}(T_i, \gamma/v) \approx c \int_0^\infty \mathrm{d}\lambda (\lambda)^{\frac{1}{z}-1} \mathcal{P}\left(0, \frac{T_i}{\lambda}, \frac{\gamma\lambda^{s+1}}{v}\right), \tag{5.82}$$

where we have explicitly indicated the two functional dependencies of $\mathcal{E}$. In Eq. (5.82) c is a proportionality constant, which is determined by the leading-order low-energy approximation (2.41) of the dispersion relation, the long-range parameters ϕ and α and the dynamical critical exponent z (4.29). More precisely, using Eq. (2.41) we find c to be

$$c = \begin{cases} \frac{1}{\pi|\Delta|} & \text{if} \quad \phi, \alpha = \infty \\ \frac{1}{\pi|\Delta a_2(\alpha)|} & \text{if} \quad \phi, \alpha > 2 \\ \frac{1}{\pi|\Delta a_1(\alpha)|(\alpha-1)} |\Delta a_1(\alpha)|^{\frac{\alpha-2}{\alpha-1}} & \text{if} \quad \phi = \infty, \alpha < 2 \\ \frac{1}{\pi|2Jb_2(\phi)|(\phi-1)} |2Jb_2(\phi)|^{\frac{\phi-2}{\phi-1}} & \text{if} \quad \phi < 2, \alpha = \infty \end{cases}, \tag{5.83}$$

where $a_1(\alpha)$, $a_2(\alpha)$ and $b_2(\phi)$ are defined in Eqs. (2.33) and (2.37), respectively. As we show next, it is possible to introduce two rescaled versions of the excitation density (5.82), each of which is a function of a single variable. The first of these, $\tilde{\mathcal{E}}_1(\tilde{T}_i)$, depends only on a rescaled initial temperature $\tilde{T}_i$. The second, $\tilde{\mathcal{E}}_2(\tilde{v})$, only varies with $\tilde{v}$, a rescaling of v/γ. By effectively reducing the excitation density to a function of a single variable in this way, we are able to analyse its dependence on T_i and v/γ in a simple and unified manner. We will refer to $\tilde{\mathcal{E}}_1(\tilde{T}_i)$ and $\tilde{\mathcal{E}}_2(\tilde{v})$ as scaling functions, and consider the two separately in the next two subsections.

5.2.4.1 Scaling Function 1: $\tilde{\mathcal{E}}_1(\tilde{T}_i)$

Here we investigate the first of the two scaling functions, $\tilde{\mathcal{E}}_1(\tilde{T}_i)$. The rescaled excitation density $\tilde{\mathcal{E}}_1$ and the rescaled initial temperature $\tilde{T}_i$ are defined as

$$\tilde{\mathcal{E}}_1 = a^{(1/z)}\mathcal{E} \qquad \text{and} \qquad \tilde{T}_i = bT_i, \tag{5.84}$$

where the a and b parameters used to perform the rescaling will be determined in due course. If we rescale $\mathcal{E}$ in Eq. (5.82) according to Eq. (5.84), and perform the change of variables $\lambda \to \lambda/a$, the rescaled excitation density is found to be

$$\tilde{\mathcal{E}}_1 \approx c \int_0^\infty \mathrm{d}\lambda (\lambda)^{\frac{1}{z}-1} \mathcal{P}\left(0, \frac{a\tilde{T}_i}{b\lambda}, \frac{\gamma\lambda^{s+1}}{va^{s+1}}\right). \tag{5.85}$$

Choosing $a = b = (\gamma/v)^{1/(s+1)}$, i.e. rescaling the excitation density $\mathcal{E}$ by $(\gamma/v)^{1/[z(s+1)]}$ and the initial temperature T_i by $(\gamma/v)^{1/(s+1)}$, eliminates the explicit γ- and v-dependence in the integral above. This immediately leads to

$$\tilde{\mathcal{E}}_1 = \mathcal{E}(\tilde{T}_i, 1), \tag{5.86}$$

where $\mathcal{E}(\tilde{T}_i, 1)$ is given by Eq. (5.82). This form (5.86) of $\tilde{\mathcal{E}}_1$ is suitable for investigating the scaling behaviour in the high $\tilde{T}_i$ regime. We now consider a second asymptotic form, which is applicable for studying the scaling behaviour of $\tilde{\mathcal{E}}_1$ when $\tilde{T}_i$ is sufficiently low. To obtain this second form of the scaling function, we

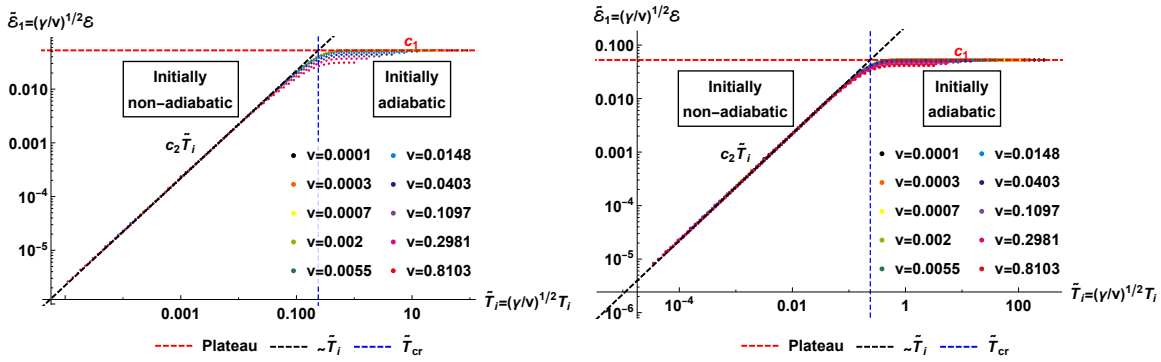

Figure 5.13: **(a)** The rescaled excitation density $\tilde{\mathcal{E}}_1$ as a function of the rescaled initial temperature $\tilde{T}_i$ for the nearest-neighbour Kitaev chain with $\gamma = 0.01$. We show the asymptotic scaling functions (5.89) and (5.90) in the two regimes, $\tilde{T}_i > \tilde{T}_{\text{cr}}$ and $\tilde{T}_i < \tilde{T}_{\text{cr}}$, as red and black dashed lines. The two cooling regimes are separated by the crossover line at $\tilde{T}_i = \tilde{T}_{\text{cr}}$. **(b)** The same as (a), but for $\gamma = 0.1$. The remaining parameters in both (a) and (b) are set as follows: $L = 4 \times 10^6$, $J = \Delta = \delta = 1$, $\lambda_c = 4000$, $\mu = \mu_c = -g_\phi(0)$ and $T_f \simeq 0$.

perform the change of variables $\lambda \to \lambda \tilde{T}_i$ in Eq. (5.85). This results in the asymptotic form

$$\tilde{\mathcal{E}}_1 = \tilde{T}_i^{\,1/z} \mathcal{E}\left(1, \tilde{T}_i^{\,s+1}\right). \tag{5.87}$$

The two forms of the scaling function introduced in Eqs. (5.86) and (5.87) describe the two asymptotic regimes of either plateauing or power-law scaling. This asymptotic behaviour is already visible in the numeric results of Section 5.2.3. To provide a quantitative description of the plateauing and power-law scaling behaviour of $\tilde{\mathcal{E}}_1$, we introduce two '*universal constants*', c_1 and c_2. These are defined as

$$c_1 = \mathcal{E}(T_i = \infty, \gamma/v = 1) \qquad \text{and} \qquad c_2 = \mathcal{E}(T_i = 1, \gamma/v = 0), \tag{5.88}$$

where c_1 is the excitation density (5.82) in the limit of very high initial temperatures, and c_2 is the excitation density (5.82) for an initial temperature of $T_i = 1$ in the limit of very fast ramp rates or very weak system–bath couplings. In fact, c_2 will correspond to the initial thermal equilibrium excitation density for a temperature of $T_i = 1$. With the universal constants (5.88), we can compactly describe the power-law scaling and plateauing in the two cooling regimes. Note that in this rescaled picture the initially adiabatic and initially non-adiabatic regimes are separated by the crossover point $\tilde{T}_{\text{cr}}$, which is a rescaled version of the crossover temperature T_{cr} in Eqs. (5.55) and (5.61). In the initially adiabatic regime, where $\tilde{T}_i > \tilde{T}_{\text{cr}}$, the rescaled excitation density approaches $\tilde{\mathcal{E}}_1 = c_1$, corresponding to the constant plateau values. When $\tilde{T}_i < \tilde{T}_{\text{cr}}$, the rescaled excitation density approaches $\tilde{\mathcal{E}}_1 = c_2 \tilde{T}_i^{\,1/z}$, which exhibits power-law scaling in $\tilde{T}_i$. Since $\tilde{\mathcal{E}}_1$ in Eqs. (5.86) and (5.87) is only dependent on $\tilde{T}_i$, we expect that for all ramp rates and system–bath couplings the data will collapse onto the functions c_1 and $c_2 \tilde{T}_i^{\,1/z}$ when in the regimes of high and low initial temperatures, respectively.

To provide a concrete example of this collapse onto a universal scaling function, we revisit the numeric results from Fig. 5.11b. For the nearest-neighbour case, both the excitation density $\mathcal{E}$ and the initial temperature T_i are rescaled by $(\gamma/v)^{1/2}$. With these rescalings, we expect the numeric data in Fig. 5.11b to collapse onto

$$\tilde{\mathcal{E}}_1 = c_1 = \mathcal{E}(\infty, 1) = \frac{1}{\pi} \int_0^\infty \mathrm{d}\lambda\, \mathcal{P}\left(0, \infty, \lambda^2\right) \approx 0.0526925 \tag{5.89}$$

when $\tilde{T}_i > \tilde{T}_{\text{cr}}$, and onto the linear function

$$\tilde{\mathcal{E}}_1 = \tilde{T}_i c_2 = \tilde{T}_i \mathcal{E}(1, 0) = \frac{\ln(2)}{\pi} \tilde{T}_i \tag{5.90}$$

when $\tilde{T}_i < \tilde{T}_{\text{cr}}$. The numeric results in Fig. 5.13a show a neat collapse of the data onto the predicted asymptotic scaling functions in the two regimes. The transition point from the asymptotic regime of power-law scaling to plateauing can be estimated by either rescaling the expression for T_{cr} in Eq. (5.55), or by

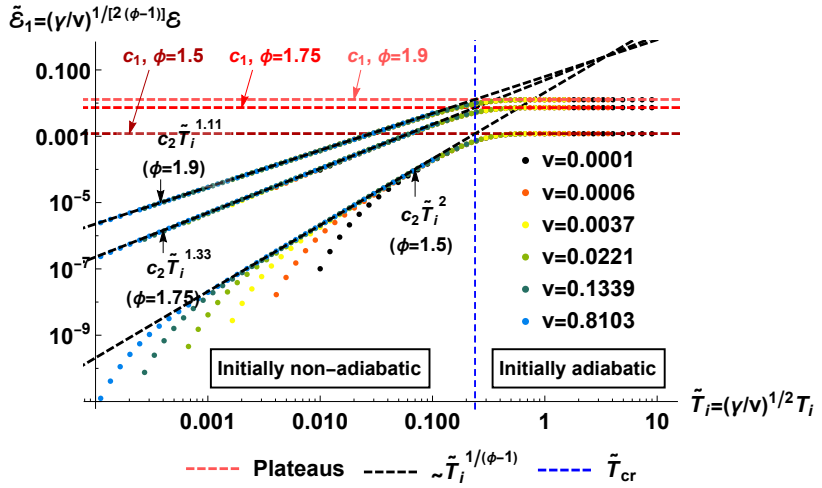

Figure 5.14: The rescaled excitation density $\tilde{\mathcal{E}}_1$ as a function of the rescaled initial temperature $\tilde{T}_i$ for the Kitaev chain with long-range hopping. The three data sets correspond to $\phi = 1.5$, $\phi = 1.75$ and $\phi = 1.9$. For each data set, the asymptotic scaling functions (5.92) in the two regimes, $\tilde{T}_i > \tilde{T}_{\text{cr}}$ and $\tilde{T}_i < \tilde{T}_{\text{cr}}$, are shown as red and black dashed lines. The crossover point at $\tilde{T}_i = \tilde{T}_{\text{cr}}$ is also indicated. The remaining parameters are set to $L = 4 \times 10^6$, $J = \Delta = \delta = 1$, $\gamma = 0.01$, $\lambda_c = 4000$, $\mu = \mu_c = -g_\phi(0)$ and $T_f \simeq 0$.

equating c_1 and $\tilde{T}_i c_2$. These two approaches produce qualitatively identical results for the transition point, with the first and second approach leading to

$$\tilde{T}_{\text{cr}} = \sqrt{\frac{3\ln(2)}{\pi^3}} \approx 0.258969 \qquad \text{and} \qquad \tilde{T}_{cr} = \frac{c_1}{c_2} \approx 0.238821. \tag{5.91}$$

The crossover point at $\tilde{T}_i = \tilde{T}_{\text{cr}}$ is evident in Fig. 5.13a, where it separates the power-law scaling behaviour from the plateauing behaviour. For faster ramp rates, or weaker system–bath couplings, we observe an imperfect collapse of the data, particularly in the initially adiabatic regime. To explain this, consider any fixed $\tilde{T}_i$, and note that a fast ramp rate v, or weak coupling γ, necessarily results in a high initial temperature T_i. This leads to the occupation of high-energy modes of which the energies are not accurately described by the leading-order approximation in Eq. (5.71). To illustrate this further, we include the numeric results for a system–bath coupling of $\gamma = 0.1$ in Fig. 5.13b. It is immediately clear that the weaker system–bath coupling $\gamma = 0.01$ used in Fig. 5.13a impacts on the quality of the collapse onto the two asymptotic scaling functions for $\tilde{\mathcal{E}}_1$.

We can test the asymptotic scaling predictions further by considering the Kitaev chain with long-range hopping. In this case, the excitation density and initial temperature are rescaled by $(\gamma/v)^{1/[2(\phi-1)]}$ and $(\gamma/v)^{1/2}$, respectively. The numeric data for all ramp rates and system–bath couplings is expected to collapse onto either

$$\tilde{\mathcal{E}}_1 = c_1 \qquad \text{or} \qquad \tilde{\mathcal{E}}_1 = c_2 \tilde{T}_i^{\,1/(\phi-1)}, \tag{5.92}$$

depending on whether $\tilde{T}_i > \tilde{T}_{\text{cr}}$ or $\tilde{T}_i < \tilde{T}_{\text{cr}}$. Figure 5.14 provides the exact numeric results for this case, which are in good agreement with the analytic predictions for three different ϕ-values. The deviation from the asymptotic behaviour at low temperatures is due to finite-size effects. It can be shown that these scaling predictions are also consistent for long-range pairing.

5.2.4.2 Scaling Function 2: $\tilde{\mathcal{E}}_2(\tilde{v})$

The second scaling function $\tilde{\mathcal{E}}_2(\tilde{v})$ depends only on the rescaled ramp rate $\tilde{v}$. We define the rescaled quantities explicitly as

$$\tilde{\mathcal{E}}_2 = a'^{(1/z)}\mathcal{E} \qquad \text{and} \qquad \tilde{v} = b'v, \tag{5.93}$$

where the rescaling parameters a' and b' will become evident shortly. Using the expression for $\mathcal{E}$ in Eq. (5.82), we can apply the rescaling (5.93), followed by the change of variables $\lambda \to \lambda/a'$, to bring $\tilde{\mathcal{E}}_2$ into the form

$$\tilde{\mathcal{E}}_2 \approx c \int_0^\infty \mathrm{d}\lambda\, (\lambda)^{\frac{1}{z}-1} \mathcal{P}\left(0, \frac{a'T_i}{\lambda}, \frac{b'\gamma\lambda^{s+1}}{\tilde{v}a'^{(s+1)}}\right). \tag{5.94}$$

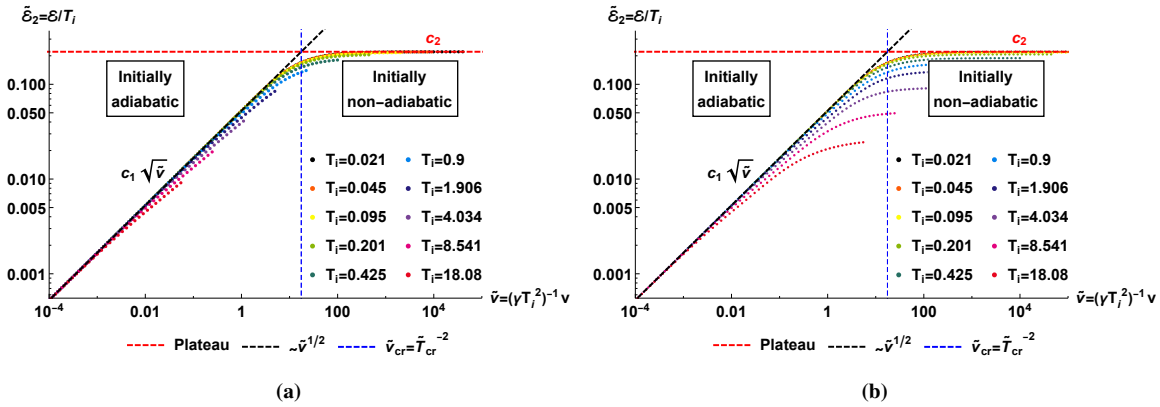

Figure 5.15: **(a)** The rescaled excitation density $\tilde{\mathcal{E}}_2$ as a function of the rescaled ramp rate $\tilde{v}$ for the nearest-neighbour Kitaev chain with $\gamma = 0.1$. The red and black dashed lines are the asymptotic scaling functions (5.95) and (5.96) in the two regimes, $\tilde{v} > \tilde{T}_{\rm cr}^{-2}$ and $\tilde{v} < \tilde{T}_{\rm cr}^{-2}$, which are separated by the crossover line at $\tilde{v}_{\rm cr} = \tilde{T}_{\rm cr}^{-2}$. **(b)** The same as (a), but for $\gamma = 0.001$. The parameters in (a) and (b) are set as follows: $L = 4 \times 10^6$, $J = \Delta = \delta = 1$, $\lambda_c = 4000$, $\mu = \mu_c = -g_\phi(0)$ and $T_f \simeq 0$.

Choosing $a' = 1/T_i$ and $b' = \left(\gamma T_i^{(s+1)}\right)^{-1}$, i.e. rescaling the excitation density $\mathcal{E}$ by $T_i^{-1/z}$ and the ramp rate v by $\left(\gamma T_i^{(s+1)}\right)^{-1}$, eliminates the explicit γ- and T_i-dependence in the integral above. As discussed in Section 5.2.4.1, we can now extract two asymptotic forms for the scaling function $\tilde{\mathcal{E}}_2$. Substituting the choices for a' and b' above into (5.94) trivially leads to

$$\tilde{\mathcal{E}}_2 = \mathcal{E}(1, \tilde{v}^{-1}), \tag{5.95}$$

where the excitation density $\mathcal{E}(1, \tilde{v}^{-1})$ is given by Eq. (5.82). This form is applicable for studying the scaling behaviour of $\tilde{\mathcal{E}}_2$ when the rescaled ramp rate $\tilde{v}$ is fast. The second asymptotic form of the scaling function is found through the change of variables $\lambda \to \tilde{v}^{1/(s+1)}\lambda$ in Eq. (5.94). This leads to

$$\tilde{\mathcal{E}}_2 = \tilde{v}^{1/[z(s+1)]}\mathcal{E}(\tilde{v}^{-1/(s+1)}, 1). \tag{5.96}$$

The form of the scaling function above is suitable for investigating the scaling behaviour in the slow $\tilde{v}$ regime.

For the scaling function $\tilde{\mathcal{E}}_2$, we find that the two asymptotic forms (5.95) and (5.96) are qualitatively similar to those encountered for the scaling function $\tilde{\mathcal{E}}_1$ in Section 5.2.4.1. More precisely, Eq. (5.95) describes a plateauing in the regime where $\tilde{v} > \tilde{T}_{\rm cr}^{-2}$, and Eq. (5.96) characterises the power-law scaling behaviour when $\tilde{v} < \tilde{T}_{\rm cr}^{-2}$. To provide a quantitative description of this plateauing and power-law scaling, we refer back to the two '*universal constants*', c_1 and c_2, in Eq. (5.88). In the initially non-adiabatic regime, where $\tilde{v} > \tilde{T}_{\rm cr}^{-2}$, the rescaled excitation density approaches $\tilde{\mathcal{E}}_2 = c_2$, corresponding to the *plateauing* behaviour. However, if the rescaled ramp rate is sufficiently slow, such that $\tilde{v} < \tilde{T}_{\rm cr}^{-2}$, then we are in the initially adiabatic regime in which $\tilde{\mathcal{E}}_2 = c_1\tilde{v}^{1/[z(s+1)]}$ exhibits power-law scaling with $\tilde{v}$. These results suggest that the scaling function $\tilde{\mathcal{E}}_2$ will be described by the universal functions c_2 and $c_1\tilde{v}^{1/[z(s+1)]}$ in the regimes where $\tilde{v} > \tilde{T}_{\rm cr}^{-2}$ and $\tilde{v} < \tilde{T}_{\rm cr}^{-2}$, respectively.

The analytic scaling functions defined above can be verified numerically. To demonstrate this, let us first revisit the numeric results for the nearest-neighbour Kitaev chain in Fig. 5.11a. If the analytic results are accurate, then rescaling the excitation density $\mathcal{E}$ by $1/T_i$ and the ramp rate v by $\left(\gamma T_i^2\right)^{-1}$ should collapse the data of Fig. 5.11a onto the two asymptotic scaling functions c_2 and $c_1\sqrt{\tilde{v}}$ for $\tilde{v} > \tilde{T}_{\rm cr}^{-2}$ and $\tilde{v} < \tilde{T}_{\rm cr}^{-2}$, respectively. Figure 5.15a supports these predictions, with the data collapsing neatly onto the two scaling functions. Despite the good agreement between the analytic and numeric results in general, the data does not collapse well for high initial temperatures. It is not unreasonable to expect this, since a high initial temperature T_i leads to the occupation of high-energy modes. The energies of these modes will not be accurately described by the leading-order approximation in Eq. (5.71), which is applied in our analytic derivation. For the same reason, weaker system–bath couplings negatively affect the collapse onto the two asymptotic scaling functions, as is evident in Fig. 5.15b. As before, we also validate the analytic results (5.95) and (5.96) for the Kitaev chain with long-range hopping. Rescaling the excitation density and the ramp rate by $T_i^{-1/(\phi-1)}$ and $\left(\gamma T_i^2\right)^{-1}$, respectively, collapses the data onto c_2 when $\tilde{v} > \tilde{T}_{\rm cr}^{-2}$ and $c_1\tilde{v}^{1/[2(\phi-1)]}$ when $\tilde{v} < \tilde{T}_{\rm cr}^{-2}$. This

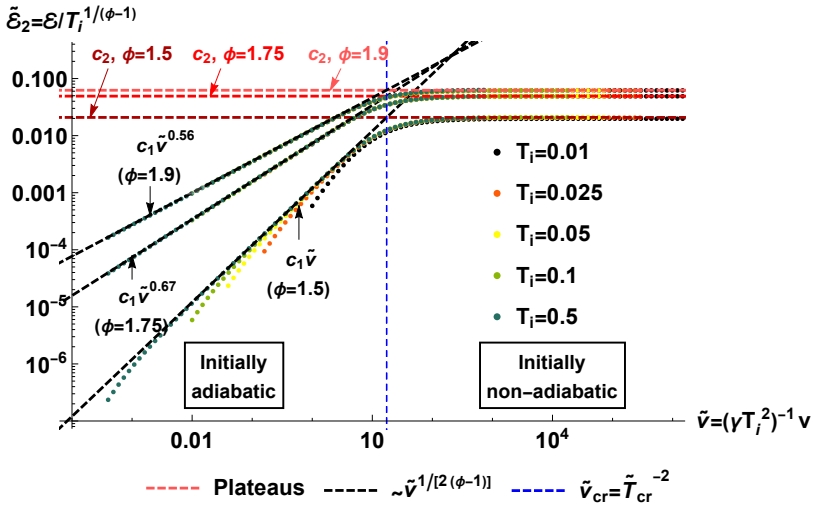

Figure 5.16: The rescaled excitation density $\tilde{\mathcal{E}}_2$ as a function of the rescaled ramp rate $\tilde{v}$ for the Kitaev chain with long-range hopping. The three data sets correspond to $\phi = 1.5$, $\phi = 1.75$ and $\phi = 1.9$. For each data set, the red and black dashed lines correspond to the asymptotic scaling functions (5.95) and (5.96). The initially adiabatic ($\tilde{v} < \tilde{T}_{\rm cr}^{-2}$) and initially non-adiabatic ($\tilde{v} > \tilde{T}_{\rm cr}^{-2}$) regimes are separated by the crossover line at $\tilde{v} = \tilde{v}_{\rm cr} = \tilde{T}_{\rm cr}^{-2}$. The remaining parameters are set to $L = 4 \times 10^6$, $J = \Delta = \delta = 1$, $\gamma = 0.01$, $\lambda_c = 4000$, $\mu = \mu_c = -g_\phi(0)$ and $T_f \simeq 0$.

is in agreement with the numeric results in Fig. 5.16 for three different choices of ϕ.

5.3 Conclusion

In this chapter we built on the work established in Chapter 4 to derive a set of scaling relations for the dissipative open Kitaev chain. We were particularly interested in two time dependencies, $\mu(t)$ and $T(t)$, where μ is the chemical potential in the Kitaev chain Hamiltonian (2.1) and T is the temperature of the thermal bath to which the system is coupled. This led to the introduction of two ramping protocols: the finite-temperature ramping protocol, whereby the chemical potential μ is ramped towards the quantum critical point $\mu = \mu_c$ at $T > 0$, and the temperature ramping protocol, in which the cooling of the Kitaev chain towards quantum criticality is investigated.

In Section 5.1 we introduced the finite-temperature ramping protocol, and monitored the density of excitations during the ramp. Studies of this nature have already been conducted by Refs. [23, 50, 85], which led to general scaling laws for the density of excitations. Our scaling results (5.30) and (5.31) corroborate those published in Ref. [50], where the excitation density was found to scale universally as a function of both the ramp rate v and the bath temperature T—even in the presence of dissipation. To derive the scaling laws for the finite-temperature ramps we considered the incoherent and coherent contributions to the excitation density independently. While this does not provide the full picture, it allowed us to conduct an in-depth study of the scaling behaviour of the incoherent contribution $\mathcal{E}_{\rm inc}$, and determine quantitative conditions under which we expect the scaling laws to be valid. To support the scaling arguments, we treated the Lindblad master equation (2.78) numerically. In all cases we observed good agreement between the analytic and numeric results.

In Section 5.2 we extended the existing results in the literature to incorporate scaling relations for the cooling of systems in the vicinity of the quantum critical point. To study the cooling of the Kitaev chain we implemented a protocol in which the temperature was ramped from some finite value $T > 0$ towards zero absolute temperature, while holding the system at the critical value $\mu = \mu_c$. Under suitable conditions, the excitation density $\mathcal{E}$ was found to exhibit scaling behaviour characterised by power laws involving the ramp rate v and the initial temperature T_i. The numeric results for the temperature ramps validated the analytic scaling predictions (5.74) and (5.76), and also suggested that an appropriate rescaling of the data can collapse the various data sets onto a universal scaling function. We explored this idea further, and established a universal description of the power-law scaling and plateauing in the two cooling regimes. Here we also found good agreement between our analytic work and the numeric results. Although we restricted the majority of our discussions to the Kitaev chain, we believe it is possible to extend the results of this chapter to other models with similar system–bath couplings.

Chapter 6

Summary and outlook

This thesis explored aspects of the non-equilibrium dynamics of quantum critical systems, with a focus on the universality of the dynamics in the vicinity of quantum critical points. We considered the density of excitations generated when linearly ramping a parameter in the system Hamiltonian towards the critical point, as well as the residual excitations present after lowering the thermal environment's temperature to zero at the critical point. In-keeping with the central ideas of the Kibble-Zurek framework, we found that these excitation densities obeyed universal scaling laws with powers determined by the equilibrium critical exponents of the phase transition.

For the bulk of the work, the analytic and numeric analyses of the universal features arising in the excitation density was specialised to the fermionic Kitaev chain. Accordingly, we started with an in-depth discussion of the model in Chapter 2, where we exploited the quadratic nature of the Hamiltonian (2.1) to map it onto a free-quasiparticle description. While this enabled us to study the unitary dynamics of the Kitaev chain, it was insufficient for exploring the effect of an external environment on the system's dynamics. To this end, we formulated the open system dynamics of the Kitaev chain in terms of an appropriate Markovian Lindblad master equation (2.78), with the thermal environment consisting of identical, independent bosonic baths. We chose a linear coupling between the baths and sites on the chain.

After introducing the Kitaev chain and its coupling to the environment we focused on solving the Lindblad dynamics of the model, which was one of the main numeric components of our work. To this end, we implemented the general method of "third quantisation", first introduced by Prosen [58]. Within this formalism, we derived the matrix differential equation (3.23) which governs the dynamics of the correlation functions relevant to calculating the excitation density. To reduce computational complexity, these correlation functions were reformulated in terms of Fourier Majorana fermions, resulting in a convenient block-diagonal structure for the matrix equation. This led to the set of decoupled, lower-dimensional matrix differential equations in (3.61), which allowed for an exact numeric treatment even for large system sizes.

The preliminary work in Chapter 2 and Chapter 3 formed the basis for our subsequent study of the isolated and open system dynamics of the Kitaev chain in the vicinity of a quantum phase transition. In Chapter 4 we focused on the dynamic Kibble-Zurek scaling for the isolated Kitaev chain. After a general description of the quantum Kibble-Zurek ramping protocol, we provided a detailed derivation of the scaling laws for the excitation density. Our results were in agreement with those of Ref. [22], and also extended the current results in the literature to include the presence of long-range hopping. A numeric treatment of the Kitaev chain was then used to verify the analytic scaling results, with good agreement observed for both weakly long-range and short-range systems.

Chapter 5 implemented the tools and methods developed in previous chapters to investigate scaling behaviour emerging in dissipative open quantum systems. Here we introduced two ramping protocols, a finite-temperature parameter ramping protocol and a protocol in which the system is cooled to quantum criticality. The former described the ramping of the chemical potential μ in the Kitaev chain Hamiltonian towards its critical value $\mu = \mu_c$ at a finite temperature $T > 0$. Provided that this temperature is sufficiently low, we observed that the system is still sensitive to the presence of the quantum critical point and that universal scaling emerges. In our derivation of the set of scaling relations, we considered the coherent $\mathcal{E}_{\text{coh}}$ and incoherent $\mathcal{E}_{\text{inc}}$ contributions separately. Later we treated the full master equation numerically to analyse the emergence of universal features in the total excitation density $\mathcal{E}_{\text{tot}}$. Based on the regimes in which the scaling laws are

expected to be valid, it was not surprising that only a certain range of parameters led to scaling behaviour emerging in $\mathcal{E}_{\text{tot}}$. The second protocol in Chapter 5 investigated the cooling of the Kitaev chain towards quantum criticality. Under certain conditions, the excitation density $\mathcal{E}$ was found to exhibit scaling behaviour characterised by power laws involving the ramp rate v and the initial temperature T_i. By introducing a universal scaling function, we established a unified description of the power-law scaling and plateauing in the two cooling regimes.

Our analytic results for the scaling laws in Chapter 4 and Chapter 5 support the emergence of dynamic universal scaling in the vicinity of the quantum phase transition, even in the presence of dissipation. This scaling behaviour is governed by the equilibrium critical exponents and, in the case of finite-temperature parameter ramps and temperature ramps, also the properties of the thermal bath to which the system is coupled. We restricted our discussions to short-range and weakly long-range chains. The strongly long-range case, where $\phi, \alpha < 1$, requires a more sophisticated numeric treatment to minimise finite-size effects, which become increasingly prominent for longer-range hopping and pairing. Despite these challenges, the strongly long-range Kitaev chain is a particularly intriguing model, as we expect it to exhibit a topological quantum phase transition at finite temperatures. One possible extension of this work is therefore to identify the footprint of this phase transition in the system's finite-temperature dynamics. This will require introducing novel non-local observables, for example the Uhlmann fidelity [95], which are sensitive to the proximity of the topological critical point. Monitoring such a topological quantity while performing a finite-temperature ramp in the vicinity of the critical point should allow for the identification of potential universal behaviour.

Another natural extension of this research would be to exploit the solvability of the Kitaev chain to study non-equilibrium stationary states. Our current description of the thermal bath is homogeneous, i.e. the Lindblad operators act on every lattice site in the same way. Coupling the sites of the chain to baths at different temperatures, i.e. using an inhomogeneous thermal environment, should permit the study of non-equilibrium stationary states. In particular, it would be interesting to initialise the system in a non-equilibrium stationary state corresponding to some parameter value μ, and then ramp μ across its critical value which, in equilibrium, corresponds to the quantum phase transition. A sensible definition of the excitations generated during such a ramp may be used to establish whether universal features emerge here. Of course, we again propose studying the dynamics for global ramps, where the control parameter couples uniformly to all lattice sites. An entirely separate, but perhaps thought-provoking question, is how this picture would change if local or nonuniform ramps are performed.

Although unrelated to the Kitaev chain itself, another interesting avenue of investigation is the dynamics of systems that exhibit true finite-temperature phase transitions, for example the long-range interacting transverse-field Ising chain or a Heisenberg chain. Both these models are known to exhibit finite-temperature phase transitions for sufficiently long-range interactions [90]. Of interest to us is the extent to which the scaling behaviour differs in weakly long-range versus strongly long-range regimes. From a numeric perspective, this will require an innovative and efficient computational scheme, which may be difficult to achieve since we would no longer be dealing with a solvable quadratic model.

The work contained in this thesis, as well as the above-mentioned extensions of the research, focuses primarily on systems which are in contact with some thermal environment. Despite its technical challenges, the theoretical study of open quantum systems is warranted by the major role these systems play in numerous applications of quantum physics, and the fact that the perfect isolation of quantum systems in experiments is not viable [50]. Consequently, it is necessary to understand the highly non-trivial interplay between the unitary quantum dynamics and the dissipation in order to address pertinent questions about quantum critical phenomena and non-equilibrium dynamics in open systems. In turn, research in this field may impact on current and future endeavours focused on the realisation of quantum-based technologies and scalable quantum computers.

References

[1] Carr, L. D. (ed.) [2010]. *Understanding Quantum Phase Transitions*, CRC Press.

[2] Vojta, M. [2003]. Quantum phase transitions, *Reports on Progress in Physics* **66**(12): 2069–2110.

[3] Chakravarty, S. [2010]. Dissipation, quantum phase transitions, and measurement, *in* L. D. Carr (ed.), *Understanding Quantum Phase Transitions*, CRC Press, chapter 2, pp. 31–58.

[4] Greiner, M., Mandel, O., Esslinger, T., Hänsch, T. W. and Bloch, I. [2002]. Quantum phase transition from a superfluid to a Mott insulator in a gas of ultracold atoms, *Nature* **415**: 39–44.

[5] Sondhi, S. L., Girvin, S. M., Carini, J. P. and Shahar, D. [1997]. Continuous quantum phase transitions, *Reviews of Modern Physics* **69**(1): 315–333.

[6] Vojta, T. [2002]. Quantum phase transitions, *in* K. H. Hoffmann and M. Schreiber (eds), *Computational Statistical Physics: From Billiards to Monte Carlo*, Springer, chapter 13, pp. 211–226.

[7] Sachdev, S. [2011]. *Quantum Phase Transitions*, Cambridge University Press.

[8] Polkovnikov, A. and Gritsev, V. [2010]. Universal dynamics near quantum critical points, *in* L. D. Carr (ed.), *Understanding Quantum Phase Transitions*, CRC Press, chapter 3, pp. 59–90.

[9] Hertz, J. A. [1975]. Quantum critical phenomena, *Physical Review B* **14**(3): 1165–1184.

[10] Greiner, M., Mandel, O., Rom, T., Altmeyer, A., Widera, A., Hänsch, T. and Bloch, I. [2003]. Quantum phase transition from a superfluid to a Mott insulator in an ultracold gas of atoms, *Physica B: Condensed Matter* **329–333**: 11–12.

[11] Dziarmaga, J. [2010]. Dynamics of a quantum phase transition and relaxation to a steady state, *Advances in Physics* **59**(6): 1063–1189.

[12] Damski, B. [2005]. The Simplest Quantum Model Supporting the Kibble-Zurek Mechanism of Topological Defect Production: Landau-Zener Transitions from a New Perspective, *Physical Review Letters* **95**(3): 035701(1–4).

[13] Kato, T. [1950]. On the Adiabatic Theorem of Quantum Mechanics, *Journal of the Physical Society of Japan* **5**(6): 435–439.

[14] Landau, L. D. [1932]. Zur Theorie der Energieübertragung II [A Theory of Energy Transfer. II], *Physikalische Zeitschrift der Sowjetunion* **2**(46).

[15] Zener, C. [1932]. Non-Adiabatic Crossing of Energy Levels, *Proceedings of the Royal Society of London. Series A, Containing Papers of a Mathematical and Physical Character* **137**(833): 696–702.

[16] Stueckelberg, E. C. G. [1932]. Theorie der unelastischen Stösse zwischen Atomen [Theory of Inelastic Collisions between Atoms], *Helvetica Physica Acta* **5**: 369–423.

[17] Majorana, E. [1932]. Atomi orientati in campo magnetico variabile, *Il Nuovo Cimento* **9**: 43–50.

[18] Vitanov, N. V. [1999]. Transition times in the Landau-Zener model, *Physical Review A* **59**(2): 988–994.

[19] Suzuki, S. and Okada, M. [2005]. Simulated quantum annealing by the real-time evolution, *in* A. Das and B. K. Chakrabarti (eds), *Quantum Annealing and Related Optimization Methods*, Springer, chapter 8, pp. 207–238.

[20] Vitanov, N. V. and Garraway, B. M. [1996]. Landau-Zener model: Effects of finite coupling duration, *Physical Review A* **53**(6): 4288–4304.

[21] del Campo, A. and Zurek, W. H. [2014]. Universality of phase transition dynamics: Topological defects from symmetry breaking, *International Journal of Modern Physics A* **29**(8): 1430018(1–49).

[22] Dutta, A. and Dutta, A. [2017]. Probing the role of long-range interactions in the dynamics of a long-range Kitaev chain, *Physical Review B* **96**(12): 125113(1–8).

[23] Patanè, D., Silva, A., Amico, L., Fazio, R. and Santoro, G. E. [2008]. Adiabatic Dynamics in Open Quantum Critical Many-Body Systems, *Physical Review Letters* **101**(17): 175701(1–4).

[24] Wubs, M., Saito, K., Kohler, S., Kayanuma, Y. and Hänggi, P. [2005]. Landau–Zener transitions in qubits controlled by electromagnetic fields, *New Journal of Physics* **7**: 218(1–14).

[25] Miladinovic, N., Hasan, F., Chisholm, N., Linnington, I. E., Hinds, E. A. and O'Dell, D. H. J. [2011]. Adiabatic transfer of light in a double cavity and the optical Landau-Zener problem, *Physical Review A* **84**(4): 043822(1–21).

[26] Sinitsyn, N. A. and Li, F. [2016]. Solvable multistate model of Landau-Zener transitions in cavity QED, *Physical Review A* **93**(6): 063859(1–12).

[27] Hasan, F. and O'Dell, D. H. J. [2016]. Parametric amplification of light in a cavity with a moving dielectric membrane: Landau-Zener problem for the Maxwell field, *Physical Review A* **94**(4): 043823(1–24).

[28] Niranjan, A., Li, W. and Nath, R. [2020]. Landau-Zener transitions and adiabatic impulse approximation in an array of two Rydberg atoms with time-dependent detuning, *Physical Review A* **101**(6): 063415(1–16).

[29] Altland, A. and Gurarie, V. [2008]. Many Body Generalization of the Landau-Zener Problem, *Physical Review Letters* **100**(6): 063602(1–4).

[30] Qian, Y., Gong, M. and Zhang, C. [2013]. Many-body Landau-Zener transition in cold-atom double-well optical lattices, *Physical Review A* **87**(1): 013636(1–6).

[31] Johansson, J., Amin, M. H. S., Berkley, A. J., Bunyk, P., Choi, V., Harris, R., Johnson, M. W., Lanting, T. M., Lloyd, S. and Rose, G. [2009]. Landau-Zener transitions in a superconducting flux qubit, *Physical Review B* **80**(1): 012507(1–4).

[32] Larson, J. [2015]. Multiple-time-scale Landau-Zener transitions in many-body systems, *Physical Review A* **91**(1): 013618(1–9).

[33] Kolovsky, A. R. and Maksimov, D. N. [2016]. Mott-insulator state of cold atoms in tilted optical lattices: Doublon dynamics and multilevel Landau-Zener tunneling, *Physical Review A* **94**(4): 043630(1–9).

[34] Ashhab, S. [2016]. Landau-Zener transitions in an open multilevel quantum system, *Physical Review A* **94**(4): 042109(1–9).

[35] Chen, R. [2020]. Landau-Zener transitions in a fermionic dissipative environment, *Physical Review B* **101**(12): 125426(1–10).

[36] Sarkar, S., Rana, D. and Mandal, S. [2020]. Defect production and quench dynamics in the three-dimensional Kitaev model, *Physical Review B* **102**(13): 134309(1–18).

[37] Kibble, T. W. B. [1976]. Topology of cosmic domains and strings, *Journal of Physics A: Mathematical and General* **9**(8): 1387–1398.

[38] Zurek, W. H. [1996]. Cosmological experiments in condensed matter systems, *Physics Reports* **276**(4): 177–221.

[39] Zurek, W. H. [1985]. Cosmological experiments in superfluid helium?, *Nature* **317**: 505–508.

[40] Chandran, A., Erez, A., Gubser, S. S. and Sondhi, S. L. [2012]. Kibble-Zurek problem: Universality and the scaling limit, *Physical Review B* **86**(6): 064304(1–16).

[41] Zurek, W., Dorner, U. and Zoller, P. [2005]. Dynamics of a Quantum Phase Transition, *Physical Review Letters* **95**(10): 105701(1–4).

[42] Polkovnikov, A. [2005]. Universal adiabatic dynamics in the vicinity of a quantum critical point, *Physical Review B* **72**(16): 161201(1–4).

[43] Dziarmaga, J. [2005]. Dynamics of a Quantum Phase Transition: Exact Solution of the Quantum Ising Model, *Physical Review Letters* **95**(24): 245701(1–4).

[44] Sen, D., Sengupta, K. and Mondal, S. [2008]. Defect Production in Nonlinear Quench across a Quantum Critical Point, *Physical Review Letters* **101**(1): 016806(1–4).

[45] Polkovnikov, A., Sengupta, K., Silva, A. and Vengalattore, M. [2011]. Colloquium: Nonequilibrium dynamics of closed interacting quantum systems, *Reviews of Modern Physics* **83**(3): 863–883.

[46] Xu, X.-Y., Han, Y.-J., Sun, K., Xu, J.-S., Tang, J.-S., Li, C.-F. and Guo, G.-C. [2014]. Quantum Simulation of Landau-Zener Model Dynamics Supporting the Kibble-Zurek Mechanism, *Physical Review Letters* **112**(3): 035701(1–5).

[47] Wang, L., Zhou, C., Tu, T., Jiang, H.-W., Guo, G.-P. and Guo, G.-C. [2014]. Quantum simulation of the Kibble-Zurek mechanism using a semiconductor electron charge qubit, *Physical Review A* **89**(2): 022337(1–6).

[48] Gong, M., Wen, X., Sun, G., Zhang, D.-W., Lan, D., Zhou, Y., Fan, Y., Liu, Y., Tan, X., Yu, H., Yu, Y., Zhu, S.-L., Han, S. and Wu, P. [2016]. Simulating the Kibble-Zurek mechanism of the Ising model with a superconducting qubit system, *Scientific Reports* **6**: 22667(1–9).

[49] Breuer, H.-P. and Petruccione, F. [2002]. *The theory of open quantum systems*, Oxford University Press.

[50] Patanè, D., Amico, L., Silva, A., Fazio, R. and Santoro, G. E. [2009]. Adiabatic dynamics of a quantum critical system coupled to an environment: Scaling and kinetic equation approaches, *Physical Review B* **80**(2): 024302(1–10).

[51] D'Abbruzzo, A. and Rossini, D. [2021]. Self-consistent microscopic derivation of Markovian master equations for open quadratic quantum systems, *arXiv:2101.09303* pp. 1–17.

[52] Müller, M., Diehl, S., Pupillo, G. and PeterZoller [2012]. Engineered Open Systems and Quantum Simulations with Atoms and Ions, *Advances in Atomic, Molecular, and Optical Physics* **61**: 1–80.

[53] Houck, A., Türeci, H. and Koch, J. [2012]. On-chip quantum simulation with superconducting circuits, *Nature Physics* **8**: 292–299.

[54] Lidar, D. A. [2019]. Lecture Notes on the Theory of Open Quantum Systems, *arXiv:1902.00967* pp. 1–131.

[55] Schaller, G. [2014]. *Open Quantum Systems Far from Equilibrium*, Springer International Publishing.

[56] Xu, X., Thingna, J., Guo, C. and Poletti, D. [2019]. Many-body open quantum systems beyond Lindblad master equations, *Physical Review A* **99**(1): 012106(1–8).

[57] Konopik, M. and Lutz, E. [2020]. Local master equations may fail to describe dissipative critical behavior, *arXiv:2012.09907* pp. 1–9.

[58] Prosen, T. [2008]. Third quantization: a general method to solve master equations for quadratic open Fermi systems, *New Journal of Physics* **10**(4): 043026(1–23).

[59] Prosen, T. [2010]. Spectral theorem for the Lindblad equation for quadratic open fermionic systems, *Journal of Statistical Mechanics: Theory and Experiment* **2010**(7): P07020(1–19).

[60] Kinoshita, T., Wenger, T. and Weiss, D. S. [2006]. A quantum Newton's cradle, *Nature* **440**: 900–903.

[61] Sadler, L. E., Higbie, J. M., Leslie, S. R., Vengalattore, M. and Stamper-Kurn, D. M. [2006]. Spontaneous symmetry breaking in a quenched ferromagnetic spinor Bose–Einstein condensate, *Nature* **443**: 312–315.

[62] Hofferberth, S., Lesanovsky, I., Fischer, B., Schumm, T. and Schmiedmayer, J. [2007]. Non-equilibrium coherence dynamics in one-dimensional Bose gases, *Nature* **449**: 324–327.

[63] Trotzky, S., Chen, Y.-A., Flesch, A., McCulloch, I. P., Schollwöck, U., Eisert, J. and Bloch, I. [2012]. Probing the relaxation towards equilibrium in an isolated strongly correlated one-dimensional Bose gas, *Nature Physics* **8**: 325–330.

[64] Cheneau, M., Barmettler, P., Poletti, D., Endres, M., Schauß, P., Fukuhara, T., Gross, C., Bloch, I., Kollath, C. and Kuhr, S. [2012]. Light-cone-like spreading of correlations in a quantum many-body system, *Nature* **481**: 484–487.

[65] Gring, M., Kuhnert, M., Langen, T., Kitagawa, T., Rauer, B., Schreitl, M., Mazets, I., Smith, D. A., Demler, E. and Schmiedmayer, J. [2012]. Relaxation and Prethermalization in an Isolated Quantum System, *Science* **337**(6100): 1318–1322.

[66] Makotyn, P., Klauss, C. E., Goldberger, D. L., Cornell, E. A. and Jin, D. S. [2014]. Universal dynamics of a degenerate unitary Bose gas, *Nature Physics* **10**: 116–119.

[67] Chen, Z., Tang, T., Austin, J., Shaw, Z., Zhao, L. and Liu, Y. [2019]. Quantum Quench and Nonequilibrium Dynamics in Lattice-Confined Spinor Condensates, *Physical Review Letters* **123**(11): 113002(1–5).

[68] Greiner, M., Mande, O., Hänsch, T. W. and Bloch, I. [2002]. Collapse and revival of the matter wave field of a Bose–Einstein condensate, *Nature* **419**: 51–54.

[69] Bloch, I., Dalibard, J. and Zwerger, W. [2008]. Many-body physics with ultracold gases, *Reviews of Modern Physics* **80**(3): 885–964.

[70] Chen, Y.-A., Huber, S. D., Trotzky, S., Bloch, I. and Altman, E. [2011]. Many-body Landau–Zener dynamics in coupled one-dimensional Bose liquids, *Nature Physics* **7**: 61–67.

[71] Lewenstein, M., Sanpera, A. and Ahufinger, V. [2012]. *Ultracold Atoms in Optical Lattices: Simulating quantum many-body systems*, Oxford University Press.

[72] Bloch, I., Dalibard, J. and Nascimbène, S. [2012]. Quantum simulations with ultracold quantum gases, *Nature Physics* **8**: 267–276.

[73] Schneider, U., Hackermüller, L., Ronzheimer, J. P., Will, S., Braun, S., Best, T., Bloch, I., Demler, E., Mandt, S., Rasch, D. and Rosch, A. [2012]. Fermionic transport and out-of-equilibrium dynamics in a homogeneous Hubbard model with ultracold atoms, *Nature Physics* **8**: 213–218.

[74] Lewenstein, M., Sanpera, A., Ahufinger, V., Damski, B., Sen(De), A. and Sen, U. [2007]. Ultracold atomic gases in optical lattices: mimicking condensed matter physics and beyond, *Advances in Physics* **56**(2): 243–379.

[75] Sengupta, K., Powell, S. and Sachdev, S. [2004]. Quench dynamics across quantum critical points, *Physical Review A* **69**(5): 053616(1–10).

[76] Rossini, D., Silva, A., Mussardo, G. and Santoro, G. E. [2009]. Effective Thermal Dynamics Following a Quantum Quench in a Spin Chain, *Physical Review Letters* **102**(12): 127204(1–4).

[77] Fagotti, M. and Calabrese, P. [2008]. Evolution of entanglement entropy following a quantum quench: Analytic results for the XY chain in a transverse magnetic field, *Physical Review A* **78**(1): 010306(1–4).

[78] Divakaran, U. [2018]. Sudden quenches in a quasiperiodic Ising model, *Physical Review E* **98**(3): 032110(1–5).

[79] Silva, A. [2008]. Statistics of the Work Done on a Quantum Critical System by Quenching a Control Parameter, *Physical Review Letters* **101**(12): 120603(1–4).

[80] Arrais, E. G., Wisniacki, D. A., Roncaglia, A. J. and Toscano, F. [2019]. Work statistics for sudden quenches in interacting quantum many-body systems, *Physical Review E* **100**(5): 052136(1–12).

[81] Puebla, R., Marty, O. and Plenio, M. B. [2019]. Quantum Kibble-Zurek physics in long-range transverse-field Ising models, *Physical Review A* **100**(3): 032115(1–15).

[82] Cui, J.-M., Gómez-Ruiz, F. J., Huang, Y.-F., Li, C.-F., Guo, G.-C. and del Campo, A. [2020]. Experimentally testing quantum critical dynamics beyond the Kibble–Zurek mechanism, *Communications Physics* **3**(1): 44(1–7).

[83] De Grandi, C., Gritsev, V. and Polkovnikov, A. [2010a]. Quench dynamics near a quantum critical point, *Physical Review B* **81**(1): 012303(1–4).

[84] De Grandi, C., Gritsev, V. and Polkovnikov, A. [2010b]. Quench dynamics near a quantum critical point: Application to the sine-Gordon model, *Physical Review B* **81**(22): 224301(1–21).

[85] Rossini, D. and Vicari, E. [2020]. Dynamic Kibble-Zurek scaling framework for open dissipative many-body systems crossing quantum transitions, *Physical Review Research* **2**(2): 023211(1–15).

[86] Hedvall, P. and Larson, J. [2017]. Dynamics of non-equilibrium steady state quantum phase transitions, *arXiv:1712.01560* pp. 1–21.

[87] Schützhold, R. and Schaller, G. [2006]. Adiabatic quantum algorithms as quantum phase transitions: First versus second order, *Physical Review A* **74**(6): 060304(1–4).

[88] Farhi, E., Goldstone, J., Gutmann, S., Lapan, J., Lundgren, A. and Preda, D. [2001]. A Quantum Adiabatic Evolution Algorithm Applied to Random Instances of an NP-Complete Problem, *Science* **292**(5516): 472–475.

[89] Gardas, B., Dziarmaga, J., Zurek, W. H. and Zwolak, M. [2018]. Defects in Quantum Computers, *Scientific Reports* **8**: 4539(1–10).

[90] Vodola, D., Lepori, L., Ercolessi, E. and Pupillo, G. [2015]. Long-range Ising and Kitaev models: phases, correlations and edge modes, *New Journal of Physics* **18**(1): 015001(1–18).

[91] Vodola, D., Lepori, L., Ercolessi, E., Gorshkov, A. V. and Pupillo, G. [2014]. Kitaev Chains with Long-Range Pairing, *Physical Review Letters* **113**(15): 156402(1–5).

[92] Nulty, S., Vala, J., Meidan, D. and Kells, G. [2020]. Constrained thermalisation and topological superconductivity, *arXiv:2001.10282* pp. 1–11.

[93] Lieb, E., Schultz, T. and Mattis, D. [1961]. Two Soluble Models of an Antiferromagnetic Chain, *Annals of Physics* **16**(3): 407–466.

[94] Gabbrielli, M. [2018]. Multipartite entanglement in quantum phase transitions, *arXiv:1810.10537* pp. 1–124.

[95] Bhattacharya, U. and Dutta, A. [2018]. Topological footprints of the Kitaev chain with long-range superconducting pairings at a finite temperature, *Physical Review B* **97**: 214505(1–7).

[96] Jordan, P. and Wigner, E. [1928]. Über das Paulische Äquivalenzverbot, *Zeitschrift für Physik* **47**: 631–651.

[97] Calabrese, P., Essler, F. H. L. and Fagotti, M. [2012]. Quantum quench in the transverse field Ising chain: I. Time evolution of order parameter correlators, *Journal of Statistical Mechanics: Theory and Experiment* **2012**(7): P07016(1–74).

[98] Greiter, M., Schnells, V. and Thomale, R. [2014]. The 1D Ising model and the topological phase of the Kitaev chain, *Annals of Physics* **351**: 1026–1033.

[99] Kitaev, A. Y. [2001]. Unpaired Majorana fermions in quantum wires, *Uspekhi Fizicheskikh Nauk* **44**(10S): 131–136.

[100] Segnorile, H. H., González, C. E. and Zamar, R. C. [2019]. Adiabatic quantum decoherence in non-interacting subsystems, induced by the coupling with a common boson bath, *arXiv:1912.12993* pp. 1–16.

[101] Sakurai, J. J. and Napolitano, J. [2017]. *Modern Quantum Mechanics*, Cambridge University Press.

[102] Prosen, T. and Žunkovič, B. [2010]. Exact solution of Markovian master equations for quadratic Fermi systems: thermal baths, open XY spin chains, and non-equilibrium phase transition, *New Journal of Physics* **12**(2): 025016(1–23).

[103] Kos, P. and Prosen, T. [2017]. Time-dependent correlation functions in open quadratic fermionic systems, *Journal of Statistical Mechanics: Theory and Experiment* **2017**: 123103(1–25).

[104] Lieu, S., McGinley, M. and Cooper, N. R. [2020]. Tenfold Way for Quadratic Lindbladians, *Physical Review Letters* **124**(4): 040401(1–6).

[105] Danielewicz, P. [1984]. Quantum theory of nonequilibrium processes, I, *Annals of Physics* **152**(2): 239–304.

[106] Molinari, L. G. [2017]. Notes on Wick's theorem in many-body theory, *arXiv:1710.09248* pp. 1–6.

[107] Kadanoff, L. P. [1966]. Scaling Laws for Ising Models near T_c, *Physics* **2**(6): 263–272.

[108] Wilson, K. G. [1971]. Renormalization Group and Critical Phenomena. I. Renormalization Group and the Kadanoff Scaling Picture, *Physical Review B* **4**(9): 3174–3183.

[109] Gradshteyn, I. S. and Ryzhik, I. [2007]. *Table of Integrals, Series and Products*, Elsevier Academic Press.

[110] Dutta, A., Aeppli, G., Chakrabarti, B. K., Divakaran, U., Rosenbaum, T. F. and Sen, D. [2015]. *Quantum Phase Transitions in Transverse Field Spin Models: From Statistical Physics to Quantum Information*, Cambridge University Press.

[111] Defenu, N., Enss, T., Kastner, M. and Morigi, G. [2018]. Dynamical Critical Scaling of Long-Range Interacting Quantum Magnets, *Physical Review Letters* **121**(24): 240403(1–6).

[112] Press, W. H., Teukolsky, S. A., Vetterling, W. T. and Flannery, B. P. [1992]. *Numerical Recipes in C: The Art of Scientific Computing*, Cambridge University Press.

[113] Polyanin, A. and Zaitsev, V. [2002]. *Handbook of Exact Solutions for Ordinary Differential Equations (2nd ed.)*, Chapman and Hall/CRC.

[114] Bhattacharjee, S. M. and Seno, F. [2001]. A measure of data collapse for scaling, *Journal of Physics A: Mathematical and General* **34**(33): 6375–6380.

[115] Santoro, G. E. [2016]. Non-equilibrium quantum systems, *International School for Advanced Studies Lecture Notes* pp. 1–148.

[116] Browder, A. [1996]. *Mathematical Analysis: An Introduction*, Springer-Verlag New York.

Appendices

Appendix A

Adiabatic-following condition

In this appendix we show how a condition for adiabatic evolution within the Landau-Zener (LZ) model can be motivated directly from the set of coupled differential equations (1.4) governing the system's dynamics. When this condition is met the system's state is therefore able to "follow" the Hamiltonian's instantaneous ground state, even as the latter changes in time. We also show how this result can be adapted to apply to the dynamics of a single η_k-mode of the isolated Kitaev chain.

A.1 Adiabatic-following condition for the standard LZ model

First we formulate the differential equations from Eq. (1.4) describing the time evolution of the LZ model in matrix form as

$$i\frac{d}{dt}\begin{bmatrix} C_1(t) \\ C_2(t) \end{bmatrix} = \underbrace{\begin{bmatrix} \varepsilon(t) & \bar{\Delta} \\ \bar{\Delta} & -\varepsilon(t) \end{bmatrix}}_{H(t)} \begin{bmatrix} C_1(t) \\ C_2(t) \end{bmatrix}. \tag{A.1}$$

Here the detuning $\varepsilon(t)$ varies linearly in time at a constant rate of $\dot{\varepsilon}(t) = \vartheta$. The unitary transformation diagonalising $H(t)$ is

$$U(t) = \begin{bmatrix} \cos[\theta(t)/2] & \sin[\theta(t)/2] \\ -\sin[\theta(t)/2] & \cos[\theta(t)/2] \end{bmatrix}, \tag{A.2}$$

where the angle $\theta(t)$ is such that $\cos[\theta(t)] = \varepsilon(t)/\sqrt{\varepsilon^2(t)+\bar{\Delta}^2}$ and $\sin[\theta(t)] = \bar{\Delta}/\sqrt{\varepsilon^2(t)+\bar{\Delta}^2}$. The eigenvalues of $H(t)$ are $\pm\Delta(t)$ with $\Delta(t) = 2\sqrt{\varepsilon(t)^2+\bar{\Delta}^2}$. Hereafter the explicit time dependence of functions will be suppressed. The system state in the adiabatic basis is $\psi = U[C_1 \;\; C_2]^{\mathsf{T}}$, of which the dynamics is governed by the Hamiltonian

$$\tilde{H} = UHU^\dagger + i\dot{U}U^\dagger = \begin{bmatrix} +\Delta/2 & i\dot{\theta}/2 \\ -i\dot{\theta}/2 & -\Delta/2 \end{bmatrix} \tag{A.3}$$

according to

$$i\dot{\psi} = \tilde{H}\psi. \tag{A.4}$$

Note that

$$\dot{\theta} = -\frac{4\bar{\Delta}\vartheta}{\Delta^2}. \tag{A.5}$$

The components of ψ are the probability amplitudes for finding the system in either its instantaneous ground or excited state. Adiabatic evolution therefore corresponds to the magnitudes of these components remaining constant. Since the diagonal entries of $\tilde{H}$ only introduce phases in these components, any deviation from adiabatic evolution must be due to the two off-diagonal entries $\pm i\dot{\theta}/2$. To formulate a condition under which the effect of these off-diagonal entries will be negligible we exploit the qualitative similarity between the equation governing ψ and the well-known example of a harmonically driven two-level system [101]. Based on this analogy we require, for adiabatic evolution, that the magnitude $|\dot{\theta}|$ of the off-diagonal entries is small compared to $\Delta/2$. This is the analogue of weak driving, and amounts to the condition

$$\frac{2|\dot{\theta}|}{\Delta} = \frac{8|\bar{\Delta}|\vartheta}{\Delta^3} \ll 1. \tag{A.6}$$

Secondly, we require that the rate at which the off-diagonal entries vary in time is slow compared to the transition frequency Δ between the ground and excited state. This condition is the analogue of the driving being off-resonance with the transition between the two states. To quantify the relative rate of change in the off-diagonal entries we use the ratio $|\ddot{\theta}/\dot{\theta}|$. The second condition therefore reads

$$\frac{1}{\Delta}\left|\frac{\ddot{\theta}}{\dot{\theta}}\right| = \frac{8|\varepsilon|\vartheta}{\Delta^3} \ll 1. \tag{A.7}$$

The conditions (A.6) and (A.7) can be conveniently combined into

$$\sqrt{\left(\frac{8|\varepsilon|\vartheta}{\Delta^3}\right)^2 + \left(\frac{8|\bar{\Delta}|\vartheta}{\Delta^3}\right)^2} = \frac{4\vartheta}{\Delta^2} \ll 1, \tag{A.8}$$

which amounts to

$$\sqrt{\vartheta} \ll \Delta(t)/2. \tag{A.9}$$

As expected, this is a comparison of the ramp rate ϑ at which the detuning $\varepsilon(t)$ in $H(t)$ varies, with the instantaneous excitation gap $2\Delta(t)$ of $H(t)$. This shows that ramping $\varepsilon(t)$ through a point where $\Delta(t)$ vanishes will result in a loss of adiabaticity, no matter how slow the ramp rate. Far from this point condition (A.9) may still be satisfied, allowing the system to evolve adiabatically.

A.2 Adiabatic-following condition for the isolated Kitaev chain

In Section 4.2.1 we describe the evolution of the excitation probability $\langle \eta_k^\dagger \eta_k \rangle(t)$ for a single η_k-mode in the Kitaev chain by mapping this problem onto the Landau-Zener model. This mapping allows us to treat each η_k-mode as an independent two-level LZ model. The time-dependent Hamiltonian $H_k(t)$ (4.5) has the same structure as the Landau-Zener Hamiltonian $H(t)$ in Eq. (A.1) of the preceding section, with eigenenergies $\pm\lambda_k(t)$ given in Eq. (4.6). Following the same set of steps presented in Section A.1, the final condition for adiabatic evolution for a single η_k-mode is found to be

$$\sqrt{v} \ll \lambda_k. \tag{A.10}$$

Appendix B

Symmetries of the BdG Hamiltonian

In the process of simplifying the dissipator $\mathcal{D}[\varrho]$ (2.71) in Section 2.2.4 we used the condition

$$V^\dagger S^* + S^{\mathrm{T}} V = 0. \tag{B.1}$$

It was claimed that this additional constraint on the V and S matrices (2.11) is due to the symmetries of the Bogoliubov–de Gennes Hamiltonian (2.10) introduced in Section 2.1.2.1. For reference, we restate the Hamiltonian below as

$$\mathbb{H} = \begin{bmatrix} Q & P \\ -P^* & -Q^* \end{bmatrix}. \tag{B.2}$$

The Hamiltonian $\mathbb{H}$ exhibits a number of symmetries, with the relevant ones here being particle-hole (PH) symmetry and time-reversal (TR) symmetry. Both of these are realised through anti-unitary operators acting on the same column vector space as $\mathbb{H}$.

We introduce the operators for PH and TR symmetry as follows:

- The operator for PH symmetry is U_{PH} and acts as

$$U_{\mathrm{PH}} \begin{bmatrix} \vec{a} \\ \vec{b} \end{bmatrix} = \begin{bmatrix} \vec{b}^* \\ \vec{a}^* \end{bmatrix}, \tag{B.3}$$

  where $\vec{a}$ and $\vec{b}$ are L-component column vectors. It can be verified that $U_{\mathrm{PH}}\mathbb{H} = -\mathbb{H}U_{\mathrm{PH}}$.

- The operator for TR symmetry is U_{TR} and acts as

$$U_{\mathrm{TR}}\mathbf{v} = \mathbf{v}^*, \tag{B.4}$$

  i.e. by complex conjugation. In Eq. (B.4), and in what follows, boldface vectors comprise of $2L$ components. Since the entries of $\mathbb{H}$ are real, we have $U_{\mathrm{TR}}\mathbb{H} = \mathbb{H}U_{\mathrm{TR}}$.

Based on the two symmetries (B.3) and (B.4) we can make some statements about the eigenvectors of $\mathbb{H}$ (B.2). It follows that if $\mathbf{v}$ in Eq. (B.4) is an eigenvector of $\mathbb{H}$ with eigenvalue λ_k, then so is $U_{\mathrm{TR}}\mathbf{v} = \mathbf{v}^*$. This implies that U_{TR} leaves the eigenspaces of $\mathbb{H}$ invariant. Secondly, we have that if $\mathbf{v}$ is an eigenvector of $\mathbb{H}$ with eigenvalue λ_k, then $U_{\mathrm{PH}}\mathbf{v}$ is an eigenvector with eigenvalue $-\lambda_k$.[1] This observation is also reflected in the matrix $\mathbb{T}$ (2.12)

$$\mathbb{T} = \begin{bmatrix} V & S \\ S^* & V^* \end{bmatrix}, \tag{B.5}$$

which diagonalises $\mathbb{H}$ as

$$\mathbb{T}^\dagger \mathbb{H} \mathbb{T} = \begin{bmatrix} \Lambda & 0 \\ 0 & -\Lambda \end{bmatrix}. \tag{B.6}$$

Here Λ is an $L \times L$ diagonal matrix containing the mode energies $\lambda_k \geq 0$. The "particle" eigenvectors $\{\mathbf{u}_k\}$ with eigenvalues $\{\lambda_k\}$ are the first L columns of $\mathbb{T}$ (B.5), while the "hole" eigenvectors $\{U_{\mathrm{PH}}\mathbf{u}_k\}$ with

[1] As will become clear, this is just the statement that for each mode we have a particle with energy $\lambda_k > 0$, created by an $\eta_k^\dagger$ operator, and a corresponding hole with energy $\lambda_k < 0$, created by η_k.

eigenvalues $\{-\lambda_k\}$ are the last L columns.[2]

Based on the statements made above, we can now motivate how the two symmetries lead to condition (B.1). Note that since $\mathbb{H}$ (B.2) is real and symmetric we can choose $\mathbb{T}$ (B.5) to be real and orthogonal. However, this is not necessarily convenient, since it prevents us from constructing modes with well-defined momenta.[3] We will therefore not require the $\mathbf{u}_k$ vectors to be real. However, for the ones corresponding to zero-energy modes we will assume that $\mathbf{u}_k$ is either real, or proportional to a real vector. Keeping these assumptions in mind, let $\mathbf{u}_k$ be a "particle" eigenvector of $\mathbb{H}$ with eigenvalue $\lambda_k \geq 0$. Its time-reversed version $U_{\text{TR}}\mathbf{u}_k = \mathbf{u}_k^*$ is then an eigenvector with the same eigenvalue. If $\lambda_k > 0$ then $U_{\text{TR}}\mathbf{u}_k = \mathbf{u}_k^*$ is orthogonal to all the non-positive eigenvalue "hole" eigenvectors $\{U_{\text{PH}}\mathbf{u}_{k'}\}$. If $\lambda_k = 0$ then, by assumption, $U_{\text{TR}}\mathbf{u}_k = \mathbf{u}_k^*$ is proportional to $\mathbf{u}_k$, and therefore also orthogonal to all the $\{U_{\text{PH}}\mathbf{u}_{k'}\}$ vectors, since $\mathbb{T}$ is unitary and has orthogonal columns. In summary, the $\{\mathbf{u}_k^*\}$ vectors, which are the columns of

$$\begin{bmatrix} V^* \\ S \end{bmatrix}, \tag{B.7}$$

are orthogonal to the $\{U_{\text{PH}}\mathbf{u}_k\}$ vectors, which are the columns of

$$\begin{bmatrix} S \\ V^* \end{bmatrix}. \tag{B.8}$$

This implies that

$$\begin{bmatrix} V^* \\ S \end{bmatrix}^\dagger \begin{bmatrix} S \\ V^* \end{bmatrix} = \begin{bmatrix} V^T & S^\dagger \end{bmatrix} \begin{bmatrix} S \\ V^* \end{bmatrix} = V^T S + S^\dagger V^* = 0. \tag{B.9}$$

Through complex conjugation we obtain the result in Eq. (B.1), which is the condition imposed in Section 2.2.4.

[2] To connect this with the second quantised formalism, note that the expansion coefficients of η_k in the site-fermion basis are the entries of $\mathbf{u}_k^*$, i.e. $\eta_k = \mathbf{u}_k^\dagger \mathbf{c}$. Similarly, $\eta_k^\dagger = (U_{\text{PH}}\mathbf{u}_k)^\dagger \mathbf{c}$.

[3] This would be like choosing the "real" combinations $\eta_k + \eta_{-k}$ and $i(\eta_k - \eta_{-k})$ instead of η_k and η_{-k}. Due to the degeneracy of these modes we can have this choice, but the real combinations are more like (discrete) "standing waves" ($\sin(kx)$ and $\cos(kx)$) than travelling waves ($\exp(\pm ikx)$).

Appendix C

Landau-Zener transition probability

It is widely accepted that under certain conditions the quasiparticle excitation probability of several integrable spin models can be calculated using a general form of the Landau-Zener (LZ) transition probability. In Section C.1 we outline the link between the probability of exciting an η_k-mode and the probability of inducing a transition in the two-level model governed by $H_k(t)$ (4.5). Since the probability of exciting the η_k-mode is exactly the probability of inducing a transition in the two-level model, we map the fermionic problem onto the LZ model. This allows us to obtain the transition probability amplitude in Section C.2. Finally, in Section C.3 we derive the well-known asymptotic form of the LZ excitation probability for a single mode in the Kitaev chain.

C.1 The link between the fermionic and Landau-Zener pictures

Consider the time-dependent Hamiltonian from Eq. (2.21) in the text, which can be written compactly as

$$H(t) = \frac{1}{2}\sum_k \Psi_k^\dagger H_k(t)\Psi_k \tag{C.1}$$

with $\Psi_k = [a_k \;\; a_{-k}^\dagger]^T$ a column vector of Fourier fermion operators. The 2×2 matrix $H_k(t)$ has the form

$$H_k(t) = \begin{bmatrix} A_k(t) & iB_k \\ -iB_k & -A_k(t) \end{bmatrix}, \tag{C.2}$$

where $A_k(t) = A_{-k}(t) = 2Jg_\phi(k) + 2\mu(t)$ and $B_k = -B_{-k} = \Delta f_\alpha(k)$. We introduce the vector Ψ_k in the Heisenberg picture, denoted as

$$\Psi_k^H(t) = [a_k^H(t) \;\; a_{-k}^{\dagger H}(t)]^T. \tag{C.3}$$

Using the fermionic anticommutation relations it can be shown that the Heisenberg equations of motion for $\psi_k^H(t)$ are

$$i\frac{d}{dt}\Psi_k^H(t) = H_k(t)\Psi_k^H(t). \tag{C.4}$$

Equation (C.4) can be rewritten as a set of ordinary scalar differential equations. We express the components of $\Psi_k^H(t)$ (C.3) as time-dependent linear combinations of the time-independent operators, $\eta_{k,i}$ and $\eta_{-k,i}^\dagger$, which are the elementary excitations associated with the *initial* Hamiltonian $H(t_i)$. This leads to

$$\begin{bmatrix} a_k^H(t) \\ a_{-k}^{\dagger H}(t) \end{bmatrix} = \underbrace{\begin{bmatrix} u_k(t) & -v_k^*(t) \\ v_k(t) & u_k^*(t) \end{bmatrix}}_{U_k(t)} \underbrace{\begin{bmatrix} \eta_{k,i} \\ \eta_{-k,i}^\dagger \end{bmatrix}}_{\Phi_{k,i}}, \tag{C.5}$$

or compactly $\Psi_k^H(t) = U_k(t)\Phi_{k,i}$. It follows that the Heisenberg equations of motion in terms of $U_k(t)$ are

$$i\frac{d}{dt}U_k(t) = H_k(t)U_k(t), \tag{C.6}$$

which reduces to

$$i\frac{d}{dt}\begin{bmatrix} u_k(t) \\ v_k(t) \end{bmatrix} = H_k\begin{bmatrix} u_k(t) \\ v_k(t) \end{bmatrix} \tag{C.7}$$

since it is only necessary to consider the first column on both sides of Eq. (C.6).

We recognise the structure of Eq. (C.7) as being that of the equation governing the dynamics of a state $|\psi(t)\rangle = u_k(t)\,|1\rangle + v_k(t)\,|2\rangle = [u_k(t), v_k(t)]^T$ evolving under the matrix Hamiltonian $H_k(t)$ within the standard Landau-Zener framework of Section 1.1.2. In this sense the dynamics of a $\{k, -k\}$ mode pair under the fermionic Hamiltonian (C.1) is completely equivalent to the dynamics of a two-level Landau-Zener model. Ultimately we are interested in calculating the excitation probability, at the end of the ramp, of an η_k mode associated with the *final* fermionic Hamiltonian $H(t_f)$. This is given by $\langle \eta_k^\dagger \eta_k \rangle(t_f)$, where the expectation value is taken with respect to the system state at $t = t_f$. The definitions above can be combined to show that the correspondence with the Landau-Zener model persists here as well, and that $\langle \eta_k^\dagger \eta_k \rangle(t_f)$ indeed equals the LZ excitation probability $p_k = |\langle e(t_f)|\psi(t_f)\rangle|^2$, where $|e(t_f)\rangle$ is the positive energy eigenvector of $H_k(t_f)$. The lecture notes by Santoro [115] provide a more detailed account of this connection between the fermionic and LZ pictures.

C.2 The Landau-Zener transition probability amplitude

The Landau-Zener transition probability amplitude $A(\chi, \omega)$ (4.11) can be obtained from the solution to the set of differential equations governing the evolution of the two-level model. In the previous section we established the link between the fermionic and Landau-Zener pictures, and from Eq. (C.7) we write the set of coupled first-order differential equations as

$$i\frac{d}{dt}u_k(t) = A_k(t)u_k(t) + iB_k v_k(t) \qquad \text{and} \qquad i\frac{d}{dt}v_k(t) = -iB_k u_k(t) - A_k(t)v_k(t), \tag{C.8}$$

where $A_k(t)$ and B_k are defined below Eq. (C.2) As a matter of convenience, we introduce the dimensionless parameters χ and ω as

$$\chi(k,t) = \frac{A_k(t)}{\sqrt{2v}} = \frac{2Jg_\phi(k) + 2\mu(t)}{\sqrt{2v}} \qquad \text{and} \qquad \omega(k) = \frac{B_k}{\sqrt{2v}} = \frac{\Delta f_\alpha(k)}{\sqrt{2v}}. \tag{C.9}$$

Now using $\frac{\mathrm{d}}{\mathrm{d}t} = \sqrt{2v}\frac{\mathrm{d}}{\mathrm{d}\chi}$ and the dimensionless parameters (C.9), we express the set of coupled differential equations (C.8) as

$$i\frac{\mathrm{d}}{\mathrm{d}\chi}u_k = \chi u_k + i\omega v_k \qquad \text{and} \qquad i\frac{\mathrm{d}}{\mathrm{d}\chi}v_k = -i\omega u_k - \chi v_k, \tag{C.10}$$

or in matrix notation as

$$i\frac{\mathrm{d}}{\mathrm{d}\chi}\begin{bmatrix} u_k \\ v_k \end{bmatrix} = \underbrace{\begin{bmatrix} \chi & i\omega \\ -i\omega & -\chi \end{bmatrix}}_{H_\chi}\begin{bmatrix} u_k \\ v_k \end{bmatrix}, \tag{C.11}$$

where we have introduced the matrix H_χ. Taking the derivative with respect to χ in Eq. (C.10), and substituting in the expressions for $\frac{\mathrm{d}u_k}{\mathrm{d}\chi}$ and $\frac{\mathrm{d}v_k}{\mathrm{d}\chi}$ (C.10), leads to the following second-order differential equations (Weber equations) [15, 20]

$$\frac{\mathrm{d}^2}{\mathrm{d}\chi^2}u_k = -(i + \chi^2 + \omega^2)u_k \qquad \text{and} \qquad \frac{\mathrm{d}^2}{\mathrm{d}\chi^2}v_k = -(-i + \chi^2 + \omega^2)v_k. \tag{C.12}$$

The parabolic cylinder (Weber) function $D_n(z)$ is a solution of the second-order differential equations (C.12) [15, 20, 109]. Based on definitions in Gradshteyn and Ryzhik [109], we find the solutions of Eq. (C.12) to be

$$u_k(\chi) = aD_{-1+\frac{i\omega^2}{2}}\left(\sqrt{2}\chi e^{\frac{3\pi}{4}i}\right) + bD_{-1+\frac{i\omega^2}{2}}\left(\sqrt{2}\chi e^{-\frac{\pi}{4}i}\right) \tag{C.13}$$

and

$$v_k(\chi) = \frac{\sqrt{2}}{\omega}e^{-\frac{\pi}{4}i}\left[aD_{\frac{i\omega^2}{2}}\left(\sqrt{2}\chi e^{\frac{3\pi}{4}i}\right) - bD_{\frac{i\omega^2}{2}}\left(\sqrt{2}\chi e^{-\frac{\pi}{4}i}\right)\right], \tag{C.14}$$

where the time dependence enters via χ, and the coefficients a and b need to be determined from the initial conditions.

To determine the coefficients a and b we first express $u_k(\chi)$ and $v_k(\chi)$ in Eqs. (C.13) and (C.14) in terms

of the parameters

$$z = \sqrt{2}\chi e^{-\frac{\pi}{4}i} \qquad \text{and} \qquad n = \frac{\omega^2}{2}. \tag{C.15}$$

This leads to

$$u_k(\chi) = aD_{-1+in}(-z) + bD_{-1+in}(z) \qquad \text{and} \qquad v_k(\chi) = \frac{\sqrt{2}}{\omega}e^{-\frac{\pi}{4}i}\left[aD_{in}(-z) - bD_{in}(z)\right] \tag{C.16}$$

The ground state of the Hamiltonian H_χ (C.11) in the limit $\chi \to -\infty$ is $[\,1 \;\; 0\,]^{\mathrm{T}}$. Therefore we want to enforce, via a and b, the initial conditions

$$\lim_{\chi\to-\infty}|u_k(\chi)| = 1 \qquad \text{and} \qquad \lim_{\chi\to-\infty}|v_k(\chi)| = 0 \tag{C.17}$$

From the second initial condition and the expression for $v_k(\chi)$ in Eq. (C.16), together with the asymptotic expansions 9.246.1 and 9.246.2 in Ref. [109] we have

$$\frac{a}{b} = \lim_{\chi\to-\infty}\frac{D_{in}(z)}{D_{in}(-z)} = e^{-\pi n} = e^{-\frac{\pi\omega^2}{2}}. \tag{C.18}$$

Applying the result above to $u_k(\chi)$ and $v_k(\chi)$ in Eq. (C.16) leads to

$$u_k(\chi) = b\left[e^{-\frac{\pi\omega^2}{2}}D_{-1+in}(-z) + D_{-1+in}(z)\right] \quad \text{and} \quad v_k(\chi) = \frac{\sqrt{2}}{\omega}e^{-\frac{\pi}{4}i}b\left[e^{-\frac{\pi\omega^2}{2}}D_{in}(-z) - D_{in}(z)\right]. \tag{C.19}$$

To enforce the first initial condition (C.17), it is required that we determine the $\chi \to -\infty$ limit of $u_k(\chi)$. We achieve this using the asymptotic expansions in 9.246.1 and 9.246.2 of Ref. [109]. Keeping only the dominant terms, we have

$$u_k(\chi) \sim b\left[-\frac{\sqrt{2\pi}}{\Gamma(1-in)}e^{(-1+in)\pi i}e^{\frac{z^2}{4}}z^{-in}\right] \tag{C.20}$$

To ensure the first condition in Eq. (C.17) is met, we first identify the phases in the expansion of $u_k(\chi)$, which do not impact on the value of the coefficient b. We find that the initial condition is satisfied when

$$b = \frac{\Gamma(1-in)}{\sqrt{2\pi}}e^{\frac{\pi}{4}n}. \tag{C.21}$$

The expressions for the coefficients (C.18) and (C.21), together with Eq. (C.16), provide the exact solution to the coupled differential equations (C.10) with the initial conditions in Eq. (C.17).

The solutions for $u_k(\chi)$ and $v_k(\chi)$ determined above can be used to calculate the transition probability at time t. Recall that the time dependence enters via the parameter χ. For convenience we impose the condition $\omega \geq 0$ in what follows. Now the probability amplitude $A(\chi,\omega)$ is given by the inner product of $\psi_k(\chi) = [\,u_k(\chi) \;\; v_k(\chi)\,]^{\mathrm{T}}$ (4.7) with the excited state $|e(\chi)\rangle$ of the Hamiltonian (C.11). Following the same steps as in Section 1.1.2, we write the $|e(\chi)\rangle$ and $|g(\chi)\rangle$ eigenvectors of the Hamiltonian (C.11) as

$$|e(\chi)\rangle = \begin{bmatrix}\cos(\theta/2)\\ -i\sin(\theta/2)\end{bmatrix} \qquad \text{and} \qquad |g(\chi)\rangle = \begin{bmatrix}\sin(\theta/2)\\ i\cos(\theta/2)\end{bmatrix}, \qquad \theta\in[0,\pi], \tag{C.22}$$

where $\sin(\theta) = \omega/\lambda$ and $\cos\theta = \chi/\lambda$ with $\lambda = \sqrt{\chi^2+\omega^2}$. This allows us to express the components of the eigenvectors (C.22) as

$$\sin(\theta/2) = \sqrt{\frac{(1-\cos\theta)}{2}} = \sqrt{\frac{1}{2} - \frac{\chi}{2\sqrt{\chi^2+\omega^2}}}, \qquad \cos(\theta/2) = \sqrt{\frac{(1+\cos\theta)}{2}} = \sqrt{\frac{1}{2} + \frac{\chi}{2\sqrt{\chi^2+\omega^2}}}. \tag{C.23}$$

The inner product

$$\langle e(\chi)|\psi_k(\chi)\rangle = A(\chi,\omega) = \begin{bmatrix}\cos(\theta/2) & i\sin(\theta/2)\end{bmatrix}\begin{bmatrix}u_k(\chi)\\ v_k(\chi)\end{bmatrix} \tag{C.24}$$

with $\sin(\theta/2)$ and $\cos(\theta/2)$ from Eq. (C.23) and $u_k(\chi)$ and $u_k(\chi)$ from Eqs. (C.19) and (C.21) leads to

$$\begin{aligned} A(\chi,\omega) = &\frac{1}{\sqrt{\pi}}(1+i)2^{-2+\frac{i\omega^2}{4}}e^{-\frac{3\pi\omega^2}{8}+\frac{i}{2}} \\ &\times\left[(1-i)\sqrt{1+\frac{\chi}{\sqrt{\chi^2+\omega^2}}}\Gamma\left(1-\frac{i\omega^2}{2}\right)\left(e^{\frac{\pi\omega^2}{2}}D_{\frac{i\omega^2}{2}-1}((1-i)\chi)+D_{\frac{i\omega^2}{2}-1}((-1+i)\chi)\right)\right. \\ &\left.-i\omega\sqrt{1-\frac{\chi}{\sqrt{\chi^2+\omega^2}}}\Gamma\left(-\frac{i\omega^2}{2}\right)\left(D_{\frac{i\omega^2}{2}}((-1+i)\chi)-e^{\frac{\pi\omega^2}{2}}D_{\frac{i\omega^2}{2}}((1-i)\chi)\right)\right]. \end{aligned} \tag{C.25}$$

C.3 The asymptotic Landau-Zener transition probability

In some cases it is useful to have the asymptotic expression for the transition, or excitation, probability $p_k = |A(\chi,\omega)|^2$, with $A(\chi,\omega)$ (C.25), at a final time $t \to \infty$. In Section 1.1.2 we provided an expression for the asymptotic LZ transition probability in Eq. (1.10). With the work in Section C.2, we show that in the limit $t \to \infty$, i.e. $\chi \to \infty$, we indeed reproduce the well-known result (1.10). First note that in the limit $\chi \to \infty$ the excited state $|e(\chi)\rangle$ of the Hamiltonian (C.11) is $[1 \;\; 0]^{\mathrm{T}}$. Hence, the asymptotic transition probability will be given by $p_k = |u_k(\chi=\infty)|^2$. From Eq. (C.19) we have

$$\lim_{\chi\to\infty}|u_k(\chi)| = \lim_{\chi\to\infty}\left|b\left[e^{-\frac{\pi\omega^2}{2}}D_{-1+in}(-z)+D_{-1+in}(z)\right]\right|, \tag{C.26}$$

with b in Eq. (C.21). The asymptotic expansions of the parabolic cylinder functions $D_{-1+in}(-z)$ and $D_{-1+in}(z)$ in Ref. [109] yields

$$\lim_{\chi\to\infty}|u_k(\chi)| = \left|e^{\frac{\pi}{4}n-2\pi n+\frac{3\pi}{4}i(-in)}\right| = e^{-\pi n}. \tag{C.27}$$

According to Eq. (C.15), $n = \omega^2/2$, which leads to the exponential form of the transition probability as

$$p_k = |u_k(\chi=\infty)|^2 = e^{-\pi\omega^2} = e^{-\pi\Delta^2 f_\alpha^2(k)/(2v)}. \tag{C.28}$$

This form matches the result in Eq. (1.10).

Appendix D

Finite-v corrections to the scaling relations of the isolated Kitaev chain

The asymptotic scaling results for the isolated Kitaev chain in Eq. (4.24) of Chapter 4 are only applicable in the limit of very slow ramp rates. It is therefore important to question the extent to which this scaling behaviour will emerge if the ramp rate v is finite. This will depend on the magnitudes of the sub-leading terms which were neglected in multiple steps of our derivation in Chapter 4. Here we provide a more detailed analysis on the expected range of validity for the scaling in the nearest-neighbour Kitaev chain when v is finite.

Early in our derivation in Chapter 4 we neglected sub-leading terms in the expansions of χ and ω around $k = 0$. The expansions of χ and ω to the lowest order in k were called χ_0 and ω_0. These approximations were subsequently introduced when we replaced the excitation probability function in the integrand by its $v \to 0$ limiting value. In addition to this, we extended the upper bound of the integral to infinity. This extension results in certain sub-leading terms in the excitation density being ignored. With this in mind, a necessary condition for the predicted scaling behaviour to emerge at finite v is therefore that the magnitudes of the neglected sub-leading terms in the excitation density are sufficiently small. These neglected sub-leading terms can be viewed as finite-v corrections to the asymptotic scaling relation. In what follows we will briefly discuss these finite-v corrections for the nearest-neighbour case. A similar analysis can be performed for the long-range hopping and pairing cases.

As motivated in Section 4.2.1, it will be convenient to introduce the dimensionless parameters χ and ω. In the nearest-neighbour case these have the form

$$\chi(k,t) = \frac{2J\cos(k) + 2\mu(t)}{\sqrt{2v}} \qquad \text{and} \qquad \omega(k) = \frac{\Delta\sin(k)}{\sqrt{2v}}. \tag{D.1}$$

For ramps ending at a final time $t = t_f$ at the critical point we have $\mu(t_f) = \mu_f = -J$, hence Eq. (D.1) becomes

$$\chi(k,t_f) = \frac{2J(\cos(k) - 1)}{\sqrt{2v}} \qquad \text{and} \qquad \omega(k) = \frac{\Delta\sin(k)}{\sqrt{2v}}. \tag{D.2}$$

Now the excitation probability for a particular mode can be formulated in terms of these parameters as

$$P(\chi(k,t_f),\omega(k)) = |A(\chi(k,t_f),\omega(k))|^2, \tag{D.3}$$

where $A(\chi,\omega)$ is the probability amplitude in Eq. (4.11). If we expand χ and ω in Eq. (D.2) around $k = 0$ we have, to lowest order in k,

$$\chi_0(k) = -\frac{Jk^2}{\sqrt{2v}} \qquad \text{and} \qquad \omega_0(k) = \frac{\Delta k}{\sqrt{2v}}. \tag{D.4}$$

The exact excitation probability in Eq. (D.3) expressed in terms of ω_0 is

$$P_v(\omega_0) = P(\chi(\omega_0\sqrt{2v}/\Delta, t_f), \omega(\omega_0\sqrt{2v}/\Delta)). \tag{D.5}$$

It is possible to verify that $P_v(\omega_0)$ has a well-defined $v \to 0$ limit.

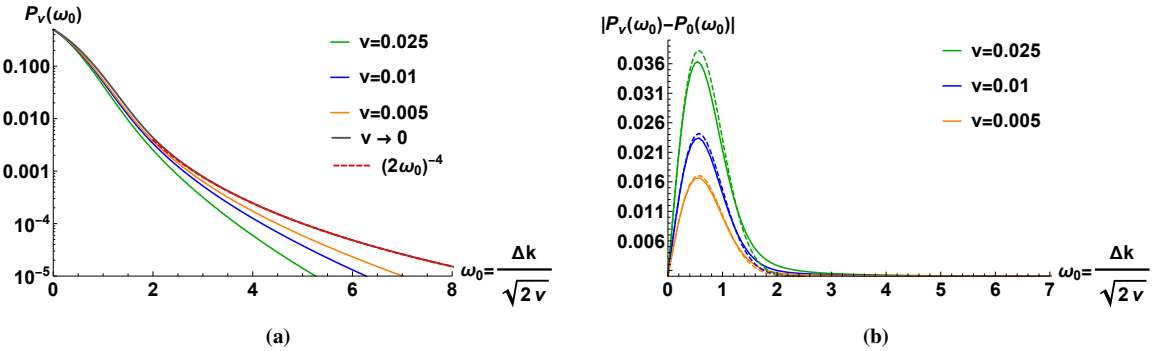

Figure D.1: **(a)** $P_v(\omega_0)$ for various choices of v, together with the exact $v \to 0$ result $P_0(\omega_0)$ and the large ω_0 approximation of the excitation probability, $P_0(\omega_0) \approx (2\omega_0)^{-4}$. **(b)** The absolute difference $|P_v(\omega_0) - P_0(\omega_0)|$ for various choices of v. The dashed lines correspond to the linear order correction term, which is given in Eq. (D.8).

The first, and most significant, finite-v correction to the excitation density comes from the replacement of $P_v(\omega_0)$ by its $v \to 0$ limit $P_0(\omega_0)$. Figure D.1a shows $P_v(\omega_0)$ for various choices of v, together with $P_0(\omega_0)$. As v decreases, $P_v(\omega_0)$ tends to $P_0(\omega_0)$, and there is good agreement in the region $\omega_0 \in [0, 3]$ where $P_0(\omega_0)$ is large (roughly $> 10^{-3}$). Figure D.1b shows the absolute value of the difference between $P_v(\omega_0)$ and $P_0(\omega_0)$, which is largest between $\omega_0 = 0$ and $\omega_0 \approx 2$. This difference provides an indication of the magnitude of the sub-leading terms which are dropped when replacing $P_v(\omega_0)$ by $P_0(\omega_0)$. The finite-v correction can therefore be estimated by expanding $P_v(\omega_0)$ to linear order in $\sqrt{v}$. To this end, we first expand $\chi(\omega_0\sqrt{2v}/\Delta, t_f)$ and $\omega(\omega_0\sqrt{2v}/\Delta)$, which are defined in Eq. (D.2), to linear order in $\sqrt{v}$ as

$$\chi(\omega_0\sqrt{2v}/\Delta) = -a\omega_0^2 \qquad \text{and} \qquad \omega(\omega_0\sqrt{2v}/\Delta) = \omega_0, \qquad \text{with} \qquad a = \frac{J\sqrt{2v}}{\Delta^2}. \tag{D.6}$$

For small-ω values, the excitation probability is given by

$$P(\chi, \omega) = P(0, \omega) + \frac{e^{-\pi\omega^2/2}\chi}{2\omega} + \mathcal{O}(\chi^2). \tag{D.7}$$

Combining Eqs. (D.6) and (D.7) yields, to linear order in $\sqrt{v}$,

$$P_v(\omega_0) \approx P_0(\omega_0) - \underbrace{\frac{e^{-\pi\omega_0^2/2}a\omega_0^2}{2\omega_0}}_{\text{Linear order correction}}. \tag{D.8}$$

The approximation above is only accurate when $\chi = -a\omega_0^2 \ll 1$, however for sufficiently small ramp rates this condition can at least be ensured for the range of ω_0 values for which $P_v(\omega_0)$ is non-negligible. Figure D.1b shows that the correction term in Eq. (D.8), indicated by the dashed lines, does an excellent job at describing the most significant deviation of $P_v(\omega_0)$ from $P_0(\omega_0)$. The maximum magnitude of this correction term, namely $a/(2\sqrt{e\pi})$, provides a good approximation for the upper bound on $|P_v(\omega_0) - P_0(\omega_0)|$.

Based on the discussions above, we can now compute the corrections to the excitation density itself, which is defined as

$$\mathcal{E}_{\text{coh}} = \frac{1}{\pi}\int_0^\pi dk\, P(\chi(k), \omega(k)). \tag{D.9}$$

Performing the change of variable $k \to \omega_0\sqrt{2v}/\Delta$ in the integral above, the expression for $\mathcal{E}_{\text{coh}}$ can be reformulated in terms of ω_0 as

$$\mathcal{E}_{\text{coh}} = \frac{1}{\pi}\frac{\sqrt{2v}}{\Delta}\int_0^{\omega_+} d\omega_0\, P_v(\omega_0), \tag{D.10}$$

where $\omega_+ = \Delta\pi/\sqrt{2v}$. A good approximation of the magnitude of the neglected sub-leading terms in $\mathcal{E}_{\text{coh}}$ when replacing $P_v(\omega_0)$ by $P_0(\omega_0)$ in Eq. (D.10) is given by the integral of the linear order correction (D.8). Accordingly we have

$$\int_0^{\omega_+} d\omega_0 \frac{e^{-\pi\omega_0^2/2}a\omega_0^2}{2\omega_0} \leq \int_0^{\infty} d\omega_0 \frac{e^{-\pi\omega_0^2/2}a\omega_0^2}{2\omega_0} = \frac{a}{2\pi}, \tag{D.11}$$

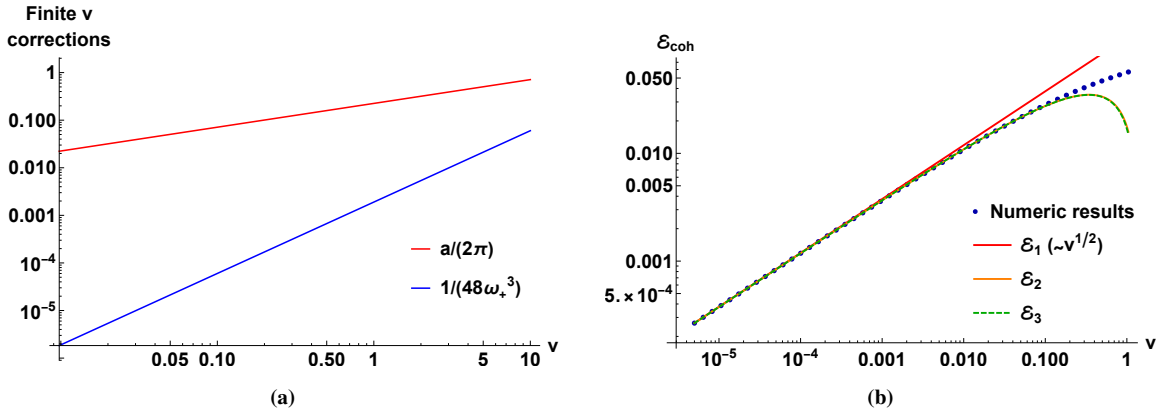

Figure D.2: **(a)** The two finite-v corrections, $a/(2\pi)$ and $1/(48\omega_+^3)$ from Eq. (D.14), as a function of the ramp rate v. Here we set $J = \Delta = 1$. It is clear that the first condition in Eq. (D.14) will imply the second, provided the ramp rate is sufficiently slow. **(b)** The exact numeric excitation density as a function of v, together with the analytic results in Eq. (D.15). The predicted scaling behaviour emerges at finite v, provided the two corrections are sufficiently small. At faster ramp rates, the corrections become large and visibly impact on the scaling of $\mathcal{E}_{\text{coh}}$.

where $a = J\sqrt{2v}/\Delta^2$ is defined in Eq. (D.6). The integral expressions in Eq. (D.11) are approximately equal once $\omega_+ > 2$. This implies that the primary finite-v correction to $\mathcal{E}_{\text{coh}}$ is well approximated by $a/(2\pi) = J\sqrt{2v}/(2\pi\Delta^2)$. As one would expect, the magnitude of this correction tends to zero as the ramp rate v decreases.

The second finite-v correction to $\mathcal{E}_{\text{coh}}$ involves the extension of the upper bound of the integral (D.10) to infinity. We have already shown that for slow ramps we can replace $P_v(\omega_0)$ by $P_0(\omega_0)$ and still capture the bulk of the contribution to $\mathcal{E}_{\text{coh}}$ accurately. Therefore, within the bounds of Eq. (D.11), we can take the excitation density to be

$$\mathcal{E}_{\text{coh}} = \frac{1}{\pi}\frac{\sqrt{2v}}{\Delta}\int_0^{\omega_+} d\omega_0\, P_0(\omega_0), \tag{D.12}$$

where the v dependence enters only in the prefactor and upper bound of the integral. Now assuming that $\omega_+ > 2$ we have

$$\int_{\omega_+}^{\infty} d\omega_0\, P_0(\omega_0) = \frac{1}{48}\frac{1}{\omega_+^3}, \tag{D.13}$$

where the large-ω_0 expansion $P_0(\omega_0) \approx (2\omega_0)^{-4}$ was used. The approximation $P_0(\omega_0) \approx (2\omega_0)^{-4}$ performs well for sufficiently large ω_0 values, as observed in Fig. D.1a. Equation (D.13) therefore provides an estimate of the correction which accounts for the extension of the integral bound to infinity.

A necessary condition for the predicted scaling in v to emerge for the nearest-neighbour Kitaev chain is that both the corrections are much smaller than one. This amounts to

$$\frac{a}{2\pi} = \frac{J\sqrt{2v}}{2\pi\Delta^2} \ll 1 \qquad \text{and} \qquad \frac{1}{48\omega_+^3} = \frac{v^{3/2}}{12\sqrt{2}(\pi\Delta)^3} \ll 1. \tag{D.14}$$

If one chooses $J = 1$ and Δ to be of order 1, the first condition will imply the second for sufficiently slow ramp rates, as seen in Fig. D.2a. The magnitudes of the corrections in Eq. (D.14) impact on the emergence of the predicted scaling behaviour, particularly at faster ramp rates where the conditions $a/(2\pi) \ll 1$ and $1/(48\omega_+^3) \ll 1$ are potentially not satisfied. To illustrate this, we plot the numeric excitation density results for the nearest-neighbour Kitaev chain in Fig. D.2b with

$$\mathcal{E}_1 = \frac{1}{\pi}\frac{\sqrt{2v}}{\Delta}\int_0^{\infty} d\omega_0\, P_0(\omega_0), \qquad \mathcal{E}_2 = \mathcal{E}_1 - \frac{a}{2\pi} \qquad \text{and} \qquad \mathcal{E}_3 = \mathcal{E}_1 - \frac{a}{2\pi} - \frac{1}{48\omega_+^3}. \tag{D.15}$$

The scaling is accurately predicted by $\mathcal{E}_1 \sim v^{1/2}$, and both the slope and intercept are in agreement with the numeric results. Combining $\mathcal{E}_1$ with the correction terms improves the agreement between the analytic and numeric results for large, finite v. Additionally, we can confirm from the plot that the correction of $a/(2\pi)$ has a significantly greater impact than the second correction $1/48\omega_+^3$. To observe the predicted scaling behaviour it is therefore important that the condition $a/(2\pi) \ll 1$ is met.

Appendix E

Linear-order approximation of the rate equation for the $k = 0$ mode

In our derivation of the scaling laws for the incoherent contribution $\mathcal{E}_{\text{inc}}$ to the excitation density in Section 5.1.2 we treated the excitation probability $\mathcal{P}_k$ to linear order in the system–bath coupling γ. A natural question that arises is under what conditions we would expect the predicted power-law scaling in Eqs. (5.30) and (5.31) to emerge. In this appendix we derive a condition for the predicted scaling in v and T to emerge by analysing the contribution to $\mathcal{E}_{\text{inc}}$ from the $k = 0$ mode within the linear-order approximation in Eq. (5.21).

We start with the rate equation (5.13), which describes the dynamics of the incoherent excitation probability $\mathcal{P}_k$. This is given by

$$\frac{\mathrm{d}}{\mathrm{d}t}\mathcal{P}_k = -\frac{1}{\tau_k}(\mathcal{P}_k - \mathcal{P}_k^{\text{th}}), \tag{E.1}$$

where τ_k^{-1} is the relaxation rate (5.17). The relaxation rate introduces the spectral density $\mathcal{J}$ of the thermal bath. Here we will consider an ohmic spectral density of the form in Eq. (2.81), with a cutoff frequency of $\lambda_c = \infty$. We proceed by considering only the $k = 0$ mode, which makes the largest contribution to the incoherent excitation density $\mathcal{E}_{\text{inc}}$. The approximations derived for the $k = 0$ mode are expected to also apply to the other k modes.

The rate equation (E.1) can be simplified if we consider only the $k = 0$ mode. First we write the dispersion relation for the $k = 0$ mode as

$$\lambda_0 = |2J + 2\mu(t)| = -(2J + 2\mu(t)), \tag{E.2}$$

where we choose $\mu(t) = vt$ as a matter of convenience. It will be useful to introduce a new variable $x = \frac{2(J+vt)}{T}$, which runs from $x_i = \frac{2(J+\mu_i)}{T} < 0$ to $x_f = 0$. Rewriting the relaxation rate τ_0^{-1} in Eq. (5.17) in terms of the ohmic spectral density (2.81) with $\lambda_c = \infty$ and the new variable x leads to

$$\tau_0^{-1} = 2\pi\gamma\delta\lambda_0(2n(\lambda_0) + 1) = 2\pi T\gamma\delta x\frac{e^x + 1}{e^x - 1}. \tag{E.3}$$

Noting that the equilibrium excitation probability $\mathcal{P}_k^{\text{th}}$ for the $k = 0$ mode is

$$\mathcal{P}_0^{\text{th}} = \frac{1}{e^{-x} + 1}, \tag{E.4}$$

the rate equation (E.1) for the $k = 0$ mode is written as

$$\frac{\mathrm{d}}{\mathrm{d}x}\mathcal{P}_0(x) = -\underbrace{\frac{\pi T^2\gamma\delta}{v}}_{a} x\frac{e^x + 1}{e^x - 1}\left(\mathcal{P}_0(x) - \frac{1}{e^{-x} + 1}\right) \qquad \text{with} \qquad a = \frac{\pi T^2\gamma\delta}{v}. \tag{E.5}$$

With the initial condition $\mathcal{P}_0(x_i) = 0$ where $x_i \to -\infty$, we can solve Eq. (E.5). We will take $x_i = -20$, since this is effectively equivalent to $x_i = -\infty$. The ramp ends at $x_f = 0$, so we analyse the excitation probability $P_0(0)$ as a function of a. The linear-order approximation which leads to perfect scaling is $\tilde{\mathcal{P}}_0(x)$,

satisfying

$$\frac{\mathrm{d}}{\mathrm{d}x}\tilde{\mathcal{P}}_0(x) = -ax\frac{e^x+1}{e^x-1}\left(0 - \frac{1}{e^{-x}+1}\right). \tag{E.6}$$

By solving for $\mathcal{P}_0(0)$ and $\tilde{\mathcal{P}}_0(0)$ numerically for various choices of $a \ll 1$ we extract the result

$$\frac{|\mathcal{P}_0(0) - \tilde{\mathcal{P}}_0(0)|}{\mathcal{P}_0(0)} \approx \frac{7}{2}a. \tag{E.7}$$

Requiring a less than 10% difference imposes the following condition on a:

$$a = \frac{\pi T^2 \gamma\delta}{v} < \frac{1}{35} \approx 0.02857. \tag{E.8}$$

This condition will hold for either sufficiently low temperatures, fast ramp rates or weak system–bath couplings.

Appendix F

Small-v/γ and small-T_i asymptotics of the excitation probability

The small-v/γ and small-T_i asymptotics of the excitation probability $\mathcal{P}_k$ (5.68) for a single η_k-mode in the Kitaev chain were used to derive the scaling relations for the temperature ramping protocol in Section 5.2.2. In this appendix we provide further information on the $v/\gamma \to 0$ and $T_i \to 0$ limits of the integrals in Eqs. (5.73) and (5.75), respectively. Section F.1 argues, via the dominated convergence theorem, that the $v/\gamma \to 0$ limit of Eq. (5.73) exists and is finite. The $T_i \to 0$ limit of Eq. (5.75) can be treated in the same way. To avoid unnecessary repetition, in Section F.2 we motivate that the limit exists and is finite using the small-T_i asymptotics of $\mathcal{P}_k$.

F.1 Small-v/γ asymptotics of the excitation probability and $v/\gamma \to 0$ limit of the integral

It is required to show that the integral

$$\int_0^\infty d\lambda\, (\lambda)^{\frac{1}{z}-1} \mathcal{P}\left(0, \frac{T_i}{\lambda (v/\gamma)^{1/(s+1)}}, \lambda^{s+1}\right) \tag{F.1}$$

from Eq. (5.73) has a well defined $\frac{T_i}{(v/\gamma)^{1/(s+1)}} \to \infty$ limit. We restate the excitation probability from Eq. (5.68) in the main text as

$$\mathcal{P}_k = \mathcal{P}\,(y, A, B) = Ce^{F(y)} + Be^{F(y)} \int_{-A}^{y} dy'\, e^{-F(y')} m(-1/y') \mathcal{P}_k^{\text{th}}\left(\frac{-1}{y'}\right) \tag{F.2}$$

with

$$C = \mathcal{P}_k^{\text{th}}(A^{-1}), \quad F(y) = -B\int_{-A}^{y} dy'\, m(-1/y') \quad \text{and} \quad m(-1/y) = 2\pi\left(\frac{2}{e^{-1/y}-1} + 1\right). \tag{F.3}$$

For convenience, we define

$$c = \frac{T_i}{(v/\gamma)^{1/(s+1)}}, \qquad A = \frac{c}{\lambda} \qquad \text{and} \qquad B = \lambda^{s+1}, \tag{F.4}$$

such that the excitation probability in Eq. (F.1) can be expressed as $\mathcal{P}(0, A, B)$. Now consider the Lebesgue's dominated convergence theorem [116]:

> *Suppose $f_n : \mathbb{R} \to [-\infty, \infty]$ is a sequence of (Lebesgue) measurable functions such that the point-wise limit $f(x) = \lim_{n\to\infty} f_n(x)$ exists, i.e. that $f_n \to f$ as $n \to \infty$. Now assume there is an integrable (summable) function $g : \mathbb{R} \to [0, \infty]$ with $|f_n(x)| \leq g(x)$, $\forall n$, for each $x \in \mathbb{R}$. Then f is integrable (summable), as is f_n for each n, and*
>
> $$\lim_{n\to\infty} \int_{\mathbb{R}} f_n d\mu = \int_{\mathbb{R}} \lim_{n\to\infty} f_n\, d\mu = \int_{\mathbb{R}} f\, d\mu. \tag{F.5}$$

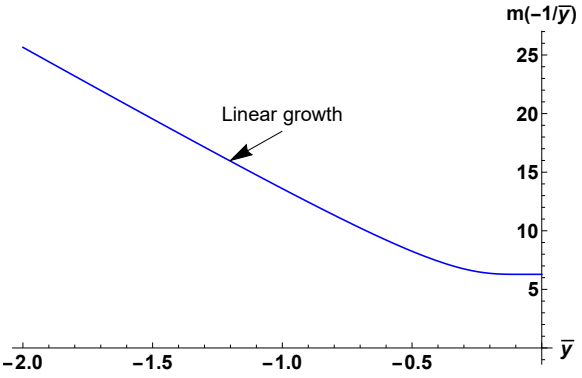

Figure F.1: The function $m(-1/\bar{y})$ (F.3) plotted as a function of $\bar{y}$, showing a clear increasing trend with $|\bar{y}|$ and linear growth for large negative $\bar{y}$.

Hence, to show that the $v/\gamma \to 0$ limit of the integral (F.1) is well defined when the integrand $\lambda^{1/z-1}\mathcal{P}(0,A,B)$ is in the asymptotic form, it is required to prove that

1. The limit of the function $\mathcal{P}(0,\infty,B) = \lim_{c\to\infty}\mathcal{P}(0,c/\lambda,B)$ exists.
2. There exists an integrable function g such that $|\mathcal{P}(0,c/\lambda,B)| \leq g(0,c/\lambda,B)$.
3. The integral $\int_0^\infty d\lambda\, \lambda^{1/z-1}\mathcal{P}(0,\infty,\lambda^{s+1})$ exists.

First, we show that the limit $\mathcal{P}(0,\infty,B) = \lim_{c\to\infty}\mathcal{P}(0,c/\lambda,B)$ exists for the small-v/γ asymptotics of the excitation probability. Noting that $F'(y) = -Bm(-1/y)$, Eq. (F.2) can be written as

$$\mathcal{P}(0,A,B) = \mathcal{P}_k^{\text{th}}(A^{-1})e^{F(0)} + \int_{-A}^{0} dy' \frac{\mathrm{d}}{\mathrm{d}y'}\left[e^{F(0)-F(y')}\right]\mathcal{P}_k^{\text{th}}(-1/y'). \tag{F.6}$$

Performing integration by parts, we obtain the form

$$\begin{aligned}\mathcal{P}(0,A,B) &= \mathcal{P}_k^{\text{th}}(A^{-1})e^{F(0)} + \mathcal{P}_k^{\text{th}}\left(\frac{-1}{y'}\right)e^{F(0)-F(y')}\Big|_{-A}^{0} - \int_{-A}^{0} dy' \frac{\mathrm{d}}{\mathrm{d}y'}\left[\mathcal{P}_k^{\text{th}}(-1/y')\right]e^{F(0)-F(y')} \\ &= -\int_{-A}^{0} dy' \frac{\mathrm{d}}{\mathrm{d}y'}\left[\mathcal{P}_k^{\text{th}}(-1/y')\right]e^{F(0)-F(y')}.\end{aligned} \tag{F.7}$$

Naively one would expect that taking the $c\to\infty$ limit of the excitation probability amounts to extending the lower bound of the integral in Eq. (F.7) to $-\infty$. While this is indeed the case, we provide a more concrete argument below.

Note that the exponential in the integrand of Eq. (F.7) is

$$e^{F(0)-F(y')} = -B\int_{y'<0}^{0} d\bar{y}\, m(-1/\bar{y}). \tag{F.8}$$

The form of the function $m(-1/\bar{y})$ is shown in Fig. F.1. Consequently, the integral (F.8) will be an increasing function of $|y'|$. The expansion of $m(-1/\bar{y})$ for large $\bar{y}$ to $\mathcal{O}\left(1/\bar{y}^4\right)$ is

$$m(-1/\bar{y}) = -4\pi\bar{y} - \frac{\pi}{3\bar{y}} + \frac{\pi}{180\bar{y}^3} + \mathcal{O}\left(\frac{1}{\bar{y}^4}\right), \tag{F.9}$$

hence for sufficiently large $\bar{y}$

$$\int_{y'<0}^{0} d\bar{y}\, m(-1/\bar{y}) \sim 2\pi y'^2. \tag{F.10}$$

It follows that the exponential function (F.8) will rapidly tend to zero with decreasing y' when $B \neq 0$. As a result, the integrand of the integral describing the excitation probability (F.7) rapidly decreases as the lower bound becomes increasingly more negative. Hence, the extension of the lower integration bound to $-\infty$ results in a well behaved integral, and the limit $\mathcal{P}(0,\infty,B) = \lim_{c\to\infty}\mathcal{P}(0,c/\lambda,B)$ exists.

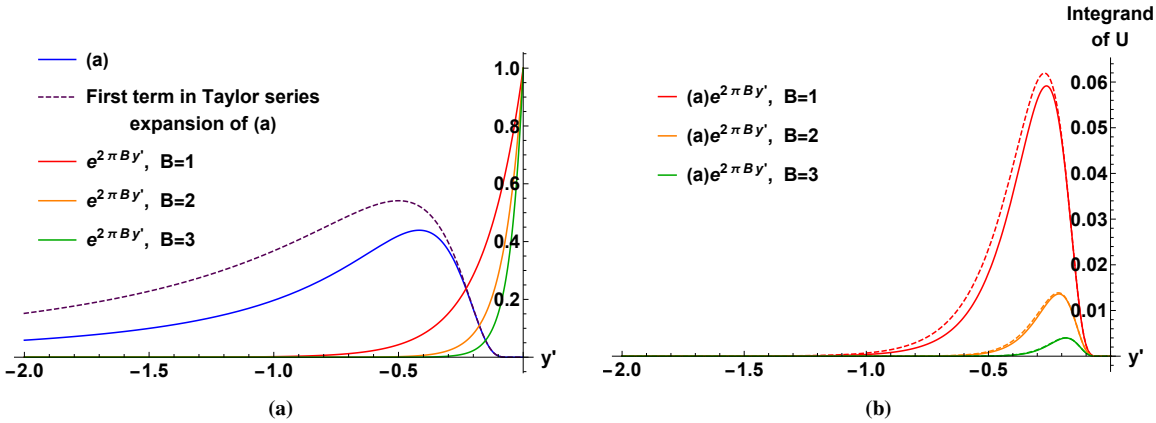

Figure F.2: (a) The two parts of the integrand in Eq. (F.13), indicated by (a) and (b). As B is increased the rapid decay of the exponential function $e^{2\pi B y'}$ results in the small-y' behaviour of (a) becoming increasingly dominant. Note that (i) function (a) tends to zero extremely rapidly as $y' \to 0$ and (ii) the first term in the Taylor series of (a), indicated by the dashed curve, well approximates the function (a) for small y'. **(b)** The product of (a) and (b), as they appear in the U integral (F.14). The solid curves correspond to the exact function in the integrand of U (F.14) for a series of B values, while the dashed curves correspond to the first term in the Taylor series of (a) multiplied by the exponential function $e^{2\pi B y'}$.

We proceed by proving points 2 and 3, i.e. that there exists an integrable function g such that $|\mathcal{P}(0, c/\lambda, B)| \leq g(0, c/\lambda, B)$, and that the integral $\int_0^\infty d\lambda\, \lambda^{1/z-1}\mathcal{P}(0,\infty,\lambda^{s+1})$ exists, which will then result in sufficient motivation for exchanging the small-v/γ limit of the integral with the integral of the limit. The integrand in Eq. (F.1) is an increasing function of c, hence

$$\lambda^{1/z-1}\mathcal{P}\left(0, \frac{c}{\lambda}, B\right) \leq \lambda^{1/z-1}\mathcal{P}(0,\infty,B), \tag{F.11}$$

where $\lambda^{1/z-1}\mathcal{P}\left(0, c/\lambda, B\right)$ is dominated by the function $\lambda^{1/z-1}\mathcal{P}(0,\infty,B)$ in the limit of slow ramp rates, i.e. in the $c \to \infty$ limit. Now it is required to prove that the integral

$$\int_0^\infty d\lambda\, \lambda^{1/z-1}\mathcal{P}(0,\infty,\lambda^{s+1}) \tag{F.12}$$

converges. Writing the integrand explicitly using Eqs. (F.7) and (F.8) leads to

$$\lambda^{1/z-1}\mathcal{P}(0,\infty,\lambda^{s+1}) = \lambda^{1/z-1}\int_{-\infty}^0 dy' \underbrace{\frac{\mathrm{d}}{\mathrm{d}y'}\left[-\mathcal{P}_k^{\mathrm{th}}(-1/y')\right]}_{(a)} \underbrace{\left[e^{-B\int_{y'}^0 d\bar{y}\, m(-1/\bar{y})}\right]}_{(b)}. \tag{F.13}$$

Referring back to the definition of the function m in Eq. (F.3) and Fig. F.1, note that $m(-1/\bar{y}) \geq 2\pi$. This implies $(b) \leq e^{2\pi B y'}$ in Eq. (F.13). We therefore define the upper bound U on the excitation probability as

$$0 \leq \mathcal{P}(0,\infty,\lambda^{s+1}) \leq U \qquad \text{with} \qquad U = \int_{-\infty}^0 dy' \frac{\mathrm{d}}{\mathrm{d}y'}\left[-\mathcal{P}_k^{\mathrm{th}}(-1/y')\right] e^{2\pi B y'}. \tag{F.14}$$

With reference to Fig. F.2, we observe that as $B \to \infty$, i.e. $\lambda \to \infty$, the small-y' behaviour of (a) (F.13) will be dominant in the upper bound U (F.14). Using the Taylor series

$$(a) = \frac{\mathrm{d}}{\mathrm{d}y'}\left[-\mathcal{P}_k^{\mathrm{th}}(-1/y')\right] = \frac{e^{1/y'}}{y'^2}\sum_{n=0}^\infty (-1)^n(n+1)e^{n/y'}, \tag{F.15}$$

the bound U is

$$U = \sum_{n=0}^\infty (-1)^n(n+1)\int_{-\infty}^0 dy' \frac{e^{(n+1)/y'}}{y'^2}e^{2\pi B y'} = \sum_{n=0}^\infty (-1)^n(n+1)\left(\frac{8\pi B}{1+n}\right)^{1/2} K_1(\sqrt{8\pi B(1+n)}) \tag{F.16}$$

where K_1 is the modified Bessel function of the second kind. From the large argument asymptotic expansion

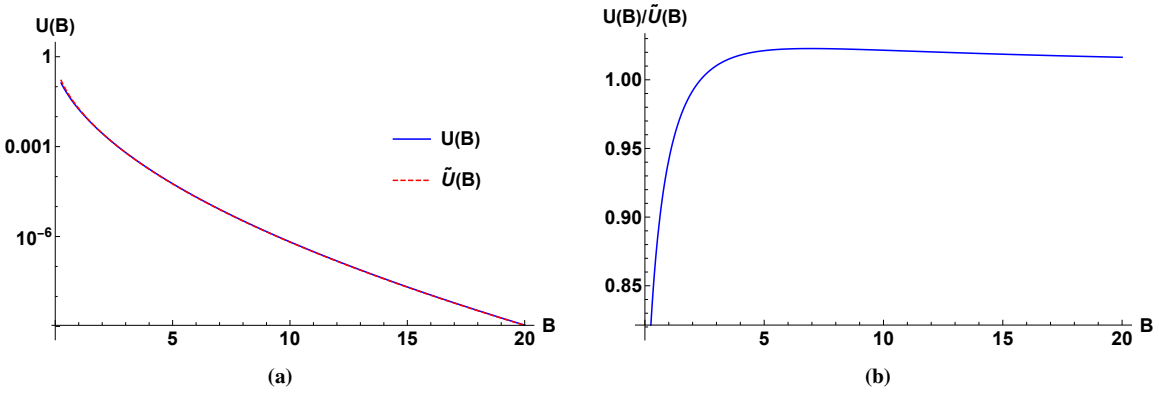

Figure F.3: **(a)** The first term of the asymptotic approximation $\tilde{U}$ (F.18) of the bound, together with the exact bound U (F.16) as a function of B. The bounds tend to zero exponentially quickly as $B \to \infty$. **(b)** The ratio $U/\tilde{U}$ of the exact and approximate bounds as a function of B, which tends to 1 as B is increased.

of K_1, the asymptotic approximation of the bound is

$$U \approx \sum_{n=0}^{\infty} (-1)^n \left[2(1+n)\pi^3 B\right]^{1/4} e^{-2[2\pi(n+1)B]^{1/2}}. \tag{F.17}$$

Since the first term in the infinite series will be dominant, we have

$$U \approx \tilde{U} = \left[2\pi^3 B\right]^{1/4} e^{-2[2\pi B]^{1/2}}, \tag{F.18}$$

which agrees well with the true bound, even for relatively small values of B. This is illustrated in Fig. F.3. Finally since $B = \lambda^{s+1}$, the bounded excitation probability $\mathcal{P}(0, \infty, \lambda^{s+1}) \leq U$ tends to zero exponentially quickly as $\lambda \to \infty$, so the integral in Eq. (F.12) converges.

F.2 Small-T_i asymptotics of the excitation probability

In this section we motivate that the $T_i \to 0$ limit of the integral

$$\int_0^{\infty} d\lambda \, (\lambda)^{\frac{1}{z}-1} \mathcal{P}\left(0, \frac{1}{\lambda}, \frac{\gamma(\lambda T_i)^{s+1}}{v}\right) \tag{F.19}$$

from Eq. (5.75) exists and is finite by using the small-T_i asymptotics of $\mathcal{P}_k$ (F.2). For simplicity, define $x = \left(\gamma T_i^{s+1}\right)/v$. The $T_i \to 0$ limit of the excitation probability $\mathcal{P}_k = \mathcal{P}\left(0, \frac{1}{\lambda}, \lambda^{s+1}x\right)$ in the integral (F.19) is

$$\lim_{x \to 0} \mathcal{P}\left(0, \frac{1}{\lambda}, \lambda^{s+1}x\right) = \mathcal{P}_k^{\text{th}}(\lambda). \tag{F.20}$$

Through a similar argument as in the previous section, it can be motivated that it is permissible to exchange the $T_i \to 0$ limit with the integral in Eq. (F.19). The resulting integral can be shown to converge.

Appendix G

Mathematical expressions

The expression for $h(\chi)$ in Eq. (4.22) is given by

$$\begin{aligned} h(\chi) = &\Big[(1+i)\chi\left(iD^{(1,0)}(0,(1-i)\chi) - iD^{(1,0)}(0,(-1+i)\chi) + \pi D(0,(-1+i)\chi)\right) \\ &\quad + D(-1,(1-i)\chi) + D(-1,(-1+i)\chi)\Big] \\ &\times \Big[(1+i)\chi\left(D^{(1,0)}(0,(-1-i)\chi) - D^{(1,0)}(0,(1+i)\chi) - i\pi D(0,(1+i)\chi)\right) \\ &\quad + D(-1,(-1-i)\chi) + D(-1,(1+i)\chi)\Big], \end{aligned} \tag{G.1}$$

where we use the notation $D(n,z) = D_n(z)$ and $D^{(1,0)}(n,z) = \frac{\mathrm{d}D_n(z)}{\mathrm{d}n}$, where $D_n(z)$ is the parabolic cylinder function satisfying the Weber differential equation [109].